Exploring the mechanisms of chlamydial cell division, peptidoglycan turnover, and persistence

Dissertation

zur

Erlangung des Doktorgrades (Dr. rer. nat.)

der

Mathematisch-Naturwissenschaftlichen Fakultät

der

Rheinischen Friedrich-Wilhelms-Universität Bonn

vorgelegt von

Julia Dannenberg

aus

Gummersbach

Bonn 2024

Angefertigt mit Genehmigung der Mathematisch-Naturwissenschaftlichen Fakultät
der Rheinischen Friedrich-Wilhelms-Universität Bonn

Gutachterin/Betreuerin: Prof. Dr. Tanja Schneider
Gutachterin: PD Dr. Christiane Dahl

Tag der Promotion: 27.03.2025
Erscheinungsjahr: 2025

-Für meine Familie-

Table of contents

Abbreviations ..... **I**
Register of tables ..... **IV**
Register of figures ..... **V**
1. Introduction **1**
1.1. Chlamydial phylogeny, pathological and epidemiological aspects 1
1.2. The developmental cycle of *Chlamydia* 4
1.3. The chlamydial cell envelope 6
1.3.1. Peptidoglycan biosynthesis 8
1.4. Cell division 11
1.5. Peptidoglycan turnover – remodeling and recycling 14
1.5.1. AmiA as a part of chlamydial PGN turnover and cell division machinery 16
1.6. Aims of this work 19
2. Material & Methods **20**
2.1. *In silico* methods, software and online tools 20
2.2. Consumables 21
2.3. Technical equipment 21
2.4. Chemicals 23
2.4.1. Special reagents 23
2.5. Kits 23
2.6. Cultivation of bacteria and mammalian cells 24
2.6.1. Media preparation and additives 24
2.6.1.1. Media for cultivation of bacteria 24
2.6.1.2. Media for cultivation of mammalian cells 25
2.6.1.3. Antibiotics and tested compounds 26
2.6.2. Used organisms 27
2.6.2.1. *E. coli* strains for plasmid propagation, subcloning and preparation of PGN sacculi 27
2.6.2.2. *E. coli* strains used for recombinant protein production 27
2.6.2.3. *E. coli* mutant strains used in complementation experiments 28
2.6.2.4. Mammalian cell lines 28
2.6.2.5. *Chlamydia* strains 28
2.6.3. Bacteriological methods 29
2.6.3.1. Preparation of chemically competent *E. coli* 29
2.6.3.2. Heat shock transformation of chemically competent *E. coli* 29
2.6.3.3. Electroporation 29
2.6.3.4. Optical density determination 29
2.6.4. Mammalian cell culture and propagation of *Chlamydia* 29
2.6.4.1. Reagents used in mammalian cell culture and microscopy 30
2.6.4.2. Cultivation of eukaryotic cells and passaging 30
2.6.4.3. Permanent cultures of mammalian cells 31
2.6.4.4. Infection of eukaryotic cells and propagation of *Chlamydia* 31
2.6.4.5. Permanent cultures of *Chlamydia* 31
2.7. Molecular methods 31
2.7.1. Isolation of genomic DNA from bacteria 31
2.7.2. Polymerase chain reaction 31
2.7.3. Reverse Transcriptase quantitative PCR (RT-qPCR) 33
2.7.4. Agarose gel electrophoresis 34
2.7.5. Purification of DNA fragments and plasmids 34
2.7.6. Photometric determination of DNA concentration 35
2.7.7. Molecular Cloning 35
2.7.7.1. Restriction of DNA with endonucleases 35
2.7.7.2. Ligation of inserts into plasmids 35
2.7.7.3. In-Fusion Cloning 36
2.7.7.4. PCR-based site-directed mutagenesis 36
2.7.8. Sequencing 36

2.7.9. Expression vectors 37
2.8. Biochemical methods 38
2.8.1. Recombinant protein production and purification 38
2.8.2. Quantification of recombinant protein with Bradford's reagent 39
2.8.3. Protein analysis by SDS-PAGE 40
2.8.4. Dialysis 40
2.8.5. Preparation of Remazol Brilliant Blue-stained E. coli PGN sacculi 40
2.8.6. Thin layer chromatography (TLC) 40
2.8.6.1. TLC for detection of lipids 40
2.8.7. In vitro assays using purified recombinant protein 41
2.8.7.1. Activity on lipid II 41
2.8.7.2. Dye release assay 41
2.8.7.3. Assessment of PGN binding properties of AmiA by pulldown assays 41
2.8.8. Mass Spectrometry 42
2.9. Complementation assays with *E. coli* mutant strains 42
2.10. Investigation of antichlamydial effects in tissue-culture based *Chlamydia* infection models 42
2.10.1. Preparation of HEp-2 cells 42
2.10.2. AlamarBlue cell viability assay 43
2.10.3. Infection of host cells with *Chlamydia* 43
2.10.4. Determination of minimal inhibitory concentrations (MIC) against chlamydial infection 43
2.10.4.1. Productive chlamydial infection 43
2.10.4.2. Chlamydial infection in penicillin G-induced persistent state 43
2.10.4.3. Chlamydial infection in interferone (IFN)-γ-induced persistence 44
2.10.5. Recovery Assay 44
2.10.6. Fluorescence microscopy 45
2.10.7. Quantitative analysis of fluorescence microscopy data 45
2.11. Introducing genetic knockdowns using CRISPRi 46
2.11.1. Transformation of *Chlamydia* and induction of CRISPRi construct expression 46
2.11.2. Collection and processing of RNA samples from infected host cells 46
2.11.3. Collection and processing of DNA samples from infected host cells 47
2.11.4. Collection and processing of samples for immunofluorescence assay 47
2.11.5. Immunofluorescence assay (IFA) 47
2.11.6. Determination of infectious progeny (IFU Assay) 48
3. Results 49
3.1. Characterization of AmiA_Ct 49
3.1.1. Comparative *in silico* analysis of AmiA_Ct 49
3.1.2. AmiA_Ct rescues cell separation in an amidase-deficient *E. coli* mutant 52
3.1.3. AmiA_Ct lyses a heterologous host strain upon overproduction 53
3.1.4. Recombinant AmiA_Ct is active *in vitro* 53
3.1.5. AmiA_Ct binds to PGN *in vitro* independently from enzymatic activity 55
3.1.6. AmiA_Ct can be inhibited by metal chelators *in vitro* 56
3.2. Effects of CRISPRi-induced conditional genetic knockdowns of *amiA* in *C. trachomatis* 58
3.2.1. Effects of *amiA* knockdown 59
3.2.2. Knockdown of *amiA* and complementation 62
3.2.3. Effects of *amiA* knockdown on PGN shown by EDA-DA PGN labeling 64
3.2.4. Effects of *amiA* knockdown on infectious progeny of *C. trachomatis* 66
3.3. Overexpression and CRISPRi-mediated knockdown of putatively cell division-associated chlamydial genes affect cell division in *C. trachomatis* 68
3.3.1. CRISPRi-induced knockdown and overexpression of *C. trachomatis rodA* 69
3.3.2. CRISPRi-induced knockdown and overexpression of *C. trachomatis namZ* 71
3.4. New insights into the substrate spectrum of chlamydial recycling enzyme YkfC 73
3.5. *C. trachomatis* nutrient starvation and persistence in tissue culture infection models 74
3.5.1. Toxicity of metal chelators on mammalian cells 74
3.5.2. Effects of metal chelators on active chlamydial infections tested in cell culture-based infection models 76

3.5.3. Effects of metal chelators on penicillin G-induced persistent chlamydial infections in cell culture-based infection models 83
3.5.4. Effects of metal chelators on interferon-γ induced persistent chlamydial infections tested in cell culture-based infection models 90
3.5.5. Rescue of chelator-treated chlamydial infections 96
3.5.6. Recovery of active and penicillin G-induced persistent chlamydial infections treated with metal chelators 100
4. Discussion 103
5. Summary 133
References 135
Veröffentlichungen 162

Abbreviations

(v/v)	volume/volume percent
(w/v)	weight/volume percent
°C	degree Celsius
µg	microgram
µL	microliter
µm	micrometer
6xH	hexahistidine tag
aa	amino acid(s)
AB	aberrant body
AmiA_Cp	AmiA from *Chlamydia pneumoniae*
AmiA_Ct	AmiA from *Chlamydia trachomatis*
AmiA_Ec	AmiA from *E. coli*
aTc	anhydrotetracycline
BSA	bovine serum albumin
bp	base pair
Cp	*Chlamydia pneumoniae*
CRISPR	clustered Regularly Interspaced Short Palindromic Repeats
CRISPRi	clustered Regularly Interspaced Short Palindromic Repeats Interference
Ct	*Chlamydia trachomatis*
CV	column bed volume
$C_{55}P$	undecaprenyl phosphate, bactoprenol lipid carrier
Da	Dalton
DAPI	4',6-Diamidin-2-phenylindol
DD-CPase	DD-carboxypeptidase
DMEM	Dulbecco's Modified Eagle Medium
DMSO	dimethylsulfoxide
DNA	desoxyribonucleic acid
dNTP	desoxynucleotide triphosphate
EB	elementary body
Ec	*Escherichia coli*
EDA-DA	ethynyl-D-alanyl-D-alanine
EDTA	ethylene diamine tetracetic acid
Fig.	figure
g	relative centrifugation force to gravity
GlcNAc	N-acetylglucosamine
h	hours

HBSS	Hank's Balanced Salt Solution
hpi	hours post infection
IFA	immunofluorescence assay
IFU	inclusion forming unit
IFN-γ	interferon-γ
IM	inner membrane
kb	kilobase
kDa	kilodalton
L	liter
LB	lysogeny broth
lipid I	undecaprenyl-pyrophosphoryl-MurNAc-pentapeptide
lipid II	undecaprenyl-pyrophosphoryl-MurNAc-GlcNAc-pentapeptide
LPS	lipopolysaccharide
M	molar
mb	megabase
MCS	multiple cloning site
MS	mass spectrometry
*m*DAP	*meso*-diaminopimelic acid
MIC	minimum inhibitory concentration
min	minute(s)
mL	milliliter(s)
mM	millimolar
MOMP	major outer membrane protein
MurNAc	N-acetylmuramic acid
ng	nanogram
nm	nanometer
OD	optical density
OD_{600}	optical density 600 nm
OM	outer membrane
PAGE	polyacrylamide gel electrophoresis
PBP	penicillin binding protein
PGN	peptidoglycan
PMA	phosphomolybdic acid
RB	reticulate body
rpm	rounds per minute
s	second(s)
SDS	sodium dodecyl sulfate

s.d.	standard deviation
SP	signal peptide
TAE	tris-acetate-EDTA buffer
TLC	thin layer chromatography
Tris	tris(hydroxymethyl)diamine
u	unit(s)
UV	ultraviolet
V	volt

Amino acid abbreviations used in this work are in accordance to the IUPAC amino acid code. Nucleotide abbreviations are in accordance to the IUPAC nucleotide code.

Register of tables

Table 1: Software and online tools.....20
Table 2: Technical equipment.....22
Table 3: Special reagents.....23
Table 4: Kits used in this work.....23
Table 5: Media used for cultivation of bacteria.....24
Table 6: Media used for cultivation of HEp-2 cells.....25
Table 7: Media used for cultivation of HEK-Blue reporter cells.....26
Table 8: Antibiotics and tested compounds.....26
Table 9: *E. coli* strains for plasmid propagation, subcloning and preparation of PGN sacculi.....27
Table 10: *E. coli* strains used for recombinant protein production.....27
Table 11: *E. coli* mutant strains.....28
Table 12: Mammalian cell lines.....28
Table 13: *Chlamydia* strains.....28
Table 14: Reagents used in mammalian cell culture.....30
Table 15: Oligonucleotides used in this work.....32
Table 16: Primers used for qPCR.....34
Table 17: gBlocks.....35
Table 18: Expression vectors.....37
Table 19: Conditions for recombinant production of AmiA_Ct and AmiA_Cp.....39

Register of figures

Figure 1: Chlamydial developmental cycle. 6
Figure 2: Proposed model of PGN biosynthesis, turnover and recycling in *Chlamydia*. 9
Figure 3: Model of chlamydial cell division. 13
Figure 4: *In silico* analysis of AmiA_Ct compared to AmiA_Cp and AmiA_Ec. 51
Figure 5: AmiA_Ct has conserved activity and assists in cell separation in an amidase-deficient *E. coli* mutant. 52
Figure 6: AmiA_Ct lyses an *E. coli* host strain upon heterologous overproduction. 53
Figure 7: Recombinant AmiA_Ct is active *in vitro* on PGN and precursor molecule lipid II mDAP. 55
Figure 8: AmiA_Ct binds to PGN *in vitro*. 56
Figure 9: AmiA_Ct is inhibited by chelators of bivalent cations *in vitro*. 58
Figure 10: Gene expression during CRISPRi-mediated knockdown over time under uninduced (blue) and induced (red) conditions in *amiA* knockdown strain *C. trachomatis* pLCRia(*amiA*). 59
Figure 11: Gene expression during CRISPRi-mediated knockdown over time under uninduced (blue) and induced (red) conditions in *C. trachomatis* pLCRia(NT). 60
Figure 12: Gene expression during CRISPRi-mediated knockdown over time under uninduced (blue) and induced (red) conditions *C. trachomatis* pLCRia-*amiA*_6xH(*amiA*). 61
Figure 13: CRISPRi-mediated knockdown of amiA leads to chlamydial phenotypes related to impaired cell division in *C. trachomatis*. 63
Figure 14: CRISPRi-mediated knockdown of *amiA* is complemented by overexpression of *amiA*. 64
Figure 15: Effects of *amiA* knockdown on PGN in *C. trachomatis*. 65
Figure 16: Effects of CRISPRi-mediated knockdown of *amiA* in *C. trachomatis* on proliferation. 67
Figure 17: Phenotypic effects of CRISPRi-mediated genetic knockdown of *rodA* in *C. trachomatis*. 69
Figure 18: Morphologic effects of *rodA* overexpression in *C. trachomatis*. 70
Figure 19: Morphologic effects of CRISPRi-mediated genetic knockdown of *namZ* in *C. trachomatis*. 71
Figure 20: Morphologic effects of *namZ* overexpression in *C. trachomatis*. 72
Figure 21: *In vitro* activity of YkfC_Ct on (non)-PGN-derived peptides (adapted from Reuter *et al.*, 2023). 73
Figure 22: Cytotoxic effects of metal chelators clioquinol, 1,10-phenanthroline and TPEN on mammalian HEp-2 host cells. 75
Figure 23: Diagram for the treatment of active chlamydial infections using metal chelators. 77
Figure 24: Effects of 28-hour clioquinol treatment on active chlamydial infections (treatment timepoint: 2 hpi). 78
Figure 25: Effects of 18-hour clioquinol treatment on active chlamydial infections (treatment timepoint: 12 hpi). 79

Figure 26: Effects of 28-hour 1,10-phenanthroline treatment on active chlamydial infections (treatment timepoint: 2 hpi).. 81
Figure 27: Effects of 18-hour 1,10-phenanthroline treatment on active chlamydial infections (treatment timepoint: 12 hpi) 82
Figure 28: Diagram for the treatment of penicillin G-induced persistent chlamydial infections using metal chelators. 83
Figure 29: Effects of simultaneous clioquinol and penicillin G treatment on chlamydial infections (treatment timepoint: 2 hpi). 84
Figure 30: Effects of 18-hour clioquinol treatment on penicillin-induced persistent chlamydial infections (treatment timepoint: 12 hpi). 86
Figure 31: Effects of simultaneous 1,10-phenanthroline and penicillin G treatment on chlamydial infections (treatment timepoint: 2 hpi). 87
Figure 32: Effects of 18-hour 1,10-phenanthroline treatment on penicillin-induced persistent chlamydial infections (treatment timepoint: 12 hpi). 89
Figure 33: Diagram for the treatment of interferon-γ-induced persistent chlamydial infections using metal chelators. 90
Figure 34: Effects of 28-hour clioquinol treatment on interferon-γ-induced persistent chlamydial infections (treatment timepoint: 2 hpi). 91
Figure 35: Effects of 18-hour clioquinol treatment on interferon-γ-induced persistent chlamydial infections (treatment timepoint: 12 hpi). 92
Figure 36: Effects of 28-hour 1,10-phenanthroline treatment on interferon-γ-induced persistent chlamydial infections (treatment timepoint: 2 hpi).. 93
Figure 37: Effects of 18-hour 1,10-phenanthroline treatment on interferon-γ-induced persistent chlamydial infections (treatment timepoint: 12 hpi). 95
Figure 38: 2,2-bipyridyl treatment led to small inclusions filled with slightly enlarged chlamydial cells. 97
Figure 39: Rescue of 1,10-phenanthroline and clioquinol-induced phenotypes by iron and zinc compounds applied 2 hpi. 98
Figure 40: Rescue of 1,10-phenanthroline and clioquinol-induced phenotypes by iron and zinc compounds applied on an established *C. trachomatis* infection 12 hpi. 99
Figure 41: Recovery clioquinol-treated infections. 101
Figure 42: Recovery of 1,10-phenanthroline-treated infections. 102

1. Introduction

Chlamydia trachomatis was first discovered in swabs from conjunctival scrapings by von Prowazeck and Halberstädter in 1907 (von Prowazek and Halberstädter, 1907). First thought to be protozoa, then viruses (Bedson and Bland, 1932), James W. Moulder discovered in 1966 that *Chlamydia* in fact is a bacterial genus, phylogenetically belonging to the order of *Chlamydiales* (Moulder, 1966, 1968). To date, nine families are included within the order, but recent molecular data suggest the existence of 181 family lineages (Lagkouvardos et al., 2014). The *Chlamydiales* order contains a wide range of important human and veterinary pathogens causing diverse clinical pictures and posing a socioeconomic burden throughout society. The most well-known pathogen within the order is *C. trachomatis*, the world's most common cause for preventable blindness and the most widespread bacterial sexually transmitted infection (STI).

Besides the clinical pictures, members of *Chlamydiales* stand out from other bacterial pathogens because of the obligate intracellular lifestyle, limiting the organisms to proliferate exclusively within eukaryotic host cells. Therefore, in contrast to free-living bacteria, intracellular bacteria are less exposed to environmental stimuli and reside within a homeostatic environment. A lot of biosynthetic pathways designed to react to biotic and abiotic stressors are indispensable for free-living bacteria but are reduced in the intracellular *Chlamydiales*. Over the course of reductive co-evolution with the eukaryotic host, chlamydial genome sizes condensed, cumulating in the highly streamlined *C. trachomatis* that is left with a genome size of about 1.0 megabase pairs (Mbp) and less than 900 open reading frames (ORFs), of which many encode housekeeping genes and approx. two thirds represent the core genome shared across species (Belland *et al.*, 2003; Elwell, Mirrashidi and Engel, 2016; Collingro, Köstlbacher and Horn, 2020). Despite this, *C. trachomatis* and all members of *Chlamydiales* retained a complex biphasic lifecyle, unique within the bacterial domain, and an outstanding cell division process. Perfectly adapted to its host and intracellular niche, *C. trachomatis* developed strategies to scavenge nutrients from the host, endure unfavorable environmental conditions and escape the hosts immune system, often allowing chlamydial infections to remain undetected. The following chapters provide the theoretical background of the research presented in this work, covering chlamydial phylogeny, pathology, and epidemiologic aspects (1.1.). Aspects of the unique biphasic lifecycle of chlamydiae are reviewed in 1.2. and the tightly interlinked processes of cell envelope biosynthesis (1.3.), cell division (1.4.) and cell envelope turnover and recycling processes (1.5.) are reviewed.

1.1. Chlamydial phylogeny, pathological and epidemiological aspects

The term *Chlamydia* originated from the ancient Greek word *khlamús,* meaning cloak. This is a reference towards the obligate intracellular lifestyle of these pathogens, that can be applied to all members of the order *Chlamydiales*. To date, *Chlamydiales* comprise nine families including *Waddliaceae*, *Simkaniaceae* and *Parachlamydiaceae* (Taylor-Brown *et al.*, 2015). The clinically most relevant family within the order is *Chlamydiaceae,* with *Chlamydia* as the only genus known to date. It

includes the major human pathogens *C. trachomatis* and *C. pneumoniae*, as well as veterinary pathogens with immense zoonotic potential.

Worldwide, *C. trachomatis* serovars D-K, subsumed under the term genital tract biovar, are the most widespread bacterial causes of STI in men and women. Transmission from infected mothers to newborns during childbirth is the only vertical mode of transmission, causes pneumonia and conjunctivitis in newborns and occurs rather rarely compared to horizontal transmission (Darville, 2005; Honkila *et al.*, 2017). In fact, the most relevant way of transmission is through unprotected sex. According to WHO estimates, 128.5 million new infections with *C. trachomatis* D-K among people aged 15 – 49 years occurred worldwide in 2020. Most recent data of Centers for Disease Control and Prevention (CDC) reports more than 1.6 million infections in 2021 in the US alone, with almost two thirds of cases in the age group of 15 – 24 years. Though very common, a representative survey among various age groups in Germany showed that only 20 % of men and women within the age group of 18-25 are aware of genital *C. trachomatis* infections as a sexually transmitted disease (Matthiesen *et al.*, 2021). *C. trachomatis* genital tract infections often proceed subclinically, with 50 % of infections in male and 80 % of female infections being asymptomatic, undetected and, therefore, untreated (Mabonga *et al.*, 2021). Possible complications of infection include urethritis and proctitis. 15 – 40 % of infections ascend to the upper genital tract, possibly entailing pelvic inflammatory disease (PID), cervicitis, adverse pregnancy outcome, ectopic pregnancy, or tubal factor infertility (Blanchard and Mabey, 1994; Paavonen, 1999; Taylor and Haggerty, 2011). Infection with *C. trachomatis* was also associated with enhanced HIV infection progression and cervical cancer (Arcia Franchini *et al.*, 2022; Dzakah *et al.*, 2022). Serovars L1-L2 of *C. trachomatis* cause lymphogranuloma venereum (LGV), another sexually transmitted condition that can cause invasive infection and is often associated with proctocolitis and can develop into severe systemic infection (Martin-Iguacel *et al.*, 2010). Serovars A-C are termed the trachoma biovar and represent the most prevalent cause for preventable blindness, causing 1.4 % of blindness in humans worldwide according to WHO (WHO, 2021). Trachoma affects 1.8 million people worldwide causing visual impairment and blindness. Further 125 million people living in trachoma-endemic areas are threatened by the disease (Solomon *et al.*, 2022). Prevalence of infection is highly elevated in sub-Saharan African countries and strongly correlated with relative poverty (Habtamu *et al.*, 2015). Repeated infections over time entail scarring of the upper eyelid conjunctiva and the subsequent inversion of lashes causes abrasion of the eyeball, opacification of the cornea and eventually blindness (Mabey, Solomon and Foster, 2003). Infection is contracted through smear infections through conjunctival liquid of infected persons and possibly also insects having come in contact with contaminated eye discharge (Cook, 2008; Last *et al.*, 2020). Through improved hygienic standards, trachoma disappeared from Europe and other industrialized countries during the 20th century (Taylor, 2009).

C. pneumoniae is the second most well-known pathogen within the *Chlamydiaceae* family and infects the upper and lower respiratory tract. Unlike the close relative *C. trachomatis* with humans as the sole possible host, *C. pneumoniae* was shown to have a broader host range including horses, frogs and koalas

(Jackson *et al.*, 1999; Mitchell *et al.*, 2010). In humans, it is responsible for 6 – 20 % of cases of community-acquired pneumonia (CAP) and can cause otitis media, sinusitis, and bronchitis (Block *et al.*, 1997; Blasi, Tarsia and Aliberti, 2009). It has also been linked with atherosclerosis and Alzheimer's disease (Shima, Kuhlenbäumer and Rupp, 2010; Khoshbayan *et al.*, 2021; Piekut *et al.*, 2022).

The *Chlamydiaceae* also include the veterinary pathogen *C. psittaci*, that causes avian chlamydiosis. In birds, infections affect the respiratory system and may cause myocarditis with mortality rates up to 30 % (Andersen and Vanrompay, 2000), making the pathogen an important factor in lifestock production. For humans, *C. psittaci* harbors an immense zoonotic potential: upon close contact with infected birds, humans can contract psittacosis, with complications ranging from mild influenza-like illness to pneumonia, endocarditis, or hepatitis (Gregory and Schaffner, 1997). Further animal pathogens within the *Chlamydiaceae* are *C. muridarum*, representing an established *in vivo* infection model in mice, *C. abortus*, *C. pecorum* and *C. felis,* among others.

Except *Chlamydiaceae*, the other families within the *Chlamydiales* order are summarized under the non-phylogenetic terms *Chlamydia*-related bacteria or environmental chlamydiae. Omnipresent in various environments, they constitute an important part of the biosphere. *Chlamydia*-related bacteria were shown to be present in freshwater and saltwater environments, soils, within biofilms in engineered water systems, such as drinking water distribution facilities, and even in anoxic environments like bioreactors or deep marine sediments (Corsaro and Venditti, 2009; Serkebaeva *et al.*, 2013; Huang, Yang and Zhang, 2016; Pizzetti *et al.*, 2016; Bertelli *et al.*, 2018; Dharamshi *et al.*, 2020). Like *Chlamydiaceae*, environmental chlamydiae are strictly intracellular. According to phylogenetic analyses, the last common ancestor of all chlamydiae is estimated to have adopted an intracellular lifestyle 1- 2 billion years ago (Kamneva *et al.*, 2012; Subtil, Collingro and Horn, 2014). Instead of higher eukaryotes, hosts of environmental chlamydiae are mostly unicellular organisms like amoebae, which are highly abundant in terrestrial and aquatic environments. Recently, some members of the *Chlamydia*-related bacteria gained importance as emerging pathogens of humans and animals. Within *Parachlamydiaceae*, the organism *Parachlamydia acanthamoebae* normally infects the amoebal species *Acanthamoeba polyphaga* (Greub and Raoult, 2002a). Due to its ability to escape amoebal phagolysosome lytic pathway, the organism was also suspected to escape human alveolar macrophages after 16S rRNA was detected in bronchoalveolar lavage (Greub and Raoult, 2002b). Shortly after, *P. acathamoebae* was confirmed as a rare agent causing pneumonia in humans (Greub *et al.*, 2003; Greub, 2009). *Acanthamoeba* spp. is the host for species also belonging to *Protochlamydia* within the *Parachlamydiaceae* family. *Pr. naegleriophila* was shown to survive within cells of the human respiratory tract and was detected in bronchoalveolar lavage of pneumonia patients, suggesting a role of the organism in pneumonia in humans (Casson *et al.*, 2008). *Simkania negevensis* was discovered as a contaminant in cell culture and was set within the newly discovered *Simkaniaceae* family at the time (Kahane, 1993; Thao *et al.*, 2003). Often associated with insects, the bacterium was shown to replicate within mammalian cells as well and to be implicated as an emerging pathogen causing pneumonia and

bronchiolitis in humans (Greenberg *et al.*, 2003; Vouga, Baud and Greub, 2017). *Waddlia chondrophila* belongs to the *Waddliaceae* family and was first isolated from bovine abortion tissue. In recent years, the organism was shown to be also involved in human miscarriage and respiratory diseases (Baud *et al.*, 2011; de Barsy and Greub, 2013). Besides host range, an interesting difference between *Chlamydiaceae* and *Chlamydia*-related bacteria becomes evident upon comparison of genome size. While the free-living model organism *Escherichia coli* has a genome size of 4.6 Mbp, *P. acanthamoebae* shows a reduced size of approx. 3 Mbp. The highly adapted *C. trachomatis* reduced genome size further to 1 Mbp, as already mentioned. The intracellular lifestyle and the consequent diminished exposure to environmental stimuli enabled this reduction. Therefore, within the nutrient-rich environment that eukaryotic host cells provide, some energy-intense biosynthetic pathways became dispensable over time, which is reflected in reduced genetic flexibility (McClarty, 1994). This reductive evolution has left an ongoing pattern: *Chlamydia*-related bacteria are evolutionary older than *Chlamydiaceae* and are deep-rooted within the phylogenetic tree (Zomorodipour and Andersson, 1999; Horn *et al.*, 2004). While amoebal cells form a barrier between the environment and the intracellular bacteria, they still provide a less homeostatic environment than cells of higher multicellular eukaryotes. Therefore, *Chlamydia*-related bacteria require larger metabolic potential to overcome environmentally challenging situations (Collingro *et al.*, 2011). Moreover, larger genetic diversity allows *Chlamydia*-related bacteria to infect a broader host range than *Chlamydiaceae*, that are well-protected within cells of eukaryotic tissue, but auxotrophic for many nutrients and highly limited in host range.

1.2. The developmental cycle of *Chlamydia*

Despite being drastically reduced in terms of genome size, *Chlamydiaceae* are far from simple. Like all members of *Chlamydiales*, they undergo a complex and unique biphasic lifecycle in which they alternate between two morphologically distinct forms. A schematic representation of the chlamydial lifecycle is presented in Figure 1. Extracellularly, *Chlamydiales* can survive in the form of an elementary body (EB) but cannot proliferate (Fig. 1a). After internalization into a eukaryotic host cell (Fig. 1b), they differentiate into reticulate bodies (RB) (Fig. 1c), which are able to divide but cannot exist extracellularly. To enter a new infectious cycle, RBs redifferentiate into EBs that exit the host cell. Within the biphasic lifecycle, a distinct pattern of gene expression corresponds to the specific chlamydial differentiation phase (Belland *et al.*, 2003). More in details, elementary bodies are round, electron dense and approx. 0.2 - 0.3 µm in diameter (Matsumoto, 1973). Due to their rigidity and ability to resist a wide range of environmental stressors, they are often termed the spore-like form of chlamydiae. Rigidity is conferred through heavy protein crosslinkage via disulfide bonds in the EB outer layer, which is rich in the major outer membrane protein (MOMP), the small cysteine-rich protein OmcA and the large cysteine-rich protein OmcB (Hackstadt, Todd and Caldwell, 1985; Hatch, Miceli and Sublett, 1986; Hatch, 1996). Long assumed to be metabolically inert, EB metabolism was shown to be highly active and synthesis of various proteins at this stage is thought to prime EBs for differentiation into RBs once inside a host cell (Saka *et al.*, 2011; Omsland *et al.*, 2014). Adhesion of EBs to eukaryotic host cells is

dependent on various factors and differences in host and tissue tropism among *Chlamydia* might be regulated by variance in adhesion factors (Elwell, Mirrashidi and Engel, 2016). In a two-step process, a low-affinity interaction between chlamydial protein OmcB and heparan sulfate proteoglycans on the surface of host cells is established (Su *et al.*, 1996). Secondly, high-affinity binding is mediated through interaction of chlamydial lipopolysaccharide (LPS) (Ajonuma *et al.*, 2010), MOMP (Mehlitz and Rudel, 2013), members of the polymorphic membrane protein (Pmp) family and more with host cell surface factors (Becker and Hegemann, 2014). Upon contact with host cells, pre-packed effector proteins are injected into the host cell cytoplasm through type III secretion system (T3SS) leading to small GTPase-dependent cytoskeletal rearrangements facilitating internalization of EBs (Bastidas *et al.*, 2013). Now present within an intracellular compartment termed inclusion, EBs start the second part of developmental cycle. The presence of the inclusion prevents, on one hand, the killing of chlamydiae by host lysosomes and, on the other, avoids host cell apoptosis. Not only mediate effector proteins the inclusion's escape from the host cell's lysosomal pathway through alteration of the inclusion surface (Hackstadt, 2000) but also the intracellular transportation along microtubules to the microtubule organizing center (MTOC) (Clausen *et al.*, 1997; Grieshaber, Grieshaber and Hackstadt, 2003; Grieshaber *et al.*, 2006). Effectors also interfere with intracellular vesicle and nutrient-rich compartment transport and induce their redirection towards the chlamydial inclusion (Omsland *et al.*, 2014). In this way, auxotrophic *Chlamydia* scavenge nutrients from the host. Furthermore, mechanisms that trigger apoptosis of the host cell are averted (Moore and Ouellette, 2014). Inside the inclusion, EBs start the primary differentiation process to become RBs (Fig. 1c). Disulfide bonds in the outer layer of EBs are reduced, increasing membrane fluidity (Nelson, 2012). With a diameter of 0.8 - 1 µm, the diderm RB is less dense and significantly larger than the EB (AbdelRahman and Belland, 2005). Within the inclusion, RBs undergo cell division by a polarized budding mechanism until the inclusion is significantly enlarged and filled with RBs (Abdelrahman *et al.*, 2016) (Fig. 1d). In an asynchronous manner, RBs differentiate back into EBs (Moulder, 1991; Nicholson *et al.*, 2003) (Fig. 1e), that exit the host cell either by lysis (Fig. 1f) or by extrusion (Fig. 1g) in membrane-coated vesicles to begin a new infectious cycle (Moulder, 1991; Hybiske and Stephens, 2007). Upon adverse environmental conditions such as nutrient deprivation (e.g. iron, amino acids) (Moulder, 1983; Coles, 1993; Raulston, 1997), viral coinfection of the host cell (Deka *et al.*, 2006), exposure to host cell cytokines, heat shock or antibiotic treatment, chlamydial cells can enter a state of persistence (Kazar, Gillmore and Gordon, 1971; Beatty, Byrne and Morrison, 1993). In most cases, cells adopt a morphologically distinct shape characterized by significantly enlarged non-dividing cells termed aberrant bodies (AB) (Fig. 1h). This process enables chlamydial cells to outlast environmentally challenging situations. Among the other inductors, β-lactam antibiotic penicillin, which targets cell wall biosynthesis in free-living bacteria, is the most characterized inductor, though some mechanistic and cellular processes are not understood yet (Beatty, Morrison and Byrne, 1994). The underlying mechanisms of persistence differ depending on the stimulus and are characterized by differential patterns of gene expression (Panzetta, Valdivia and Saka, 2018). Once the

stressor is removed, RBs asynchronously constrict from ABs in a budding-like mechanism and chlamydial cells reenter the developmental cycle as it was shown for penicillin-induced persistence (Skilton *et al.*, 2009). Depending on the chlamydial species and the host cell, durations of the lifecycle stages may vary. On average, primary differentiation from EBs to RBs occurs within two to six hours post infection. Division of RBs starts approx. 12 hours post infection and reaches its peak 18 to 24 hours after infection. After redifferentiation, EBs exit the host cell 48 to 72 hours post infection (Nicholson *et al.*, 2003).

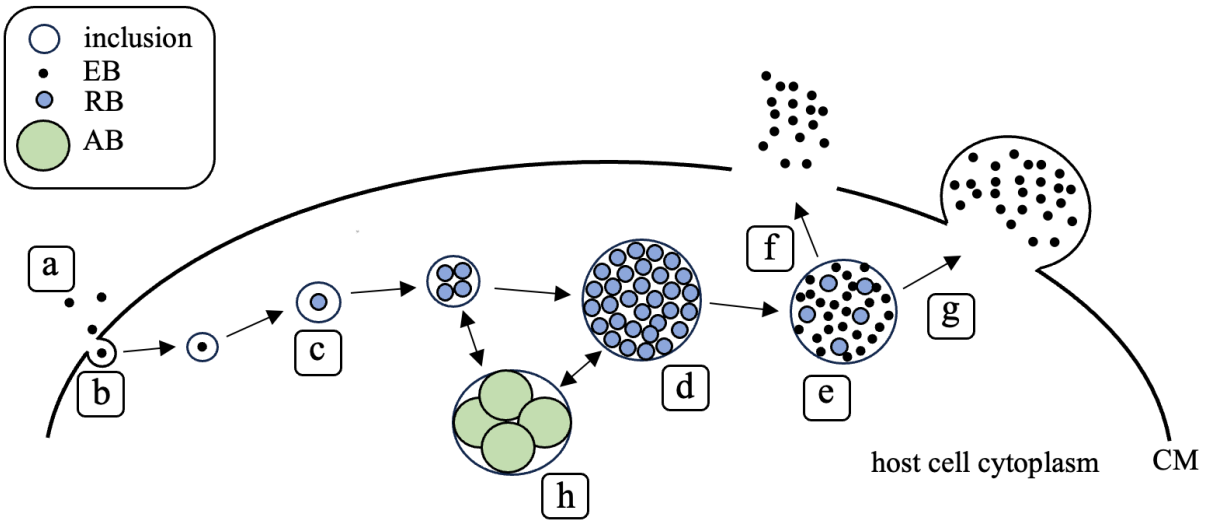

Figure 1: Chlamydial developmental cycle. The biphasic lifecycle begins extracellularly with the infectious elementary bodies (EB) (a) that are internalized by a eukaryotic host cell (b). Within an intracellular compartment termed inclusion, EBs undergo primary differentiation into non-infectious but replicative reticulate bodies (RBs) (c), that undergo cell division. Once the inclusion is filled up with RBs (d), asynchronous redifferentiation to EBs is commenced (e). EBs exit the host cell by either host cell lysis (f) or membrane extrusion (g). Upon adverse environmental conditions, the developmental cycle can be interrupted and chlamydial cells become aberrant bodies (ABs) (h) in a reversible persistent state. Upon removal of the stressor, the developmental cycle can be resumed. CM = cytoplasmic membrane.

1.3. The chlamydial cell envelope

All members of the *Chlamydiales* are diderm bacteria with an outer and an inner membrane. The outer membrane contains cysteine-rich major outer membrane protein (MOMP), forming approx. 60 % of chlamydial protein mass (Hepler *et al.*, 2018), and other cysteine-rich proteins like OmcA and OmcB. A genus-specific lipopolysaccharide (LPS) is embedded into the outer membrane. In free-living Gram-negative bacteria, LPS is one of the major constituents of the cell envelope. It consists of the membrane anchor lipid A, a conserved core polysaccharide and a species-specific polysaccharide O-antigen distal to the membrane anchor (Whitfield and Trent, 2014). In the bacterial cell, LPS serves as a permeability barrier for hydrophobic compounds that otherwise could damage the outer membrane or the entire cell and often is essential for bacterial proliferation (Nikaido, 2003; Zhang, Meredith and Kahne, 2013).

Chlamydial LPS does not contain an O-antigen and its core polysaccharide consists of three sugar moieties, making it the smallest known LPS structure (Kosma, 1999). The composition of chlamydial lipid A is altered compared to free-living Gram-negative bacteria and displays less immunogenic potential (Yang *et al.*, 2019). In Gram-negative bacteria, a PGN layer is sandwiched between the outer membrane and the cytoplasmic membrane and is also referred to as the cell wall. Also referred to as murein, it is a large macromolecule consisting of β-1,4-linked monosaccharide units of *N*-acetylmuramic acid and *N*-acetylglucosamine. Attached to the sugar moieties, peptide side chains enable crosslinking to strengthen the network (Schleifer and Kandler, 1972). PGN encases the bacterial cell and provides rigidity, shape, and osmotic protection. As a PGN sacculus similar to the one in free-living bacteria is missing in *Chlamydia*, proteins MOMP, OmcA and OmcB that are highly cross-linked via disulfide bridges in the outer layers of EBs were long regarded as the functional equivalent to a cell wall (Everett and Hatch, 1995). However, traces of muramic acid, the hallmark for PGN, were detected in *C. trachomatis* and *C. psittaci*, raising the question if *Chlamydia* does in fact contain PGN (Jenkin, 1960; Perkins and Allison, 1963). Due to its intracellular lifestyle and the protection that host cells provide against environmental influences, it was hypothesized that *Chlamydia* reduced its cell wall entirely over the course of coevolution with the host. However, more hints towards PGN in *Chlamydia* were discovered over the years, such as chlamydial persistence induced by β-lactam antibiotics (Matsumoto and Manire, 1970), that target the transpeptidase domain of penicillin binding proteins (PBPs) which execute the final steps of cell wall biosynthesis in free-living bacteria (Park and Strominger, 1957). Susceptibility towards cell wall-targeting antibiotics despite the absence of a cell wall was regarded the chlamydial anomaly. However, Barbour *et al*. confirmed three PBPs in *Chlamydia* and demonstrated penicillin binding (Barbour *et al.*, 1982). Over the years, not only pathways for the synthesis of cell wall metabolites, such as PGN-associated unusual amino acids *m*DAP and D-Glu, were elucidated in *Chlamydia* (McCoy *et al.*, 2006; De Benedetti *et al.*, 2014; Liechti, Singh, Patricia L. Rossi, *et al.*, 2018), but also a complete pathway with functional conservation for the synthesis of the PGN precursor lipid II (Stephens *et al.*, 1998a; Henrichfreise, Schiefer, Schneider, Nzukou, Poellinger, T. Hoffmann, *et al.*, 2009). Pilhofer *et al.* could demonstrate the existence of PGN sacculi in the *Chlamydia*-related bacterial species *Pr. amoebophila* by electron microscopy and labeling by D-amino acid probes that were incorporated into PGN by the organism (Pilhofer *et al.*, 2013). Despite efforts to reproduce the labeling technique introduced by Pilhofer *et al.*, PGN in *Chlamydia* was not identified until 2014, when Liechti *et al.* used diamino acid probes instead of single amino acids and subsequent click chemistry for visualization (Liechti *et al.*, 2014). Hereby, the existence of PGN in *Chlamydia* was proven. Two years later, PGN was shown to form a narrow ring-like structure at the septal region between dividing chlamydial cells instead of a complete sacculus (Liechti, Kuru, Packiam, Hsu, Tekkam, Hall, Jonathan T. Rittichier, *et al.*, 2016). Moreover, PGN in *Chlamydia* is only present in RBs, but not in EBs, where it was searched for a long time due to their rigidity (Chopra *et al.*, 1998). This finding was in line with observations of transcriptomic data, according to which genes involved in the lipid II biosynthesis

pathway were upregulated in the intracellular RBs, but not in EBs (Belland *et al.*, 2003). This discovery added to the successful isolation of PGN material from *Chlamydia*-related *Waddlia*, where not only a PGN ring structure with septal localization, but also a complete PGN sacculus is assumed (Frandi *et al.*, 2014; Jacquier *et al.*, 2015; Jacquier, Viollier and Greub, 2015). In contrast to free-living bacteria, PGN in *Chlamydia* does not serve as a structural component. The role of the polymer is further described in the following sections after an overview of biosynthetic processes in comparison to free-living bacteria is provided in the next subchapter.

1.3.1. Peptidoglycan biosynthesis

Catalytic steps of PGN biosynthesis in Gram-negative bacteria span three cellular compartments, beginning in the cytoplasm, proceeding to the inner membrane until finalizing in the periplasmic space, where precursors are incorporated into the existing PGN meshwork. The first cytoplasmic step is performed by UDP-N-acetylglucosamine enolpyruvyl transferase MurA, that adds enolpyruvate to N-acetylglucosamine (Heijenoort, 2001). UDP-N-acetylmuramic acid is produced by subsequent reduction by MurB (McCoy, Sandlin and Maurelli, 2003). The pentapeptide side chain is attached to the activated amino sugar by ligases MurC – MurF. In Gram-negative bacteria, the pentapeptide is usually formed by L-Ala-γ-D-Glu-*m*DAP-D-Ala-D-Ala (Schleifer and Kandler, 1972; Vollmer and Bertsche, 2008), but, when resolving the structure of chlamydial muropeptides, Packiam *et al.* also isolated a stem peptide variant with glycine at position 1 of the stem peptide (Packiam *et al.*, 2015). Hesse *et al.* could show that chlamydial MurC is fused to D-alanyl-D-alanine ligase Ddl and that the MurC domain lacks specificity towards alanine over glycine or serine (Hesse *et al.*, 2003; McCoy and Maurelli, 2005). The stem peptide in bacterial PGN contains non-proteinogenic amino acids that are highly specific for this structure and cannot be acquired from the host cell (Klöckner *et al.*, 2018). *Chlamydia* therefore need to employ own biosynthetic pathways for γ-D-Glu, D-Ala and *m*DAP. Liechti *et al.* showed that chlamydial DapF is a bifunctional enzyme, not only catalyzing the final biosynthetic step towards *m*DAP, predecessed by L,L-diaminopimelate aminotransferase DapL, but also performing the racemase reaction yielding γ-D-Glu from L-Glu (Liechti, Singh, Patricia L. Rossi, *et al.*, 2018; Singh, Slade, *et al.*, 2020). In free-living Gram-negative bacteria such as *E. coli*, these enzymatic steps are separate and carried out by DapF and MurI, respectively (Doublet *et al.*, 1993; Singh, Slade, *et al.*, 2020). In *Chlamydia*, D-Ala is synthesized by serine hydroxymethyltransferase GlyA, which was shown to have weak alanine-racemase activity, previously known only as a side activity of *E. coli* GlyA (Shostak and Schirch, 1988; De Benedetti *et al.*, 2014). D-Ala is especially important in bacterial PGN biosynthesis, as crosslinkage of the polymer is dependent on the dibasic characteristics of *m*DAP and D-Ala moieties. In PGN precursor biosynthesis, the final step of the stem peptide synthesis is carried out by MurF, ligating D-Ala-D-Ala to MurNAc-tripeptide and thereby yielding the last soluble PGN precursor UDP-MurNAc-pentapeptide (Patin *et al.*, 2012). Like mentioned before, the D-Ala-D-Ala dipeptide is obtained by the Ddl domain of the bifunctional MurC/Ddl enzyme complex in *Chlamydia*. In *E. coli*, instead, alanine racemases Alr and DadX isomerize L-alanine to D-alanine, which is subsequently fused by single

enzyme Ddl. Interestingly, homologs of *E. coli* genes encoding racemases Alr and DadX are conserved in *Waddlia*, *Parachlamydia* and *Protochlamydia* but not in *Chlamydia* genomes (Klöckner *et al.*, 2018).

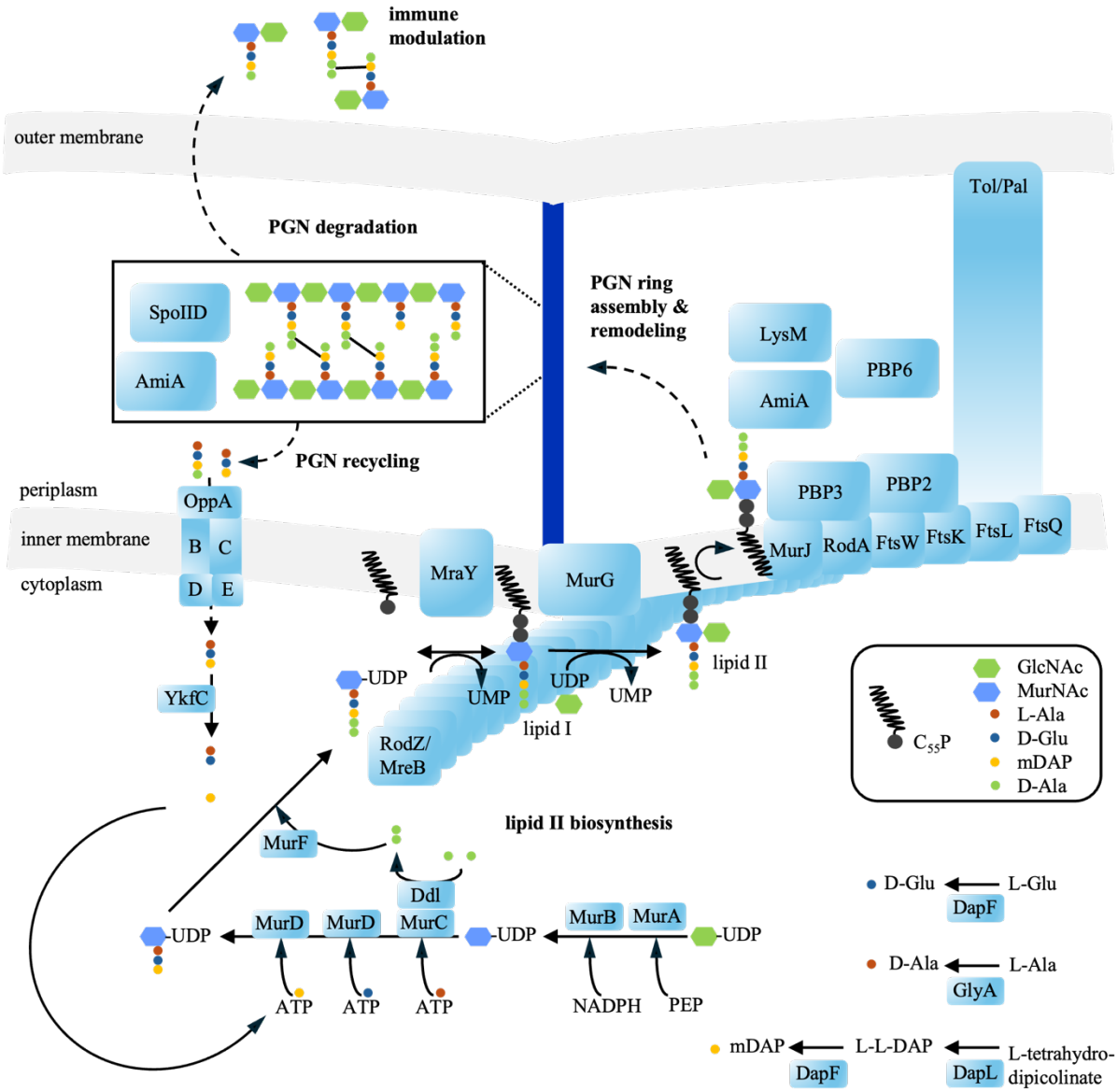

Figure 2: Proposed model of PGN biosynthesis, turnover and recycling in *Chlamydia*. A PGN sacculus like in free-living bacteria is missing in *Chlamydia*. Instead, a transient PGN ring (indicated in dark blue) is synthesized at the septum between dividing RBs and is required for cell division (indicated in dark blue). In the absence of FtsZ, the multi-enzyme machinery of PGN biosynthesis and cell division is coordinated by MreB and RodZ. In the cytoplasm, precursor molecule UDP-MurNAc-pentapeptide is synthesized by MurA-MurF. The stem peptide contains D-amino acids D-Glu and D-Ala, which are synthesized by DapF and GlyA from their L-enantiomers, respectively (De Benedetti *et al.*, 2014; Liechti, Singh, Patricia L Rossi, *et al.*, 2018). Unusual dibasic amino acid mDAP is synthesized from L-tetrahydrodipicolinate by DapL and DapF (Singh, Slade, *et al.*, 2020). UDP-MurNAc-pentapeptide is fused to membrane anchor bactoprenol ($C_{55}P$) by membrane enzyme MraY yielding lipid I. Lipid II is obtained by N-acetylglucosamine addition to lipid I by MurG (Henrichfreise, Schiefer, Schneider,

Nzukou, Poellinger, T.-J. Hoffmann, *et al.*, 2009). Likely, lipid II is then translocated across the cytoplasmic membrane by MurJ (Sham *et al.*, 2014). In the periplasm, the precursor is incorporated by PBP-SEDS transpeptidase-glycosyltransferase pairs. The divisome components FtsK, FtsQ, FtsL, FtsW and the Tol-Pal-complex, connecting membrane compartments in free-living bacteria and mediating invagination during cell division, have been conserved in Chlamydia (Ouellette, Lee and Cox, 2020). PGN remodeling is achieved by DD-carboxypeptidase activity conferred by monofunctional PBP6, AmiA, which has additional D-carboxypeptidase activity in C. pneumoniae and LysM protein Cpn0902 (Klöckner *et al.*, 2014; Otten *et al.*, 2015). Degradation of PGN is achieved by amidase activity of AmiA and probably of SpoIID homolog activity, that acts as a lytic transglycosylase in *Waddlia* and is conserved in *Chlamydia* (Jacquier *et al.*, 2019). PGN fragments can be immunostimulatory upon release. Oligopeptides can be reimported into the cytoplasm through transporter OppABCDF (Singh, Liechti, *et al.*, 2020) and endopeptidase YkfC was shown to cleave γ-D-Glu-mDAP bonds, making stem peptide components available for new biosynthesis of PGN precursors (Reuter *et al.*, 2023).

At the inner leaflet of the cytoplasmic membrane, UDP-MurNAc-pentapeptide is linked to membrane carrier bactoprenol (C_{55}-P) by activity of membrane protein MraY, producing the first membrane-bound precursor lipid I. Chlamydial transferase MurG adds aminosugar N-acetylglucosamine to lipid I, forming lipid II (Henrichfreise, *et al.*, 2009). To continue PGN building, lipid II must be flipped over the membrane into the periplasmic space, which is likely achieved by action of MurJ (Sham *et al.*, 2014). The bactoprenol carrier is recycled by the activity of pyrophosphorylases in free-living bacteria, all of which have not been retained in *Chlamydia*. In *Waddlia*, *Protochlamydia* and *Parachlamydia*, only UppP is involved in membrane carrier recycling, whereas free-living *E. coli* additionally encodes YeiU, YbjG and PgpB (Tatar *et al.*, 2007; Klöckner *et al.*, 2018). In the periplasm, precursor lipid II is incorporated into the existing PGN meshwork by PBPs. In *Chlamydia*, three PBPs have been retained: PBP2 and PBP3, predicted monofunctional transpeptidases (class B PBPs), and low molecular weight PBP6 with DD-carboxypeptidase activity (Otten *et al.*, 2015). Transpeptidases perform crosslinking of cell wall building blocks by connecting the dibasic *m*DAP moiety at position three of the stem peptide to D-Ala-D-Ala. PBP6 is involved in this process by cleaving of terminal D-Ala moieties from the stem peptide, thereby regulating the D-Ala-D-Ala availability for crosslinking. Unlike *E. coli*, *Chlamydia* do not encode for a bifunctional PBP, which would also confer glycosyltransferase activity. Therefore, transglycosylation of the aminosugar backbone of PGN was prone to speculation. However, *Chlamydia* retained homologs of the SEDS (shape, elongation, division, sporulation) proteins, that were proposed to act as novel glycosyltransferases together with their cognate class A PBP as a glycosyltransferase-transpeptidase pair involved in PGN polymerization (Henrichfreise, Brunke and Viollier, 2016; Meeske *et al.*, 2016). In free-living bacteria, FtsW in combination with PBP3, both of which proteins are conserved in *Chlamydia*, was able to perform PGN polymerization (Taguchi *et al.*, 2019). Another suggested glycosyltransferase-transpeptidase pair conserved in chlamydial proteomes is RodA-PBP2. Liechti *et al*. suggest that both SEDS-class B PBP pairs carry out distinct roles within the PGN

machinery in *Chlamydia*: both RodA-PBP2 and FtsW-PBP3 are needed for the PGN ring to expand and contract during the cell division process described in a later section, respectively (Liechti, 2021). The integral importance PGN plays in chlamydial cell division is further described in the next chapter.

1.4. Cell division

Cell division of Gram-negative bacteria involves multiple processes that are tightly interlinked. Among them, PGN synthesis is one of the most important. Gram-negative model organism *E. coli* divides by binary fission and employs a constrictive mechanism that involves synthesis of a PGN septum at mid-cell, its splitting and accompanying invagination of the cytoplasmic and outer membrane at the same time (Egan and Vollmer, 2013). The PGN septum is shared between the two nascent daughter cells until cell separation and represents one of the most sensitive areas in bacterial cell division. Uncontrolled cleavage of the septum during division could impair the integrity of PGN sacculi and potentially could entail lethal consequences on one or both nascent daughter cells. Prior to cell division, some bacteria like e.g. *Caulobacter crescentus* and to a limited extend *E. coli,* undergo a phase of preseptal elongation, in which cells lengthen along the longitudinal axis (de Pedro *et al.*, 1997; Aaron *et al.*, 2007). This process aids in the maintenance of equal cell sizes of daughter cells after cytokinesis. Cell division is initiated by assembly of the cell division complex at mid cell, which synthesizes and ultimately also cleaves septal PGN. This complex is termed the divisome. The assembly of the divisome components can be subdivided into an early and a late phase (Aarsman *et al.*, 2005; Egan and Vollmer, 2013). The early phase often coincides with preseptal elongation and involves the recruitment of proteins FtsZ, FtsA, ZipA, ZapA, ZapC, ZapD, FtsEX and others. Central to the divisome is tubulin ortholog FtsZ. The protein polymerizes GTP-dependently and forms filaments that move around the prospective division site below the cytoplasmic membrane. This structure is also referred to as the Z-ring (Li *et al.*, 2007; Erickson, Anderson and Osawa, 2010). The location of the Z-ring determines the area of septum formation and cell division and, for the cell to undergo binary fission, has to be placed at mid cell (Egan and Vollmer, 2013). Various mechanisms ensure the correct localization of the Z-ring. FtsZ recruits and regulates divisome components and therefore its location needs to be coordinated with chromosome replication and separation. Nucleoid occlusion ensures that septum formation does not interfere with the bacterial chromosome, which could lead to breakage and be lethal to the bacterial cell (Bernhardt and de Boer, 2005). The Min system averts the formation of division septa near the cell poles, which could lead to the formation of small cells without any nucleoid. MinE drives the oscillation of MinD and MinC between cell poles, and FtsZ polymerization occurs at midcell, where relative MinC and MinD concentrations are lowest (Raskin and de Boer, 1999; Hale, 2001). The movement of the Z-ring is referred to as treadmilling and its motion aids to distribute divisome components across the cell perimeter (Bisson-Filho *et al.*, 2017). Interestingly, divisome component FtsW exists in a motile form associated to FtsZ and, independently, as a stationary form in *E. coli* (Yang *et al.*, 2021). The early divisome proteins interdependently recruit other proteins involved in PGN synthesis and remodeling, before the late stage of divisome assembly begins immediately before constriction (Aarsman *et al.*,

2005). Among the late divisome proteins are ATPase FtsK, which is involved in bacterial chromosome segregation (Aussel *et al.*, 2002; Di Lallo *et al.*, 2003; Grenga *et al.*, 2008), FtsQ, FtsL, FtsB, FtsW, PBP3, PBP1B, FtsN and others (Aarsman *et al.*, 2005). Constriction of the septal region does not only involve PGN, but also the outer and cytoplasmic membranes of Gram-negative bacteria. In *E. coli*, the outer membrane is connected to the PGN layer by Braun's lipoprotein Lpp (Hantke and Braun, 1973). Further, the Tol-Pal-complex is involved in simultaneous constrictions of all compartments. Cells with inactivated Tol-Pal proteins showed cell division defects, indicating a central role of this complex in bacterial cell division (Bernadac *et al.*, 1998; Cascales *et al.*, 2002). TolQ, TolR and TolA are integral membrane proteins within the cytoplasmic membrane and act as a motor complex. TolB is a soluble periplasmic protein and Pal localizes in the outer membrane at midcell during cell division. Through interaction of these proteins, all compartments of the bacterial cell are connected to each other (Gerding *et al.*, 2007). Inner membrane invagination is thought to be a result of septal PGN biosynthesis applying an inward-pushing force, likely pulling the complex inwards as well, and a self-constrictive mechanism of FtsZ (Xiao and Goley, 2016; Yakhnina and Bernhardt, 2020). In *Chlamydia*, PGN biosynthesis does not lead to septum formation during cell division as observed in free-living bacteria like *E. coli*, that are encased by a PGN sacculus as a major osmoprotective element. Instead, a PGN ring structure is synthesized in *Chlamydia* solely for cell division purposes and is degraded immediately afterwards (Liechti, Kuru, Packiam, Hsu, Tekkam, Hall, Jonathan T Rittichier, *et al.*, 2016). Chlamydial PGN synthesis occurs only at the future division site by the formation of a discrete and dense PGN patch, that is suggested to form a disc in the process. Due to outward degradation, a ring structure emerges and is subject to remodeling and ultimately constriction, as daughter cells separate from each other (Liechti, 2021). This process, which is presented as a sketch in Figure 3, suggests an exact spatiotemporal organization of PGN synthesis in these bacteria, that is inevitable for cell division (Henrichfreise, Schiefer, Schneider, Nzukou, Poellinger, T.-J. Hoffmann, *et al.*, 2009).

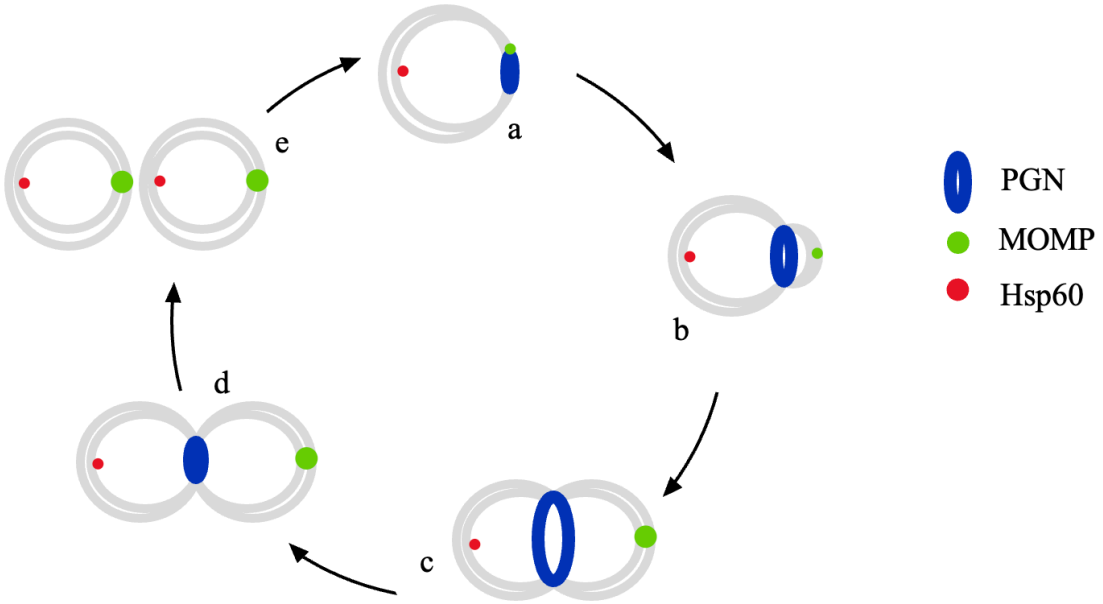

Figure 3: Model of chlamydial cell division. Chlamydial RBs divide by a budding mechanism. (a) At the prospective budding site, a PGN disc is synthesized near the MOMP-positive pole of the cell. (b) The MOMP-positive pole expands and forms the nascent bud, while through PGN remodeling, the PGN disc is rendered into a ring structure. (c) Nascent daughter cells grow to approx. the same size as the mother cell and the PGN ring expands. (d) Constriction of the ring is achieved through PGN degradation and is pursued until daughter cells are separated from each other. (e) Daughter cells are devoid of PGN structures, and, in both daughter cells, either a new Hsp60- or MOMP-rich pole is formed.

Astoundingly, the central divisome organizer FtsZ is missing in *Chlamydia* and *Chlamydia*-related bacteria (Stephens *et al.*, 1998b). Instead, cell division in these organisms is organized by the actin superfamily member MreB. The protein is highly prevalent in rods, spirillae and vibrio forms, as it governs PGN synthesis associated with elongation and incorporates PGN precursors into the existing network during longitudinal growth (Carballido-López, 2006). If the protein is deleted, elongated cells become round (Barton, Grinnell and Morgenstein, 2021). *Chlamydia,* however, despite having spherical shapes, employ MreB for the functional organization of PGN synthesis and the recruitment of divisome proteins. In analogy to its *B. subtilis* homolog, chlamydial MreB was shown to polymerize and to interact with key PGN synthesis enzymes MurF, MurG and MraY *in vitro* (Gaballah *et al.*, 2011). A ring-shape localization of MreB in *Chlamydia* could be demonstrated by superresolution microscopy (Billaudeau *et al.*, 2019). RodZ, which serves as a transmembrane anchor for MreB filaments in *E. coli* (Morgenstein *et al.*, 2015), was also retained in *Chlamydia* and was shown to interact with MreB (Kemege *et al.*, 2015; Lee, Cox and Ouellette, 2020). Ranjit *et al.* demonstrated that chlamydial MreB, with cognate RodZ, allows division in FtsZ-less *E. coli* cells, suggesting a central role for this enzyme pair in *Chlamydia* comparable to central organizer FtsZ in free-living bacteria (Ranjit, Liechti and Maurelli, 2020). In *Waddlia*, RodZ was shown to localize at the division site even earlier than MreB, suggesting a role in MreB recruitment prior to division (Jacquier *et al.*, 2014). MreB-dependent recruitment of cell division proteins to the future septum can also be subdivided into an early and late phase. While early cell division

proteins, like e.g. FtsA, have not always been retained in chlamydial proteomes, the late phase is comparable to free-living bacteria (Ouellette, Lee and Cox, 2020). Recently, MreB localization to the septal region was found to be dependent on the synthesis of cardiolipin, which is highly polarized in chlamydial cells and accumulates at the future division site (Ouellette *et al.*, 2022). Further polarization characteristics of chlamydial cells became evident when the mode of cell separation of chlamydial cells was discussed. Binary fission is not the only mode of cell division among bacteria: alternatives include endospore formation, multiple fission after filament formation and budding processes (Angert, 2005). While binary fission is the established model in case of *E. coli*, the mode of chlamydial cell division was not fully understood for a long time. Images obtained from chlamydial cell division events suggested a binary fission model as well and Lee *et al.* presented a model according to which RBs divide approx. six times by binary fission and thereby reduce cell size at each division. This process was suggested to precede redifferentiation to infectious EBs (Lee *et al.*, 2018). However, Abdelrahman *et al*. observed that MOMP and Hsp60, a cytoplasmic chaperone heat shock protein, localized discretely at opposing cell poles and that cell division did not occur in cells that were not positive for both proteins (Abdelrahman *et al.*, 2016). Localizations of MOMP and Hsp60 are also indicated in Figure 3. With observations of the MOMP-positive pole expanding asymmetrically and subsequent septum and PGN ring formation between the emerging daughter cell and the mother cell, chlamydial cell division was found to occur via a budding mechanism (Abdelrahman *et al.*, 2016). After cytokinesis, a new Hsp60 pole emerges in the daughter cell and a new MOMP-pole forms in the cell that served as the mother cell. Though earlier experiments hinted towards the budding theory, it was never pursued and, as daughter cells grow to approx. the same size as the mother cells prior to cell division, a binary fission model was considered plausible. This process of cell division is repeated, until all RBs redifferentiate to EBs after multiple rounds of cell division. During the process itself, PGN is subject to constant turnover processes, that involve remodeling and recycling, that are further described in the next chapter.

1.5. Peptidoglycan turnover – remodeling and recycling

Over the course of cell division, PGN is subjected to remodeling processes in both free-living and intracellular bacteria like *Chlamydia*, even if they do not synthesize a classical sacculus. In free-living bacteria, these processes include longitudinal elongation of the PGN sacculus prior to septation, sacculus growth, formation and ultimately degradation of the septum (Alvarez *et al.*, 2014). Chlamydial PGN requires continuous remodeling during the different steps of PGN ring formation, outward degradation, constriction, and final degradation after completed cell division (Jacquier, Viollier and Greub, 2015; Liechti, 2021). A second important process dealing with PGN turnover is recycling of PGN fragments that reenter a new cycle of biosynthesis after degradation process. Recycling of PGN fragments is favorable in two ways: reducing the metabolic burden of *de novo* PGN biosynthesis, reusing PGN fragments is an energy-efficient strategy (Singh, Liechti, *et al.*, 2020; Reuter *et al.*, 2023). In growth experiments with model organism *E. coli*, Goodell and Schwartz could show that the organism releases only 6-8 % of its muropeptides into the surrounding medium (Goodell and Schwarz, 1985). *E. coli*

processes these fragments within a multi-enzyme machinery and degradation products enter a new biosynthetic cycle. Hydrolases are key enzymes for PGN remodeling and recycling processes and include carboxypeptidases, lytic transglycosylases and amidases. Carboxypeptidases play an important role during PGN remodeling, as they control amounts of donor and acceptor peptides for transpeptidation. As mentioned earlier, DD-carboxypeptidases trim pentapeptides and yield tetrapeptide stems. Similarly, LD-carboxypeptidases yield tripeptides, while DL-carboxypeptidases yield dipeptide stems (Egan and Vollmer, 2013). PBP5, a monofunctional carboxypeptidase in *E. coli,* is not only involved in remodeling processes, but also influences cell division by being involved in the correct positioning of the Z-ring (Potluri, de Pedro and Young, 2012). In *E. coli,* activity of lytic transglycosylases such as SltY, MltA and MltB yields GlcNAc-anhydro-MurNAc peptides (Ehlert, Höitje and Templin, 1995; Lommatzsch *et al.*, 1997; Park and Uehara, 2008), which are transported into the cytoplasm by permease AmpG (Cheng and Park, 2002). All in all, *E. coli* encodes for seven lytic transglycosylases that have different specificities in their action on PGN (Egan and Vollmer, 2013). Similarly to lytic transglycosylase products, GlcNAc-anhydro-MurNAc dissacharides resulting from outer membrane anhMurNAc-L-Ala amidase AmiD (Uehara and James T Park, 2007) are ferried across the membrane by AmpG. Stem peptides resulting from PGN hydrolysis reenter the cytoplasmic space through MppA and peptide transporter OppABCDF (Ames, Mimura and Shyamala, 1990; Park *et al.*, 1998). Recently, also CadB was identified as a permease facilitating the import of muropeptides into the cytoplasm (Simpson *et al.*, 2024). In the cytoplasm, GlcNAc-anh-MurNAc-peptides are processed by cytoplasmic amidase AmpD, yielding the free disaccharide GlcNAc-anhMurNAc and the peptide stem (Höltje *et al.*, 1994). The disaccharide is cleaved by NagZ, resulting in GlcNAc and anhMurNAc, which are, then, phosphorylated by kinases NagK and AnmK, respectively, producing GlcNAc-6-P and MurNAc-6-P, which is finally transformed to GlcNAc-6P by etherase MurQ (Uehara and Park, 2004; Jaeger, Arsic and Mayer, 2005; Uehara *et al.*, 2005, 2006). At this point, the stem peptide, usually consisting of four amino acids (L-Ala-D-Glu-*m*DAP-D-Ala), is further processed by LdcA, yielding free D-Ala and a tripeptide (Ursinus, Steinhaus and Höltje, 1992). Tripeptides enter *de novo* PGN biosynthesis, being attached to UDP-MurNAc by ligase MpI or are subjected to further degradation by MpaA. MpaA action yields the dipeptide L-Ala- D-Glu (Mengin-Lecreulx, van Heijenoort and Park, 1996; Hervé *et al.*, 2007), which is epimerized to L-Ala-L-Glu by YcjG. These dipeptides can be degraded by PepD, resulting in the single amino acids L-Ala and D-Glu, which can be adjoined into a new cycle of PGN biosynthesis (Schroeder *et al.*, 1994; Schmidt, Hubbard and Gerlt, 2001). Recycling is also favorable in light of immune modulation. Since PGN fragments are also recognized as pathogen-associated molecular patterns (PAMPs), especially intracellular bacteria like *Chlamydia* are constantly at risk of being detected and eliminated by the host's immune system. Innate immunity factors NOD1 and NOD2 detect PGN segments and trigger immune response. Besides other mechanisms of immune evasion and modulation that can be triggered by the type III secretion system (T3SS), recycling of PGN fragments is another efficient strategy. Avoiding shed of PGN fragments into the surroundings enables

the pathogen to remain unnoticed within its intracellular niche. Like in free-living bacteria, chlamydial genomes encode different enzymes enabling the organisms to efficiently remodel and then reuse PGN fragments. SpoIID in *Chlamydia*-related bacterium *W. chondrophila* was shown to act as a lytic transglycosylase on PGN and as a muramidase on denuded PGN strands *in vitro*. Homologs of this protein are found in *C. trachomatis* and *C. pneumoniae* proteomes (Jacquier *et al.*, 2019). Chlamydial PBPs and *C. pneumoniae* LysM protein Cpn0902 act as DD-carboxypeptidases, releasing terminal D-Ala moieties from the stem peptides (Klöckner *et al.*, 2014; Otten *et al.*, 2015). PGN-derived peptides are suggested to be transported into the cytoplasm by transporter OppABCDF, which is conserved in *Chlamydia* and identified in *C. trachomatis,* to enable recycling processes (Singh, Liechti, *et al.*, 2020). Likely, recycling of PGN-derived fragments is important for the organism to maintain a cycle of PGN ring synthesis and cell division. Moreover, reusing PGN is an energy-efficient strategy and might contribute to immune evasion. Despite apparent importance of PGN recycling, almost nothing is known about this process in *Chlamydia*, as the organism lacks all enzymes known to catalyze the process in model organism *E. coli*. Reuter *et al.* identified an NlpC/P60 enzyme to catalyze a critical step in degradation of PGN ring-derived peptides in *C. trachomatis* and the data indicate that the enzyme not only recycles energy-intense components that would otherwise have to be synthesized *de novo*, but also breaks down the minimal recognition motif of innate immune factor NOD1 (Reuter *et al.*, 2023). Stem peptides are released from PGN by the activity of cell division amidase AmiA in *Chlamydia*. Amidases represent an important enzyme class in bacterial cell division and are further introduced in the next chapter.

1.5.1. AmiA as a part of chlamydial PGN turnover and cell division machinery

PGN hydrolases cleave bonds within either polymeric PGN or soluble fragments and precursor molecules (Shockman and Höltje, 1994; Shockman *et al.*, 1996). Being involved in regulation of cell wall growth and enlargement, PGN turnover and recycling, sporulation and germination processes and cell separation, hydrolases represent a universally important enzymatic class in bacteria (Vollmer *et al.*, 2008). Besides carboxypeptidases and lytic transglycosylases, *N*-acetylmuramyl-L-alanine amidases also referred to as PGN amidases are part of this class (Höltje, 1995). PGN amidases cleave the amide bond between the muramic acid unit and the first residue of the stem peptide, thereby cleaving off the peptide side chain. Denuded glycans and peptide stems are subjected to turnover and recycling processes as described in the previous chapter. Model organism *E. coli* encodes five amidases: outer membrane amidase AmiD, cytoplasmic amidase AmpG and three periplasmic amidases AmiA, AmiB and AmiC (Jacobs *et al.*, 1995; Heidrich, Templin, Ursinus, Merdanovic, Berger, Schwarz, De Pedro and J. Höltje, 2001; Uehara and James T. Park, 2007). The three latter enzymes are zinc-dependent metalloenzymes that are transported to the periplasm by signal peptides: while AmiA and AmiC are exported tat-dependently, AmiB is exported via the sec pathway (Bernhardt and De Boer, 2003). During cell division, amidases cleave septal PGN that is initially shared between daughter cells. In Gram-negative bacteria, where septum formation, membrane invagination and splitting of the septum occur simultaneously, the

process of PGN cleavage must be tightly coordinated to avoid lethal consequences. Though the function of the three periplasmic amidases in *E. coli* seems to be redundant, deletions produce different phenotypes: upon knockout of AmiC, 20 – 30 % of *E. coli* cells are present in chains of various lengths that are not able to cleave septal PGN and therefore do not separate. Concomitantly, these cells are more sensible towards detergents and antibiotics, indicating permeability barrier impairments (Heidrich, Templin, Ursinus, Merdanovic, Berger, Schwarz, De Pedro and J. Höltje, 2001). When AmiA is deleted, the chain-forming phenotype affects 5 – 10 % of cells, while AmiB deletion does not affect cell division (Heidrich, Templin, Ursinus, Merdanovic, Berger, Schwarz, De Pedro and J. Höltje, 2001; Heidrich *et al.*, 2002). AmiA is the smallest of the three periplasmic amidases in *E. coli*, comprising just one single globular amidase domain of approx. 28 kDa with six β-sheets and six α-helices (Cook *et al.*, 2023). Besides this amidase domain, AmiB and AmiC have an additional N-terminal domain that is likely important for septal recruitment and anchoring of the enzymes to the septal ring (de Souza *et al.*, 2008; Rocaboy *et al.*, 2013). Cell division amidases are subject to a carefully controlled mechanism to prevent unintended lysis. In their resting state, amidases are autoinhibited by a blocking helix structure that occludes the active site and require activation by proteins with LytM domains (Bernhardt and De Boer, 2004; Uehara, Dinh and Bernhardt, 2009; Uehara *et al.*, 2010). This mechanism of regulation is probably conserved and has been shown also for amidase AmiB in *V. cholerae* (Yang *et al.*, 2012). AmiA and AmiB require periplasmic EnvC and AmiC is activated by outer membrane lipoprotein NlpD (Uehara *et al.*, 2010). Mutants in which NlpD and EnvC are deleted displayed the same chain-forming phenotype observed in amidase-deficient mutants, indicating central roles for these enzymes in cell division (Uehara, Dinh and Bernhardt, 2009). In a crystal structure of *E. coli* AmiA obtained by Cook *et al.*, a conserved glutamate residue within the blocking helix was shown to function as the latch holding the inhibitory domain in place (Cook *et al.*, 2023). Activation of amidases is suggested to be part of a larger enzymatic cascade, involving not only LytM factors but also divisome protein FtsEX (Cook *et al.*, 2023). FtsEX is an ABC transporter-like complex with ATPase domain FtsE on the cytoplasmic site and transmembrane domain-containing FtsX reaching inside the periplasm (Yang *et al.*, 2011). LytM factors themselves are also suggested to be autoinhibited by a regulatory helix, occluding the LytM domain vicinity (Cook *et al.*, 2020). Through cytoplasmic ATP binding of FtsE and interaction of EnvC with the periplasmic loop of FtsX, a conformational change is suggested to occur in EnvC, retrieving its autoinhibitory domain from the LytM domain of the cognate amidase activator protein (Cook *et al.*, 2023). Besides the blocking helix occluding the active site, cell division amidases are proposed to interact with the LytM domain via an interaction helix. The binding of the interaction helix to the LytM domain of EnvC is probably mediated by hydrophobic interaction and is suggested to trigger a conformational change, which in turn withdraws the blocking helix from the amidase active site, activating the enzyme (Cook *et al.*, 2023). The system is reset by ATP hydrolysis in the cytoplasm, after which the enzymes switch to their resting states until further activation (Yang *et al.*, 2011). Sequential recruitment of LytM factors and cell division amidases to the forming septum ensures a coordinated way

of PGN cleavage during cell division (Peters, Dinh and Bernhardt, 2011). *In vitro*, the autoinhibited state results in very low basal activity of *E. coli* cell division amidases on PGN substrates (Lupoli *et al.*, 2009). Upon mutagenization of residues in the blocking helix, activity could be resumed (Uehara *et al.*, 2010; Yang *et al.*, 2012). In the active state, two histidine residues (H65, H133) and one glutamic acid residue (E80) are proposed to coordinate a zinc atom in the active center (Lupoli *et al.*, 2009). In the resting state, two additional residues, N135 and E167, are involved in coordination, while the latter residue represents the proposed latch connecting the blocking helix to the active center (Cook *et al.*, 2023). An additional glutamate residue (E242) is proposed to act as a base catalyst (Lupoli *et al.*, 2009). This active site domain architecture is shared between periplasmic cell division amidases in *E. coli.* *Chlamydia* do not synthesize a PGN septum like free-living bacteria and, thus, do not require septal splitting at the end of cell division. Instead, the transient PGN ring emerging at the division plane during chlamydial cell division requires remodeling to grow and to constrict. Instead of three periplasmic amidases of *E. coli*, just an AmiA homolog has been retained in *Chlamydia* and *Chlamydia*-related bacteria. Active site architecture is conserved compared to the active site in *E. coli*, with a zinc atom being coordinated by two histidine and two glutamate residues. In *C. trachomatis* AmiA, hereinafter referred to as AmiA_Ct, these residues are H67, H136, E80 and E205, which, upon sequence comparison, align with the corresponding residues in the *E. coli* AmiA active site. However, a major difference between amidases of free-living bacteria and chlamydial AmiA seems to be that the latter is active by default. Neither a regulatory helix, nor an interaction helix, as described by Cook *et al.* for *E. coli* AmiA, is present in the *C. pneumoniae* homolog, leaving the enzyme's active center constantly exposed (Klöckner *et al.*, 2014). Moreover, activator proteins EnvC and NlpD are not encoded in chlamydial genomes, though LysM protein Cpn0902 from *C. pneumoniae* was misannotated as a NlpD homolog (Klöckner *et al.*, 2014). Thus, a regulatory mechanism controlling the activity of chlamydial AmiA is not known to date. This raises the question on how *Chlamydia* maintains PGN ring integrity during cell division processes. AmiA from *C. pneumoniae* (AmiA_Cp) has been extensively characterized by Klöckner *et al.*, who could show that AmiA_Cp cleaves PGN and precursor lipid II *in vitro*, whereas the homologous *E. coli* enzyme was suggested to require substrates containing at least a tetrasaccharide backbone to be active (Lupoli *et al.*, 2009; Klöckner *et al.*, 2014). The cell chain phenotype of an amidase deficient *E. coli* mutant could be rescued upon heterologous expression of *amiA* from *C. pneumoniae* and producer strains were lysed by AmiA activity upon overproduction of the protein. Interestingly, AmiA_Cp was shown not only to act as a PGN amidase, but to be a bifunctional enzyme comprising an additional carboxypeptidase activity. The latter was proven to be penicillin-sensitive, adding this function of AmiA_Cp to the list of penicillin targets in *Chlamydia* (Klöckner *et al.*, 2014). Besides AmiA_Cp, the previously misannotated Cpn0902 and PBP6 also exert carboxypeptidase activity in *C. pneumoniae*. As AmiA is the only amidase that has been retained in *Chlamydia*, the enzyme is thought to play a central role in the tightly interlinked processes of PGN turnover, recycling, cell division and PGN remodeling.

1.6. Aims of this work

This work mainly aimed to provide novel insights on the role that chlamydial amidase AmiA plays in the tightly connected interplay of PGN synthesis, cell division, PGN turnover and recycling in the human pathogen *C. trachomatis*. AmiA is the only cell division amidase that has been retained in the genetically reduced *Chlamydia* and the first aim was to characterize AmiA in *C. trachomatis*. Overexpression experiments in heterologous host systems aimed to investigate whether the chlamydial enzyme has conserved function compared to cell division amidases of model organism *E. coli*. *In vitro* experiments with the purified enzyme were performed to evaluate substrate spectra and elucidate enzymatic activity of *C. trachomatis* AmiA. A comparative approach with the previously characterized AmiA homolog from *C. pneumoniae* intended to test for possible differences between these two closely related amidases, that nevertheless show remarkable differences in amino acid sequences. To analyze the further turnover of reaction products derived from amidase AmiA activity, this work contributed to specify the substrate spectrum of chlamydial recycling enzyme YkfC. To learn more about the active site and enzymatic function of *C. trachomatis* AmiA, a subset of putative inhibitors was investigated within an established *in vitro* assay platform.

Recent advances in the genetic manipulation of *Chlamydia* enabled the investigation of genetic knockdowns and overexpression of genes encoding enzymes within the cell division and PGN turnover machinery and the direct assessment of the effects of these manipulations using fluorescence microscopy. To yield novel information about the role AmiA plays in chlamydial life cycle progression and cell division, CRISPRi technology was employed to investigate the cellular effects of an *amiA* knockdown in active chlamydial infections. Leveraging the genetic manipulation assay platform employed for assessing the effects of *amiA* knockdown, the method was also used to elucidate effects of knockdown and overexpression of genes encoding RodA and NamZ, proteins that are likely to play important roles in chlamydial cell division and PGN recycling.

Furthermore, the establishment of a novel persistence model was pursued. Besides exposure to antibiotics like β-lactams or host cell cytokines, that are known to induce persistence in *Chlamydia*, nutrient starvation trigger chlamydial cells to pause their developmental cycle to outlast environmentally unfavorable conditions. To gain deeper insight into nutrient starvation-induced persistence mechanisms in Chlamydia, compounds sequestering essential micronutrients like iron were analyzed. To compare effects of nutrient starvation in different backgrounds and to identify potential synergies, active chlamydial infections and already established antibiotic-induced persistent infections were treated with these compounds and effects were assessed using a tissue culture-based infection model and a microscopy-based evaluation method.

2. Material & Methods

2.1. *In silico* methods, software and online tools

Software, online tools and applications used in this work are listed in table 1.

Table 1: Software and online tools.

Tool	Application	Weblink	Reference(s)/Source
Basic Local Alignment Search Tool (BLAST)	Identification of regions of similarity of nucleotide and amino acid sequences	blast.ncbi.nlm.nih.gov/Blast.cgi	(Altschul *et al.*, 1990)
CellProfiler	Quantitative analysis of microscopy data	-	(Carpenter *et al.*, 2006)
Chimera (USFC Chimera)	Visualization and analysis of molecular structures	-	(Pettersen *et al.*, 2004)
Clustal Omega	Sequence alignments	www.ebi.ac.uk/Tools/msa/clustalo/	(Goujon *et al.*, 2010; Sievers *et al.*, 2011)
Expasy ProtParam	Computation of physical and chemical parameters of a protein	web.expasy.org/protparam/	(Wilkins *et al.*, 1999)
GraphPad Prism 10	Data visualization and statistical analysis	-	GraphPad Software, LLC (USA)
i-control™	Operation of Tecan Infinite® 200	-	Tecan Group AG (Männedorf, Switzerland)
ImageLab	Photography of SDS and Agarose gels, band quantification	-	Bio-Rad (Hercules, CA, USA)
In-Fusion Cloning Tool	Primer Design and *in silico* Cloning for In-Fusion Cloning	www.takarabio.com/learning-centers/cloning/primer-design-and-other-tools	Takara Bio (Kusatsu, Japan)
InterPro	Functional *in silico* analysis of proteins	www.ebi.ac.uk/interpro/	(Paysan-Lafosse *et al.*, 2023)

KEGG	Database of genome and proteome sequences	www.genome.jp/kegg/	(Kanehisa and Goto, 2000)
Mendeley	Reference Manager	www.mendeley.com/reference-management/mendeley-cite	Mendeley Ltd.
Phyre^2	Homology-based 3D *in silico* modeling of proteins	www.sbg.bio.ic.ac.uk/~phyre2/html/page.cgi?id=index	(Kelley *et al.*, 2015)
PsiPred	Prediction of protein secondary structures	bioinf.cs.ucl.ac.uk/psipred/	(McGuffin, Bryson and Jones, 2000)
QuantStudio™ Design & Analysis Software	Operation system of QuantStudio 3	-	Thermo Fisher Scientific (Waltham, MA, USA)
QuikChange Primer Design Tool	Primer design for site-directed mutagenesis	www.agilent.com/store/primerDesignProgram.jsp	Agilent (Santa Clara, CA, USA)
SnapGene® 6.0.2.	Visualization and in silico editing of genetic constructs	-	GSL Biotech LLC (San Diego, CA, USA)
SparkControl (Magellan V 6.5)	Operation of Tecan Spark	-	Tecan Group AG (Switzerland)
UniProt	Protein database	www.uniprot.org/	(Bateman *et al.*, 2023)
Zen	Operation software of Zeiss fluorescence microscopes	-	Zeiss (Jena, Germany)

2.2. Consumables

If not stated otherwise, plastic and glassware consumables were purchased from Schott (Mainz, Germany), Eppendorf (Hamburg, Germany) or Sarstedt (Nümbrecht, Germany).

2.3. Technical equipment

Technical equipment used in this work is listed in table 2.

Table 2: Technical equipment.

Equipment	Manufacturer
Apotome 2 & Apotome 3	Zeiss
Avanti JXN-25 (centrifuge)	Beckman Coulter (Brea, CA, USA)
AxioObserver Z.1 fluorescence microscope	Zeiss
Biometra TI 1 (UV lamp)	Biometra (Jena, Germany)
Freezers (-20 °C)	Liebherr (Bulle, Switzerland)
Freezers (-80 °C)	Thermo Fisher Scientific
Gelaire Laminar Airflow	Gelaire (Sydney, Australia)
Refridgerators	Liebherr
FastGene PAGE Protein System	Nippon Genetics Europe (Düren, Germany)
GelDoc XR+	Bio-Rad
Heating block	Cenco Instruments (Chicago, IL, USA)
Heating block Grant QBH2	Wolflabs (Pocklington, UK)
Heraeus™ Fresco21	Thermo Fisher Scientific
Heraeus™ Megafuge 40R	Thermo Fisher Scientific
Heraeus™ Megafuge 8R	Thermo Fisher Scientific
Hot magnetic stirrer	IDL GmbH & Co. KG (Nidderau, Germany)
Ice machine	Ziegra (Isernhagen, Germany)
InFors HT Ecotron	Infors AG (Bottmingen, Switzerland)
JLA-8.1 (rotor)	Beckman Coulter
L-25.50 (rotor)	Beckman Coulter
Mars Safety Classe 2	LaboGene (Lillerod, Denmark)
Mediaclav 10	Integra Biosciences AG (Zizers, Switzerland)
miniSpin centrifuge	Eppendorf AG (Hamburg, Germany)
Nano Photometer	Implen (Munich, Germany)
Optima LE-80K ultracentrifuge	Beckman Coulter
PeqStar Thermocycler Gradient 2x48 well	VWR (Radnor, PA, USA)
Power Source	VWR
PowerPac 200	Bio-Rad
QuantStudio 3	Thermo Fisher Scientific
Sartorius Analytics fine scale	Sartorius (Göttingen, Germany)
Sartorius universal scale	Sartorius
Sonifier cell disruptor B15	Branson (Danbury, CT, USA)
Sorvall MX120 ultracentrifuge	Thermo Fisher Scientific
T100 Thermal Cycler	Bio-Rad

Tecan inifinite M200 plate reader	Tecan Group AG
Tecan Spark	Tecan Group AG
Ultrafine scale	Sartorius
Vacuum pump	KLEMM (Drolshagen, Germany)
Viaflo 8 channel pipette	Integra Biosciences AG
Vortex Genie 2	Scientific Industries Inc. (Bohemia, NY, USA)
Xcell SecureLock Electrophoresis Cell	Invitrogen

2.4. Chemicals

Unless stated otherwise, chemicals used in this work were purchased from Merck (Darmstadt, Germany), Thermo Fisher Scientific, Carl Roth (Karlsruhe, Germany), AppliChem (Darmstadt, Germany) and VWR.

2.4.1. Special reagents

Special reagents used in this work are listed in table 3.

Table 3: Special reagents.

Reagent	Manufacturer
1,10-phenanthroline	Sigma Aldrich (St. Louis, MO, USA)
Ampuwa	Fresenius Kabi (Bad Homburg an der Höhe, Germany)
Atorvastatin	Sigma Aldrich
Clioquinol	Sigma Aldrich
N,N,N',N'-Tetrakis-(2-pyridylmethyl)-ethylendiamin (TPEN)	Alfa Aesar (Haverhill, MA, USA)

2.5. Kits

Kits used in this work are listed in table 4.

Table 4: Kits used in this work.

Kit	Application	Manufacturer
DNeasy® Blood and Tissue Kit	Purification of DNA from tissue culture	Qiagen (Hilden, Germany)
GeneJet Gel Extraction Kit	Purification of DNA fragments from agarose gels	Thermo Fisher Scientific (Waltham, MA, USA)
GeneJet Plasmid MiniPrep Kit	Purification of plasmids from liquid bacterial cultures	Thermo Fisher Scientific (Waltham, MA, USA)
NEBuilder® HiFi DNA Assembly Master Mix	Ligation of gBlocks into CRISPRi expression vectors	New England Biolabs (Ipswich, MA, USA)

In-Fusion® HD Cloning Kit	Cloning	Takara Bio
QIAquick PCR purification Kit	Purification of PCR products	Qiagen (Hilden, Germany)
QIAprep spin miniprep Kit	Purification of plasmids from liquid bacterial cultures	Qiagen (Hilden, Germany)
QuikChange Lightning Site-Directed Mutagenesis Kit	Site directed mutagenesis	Agilent
Turbo DNA-free kit™	DNA digest in RNA samples from tissue culture	Invitrogen (Waltham, MA, USA)

2.6. Cultivation of bacteria and mammalian cells

2.6.1. Media preparation and additives

All media used to grow bacteria were sterilized by autoclaving at 121 °C for 20 minutes. Heat sensitive additives were sterile-filtered and added after autoclaving. For solid media, 1.5 % (w/v) agar-agar were added to media before autoclaving.

2.6.1.1. Media for cultivation of bacteria

Media used for the cultivation of bacteria are listed in table 5. Routinely, lysogeny broth (LB) was used for cultivation of *E. coli* strains in liquid or solid form (Bertani, 1951). Following heat-shock transformation, cells were grown in SOC-medium. For overproduction of AmiA_Cp, salt-free LB was prepared as described in Klöckner *et al.* (2014). For overproduction of AmiA_Ct, terrific broth (TB) (Tartoff and Hobbs, 1987) was used with additional zinc autoinduction components (Studier, 2005).

Table 5: Media used for cultivation of bacteria.

Media	**Components**	**pH**
Lysogeny broth (LB)	10 g/L tryptone, 5 g/L yeast extract, 10 g/L NaCl	7.2
SOC outgrowth medium (SOC) (New England Biolabs, Ipswich, MA, USA)	2 % (w/v) vegetable peptone, 0.5 % (w/v) yeast extract, 10 mM NaCl, 2.5 mM KCl, 10 mM $MgCl_2$, 10 mM $MgSO_4$, 20 mM glucose	-
Terrific broth (TB)	12 g/L tryptone, 24 g/L yeast extract, 4 g/L glycerol	7.2
Terrific broth (TB) with autoinduction components	12 g/L tryptone, 24 g/L yeast extract, 4 g/L glycerol Phosphate buffer solution: 0.17 M KH_2PO_4, 0.72 M K_2HPO_4, after autoclaving add 100 mL to 900 mL TB medium, additives: 10 mM $MgSO_4$, 10 mM $MgCl_2$, 20 µM $ZnCl_2$, 0.5 g/L glucose, 2 g/L lactose	7.2

2.6.1.2. Media for cultivation of mammalian cells

To cultivate mammalian HEp-2 cells, Dulbecco's Minimum Essential Medium (DMEM) high glucose, GlutaMAX supplement with pyruvate medium was prepared under sterile conditions according to the composition presented in table 6. For media used in cytotoxicity assays and MIC determination, gentamicin and amphotericin B were omitted (DMEM-MIC). For cryoconservation, media was supplemented with 5 % (v/v) DMSO. Medium for HeLa and McCoy cells was similar to HEp-2 cell medium, with omission of MEM non-essential amino acids, MEM vitamins solution and amphotericin B. Media composition used for cultivation of reporter cell lines HEK™-Blue hNOD1, HEK™-Blue hNOD2, HEK™-Blue Null1 and HEK™-Blue Null2 are listed in table 7. Blasticidin was omitted in HEK™-Blue Null1 and HEK™-Blue Null2 cells. Media used for cytotoxicity assays was prepared without addition of antibiotics. Frozen stocks of HEK™-Blue reporter cells are prepared in DMEM medium containing 20 % (v/v) fetal bovine serum (FBS) and 10 % (v/v) DMSO.

Table 6: Media used for cultivation of HEp-2 cells.

Component	Added volume (mL)	Final concentration
Dulbecco's Minimum Essential Medium (DMEM) high Glucose, GlutaMAX supplement, pyruvate (Thermo Fisher Scientific)	500	-
FBS (Thermo Fisher Scientific), heat-inactivated according to the manufacturer's instructions	50	10 % (v/v)
MEM Non-Essential Amino Acids (100x) (Thermo Fisher Scientific)	5	1x
MEM Vitamins solution (100x) (Thermo Fisher Scientific)	5	1x
Gibco™ Amphotericin B (250 µg/mL) (Thermo Fisher Scientific)	5	2.5 µg/mL
Gibco™ Gentamicin sulfate (50 mg/mL) (Thermo Fisher Scientific)	0.5	50 µg/mL

Table 7: Media used for cultivation of HEK-Blue reporter cells.

Component	Added volume (mL)	Final concentration
Dulbecco's Minimum Essential Medium (DMEM) high Glucose, GlutaMAX supplement, pyruvate (Thermo Fisher Scientific)	500	-
Fetal bovine serum (Thermo Fisher Scientific), heat-inactivated according to the manufacturer's instructions	50	10 % (v/v)
Gibco™ L-Glutamin (200 mM) (Thermo Fisher Scientific)	5	1x
Gibco™ Penicillin-Streptomycin (10.000 U/mL) (Thermo Fisher Scientific	5	100 U/mL
Normocin™ (InvivoGen, San Diego, CA, USA)	1	100 µg/mL
Blasticidin (InvivoGen)	1.5	30 µg/mL
Zeocin® (InvivoGen)	1	100 µg/mL

2.6.1.3. Antibiotics and tested compounds

Antibiotics and tested compounds used in this work are listed in table 8.

Table 8: Antibiotics and tested compounds.

Substance	Solvent	Stock concentration (mg/mL)	storage conditions	Final concentration (µg/mL)	Source
Ampicillin sodium salt	H_2O	100	- 20 °C	100	Carl Roth
Anhydrotetracycline	DMF	2	- 20 °C kept in the dark	200 µg/L	IBA Lifesciences (Göttingen, Germany)
Chloramphenicol	Ethanol	100	- 20 °C	34	Carl Roth
Clovibactin	H_2O + 0.002 % (v/v) Tween	10	4 °C	1-128	Novobiotic (Cambridge, MA, USA)

Cycloheximide	Hank's Balanced Salt Solution (HBSS)	0.1	- 20 °C	1.2	Sigma-Aldrich
D-Cycloserine	H_2O	10 mg/mL	- 20 °C	1-128	Sigma-Aldrich
Pacidamycin D	H_2O	10 mg/mL	- 20 °C	1-128	
Pacidamycin S	H_2O	10 mg/mL	- 20 °C	1-128	
Penicillin G	H_2O	10 mg/mL	- 20 °C	64.5	Carl Roth
Teixobactin	DMSO	10 mg/mL	- 20 °C	1-128	Novobiotic

2.6.2. Used organisms

2.6.2.1. *E. coli* strains for plasmid propagation, subcloning and preparation of PGN sacculi

E. coli strains for plasmid propagation, subcloning and preparation of PGN sacculi are listed in table 9.

Table 9: *E. coli* strains for plasmid propagation, subcloning and preparation of PGN sacculi.

Strain	Genotype	Application	Source
E. coli NEB5a (DH5α)	*fhuA2Δ_(fhuA2 Δ(argF-lacZ)U169 phoA glnV44 Φ80Δ (lacZ)M15 gyrA96 recA1 relA1 endA1 thi-1 hsdR17*	Plasmid propagation, subcloning, permanent storage	NEB
E. coli W3110	*F- lambda- IN(rrnDrrnE) 1 rph-1*	PGN sacculi preparation	DSM5911

2.6.2.2. *E. coli* strains used for recombinant protein production

E. coli strains used for recombinant protein production are listed in table 10.

Table 10: *E. coli* strains used for recombinant protein production.

Strain	Genotype	Application	Source
E. coli C43(DE3)	*F– ompT gal dcm hsdSB(rB- mB-)(DE3)*	Production of AmiA_Ct	Wagner *et al.* (2008)
E. coli JM83	*rpsL ara Δ(lac-proAB) Φ80dlacZΔM15*	Production of AmiA_Cp	DSM3947

2.6.2.3. *E. coli* mutant strains used in complementation experiments

E. coli mutant strains used for complementation experiments are listed in table 11.

Table 11: *E. coli* mutant strains.

Strain	Genotype	Application	Source
E. coli ADE24 + pBAD33-*amiC*	*ΔamiA, amiB, amiC*	Complementation experiments	Prof. W. Vollmer, Newcastle University. Present affiliation: The University of Queensland

2.6.2.4. Mammalian cell lines

Mammalian cell lines were used in cytotoxicity assays and in chlamydial infection models determining minimum inhibitory concentrations (MIC). All cell lines used in this work are listed in table 12.

Table 12: Mammalian cell lines.

Cell line	Application	Source
HEp-2 subclone B	Cytotoxicity assays, propagation of *Chlamydia* D/UW-3/CX, MIC determination	ATCC CCL-23
HEK™-Blue hNOD1	Cytotoxicity assays, NOD Assays	InvivoGen
HEK™-Blue hNOD2	Cytotoxicity assays, NOD Assays	InvivoGen
HEK™-Blue hNULL1	Cytotoxicity assays, NOD Assays	InvivoGen
HEK™-Blue hNULL2	Cytotoxicity assays, NOD Assays	InvivoGen
HeLa	Propagation of *Chlamydia trachomatis* L2P-	ATTC CCL-2
McCoy	Propagation of chlamydial transformants	ATTC CRL-1696

2.6.2.5. *Chlamydia* strains

Chlamydial strains used in this work are listed in table 13.

Table 13: *Chlamydia* strains.

Strain	Application	Source
Chlamydia trachomatis D/UW-3/CX	Chlamydial MIC determinations	Kind gift of K. Shima, University of Lübeck - Stephens *et al.* 1998
Chlamydia trachomatis L2P-	Transformation	Kind gift of K. Mölleken, University of Düsseldorf – Peterson *et al.* (1990)

2.6.3. Bacteriological methods

Unless stated otherwise, *E. coli* was grown in LB medium or on LB agar plates at 37 °C. For cryoconservation, cells were grown overnight and added to an equal volume of 100 % (v/v) glycerol and stored at – 80 °C.

2.6.3.1. Preparation of chemically competent *E. coli*

For the preparation of chemically competent cells, *E. coli* was grown to OD 0.4 in LB medium and then harvested at 4000 x g and 4 °C. Cell pellets were resuspended in chilled 0.1 M $CaCl_2$ solution and incubated at 4°C for 20 min. Cells were pelleted again as described previously and then resuspended in 2 mL chilled 0.1 M $CaCl_2$ solution supplemented with 15 % (v/v) glycerol. Aliquots of 50 µL each were prepared and stored at -80 °C.

2.6.3.2. Heat shock transformation of chemically competent *E. coli*

Chemically competent cells were thawed on ice and mixed with 10 – 100 ng plasmid DNA and further incubated on ice for 30 min. In a heating block unit, cells were incubated at 42 °C for 90 s and subsequently cooled on ice for two minutes. 1 mL of SOC medium (NEB) was added to the cells before incubation at 37 °C at 120 rpm for one hour. Cells were then plated on agar plates containing appropriate antibiotics for selection and incubated over night at 37 °C.

2.6.3.3. Electroporation

For complementation experiments, the plasmid encoding *amiA*_Cp had to be introduced to *E. coli* ADE24 by electroporation. Cells were thawed on ice, mixed with 70 – 100 ng plasmid DNA and transferred into an electroporation cuvette. The cuvette was placed into a MicroPulser (Bio-Rad) and cells were pulsed for 6 ms. Cells were supplemented with 1 mL prewarmed LB medium and incubated at 37 °C and 120 rpm for one hour. Cells were then plated on agar plates containing appropriate antibiotics for selection and incubated over night at 37 °C.

2.6.3.4. Optical density determination

To determine a liquid culture's optical density, 1 mL of culture was transferred into a polystyrene cuvette and measured in a photometer at 600 nm. If the optical density exceeded 0.3, the liquid culture was diluted five to ten fold to avoid light scatter effects.

2.6.4. Mammalian cell culture and propagation of *Chlamydia*

Mammalian cells were routinely grown in CellStar® TC cell culture flasks (Greiner Bio-One, Kremsmünster, Austria) on 25 – 175 cm^2 and incubated in appropriate media at 37 °C and 5 % CO_2 atmosphere between passages. Confluency of cells was checked by light microscopy. HEp-2 and HEK™- cells were passaged every 72-96 h, while HeLa ad McCoy cells were passaged every 48 h. Cells were routinely tested for *Mycoplasma* contamination using Venor® GeM OneStep – Mycoplasma Detection Kit for conventional PCR according to the manufacturer's instructions.

2.6.4.1. Reagents used in mammalian cell culture and microscopy

Reagents used in mammalian cell culture and microscopy are listed in table 14.

Table 14: Reagents used in mammalian cell culture.

Reagent	Application	Source
0.5 % Trypsin-EDTA (10x), no phenol red	Passaging of HEp-2, HeLa and McCoy cells	Thermo Fisher Scientific
4',6-diamidino-2-phenylindol (DAPI)	Staining of host cell nuclei for fluorescence microscopy	Thermo Fisher Scientific
alamarBlue™ cell viability reagent	Cytotoxicity assays	Thermo Fisher Scientific
Cycloheximide	Cultivation of *Chlamydia*	Merck
DPBS	Experiments with chlamydial transformants in HeLa and McCoy cells	Thermo Fisher Scientific
Hank's Balanced salt solution (HBSS)	Routine maintenance of tissue culture and infection of HeLa and McCoy cells	Thermo Fisher Scientific
Pathfinder *Chlamydia* Culture Confirmation System	Immunostaining of infected host cells for fluorescence microscopy	Bio-Rad
PBS	Routine maintenance of tissue culture and passaging of HEK cells	Thermo Fisher Scientific
Sucrose-phosphate buffer (SPG)	Cryoconservation of *Chlamydia,* 220 mM sucrose, 3.82 mM KH_2PO_4, 10.8 mM Na_2HPO_4 x 2 H_2O, 4.36 mM glutamic acid x H2O, pH 7.5	-
Venor® GeM OneStep – Mycoplasma Detection Kit for conventional PCR	Maintenance – testing for contamination with Mycoplasma	Minerva Biolabs GmbH (Berlin, Germany)

2.6.4.2. Cultivation of eukaryotic cells and passaging

All cell lines were cultivated in DMEM medium with different additives (see 2.6.1.2.) in coated cell culture flasks on 25 – 175 cm^2. When HEp-2, HeLa and McCoy cells reached confluency, cells were passaged into new flasks with fresh media. Therefore, media was aspirated and cells were rinsed with HBSS (HEp-2) or DPBS (HeLa, McCoy). Trypsin-EDTA solution was added to the cells (2 mL for T75 flasks) and flasks were incubated at 37 °C for 5 minutes until cells were detached. At least the doubled volume of media compared to trypsin-EDTA was added to the cells. Of this suspension, defined volumes were pipetted into new flasks containing fresh medium. HEK™ cells were passaged once they reached

70-80 % confluency. Passaging procedure is equal to the process described before, but detaching of cells was achieved with prewarmed PBS.

2.6.4.3. Permanent cultures of mammalian cells

To produce permanent cultures of mammalian cells, cells were detached from culturing flasks as described previously. Cell counts were determined using a Bürker-Türk/Thoma counting chamber and cell density was adjusted to the supplier's recommendations. HEp-2, HeLa and McCoy cells were frozen in DMEM medium supplemented with 5 % (v/v) DMSO in 1 mL aliquots at a cooling rate of 1 °C/min using the mammalian cell line freezing container Nalgene™ Mr. Frosty (Thermo Fisher Scientific) according to the manufacturer's instructions. HEK™ cells were frozen similarly in DMEM medium containing no additives except for 20 % (v/v) FBS and 10 % (v/v) DMSO. For reintroducing cells into tissue culture, the supplier's instructions were followed.

2.6.4.4. Infection of eukaryotic cells and propagation of *Chlamydia*

To infect mammalian cells with *Chlamydia*, cells grown in flasks or plates were first rinsed with HBSS. Inocula were prepared in DMEM MIC-medium without added antibiotics to an appropriate MOI using frozen *Chlamydia* stocks. Following inoculation, plates were incubated at 37 °C and 5 % CO_2 for two hours. Cells infected within flasks were supplemented with 1.2 µg/mL cycloheximide and incubated for three hours at 37 °C and 5 % CO_2. After incubation, medium in flasks and plates was aspirated and replaced with fresh medium.

2.6.4.5. Permanent cultures of *Chlamydia*

To produce permanent cultures of *Chlamydia*, mammalian cells of multiple flasks were infected with *Chlamydia* as described in the previous section. Infected cells were incubated for 48-36 hours and then scraped into the medium. Mammalian cells were lysed mechanically by vortexing with glass beads for 30 s. To pellet eukaryotic cell debris, the suspension was centrifuged at 1480 x g for 10 min at room temperature. The supernatant containing chlamydial EBs was transferred into new tubes and centrifuged again at 12100 x g for 20 min at room temperature. Pelleted EBs were resuspended in a small volume of SPG-buffer and frozen at – 80 °C.

2.7. Molecular methods

2.7.1. Isolation of genomic DNA from bacteria

Genomic DNA from *C. pneumoniae* GiD was kindly provided by RG Hegemann (University of Düsseldorf). Genomic DNA of *C. trachomatis* D/UW-3/CX was isolated using the DNeasy® Blood & Tissue Kit (Qiagen) and was kindly provided by Dr. H. Bühl (RG Henrichfreise).

2.7.2. Polymerase chain reaction

Polymerase chain reaction (PCR) (Mullis *et al.*, 1986) is used to exponentially amplify specific DNA segments. In a cyclic temperature-mediated succession of denaturation, annealing and elongation,

targeted DNA sequences framed by oligonucleotides are synthesized in 5'-3' direction by DNA polymerases. In this work, PCR was used for cloning, validation of genetic constructs and site-directed mutagenesis. Bio-Rad T100 Thermal Cycler (Bio-Rad) and PeqStar Thermocycler Gradient 2x48 well (VWR) were used. For Cloning, either purified genomic DNA or plasmids were used as templates for gene amplification. Either Q5® High-Fidelity DNA Polymerase (NEB) or Q5® Hot Start High Fidelity DNA Polymerase (NEB) were used with supplied reaction buffers according to the manufacturer's instructions. For validation of genetic constructs with purified plasmids as templates or for colony PCR, Taq DNA Polymerase, recombinant, 5 U/µL (Thermo Fisher Scientific) was used according to the manufacturer's instructions. For colony PCR, small amounts of colony material were used as templates for PCR. Site-directed mutagenesis was achieved by using QuikChange Lightning Site-Directed Mutagenesis kit (Agilent, Santa Clara, CA, USA). Oligonucleotides for In-Fusion Cloning and site-directed mutagenesis were designed using the In-Fusion Primer Design tool (Takara Bio, Kusatsu, Japan) and the QuikChange Primer Design Tool (Agilent), respectively. A list of oligonucleotides used in this work is provided in table 15.

Table 15: Oligonucleotides used in this work.

Name	Sequence (5'-3')	# nt	Application
AmiA_CtS140A_fw	CTAAAGCAGATGTATTAGACGCGTGATTACAGTGGATACTAAC	43	*ct268* mutagenesis
AmiA_CtS140A_rev	GTTAGTATCCACTGTAATCACGCGTCTAATACATCTGCTTTAG	43	*ct268* mutagenesis
CT_268_XmaI_52b_for	GCGCGCCCCGGGAGGGGTATCAGATCTTCAAAC	33	Cloning of *ct268* into pET-52b
CT_268-SP_XmaI_52B_for	GCGCGCCCCGGGGCGGGGATTCCTAAGG	28	Cloning of *ct268* into pET-52b (residues 148-780)
CT_268_EagI_52b_rev	GCGCGCCGGCCGTTATTTATGCACTTTTTTTGCTC	35	Cloning of *ct268* into pET-52b
*ct268*H67A_for	TGAACTTATAGTCATAGATCCTGGTGCTGGCGGTAAAGACG	40	*ct268* mutagenesis
*ct268*H67A_rev	CGTCTTTACCGCCAGCACCAGGATCTATGACTATAAGTTCA	41	*ct268* mutagenesis

*ct268*H136A_for	GATGTATTAGACGAGTGAT TACAGGCGATACTAACAAA AACATCAGCCTT	50	*ct268* mutagenesis
*ct268*H136A_rev	AAGGCTGATGTTTTTGTTA GTATCGCCTGTAATCACTC GTCTAATACATC	50	*ct268* mutagenesis
*ct268*E205A_for	CCTGCGGTCCTTGTGGCAA CAGGGTTTCTTTCC	33	*ct268* mutagenesis
*ct268*E205A_rev	GGAAAGAAACCCTGTTGCC ACAAGGACCGCAGG	33	*ct268* mutagenesis
ct268+_pASK3_vec_fw	TGGAGCCACCCGCAGTTC	18	Linearization of pASK3C
ct268+_pASK3_vec_rev	TTCTCTATCACTGATAGGG AGTGG	24	Linearization of pASK3C
ct268+_pASK3_ins_fw	ATCAGTGATAGAGAAATG AGGGGTATCAGATCTTCAA ACA	40	Amplification of *ct268*
*ct268*_pASK3_ins_rev	CTGCGGGTGGCTCCATTTA TGCACTTTTTTTGCTCCTGA	39	Amplification of *ct268*
*ct268*ΔSP_pASK3_ins_fw	ATCAGTGATAGAGAAGCG GGGATTCCTAAGGTAAGT	36	Amplification of *ct268* (residues 148-780)
pASK3_*amiA*Ct_ins_fw	ATCAGTGATAGAGAAATG AGGGGTATCAGATCTTCAA ACA	40	Amplification of *ct268*
pASK3_*amiA*Ct_ins_rev	CTGCGGGTGGCTCCATTTA TGCACTTTTTTTGCTCCTGA	39	Amplification of *ct268*
pASK3_*amiA*Ct_vec_fw	TGGAGCCACCCGCAGTTC	18	Linearization of pASK3
pASK3_*amiA*Ct_vec_rev	TTCTCTATCACTGATAGGG AGTGG	24	Linearization of pASK3

2.7.3. Reverse Transcriptase quantitative PCR (RT-qPCR)

RT-qPCR was used to quantify levels of mRNA to assess the level of gene expression. Isolated RNA was transcribed to cDNA using SuperScript™ III Reverse Transcriptase (Invitrogen) according to the manufacturer's instructions with reagents provided. cDNA was diluted 10 fold with nuclease-free water and frozen at – 80 °C. Equal volumes of cDNA were used in a total volume of 25 µL for qPCR with SYBR green master mix (Applied Biosystems, Waltham, MA, USA) and quantified on a QuantStudio 3 (Applied Biosystems/Thermo Fisher Scientific) using standard amplification cycle with melting curve analysis. For analysis of *amiA* expression during conditional knockdowns, levels of *murE* expression

were also analyzed to rule out polar effects of knockdown. As controls, cDNA levels of *euo* (early upstream open reading frame) and *omcB* (large cysteine-rich periplasmic protein) as early and late genes, respectively, were analyzed as well. Results were compared to a standard curve generated against purified *C. trachomatis* L2 genomic DNA. A list of qPCR primers is provided in table 16.

Table 16: Primers used for qPCR.

Name	Sequence (5'-3')	# nt	Application
*amiA*_fw	GACGAGGGAACTGCAGAAAG	20	*amiA* cDNA amplification
*amiA*_rev	CATCCGTAGCCCTTGTCATTAT	22	*amiA* cDNA amplification
*euo*_fw	CGAAGACTACTCGTTGGGAAATA	23	*euo* cDNA amplification
*euo*_rev	AACAGAAGCTCTCCTTGATAAGT	23	*euo* cDNA amplification
*murE*_fw	CCTTCAAGGCATCTGGATGTAA	22	*murE* cDNA amplification
*murE*_rev	CTTCTTCCTGAACGCTCCATAA	22	*murE* cDNA amplification
*omcB*_fw	CGGTAGGATCTCCCTATCCTATT	23	*omcB* cDNA amplification
*omcB*_rev	CGAACTCTGCTTCACATGGTA	22	*omcB* cDNA amplification

2.7.4. Agarose gel electrophoresis

Agarose gel electrophoresis was used to purify and identify DNA fragments. DNA samples were loaded onto an agarose gel which was subjected to an electric field. Due to the negatively charged phosphate backbone, DNA samples migrate towards the cathode electrode. DNA segments are separated by molecular weight, which is proportional to negative charge. Routinely, 1 % (w/v) agarose gels were cast using Agarose NEEO Ultra-Qualität (Carl Roth) and 1 x TAE buffer (40 mM Tris-HCl, 1 mM EDTA, 0.11 % (v/v) acetic acid, pH 8.3) containing GelRed™ Nucleic Acid Stain (VWR). Samples were mixed with Gel Loading Dye, Purple (6x) (NEB) and loaded into the gel pockets. Routinely, GeneRuler 1 kb DNA ladder was used as a standard. After electrophoresis at 80-100 V for 45-60 min, bands were visualized using a GelDoc Molecular Imager® (Bio-Rad) and ImageLab software (Bio-Rad).

2.7.5. Purification of DNA fragments and plasmids

For purification of DNA from tissue culture, DNeasy® Blood and Tissue Kit (Qiagen) was used. For plasmid purification from liquid bacterial cultures, either GeneJet Plasmid MiniPrep Kit (Thermo Fisher Scientific) or QIAprep spin miniprep Kit (Qiagen) was used. QIAquick PCR purification Kit (Qiagen) was employed for PCR product purification. DNA fragments cut from agarose gels were purified using GeneJet Gel Extraction Kit (Thermo Fisher Scientific). All Kits were used according to the manufacturer's instructions.

2.7.6. Photometric determination of DNA concentration

Concentrations of purified DNA fragments or plasmids were measured at 280 nm using a NanoPhotometer (Implen, Munich, Germany).

2.7.7. Molecular Cloning

Molecular Cloning of DNA fragments into expression and propagation vectors was achieved by restriction digest and ligation in case of construction of *amiA* overexpression construct pET-52b_ct268 and related constructs. CRISPRi-mediated knockdown constructs were established using gBlocks (Integrated DNA Technologies (Coralville, IA, USA) that were ligated into digested vectors pretreated with alkaline phosphatase (FastAP, Thermo Fisher Scientific) using NEBuilder® HiFi DNA Assembly Master Mix (NEB). Else, propagation and overexpression vectors were constructed using In-Fusion® HD Cloning Kit (Takara Bio). PCR-based site-directed mutagenesis was achieved by using the QuikChange Lightning Site-Directed Mutagenesis Kit (Agilent).

2.7.7.1. Restriction of DNA with endonucleases

For construction of pET-52b_*ct268,* both vector pET-52b and *C. trachomatis* D/UW-3/CX genomic DNA were digested with XmaI and EagI restriction enzymes (NEB) at 37 °C for 5 – 15 min with reagents provided. For validation of CRISPRi constructs, candidate constructs were digested using FastDigest NcoI and SacI (Thermo Fisher Scientific) at 37 °C for 5 – 15 min.

2.7.7.2. Ligation of inserts into plasmids

Before ligation, vectors were treated with FastAP Alkaline Phosphatase (Thermo Fisher Scientific) to prevent recircularization. T4 ligase (Thermo Fisher Scientific) was used to ligate the insert encoding *ct268* into restricted pET-52b. CRISPRi constructs targeting *murJ*, *rodA* and *namZ* were established by ligation of gBlocks into pLCRia vector backbones digested by FastDigest enzymes EagI and KpnI (Thermo Fisher Scientific). For ligation, NEBuilder® HiFi DNA Assembly Master Mix (NEB) was used according to the manufacturer's instructions. gBlocks were pretreated according to the manufacturer's instructions. Sequences are listed in table 17.

Table 17: gBlocks.

Name	Sequence (5'-3')	# nt	Application
*murJ*_ct624_LCRia_gRNA rev	TGAATATAATTTTAATTATATCACGCACTAGCTCAGATTCAGTAGACCGCTGTTGATAAAACGAAAGGCCCAGTCTTTCGACTGAGCCTTTCGTTTTATTTGAAAAATCTCGCCAACAAGTTGACGAGATAAACACGGCATTTTGCCTTGTTTTAGTAGATTCTGTTTCCAGAGTACTAAAACTAGTAGCATCTTTTTGGCTGGGGTGTCATTATAAGAAAACCGTCT	294	Construction of pLCRia(*murJ*)

	CCACCGGTGAATGCATGATCTACGTGCGTCAC ATGCAGTACCGACGTCTTAAGACCCACTTTCA CA		
*namZ*_ct605_L CRia_gRNA rev	TGAATATAATTTTAATTATATCACGCAC TAGCTCAGATTCAGTAGACCGCTGTTGATAAA ACGAAAGGCCCAGTCTTTCGACTGAGCCTTTC GTTTTATTTGAAAAATCTCGCCAACAAGTTGA CGAGATAAACACGGCATTTTGCCTTGTTTTAGT AGATTCTGTTTCCAGAGTACTAAAACAGGAGA TTATGAAAACAATCTGGTGTCATTATAAGAAA ACCGTCTCCACCGGTGAATGCATGATCTACGT GCGTCACATGCAGTACCGACGTCTTAAGACCC ACTTTCACA	294	Construction of pLCRia(*namZ*)
*rodA*_ct726_LC Ria_gRNA rev	TGAATATAATTTTAATTATATCACGCACTAGCT CAGATTCAGTAGACCGCTGTTGATAAAACGAA AGGCCCAGTCTTTCGACTGAGCCTTTCGTTTTA TTTGAAAAATCTCGCCAACAAGTTGACGAGAT AAACACGGCATTTTGCCTTGTTTTAGTAGATTC TGTTTCCAGAGTACTAAAACCTTATGAGCATA AGTGTGATTGGTGTCATTATAAGAAAACCGTC TCCACCGGTGAATGCATGATCTACGTGCGTCA CATGCAGTACCGACGTCTTAAGACCCACTTTC ACA	294	Construction of pLCRia(*rodA*)

2.7.7.3. In-Fusion Cloning

For In-Fusion Cloning, In-Fusion® HD Cloning Kit (Takara Bio) was used according to the manufacturer's instructions.

2.7.7.4. PCR-based site-directed mutagenesis

Site-directed mutagenesis of plasmids was achieved by using QuikChange Lightning Site-Directed Mutagenesis Kit (Agilent) according to the manufacturer's instructions.

2.7.8. Sequencing

Colonies bearing constructs were sent to Microsynth Seqlab (Göttingen, Germany) for Sanger-based *E.coli* NightSeq Sequencing.

2.7.9. Expression vectors

Expression vectors, encoded genes, additional features and sources are listed in table 18.

Table 18: Expression vectors.

Name	Encoded gene	Features	Reference/Source
pASK-IBA2C	-	CamR, TetO/TetP, MCS, OmpA, C-terminal Strep-tag II	IBA Lifesciences
pASK-IBA2C-*amiA*Cpn	*cpn0417*/*amiA*Cp	Derivate of IBA2C	This work
pASK-IBA3	-	AmpR, TetO/TetP, C-terminal Strep-tag II	IBA Lifesciences
pASK-IBA3-*ct268*	*ct268*/*amiA*Ct	Derivate of IBA3	This work
pASK-IBA3C	-	CamR, TetO/TetP, C-terminal Strep-tag II	IBA Lifesciences
pASK-IBA3C-*ct268*	*ct268*/*amiACt*	Derivate of IBA3C	This work
pASK-IBA3C-*ct268*ΔSP	*ct268*/*amiACt*ΔSP	Derivate of IBA3C	This work
pASK-IBA3C-*ct268*H67A	*ct268*/*amiACt* H67A	Derivate of IBA3C	This work
pASK-IBA3C-*ct268*H136A	*ct268*/*amiACt* H136A	Derivate of IBA3C	This work
pASK-IBA3C-*ct268*E205A	*ct268*/*amiACt* E205A	Derivate of IBA3C	This work
pET-52b(+)	-	*AmpR, T7, MCS, N-terminal Streptag II*	Merck
pET-52b-*ct268*	*ct268*/*amiACt*	Derivate of pET-52b(+)	This work
pET-52b-*ct268*ΔSP	*ct268*/*amiACt*ΔSP	Derivate of pET-52b(+)	This work
pET-52b-*ct268*H67A	*ct268*/*amiACt* H67A	Derivate of pET-52b(+)	This work
pET-52b-*ct268*H136A	*ct268*/*amiACt* H136A	Derivate of pET-52b(+)	This work
pET-52b-*ct268*E205A	*ct268*/*amiACt* E205A	Derivate of pET-52b(+)	This work

pBOMBL	-	PenR, Vaa degradation tag, weakened ribosome binding site, GFP, TetO/TetP	(Ouellette *et al.*, 2021a)
pBOMBL-*murJ*-6xH	*murJ*-6xH	Derivate of pBOMBL	This work
pBOMBL-*namZ*-6xH	*namZ*-6xH	Derivate of pBOMBL	This work
pBOMBL-*rodA*-6xH	*rodA*-6xH	Derivate of pBOMBL	This work
pBOMBLCRia::L2/ pLCRia	-	PenR, Vaa degradation tag, weakened ribosome binding site, GFP, TetO/TetP-inducible dCas9	Ouellette *et al.*, 2021
pLCRia(*amiA*)	dCas9 targeting *ct268/amiACt*	Derivate of pLCRia	Prof. Dr. SP Ouellette
pLCRia-*amiA*-6xH(*amiA*)	dCas9 targeting ct268/*amiACt*, overexpression of *amiACt*-6xH	Derivate of pLCRia	Prof. Dr. SP Ouellette
pLCRia(*murJ*)	dCas9 targeting *murJ*	Derivate of pLCRia	This work
pLCRia(*namZ*)	dCas9 targeted against *namZ*	Derivate of pLCRia	This work
pLCRia(NT)	Non-targeting dCas9	Derivate of pLCRia	Prof. Dr. SP Ouellette
pLCRia(*rodA*)	dCas9 targeting *namZ*	Derivate of pLCRia	This work

2.8. Biochemical methods

2.8.1. Recombinant protein production and purification

Production strains were transformed with expression plasmids encoding the gene of interest and plated on selective agar plates for overnight incubation. For precultures, 2-3 colonies were added to LB medium containing appropriate antibiotics. Precultures were incubated at 37 °C and 120 rpm for approx. eight hours or until an appropriate cell density was reached. Main cultures were inoculated with precultures in a 1 % ratio and incubated at 120 rpm at the permissive temperature. Unless stated otherwise, recombinant proteins were produced in a total volume of 4 L. Production conditions for AmiA_Ct and AmiA_Cp are presented in table 19. Exact TB medium composition is shown in table 5. After protein production, cultures were harvested at 3100 x g and 10 °C. AmiA_Cp was produced as already described previously by Klöckner *et al.* (2014).

Table 19: Conditions for recombinant production of AmiA_Ct and AmiA_Cp.

Protein	Strain	Medium	Induction	Temperature	Duration
AmiA_Ct	*E. coli* C43(DE3) + pET-52b-*ct268*	TB+ autoinduction solution	Autoinduction	37 °C	16 h / overnight
AmiA_Cp	*E. coli* JM83 + pASK-IBA2C-*amiA*Cp	LB (salt-free) + 300 mM sucrose	AHT, 200 ng/L OD = 0.6	30 °C	3 h

For AmiA_Ct, pellets were resuspended in buffer A (25 mM MOPS pH 7.2, 1000 mM NaCl, 2 mM $MgCl_2$) supplemented with 1 U/mL benzonase, 2 mg/mL polymyxin B and 1 mM phenylmethylsulfonylfluoride (PMSF) in a total volume of 50 mL and lysed by sonication. Lysed cells were solubilized with 0.25 % (w/v) 3-((3-cholamidopropyl)dimethylammonio)-1-propanesulfonate (CHAPS) at 4 °C for 60 min. Ultracentrifugation at 139000 x g and 4 °C was performed to obtain cleared lysate. For purification, 2 mL Strep-Tactin® XT superflow® (IBA Lifesciences), yielding 1 mL of column volume (CV). After equilibration with 5 x CV buffer A, the lysate loaded onto the column completely. The column material was washed with 5 x 2 CV buffer B (25 mM MOPS pH 7.2, 300 mM NaCl, 2 mM $MgCl_2$, 10 % (v/v) glycerol). Samples were eluted with 6 x 0.5 CV Strep-Tactin® XT buffer BXT (IBA Lifesciences) supplemented with 10 % (v/v) glycerol. All fractions were collected separately. For AmiA_Cp, pellets were resuspended in 8 mL buffer P (100 mM Tris-HCl pH 8.0, 500 mM sucrose, 1mM EDTA). The suspension was supplemented with 100 µg/mL lysozyme and 20 U/mL benzonase and incubated at 4 °C for 30 min and 15 min, respectively. To obtain clear lysate, the suspension was centrifuges at 15000 x g and 4 °C for 30 min. After loading the sample similar to the process of AmiA_Ct purification, the column was washed with 20-30 x CV buffer W (100 mM Tris-HCl pH 8.0, 150 mM NaCl, 1 mM EDTA). Proteins were eluted using 9 x 0.5 CV Strep-Tactin® XT buffer BXT (IBA Lifesciences).

2.8.2. Quantification of recombinant protein with Bradford's reagent

Quantification of purified protein was performed according to the Bradford method using (Bradford, 1976) Protein Assay Dye Reagent Concentrate (Bio-Rad). If necessary, eluted protein was diluted. A volume of 20 µL of protein was mixed with 200 µL Bradford reagent and incubated in the dark at room temperature for 10 min. Absorbances were measured at 595 nm using microplate reader GloMax Explorer (Promega, Madison, WI, USA). Defined BSA-solutions were used as standard to determine concentration.

2.8.3. Protein analysis by SDS-PAGE

SDS-PAGE was performed to assess purity of purified proteins. PAGE was run with Precast NuPAGE™ 4-12% Bis-Tris Protein Gels, 1.0 mm, 15-well (Thermo Fisher Scientific) were used with Tris-MOPS-SDS Running Buffer (GenScript, Piscataway Township, NJ, USA). Samples were mixed with Novex NuPAGE™ LDS Sample Buffer (4X) (Invitrogen) and loaded into the gel pockets. Gels were loaded into FastGene PAGE Protein Systems (Nippon) and run at 200 V and 130 mA for 40 min. Bands were visualized with either Quick Coomassie Stain (ProteinArk, Rotherham, UK) or PageBlue™ Protein Staining Solution according to the manufacturer's instructions.

2.8.4. Dialysis

After protein purification, dialysis was performed for buffer exchange. Elution fractions with high yield were pooled within D-Tube™ Dialyzer Maxi, MWCO 6-8 kDa (Merck) and placed in stirring dialysis buffer (25 mM MOPS pH 7.0, 300 mM NaCl, 2mM $MgCl_2$, 20 µM $ZnCl_2$, 10 % (v/v) glycerol) at 4 °C. After one hour, buffer was renewed and dialysis was continued overnight.

2.8.5. Preparation of Remazol Brilliant Blue-stained *E. coli* PGN sacculi

Remazol Brilliant Blue-stained PGN sacculi (RBB-PGN) were used as a substrate in dye release assays and prepared as described in Farris *et al.* (2016) and Zhou *et al.* (1988) with modifications: *E. coli* W3110 was grown to an optical density of 0.6 in 4 L TB medium. Pelleted cells were resuspended in a final volume of 40 mL chilled H_2O and boiled in 160 mL 5 % (w/v) SDS solution. Following overnight incubation at room temperature, sacculi were harvested by centrifugation at 9600 x *g* for 30 min. After washing with H_2O, material was stained with 20 mM RBB solution in 0,25 M NaOH. Unbound dye was removed by multiple washing and centrifugation steps. RBB-PG was stored at –20 °C after lyophilization and dissolved in 0,2 % (v/v) Triton X-100 prior to use.

2.8.6. Thin layer chromatography (TLC)

Thin layer chromatography was performed to analyze reaction products of *in vitro* assays with purified recombinant protein. Routinely, TLC Silica Gel 60 F254 plates (Merck) were used as stationary phase.

2.8.6.1. TLC for detection of lipids

To detect hydrolytic activity towards lipid II, assays were terminated by adding n-butanol pyridine acetate (4:1, v/v) in a 1:1 ratio to the reaction mixture to extract reaction products into the organic phase. After vortexing the mixture for three minutes, tubes were centrifuged at 17000 x g for 5 min for phase separation. The complete upper phase was spotted stepwise onto silica plates. The mobile phase was prepared according to Rick *et al.*, (1998) using chloroform, methanol, water and ammonia in a 88:48:10:1 ratio. After running the TLC in mobile phase, reaction products were visualized by staining the silica plate in phosphomolybdic acid stain (2.5 % (w/v) phosphomolybdic acid, 1 % (w/v) cerium(IV)-sulfate dissolved in 6 % (v/v) sulfuric acid) and subsequent drying and heating. Alternatively, TLCs were transiently stained by iodine stain to enable subsequent mass spectrometry.

Therefore, after running, the silica plate was placed within an airtight glass chamber with a vessel containing a small amount of elemental iodine (I_2) until bands were stained. The silica plate was imaged and then left until bands were destained by iodine sublimation.

2.8.7. *In vitro* assays using purified recombinant protein

Purified recombinant protein was used in different *in vitro* activity assays. Chlamydial amidases were used in TLC-based activity assays (2.8.5.1.) and in dye-release assays (2.8.5.2.). To determine putative effects of inhibitory compounds, dye release assays were modified. To test if purified AmiA could bind to PGN, pulldown assays were performed (2.8.5.3.).

2.8.7.1. Activity on lipid II

Activity of AmiA_Ct on lipid II was determined similarly to the method described by Klöckner *et al.* (2014) for AmiA_Cp. The PGN precursor lipid II *m*DAP was used as a substrate. After desiccation of 2 nmol lipid II, the substrate was dissolved in H_2O, 50 mM Tris-HCl pH 7 and 5 % (v/v) DMSO calculated to a total volume of 40 µL by vortexing for one minute. The reaction was started by adding 2 µM enzyme and incubated at 37 °C overnight. Reactions were analyzed by TLC according to section 2.8.6.1.

2.8.7.2. Dye release assay

Dye release assays were used to determine amidase activity of purified recombinant chlamydial amidases, to test pH dependency and inhibition by metal chelators. The experiment is based on the release of azo dye Remazol Brilliant Blue (RBB) bound to PGN sacculi upon amidase activity. RBB-stained PGN sacculi were prepared from *E. coli* W3110 (2.8.5.) Assays had a total volume of 50 µL containing 2 µM enzyme, 0,5 mg/mL RBB-PGN, 50 mM Tris-HCl pH 8.5, 150 mM NaCl, 2 mM $MgCl_2$, 20 µM $ZnCl_2$ and 0,1 % (v/v) Triton X-100. For inhibitor assays, the DMSO-dissolved compounds were added in a 1:100 molar ratio (enzyme:inhibitor). pH was adjusted with MES pH 5.5, MES pH 6.5, MOPS pH 7.5 and CHES pH 9.5 for pH dependency analysis. Enzyme was always added last. Dye release assays were incubated at 37 °C for 1 h. Absorbance of the supernatant was measured at 595 nm in a plate reader and was proportional to enzymatic activity.

2.8.7.3. Assessment of PGN binding properties of AmiA by pulldown assays

Pulldown assays were performed to determine binding affinity to PGN by AmiA_Ct. To eliminate non-functional and insoluble protein prior to the experiment, enzymes were pre-incubated for 30 min in buffer (50 mM Tris-HCl pH 8.5, 150 mM NaCl, 2 mM $MgCl_2$, 20 µM $ZnCl_2$). After centrifugation at 134,000 x *g* at 4 °C for 30 min, the protein-containing supernatant was added to to an equal volume of a 2 mg/mL suspension of PGN from *Bacillus (B.) subtilis* (Sigma-Aldrich), which was heat-inactivated at 100 °C for 10 min prior to the experiment. Tubes were incubated at 4 °C for 30 min and then centrifuged again. Samples taken from the supernantant represent unbound enzyme, while pellets were resuspended in 200 µL buffer and incubated on ice for 30 min, then centrifuged again. Supernatants and

pellets were sampled and represent washing fraction and bound enzyme, respectively. Samples were analyzed by SDS-PAGE.

2.8.8. Mass Spectrometry

Mass spectrometry was performed for detection of reaction products of AmiA_Ct cleaving PGN precursor lipid II. ESI-MS(-) was performed RG Priv. Doz. Dr. Marianne Engeser (Kekulé institute for organic chemistry and biochemistry, University of Bonn).

2.9. Complementation assays with *E. coli* mutant strains

To determine if AmiA_Ct is able to rescue cell separation in AmiA-deficient *E. coli* mutant strains, *in vivo* complementation assays with *E. coli* ADE24 were performed. The strain is deficient in AmiA, AmiB and AmiC, but harbors *amiC* on an arabinose-inducible pBAD33 plasmid. The mutant was transformed with pASK-IBA3-*ct268* encoding AmiA_Ct and grown in the presence of 0.8 % glucose, 100 ng/mL anhydrotetracycline (aTc) and 0.5 mM $ZnCl_2$. At an OD of 0.4, 2.5 µL of the culture were sampled, stained and analyzed on agarose slides on a Zeiss AxioObserver Z.1 using a 100 x magnification objective with immersion oil.

2.10. Investigation of antichlamydial effects in tissue-culture based *Chlamydia* infection models

Different compounds were used in tissue culture-based chlamydial infection models to discover putative effects on *C. trachomatis* and to determine the minimal inhibitory concentration (MIC) Therefore, eukaryotic host cells were infected with *C. trachomatis* and treated with compounds of interest. Potential effects of respective compounds on the host cell were determined beforehand with AlamarBlue cell viability assays (2.10.2.). Additionally, compounds were used in recovery model experiments. All experiments except for the AlamarBlue cell viability assay were evaluated using fluorescence microscopy (2.10.6.).

2.10.1. Preparation of HEp-2 cells

Routinely, HEp-2 cells were used for cytotoxicity assays, MIC determination and recovery assays with *C. trachomatis* D/UW-3/CX. Cells were passaged as described in section 2.6.4.2. and plated into 96 well plates for cytotoxicity assays and MIC determinations and into 12 well dishes for recovery assays. Therefore, cells were counted with a Bürker-Türk/Thoma chamber. For counting, cell suspensions were mixed 1:1 with 0.4 % trypan blue (Thermo Fisher Scientific) to distinguish live and dead cells. Based on the cell number, cells were diluted in DMEM-medium to an appropriate volume and transferred to a plate. Routinely, cells were incubated for 72 h prior to infection. For microscopy, cells were plated into black 96 well plates (µ-Plate 96 well black, Ibidi, Gräfeling, Germany). For cytotoxicity assays, flat-base clear 96 well plates (Sarstedt, Nümbrecht, Germany) were used. In 96 well plates, 35000 cells/mL corresponding to 7000 cells/well were plated. For recovery assays, cells were plated into transparent Cellstar TC 12 well plates (Greiner Bio-One). Here, 25000 cells/mL corresponding to 50000 cells/well were prepared.

2.10.2. AlamarBlue cell viability assay

The AlamarBlue cell viability assay is based on the reduction of resazurin to highly fluorescent resorufin by living cells. Here, the fluorescence intensity of resorufin is proportional to cell viability. Cells in 96 well plates were rinsed once with DMEM-MIC and supplemented with fresh DMEM-MIC. In technical duplicates, compounds and solvent controls were applied in serial dilutions. Routinely, cells were treated with compounds for 18 hours and for 28 hours. After treatment, cells were rinsed twice with HBSS before AlamarBlue cell viability reagent diluted with HBSS was applied. Plates were incubated for one hour at 37 °C in the dark. Fluorescence was measured in a Tecan Spark® microplate reader (Tecan Group AG) and the Sparkcontrol Magellan 1.2 software (Tecan Group AG) at 570 nm.

2.10.3. Infection of host cells with *Chlamydia*

Prior to infection of HEp-2 cells with *C. trachomatis*, media was aspirated and cells were rinsed once with DMEM-MIC. Infection of host cells was achieved using frozen stocks of *C. trachomatis* EBs. The EB suspension was diluted in DMEM-MIC to an appropriate multiplicity of infection (MOI) and was transferred into the plate with host cells. For 96 well plates and 12 well plates, 100 µL/well and 1 mL/well were used for infection, respectively. To enable *Chlamydia* to enter the host cell, plates were incubated at 37 °C and 5 % CO_2 for two hours. The inoculum was aspirated and cells were washed two times with DMEM-MIC before being supplemented with fresh DMEM-MIC.

2.10.4. Determination of minimal inhibitory concentrations (MIC) against chlamydial infection

Compounds were tested for their MICs against chlamydial infections. Therefore, compounds were applied in serial dilutions to HEp-2 cells that prior have been infected with *C. trachomatis* D/UW-3/CX as described in 2.10.3. in 96 well plates for microscopy. Routinely, compounds were applied 2 hours post infections (hpi) and 12 hours post infection. These two points enabled to assess MICs for both distinct chlamydial morphological forms in productive chlamydial infections, EBs 2 hpi and RBs 12 hpi. Experiments were terminated 30 hpi by methanol fixation. Therefore, cells were rinsed twice with HBSS before 100 µL/well chilled 100 % (v/v) methanol was applied. Cells were incubated on ice for five minutes. Methanol was completely aspirated and cells were either stored at – 80 °C until further processing or immediately stained for microscopy.

2.10.4.1. Productive chlamydial infection

MICs for productive chlamydial infections were assessed by infection of HEp-2 cells as described in section 2.10.3 and 2.10.4. At the indicated points, tested compounds were applied onto infected cells in serial dilutions in technical duplicates. Solvent controls were also applied in technical duplicates at the same points. Experiments were terminated at 30 hpi.

2.10.4.2. Chlamydial infection in penicillin G-induced persistent state

For the determination of MICs on chlamydial infections that are in a penicillin G-induced persistent state, additional penicillin treatment was necessary after infection of the host cells. Therefore, 100 U/mL

penicillin G were added to infected cells 2 hpi. Additionally, serial dilution of tested compounds was performed in the penicillin-containing media at the indicated points. Experiments were terminated at 30 hpi.

2.10.4.3. Chlamydial infection in interferone (IFN)-γ-induced persistence

To induce IFN-γ-persistence in *C. trachomatis*, cells in 96 well plates were treated with 40 U/mL IFN-γ 48 hours after plating and 24 hours before infection. For infection, regular DMEM-MIC was used. Treatment with tested compounds and solvent controls at the indicated points was again performed in DMEM-MIC containing 40 U/mL IFN-γ. Experiments were terminated at 30 hpi.

2.10.5. Recovery Assay

To test whether *C. trachomatis* is able to recover and to reenter the developmental cycle after treatment with compounds of interest, recovery assays were performed. To assess recovery, infectious progeny of compound-treated chlamydial infections was assessed. HEp-2 cells were plated into 12 well dishes as described in 2.10.1 and incubated for 72 h. Cells were rinsed once with DMEM-MIC and subsequently infected with *C. trachomatis* D/UW-3/CX at an appropriate MOI as described in 2.10.3. After two hours, inocula were aspirated and infected cells were supplemented with fresh DMEM-MIC. For recovery of compound-treated penicillin G-induced persistent infections, media with 100 U/mL penicillin G was used to induce persistence. In serial dilutions, four different concentrations and corresponding solvent controls were applied at the indicated timepoints. To assess a suitable concentration range for the compound, prior results from cytotoxicity and MIC experiments should be considered. At 30 hpi, media containing compounds and solvent controls was aspirated and replaced with fresh DMEM-MIC without added compounds to allow for recovery. For active infections, plates were incubated at 37 °C and 5 % CO_2 for further 48 hours. Penicillin G-induced persistent infections were incubated for 72 hours. Meanwhile, HEp-2 cells were passaged and plated into a 96 well plate suited for microscopy with 35000 cells/mL as described in 2.10.2. and incubated for 72 hours. After incubation of infected cells allowing for recovery, infectious progeny of chlamydial infections was determined. Therefore, cells were scraped into the surrounding medium with a cell scraper and transferred into tubes containing glass beads. Cells were mechanically lysed by vortexing for one minute. Lysates were transferred into 2 mL tubes and centrifuged at 1500 x g for ten minutes. Meanwhile, cells plated in 96 well plates were rinsed once with DMEM-MIC. After centrifugation of the tubes containing cell lysates, supernatants were used to infect fresh monolayers in 96 well plates in suitable dilutions. Prior to harvest of infected cells, it is advisable to check for infection rates. If infection rates are high, supernatants used to infect fresh monolayers should be diluted 1:20 to 1:50. For low infection rates, supernatants can be applied in 1:2 to 1:5 dilutions in DMEM-MIC. For each condition, two dilutions should be applied onto fresh monolayers in four well per dilution. Other than in usual infections, cells are incubated for further 24 hours without a medium change 2 hpi. Then, experiments were terminated by methanol fixation. Until further processing, plates were stored at – 80 °C or stained immediately for fluorescence microscopy. For determination of

infectious progeny, 6 images per well were taken using fluorescence microscopy. By inclusion count and with regard to dilution factor and number fields of view, rates of infectious progeny could be determined.

2.10.6. Fluorescence microscopy

MICs for compounds used in chlamydial treatment and recovery rates of treated chlamydiae were determined by fluorescence microscopy. Prior to microscopy, fixated cells were stained using Pathfinder *Chlamydia* Culture Confirmation System (Bio-Rad) and DAPI. Pathfinder solution contains fluorescin-conjugated monoclonal murine antibodies specific for chlamydial lipopolysaccharide (LPS) and the dye Evan's blue that allows for staining of host cytoplasm. The solution was diluted 1:10 in PBS and stored in the dark at 4 °C until reuse. For staining, fixated cells were rinsed once with PBS before 100 µL/well Pathfinder staining solution were applied. Plates were incubated in the dark at 37 °C for 30 min. Afterwards, host cell nuclei were stained using the DNA-intercalating and binding substance DAPI. DAPI was applied at 0.1 µg/mL to the cells and incubated at room temperature for one minute. Afterwards, cells were rinsed two times with PBS and finally supplemented with 100 µL/well PBS for fluorescence microscopy. For MIC determinations and recovery rates, a Zeiss AxioObserver Z.1. fluorescence microscope (Zeiss) with 40 x magnification and Zen 3.6 (blue edition) software were used. For detailed images of chlamydial inclusions, a Zeiss AxioObserver with an Apotome 3 (Zeiss) was used with a 100 x magnification objective used with immersion oil and Zen 3.7 software was used. As light source, a TL LED was used and images were taken using an AxioCam 820 mono (Zeiss).

2.10.7. Quantitative analysis of fluorescence microscopy data

To determine MICs, data resulting from fluorescence microscopy were analyzed in a quantitative way. Therefore, CellProfiler software (Carpenter *et al.*, Broad Institute, MA, USA) was used. MIC determination in intracellular bacteria is different than in free-living bacteria, and definitions on determination mode can vary. In this work, the definition of Donati *et al.* (1999), that determines the MIC by ≥ 90 % reduction of infection rate was followed. Further, MIC was determined based on (Suchland, Geisler and Stamm, 2003) by ≥ 90 % reduction of inclusion size and ≥ 90 % alteration of chlamydial phenotype. Using CellProfiler software, inclusion sizes were determined from image data and converted to metric units. Infection rates were determined by ratio of infected cells in relation to uninfected cells. Determination of phenotype alteration was performed manually. Unless stated otherwise, two biological replicates with two technical replicates each were used for MIC determination. For graphic depiction, GraphPad Prism was used. Inclusion sizes were visualized by scatter plots, and mean values for each technical replicates and the mean and standard deviation of individual mean values was determined. For infection rates and phenotypes, bar charts and stacked bar charts were created, respectively. Statistical significance was determined by ordinary One-Way ANOVA.

2.11. Introducing genetic knockdowns using CRISPRi

CRISPRi technology was used to introduce conditional genetic knockdowns in *Chlamydia*. The method described in Ouellette (2018) and Ouellette et al. (2021) is based on an inactivated version of Cas9 protein, which is termed dCas9. In contrast to functional Cas9, dCas9 does not induce DNA cleavage, but reversibly binds to target DNA, and thereby prevents transcription. The method was used to generate genetic knockdowns for target genes *amiA, rodA, murJ* and *namZ*. Plasmid construction is further described in sections 2.7.7. and 2.7.7.2.

2.11.1. Transformation of *Chlamydia* and induction of CRISPRi construct expression

2.6 x 10^6 EBs of *C. trachomatis* L2P- were incubated with 2 µg of plasmid in a total volume of 50 µL buffer (10 mM Tris, 50 mM $CaCl_2$, pH 7.4) at room temperature for 30 min. Meanwhile, McCoy cell monolayers plated in 6 well dishes 24 hours prior were washed with 2 mL HBSS/well before 1 mL HBSS/well was added back. The transformation inoculum was mixed with 1 mL HBSS and added to cell monolayers for infection. For synchronous infection, cells were centrifuged at 400 *x g* for 15 min at RT and incubated at 37 °C for 30 min. Afterwards, inocula were aspirated and exchanged with DMEM + 10 % FBS + 10 µg/mL gentamycin. 8 hpi, media was replaced with DMEM containing the same amounts of FBS and gentamycin, and 1 µg/mL cycloheximide. For knockdowns of *rodA* and *namZ*, 500 µg/mL spectinomycin were added for selection. 48 hpi, chlamydial transformants were harvested and used for infection of fresh McCoy monolayers as described until a stable population of transformants was established. Transformation efficiency was assessed by GFP expression in fluorescence microscopy. EBs were harvested and stored in sucrose-phosphate buffer (2SP) at – 80 °C. Transformants were verified by isolation of plasmid DNA, restriction digest and sequencing. Once a construct for genetic knockdown was established, *C. trachomatis* L2P- was transformed as described previously and used for infection of McCoy cells in 6 well dishes at an MOI of 0.1. At 10 hpi, construct expression was induced by adding 5 nM aTc. Control wells were not added aTc. After CRISPRi knockdown construct expression, cells were sampled for DNA and RNA to quantify the level of construct expression and knockdown efficacy of genes of interest. Additionally, an immunofluorescence assay control was included. Therefore, McCoy cells were plated onto coverslips, enabling infected cells to be monitored using fluorescence microscopy later. Cells were sampled 10 hpi, 14 hpi and 24 hpi. For each condition, cells that were not treated with aTc were sampled.

2.11.2. Collection and processing of RNA samples from infected host cells

For RNA isolation, wells were rinsed once with 1 mL DPBS before cells were detached by addition of TRIzol™ reagent. By pipetting up and down, detached cells were transferred into tubes to which 200 µL $CHCl_3$ is added. Each tube was vortexed three times for 15 seconds, leaving 10 seconds in between vortexing steps. After incubation at room temperature for five minutes, tubes were briefly vortexed again and centrifuged at 3000 x g for 15 min for phase separation. After centrifugation, 500 µL of the upper phase were transferred into fresh tubes containing pure isopropanol. RNA samples were stored at – 80

°C until further use. For purification, RNA samples were centrifuged at 4 °C and 15000 x g for 15 minutes. The supernatant was poured off, and for washing, 0.5 mL 80 % (v/v) chilled ethanol was added to the pellets. Tubes were centrifuged at 16900 x g for 5 minutes. The washing step was repeated twice. Pellets were dried and then resuspended in 50 µL Tris-HCl pH 7.0. After quantification of RNA, 10 µg of each sample were transferred to fresh tubes and filled up to a total volume of 45 µL using nuclease-free water. To digest residual DNA, Turbo DNA-free kit™ (Invitrogen) was used. 5 µL of 10 x reaction buffer was added to the sample followed by 1.5 µL Turbo DNase. Samples were incubated at 37 °C for 30 min. Addition of Turbo DNase and incubation at 37 °C was repeated once. After addition of DNase inactivation reagent and vortexing every minute for five minutes, samples were spinned for two minutes at 16900 x g. A volume of 50 µL of wach samples was transferred into fresh tubes. To precipitate RNA, 50 µL of 5 M NH_4OAc were mixed with the sample before 300 µL pure ethanol was added. DNAsed RNA samples were stored at – 80 °C for at least 24 hours to precipitate. After thawing, samples were spinned at 15000 x g for 15 minutes at 4 °C. Supernatants were discarded and pellets were washed with 500 µL chilled 80 % (v/v) ethanol and by centrifugation at 16900 x g for 5 minutes. Supernatant was discarded and pellets were dried. Finally, pellets were resuspended in 15 µL Tris-HCl pH 7.0. After RNA quantification, samples were stored at – 80 °C until application in RT-PCR.

2.11.3. Collection and processing of DNA samples from infected host cells

For DNA sample collection, cells were washed with 1 mL DPBS per well. Cells were detached using 500 µL trypsin-EDTA and incubation at 37 °C for five minutes. Detached cells were transferred into fresh tubes and centrifuged at 3000 x g for 15 minutes. Supernatants were discarded and pellets were resuspended in 200 µL DPBS. Until further usage, samples were stored at – 80 °C. DNA was purified using DNeasy blood & tissue kit (Qiagen) according to the manufacturer's instructions and quantified using a NanoDrop. Equal DNA quantities were used in qPCR with an *euo* primer set to quantify chlamydial genomes to normalize respective transcript data.

2.11.4. Collection and processing of samples for immunofluorescence assay

In parallel to collection of RNA and DNA samples, immunofluorescence assay controls were established to monitor effects of genetic knockdowns using fluorescence microscopy. Therefore, McCoy cells were plated into 6 well dishes onto coverslips. Infection and induction was performed as described previously. At timepoints were sampling of RNA and DNA was performed, infected cells plated on coverslips were rinsed with 1 mL DPBS per well and then fixated by adding pure methanol. Cells were incubated at room temperature for 10 minutes. Methanol was withdrawn from cells and replaced with PBS-azide (0.025 %). Plates were stored at 4 °C until further processing.

2.11.5. Immunofluorescence assay (IFA)

To prepare samples for immunofluorescence microscopy, coverslips were transferred into 24 well dishes and rinsed twice with PBS-azide. Staining was performed by using primary and secondary antibodies, of which 250 µL were used per well. Each antibody reaction was incubated for 60 min at 37 °C. For

dCas9 visualization, RbαdCas9 (1:500) was used as primary antibody directed against dCas9 and DαR594 was used as secondary antibody. GtαMOMP (1:750) directed against chlamydial major outer membrane protein (MOMP) and DαG488 were used for visualization of MOMP.

2.11.6. Determination of infectious progeny (IFU Assay)

Infectious progeny was determined by reinfection of a cell monolayer with chlamydial EBs harvested from a primary infection. HeLa cells were infected with chlamydial transformants bearing constructs of interest. After induction or not with 5 nM aTc 10 hpi, EBs were harvested at 24 hpi by scraping cells in 2SP buffer. Samples were lysed during one freeze-thaw cycle, serially diluted and used to infect a new HeLa monolayer. To verify construct expression, infected cells plated on coverslips were fixated with 100 % MeOH for 5min and immunostained for MOMP and dCas9 and imaged as described previously. The secondary infection was maintained for 24h, then fixated with 100 % MeOH for 5 min and immunostained against MOMP. IFU titers were obtained by calculating the total number of inclusions per field of view based on counts of 15 fields of view.

3. Results

The main part of this work contributed to a better understanding of chlamydial cell division and the tightly interlinked processes of PGN remodeling and recycling. Cell division amidase AmiA of *C. trachomatis* (AmiA_Ct) was characterized *in silico*, *in vitro* and in overexpression hosts. Compounds with an inhibitory effect on AmiA_Ct were identified and included in *in vitro* experiments. Moreover, CRISPRi, a novel tool of genetic manipulation in *Chlamydia,* was used to assess the cellular effects of an *amiA* genetic knockdown in *C. trachomatis*. Further experiments investigated the effects of genetic knockdowns of components that are likely essentially involved in chlamydial PGN synthesis and cell division. The second part of this work focused on the establishment of a nutrient starvation-induced persistence model in *C. trachomatis* as a comparative tool to β-lactam induced persistence using compounds that chelate bivalent cations.

3.1. Characterization of AmiA_Ct

3.1.1. Comparative *in silico* analysis of AmiA_Ct

Through homology-based sequence comparison, an AmiA homolog (AmiA_Ct) was found to be encoded in *C. trachomatis* by gene *ct268*. The protein sequence has 59 % identity compared to AmiA of *C. pneumoniae* (AmiA_Cp) and 36 % identity compared to AmiA of *E. coli* (AmiA_Ec). The catalytic site of AmiA in the Gram-negative model organism *E. coli* is composed of three histidine residues, one aspartic acid and one glutamic acid coordinating a zinc atom (Cook *et al.*, 2023). An additional glutamic acid residue is described to act as a base catalyst in AmiA_Ec (Lupoli *et al.*, 2009). A schematic of the alignment (Fig. 4b) and the aligned amino acid sequences (Fig. 4c) reveal positional conservation of active site residues in chlamydial amidases compared to AmiA_Ec, except for residues D135 and E167. Moreover, Phyre2 predictions suggest that one histidine residue and one glutamic acid in all AmiA homologs shown here (H133 and E242 in *E. coli* AmiA) are located within β-sheets that form a binding grove within the enzymes (Fig. 4a). While this grove is clearly visible in chlamydial amidases according to the prediction, the supposed active site of AmiA_Ec is occluded by a helix structure that is part of a regulatory domain constructed by two helices (Yang *et al.*, 2012). In the inactive state, the inhibitory helix, depicted in green, occludes the active site of AmiA_Ec and is withdrawn through a conformational switch induced by interplay of the interaction helix (Fig. 4a, yellow) with a LytM factor-containing activator protein (Cook *et al.*, 2023). Such a regulatory structure is missing in chlamydial amidases, leaving the catalytic centers exposed constantly. In sequence alignments, this is reflected in two predicted helix structures within AmiA_Ec that do not align with chlamydial sequences (Fig. 4c). Another structural difference among the analyzed chlamydial proteins reflects the fact that AmiA_Cp was shown to have dual activity as amidase and carboxypeptidase mediated by an active serine within the PBP motif SxxK (Klöckner *et al.*, 2014). An additional SxN PBP motif is present in AmiA_Cp starting at S140. In Phyre2 models and sequence analyses, these residues are depicted in blue (Fig 4a-c).

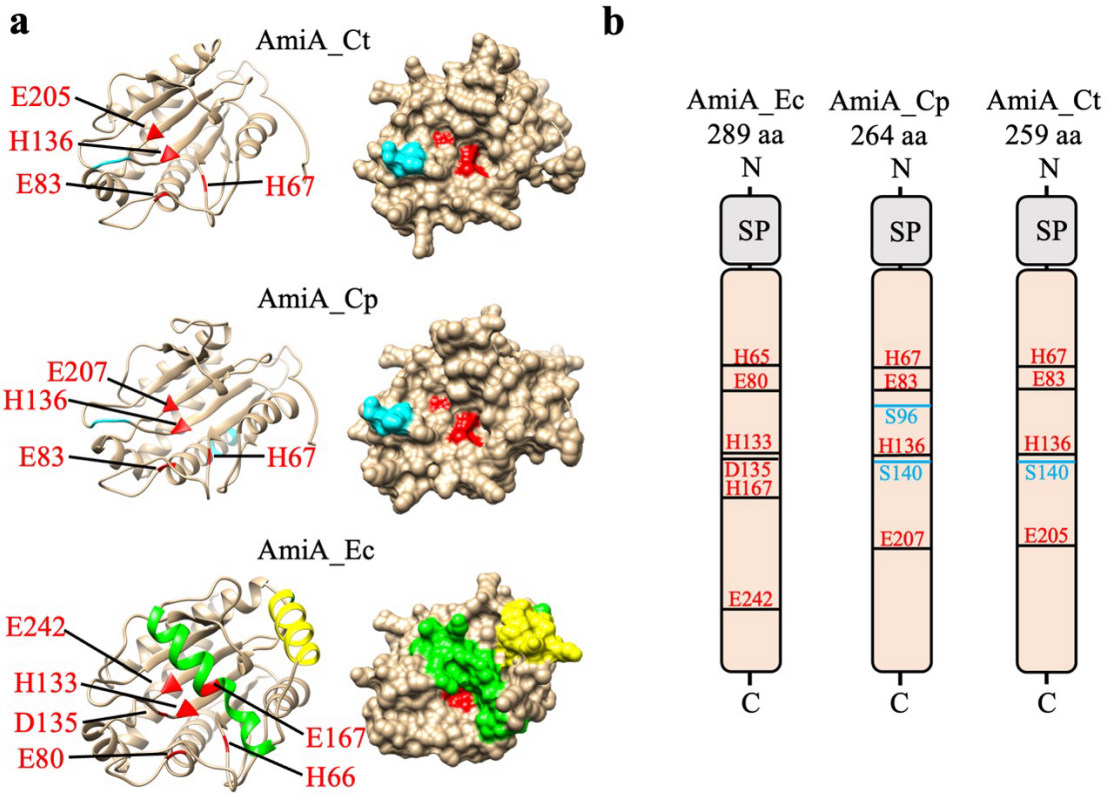

c

```
AmiA_Ec      -----MSTFKPLKTLTSRRQV--------LKAGLAALTLSGMSQAIAKDELLKTSNGHSK   47
AmiA_Ct      MRGIRSSNIRRLSLMIERLCVKPWQPFVNLTLLLLLLTLSSPVSCFA----------DA-   49
AmiA_Cp      MKLTKYLNTKQLRSMISRLFVRYSLPMSKQLSFFALCVL-GSHPIFA----------QTP   49
                    . : *  : .*  *            :   .* .    :*          .:

AmiA_Ec      PKAKKSGGKRVVVLDPGHGGIDTGAIGRN-GSKEKHVVLAIAKNVRSILRNHGIDARLTR  106
AmiA_Ct      AGIPKVSRNELIVIDPGHGGKDEGTADKELRYKEKTLALSIALSVQGCLRRMGYKTIMTR  109
AmiA_Cp      NPPQRVRRSEVIFIDPGHGGKDQGTASKELHYEEKSLTLSLALTVQSYLKRMGYKPQLTR  109
                 :   ..::.:****** * *: .::   :** :.*::* .*:. *:. * .  :**

AmiA_Ec      SGDTFIPLYDRVEIAHKHGADLFMSIHADGFTNPKAAGASVFALSNRGASSAMAKYLSER  166
AmiA_Ct      ATDVYVDLSKRAAIANQNKADVFVSIHCNHSSNTSALGTEIYFYNDKNI----------L  159
AmiA_Cp      SSDVYVDLGKRVALSNRGQGDVFISIHCNHSSNAAAFGTEVYFYNGKVGSP--------T  161
             : *.:: * .*. ::::  .*:*:***.:  :*  * *:.::  ..:

AmiA_Ec      ENRADEVAGKKATDKDHLLQQVLFDLVQTDTIKNSLTLGSHILKKIKPVHKLHSRNTEQA  226
AmiA_Ct      RT-----------------------------RKSESLGKSILAFMQKNGALRERKVKEG  189
AmiA_Cp      RN-----------------------------RMSEVLGKNILAAMEKNGILKSRGLKTA  191
             ..                             : *  **. **  ::    *:.*  : .

AmiA_Ec      AFVVLKSPSVPSVLVETSFITNPEEERLLGTAAFRQKIATAIAEGVISYFHWFDNQKAHS  286
AmiA_Ct      NFAVIRETTMPAVLVETGFLSNSKERAALLDARYRSHLAKGIAEGIHAFILNRQVDKTVS  249
AmiA_Cp      NFVVIRDTSMPAVLVETGFLSNSRERAALQDARYRMHVAKGIAEGVHNFLSGPSFQKPKQ  251
              *.*::. ::*:*****.*::* .*.  *  * :* ::*..****:  ::   . :*  .

AmiA_Ec      KKR----------                                                  289
AmiA_Ct      VSSGAKKVHK---                                                  259
AmiA_Cp      NIAKIRKPQIQAN                                                  264
                    *
```

d

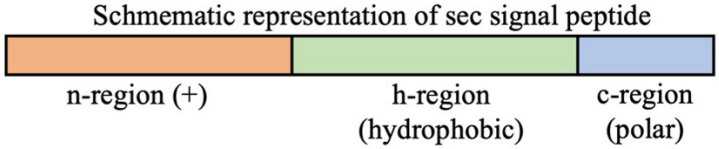

AmiA_Ct signal sequence (+3):
MRGIRSSNIRRLSLMIERLCVKPWQPFVNLTLLLLLLTLSSPVSCFADAA

AmiA_Cp signal sequence (+3):
MKLTKYLNTKQLRSMISRLFVRYSLPMSKQLSFFALCVLGSHPIFAQTP

Figure 4: *In silico* analysis of AmiA_Ct compared to AmiA_Cp and AmiA_Ec. (a) Phyre2 predictions of AmiA homologs of *E. coli, C. trachomatis* and *C. pneumoniae* show positions of catalytic residues (red), PBP motifs (blue) and the regulatory domain of *E. coli* AmiA (green + yellow) in ribbon models (left) and surface models (right). (b) Schematics of primary sequences of AmiA homologs reveal positional conservation of catalytic residues and conservation of PBP motif SxN starting at position 140 between chlamydial amidases. (c) Clustal Omega sequence alignment, confirming positional conservation of catalytic residues (red), also shows that AmiA_Ec has a regulatory domain consistent of two helix structures (green + yellow) which are absent in chlamydial amidases. Partial conservation in terms of positioning of PBP motifs (blue) is also confirmed for chlamydial amidases. Other conserved residues are highlighted in orange. Asterisks (*) indicate fully conserved residues between input sequences. Colons (:) indicate conservation of strongly similar properties, while periods (.) indicate conservation of weakly similar properties based on Gonnet PAM 250 matrix. (d) A schematic overview of the structure and physicochemical properties of sec signal peptides. In the amino acid sequences of predicted signal peptides of AmiA_Cp and AmiA_Ct, positively charged amino acids are depicted in orange, while hydrophobic amino acids are shown in green. Polar amino acids are highlighted in blue. Like shown for AmiA_Cp, periplasmic export of AmiA_Ct is likely to be mediated sec-dependently.

Sequence analysis revealed that only a SxN motif, but not the SxxK motif with the active serine residue, is conserved in AmiA_Ct and that these residues are not conserved in terms of positioning in AmiA_Ec. For the AmiA homologs considered here, a periplasmic localization is predicted. For *E. coli*, a tat-dependent export has been shown (Vollmer, Blanot and De Pedro, 2008), which is not feasible for chlamydial amidases, as a tat-system is absent in chlamydiae. Instead, a sec-dependent export for AmiA_Cp was shown (Klöckner *et al.*, 2014). A schematic overview of components found within the sequences of sec signal peptides confirms that AmiA_Cp contains the positively charged amino acids in the n-region, the hydrophobic amino acids in the h-region and the polar amino acids in the c-region typical of this secretion system (Fig. 4d). The predicted signal peptide of AmiA_Ct also matches these criteria, increasing the likelihood that AmiA_Ct is also exported into the periplasmic space in a sec-dependent manner. Taken together, *in silico* analysis showed positional conservation of the active site residues in AmiA_Ct compared to the AmiA homolog in *E. coli*. Sequence alignments reveal that PBP motifs as in AmiA_Cp are only partially conserved in AmiA_Ct and that a regulatory helix as found in AmiA_Ec is not present in chlamydial amidases, which could also be shown through structure prediction models.

3.1.2. AmiA_Ct rescues cell separation in an amidase-deficient *E. coli* mutant

To determine if AmiA_Ct can take over the function of the *E. coli* homolog and to investigate whether AmiA_Ct can complement an amidase-deficient *E. coli* mutant, a complementation assay with the mutant strain *E. coli* ADE24 was performed. Amidase triple mutant *E. coli* ADE24 (kindly provided by Prof. Waldemar Vollmer, University of Queensland) was transformed by electroporation with pASK-IBA3 encoding AmiA_Ct. Cells were grown in the presence of anhydrotetracyclin (aTc) to induce expression of *amiA*. At an OD_{600} of 0.4, microscopy was performed. Results showed that AmiA_Ct rescues cell separation in *E. coli*: under uninduced conditions, cells were predominantly present in chains of varying length, while induction of the *amiA*-overexpressing construct led to a prevalent single cell phenotype (Fig. 5a). An empty vector control was included in the experiment and confirmed the separation defect phenotype under uninduced and induced conditions. Indeed, quantitative analysis revealed > 50 % single cells under induced conditions compared to < 20 % single cells in the uninduced cells containing AmiA_Ct (Fig. 5b). In contrast, cells bearing the empty vector were almost exclusively present in unseparated aggregations. In sum, these results indicate that AmiA_Ct is functionally conserved. Like previously shown for AmiA of *C. pneumoniae* by Klöckner *et al.* (2014), AmiA_Ct is active in free-living bacteria and is likely able to take over the function of the *E. coli* protein.

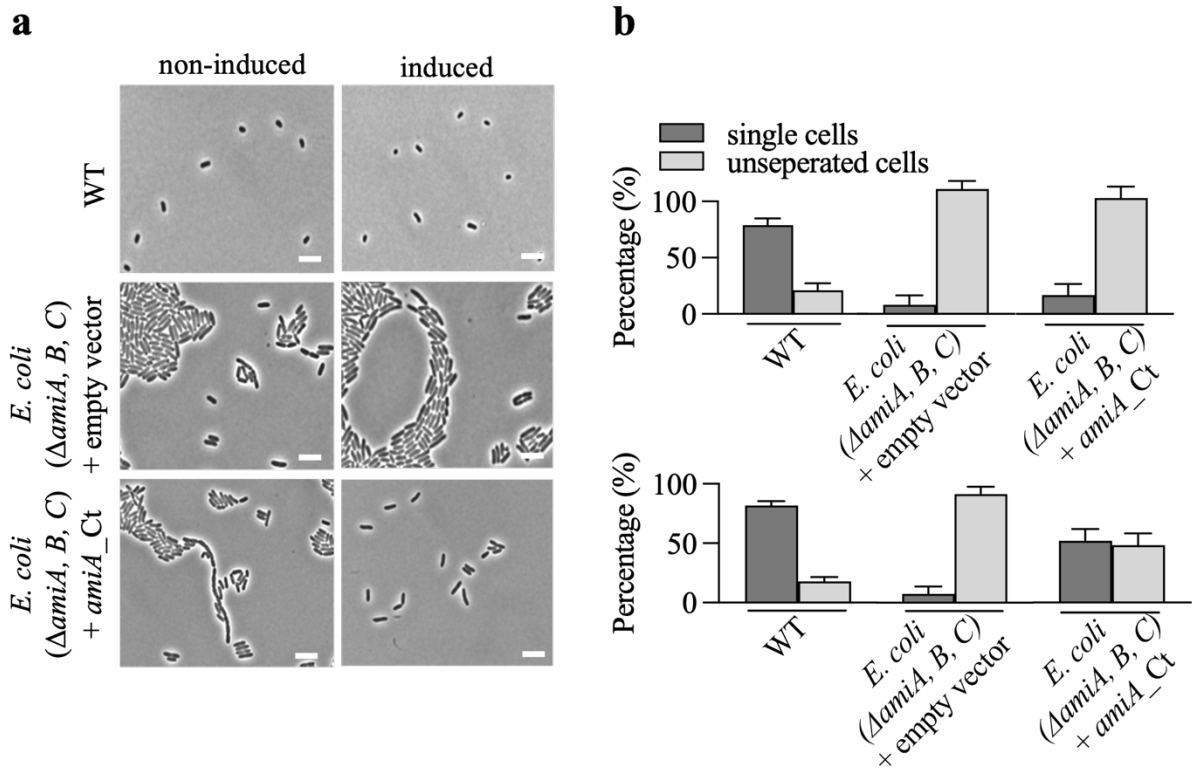

Figure 5: AmiA_Ct has conserved activity and assists in cell separation in an amidase-deficient *E. coli* mutant. Microscopy (a) and quantitative analysis (b) of amidase-deficient *E. coli* mutants expressing *amiA* of *C. trachomatis*. Induction of *amiA* expression with aTc rescued the cell separation deficient phenotype of *E. coli* triple knockout mutants and enabled cells to separate into single cells. Error bars indicate ± s.d. (n=3). Scale bar = 10 µm.

3.1.3. AmiA_Ct lyses a heterologous host strain upon overproduction

To further investigate AmiA_Ct function, we used an *E. coli* host for *amiA* overexpression. If AmiA_Ct is capable of cleaving PGN, the enzyme should lyse its producer strain upon overproduction like previously shown for AmiA homologs of *E. coli* and *C. pneumoniae* (Heidrich, Templin, Ursinus, Merdanovic, Berger, Schwarz, De Pedro and J.-V. Höltje, 2001; Klöckner *et al.*, 2014). *E. coli* JM83 was transformed with pASK-IBA3C-constructs encoding native *amiA*_Ct and three active site mutants. Additionally, an empty vector control and a construct encoding AmiA_Ct without its native signal peptide (AmiA_CtΔSP) were included. Only native AmiA_Ct lysed the producer strain, while active site mutants and AmiA_CtΔSP could not. Growth curves indicate that lysis due to AmiA_Ct started few hours after induction at an OD_{600} of approx. 0.5 and continued for several hours before reaching a plateau (Fig. 6). Periplasmic export of the protein was mediated by the native signal peptide of AmiA_Ct. Growth curves showed that all AmiA_Ct active site mutants failed to lyse the producer strain, indicating that both histidine residues and the glutamic acid residue are equally important for enzymatic activity.

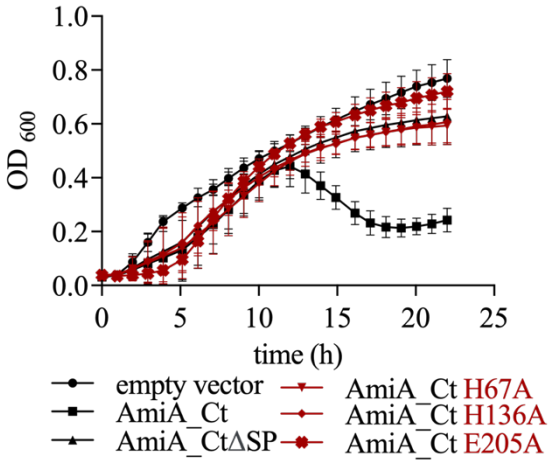

Figure 6: AmiA_Ct lyses an *E. coli* host strain upon heterologous overproduction. *E. coli* JM83 was transformed with pASK-IBA3C encoding either native *amiA*_Ct or *amiA*_CtΔSP, or the active site mutants. In a 96 well plate, cells were cultivated in LB medium at 37 °C in a Tecan microplate reader after inoculation with 1 % overnight precultures. Expression was induced at OD_{600} 0.2 - 0.4 using 200 ng/mL aTc. Cells were grown over night and optical density was monitored every 15 min after brief shaking of the plate at constant temperature of 37 °C. *E. coli* JM83 was lysed by native AmiA_Ct, but not by AmiA_CtΔSP and active site mutants. Error bars indicate ± s.d. (n=3).

3.1.4. Recombinant AmiA_Ct is active *in vitro*

To determine *in vitro* activity of AmiA_Ct, the protein was heterologously overproduced fused to a Strep-Tag II and purified by affinity chromatography. PGN sacculi prepared from *E. coli* W3110 were stained with the azo dye Remazol Brilliant Blue (RBB) and used in dye release assays to assess activity of AmiA_Ct on PGN. Upon cleavage of RBB-PGN, the dye is released and can be quantified in the supernatant after centrifugation by measuring absorbance at 595 nm. Results from dye release assays showed that AmiA_Ct cleaved RBB-stained PGN *in vitro*, while a purified active site mutant did not

(Fig. 7a). Moreover, the activity of AmiA_Ct on RBB-PGN was comparable to the activity of AmiA_Cp and of lysozyme, which were included as positive controls. By performing the experiment in different buffer conditions, pH dependency of the reaction could be demonstrated (Fig. 7b). AmiA_Ct showed highest activity at pH 9.5, indicating that the reaction optimum is at alkaline pH conditions. To investigate if AmiA_Ct was also able to cleave the PGN precursor and not only the mature PGN, purified lipid II *m*DAP was used as a substrate. AmiA_Ct was incubated with lipid II *m*DAP at 37 °C overnight and after extraction with butanol-pyridine acetate, reaction products were analyzed by thin layer chromatography. Results confirmed that AmiA_Ct, but not its active site mutant (AmiA_Ct H67A) cleaves off the peptide side from lipid II *m*DAP, yielding a peptide and an undecaprenyl-pyrophosphoryl-MurNAc-GlcNAc moiety (Fig. 7c). Activity of AmiA_Ct on lipid II *m*DAP was confirmed by mass spectrometry (Fig. 7d-e). The molecular mass of the product undecaprenyl-pyrophosphoryl-MurNAc-GlcNAc could be detected in the reaction containing AmiA_Ct (lower panel), whereas it was not present in the negative control reaction without any enzyme (upper panel). Instead, in this reaction the educt lipid II *m*DAP was detected by mass. Moreover, in contrast to AmiA from *C. pneumoniae,* which was characterized as a bifunctional enzyme conferring additional carboxypeptidase activity, biochemical analysis revealed that, in line with *in silico* analysis, AmiA_Ct is a monofunctional amidase.

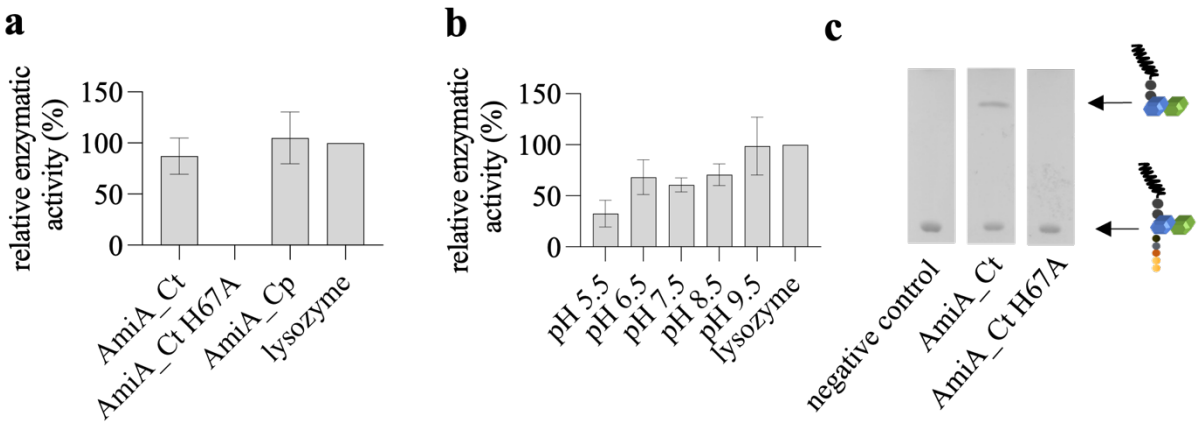

d

Sample	m/z calculated	m/z measured	Symbol
Undecaprenyl-pyrophosphoryl-MurNAc-(GlcNAc)-pentapeptide (lipid II *m*DAP)	1919.05	958.51 $[M-H]^{2-}$	
Undecaprenyl-pyrophosphoryl-MurNAc-(GlcNAc)	1332.79	1331.78 $[MH]^{-}$	

e

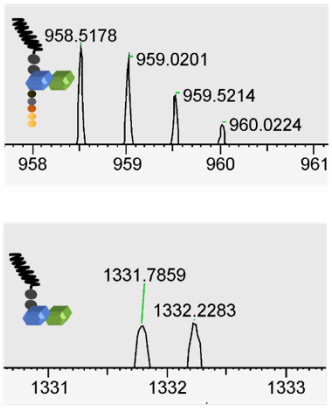

Figure 7: Recombinant AmiA_Ct is active *in vitro* on PGN and precursor molecule lipid II mDAP. (a) Dye release assays showed PGN-cleaving activity of AmiA_Ct which was comparable to activity of AmiA_Cp and lysozyme, whereas an active site mutant of AmiA_Ct did not show any activity. (b) pH-dependency of the reaction could be shown in further dye release assays, demonstrating an alkaline pH optimum for AmiA_Ct. (c) While an active site mutant did not show any activity, AmiA_Ct cleaved PGN precursor lipid II mDAP *in vitro* and functioned as a monofunctional amidase. (d,e) The reaction product undecaprenylpyrophosphoryl-MurNAc-(GlcNAc) was identified by mass spectrometry, as well as the educt lipid II mDAP in the negative control. Error bars indicate ± s.d. (n=3).

3.1.5. AmiA_Ct binds to PGN *in vitro* independently from enzymatic activity

In a dye release assay in which AmiA_Ct and its active site mutant AmiA_Ct H67A were incubated in an equimolar ratio, a significant decline in activity was observed compared to assay conditions that included only AmiA_Ct (Fig. 8a). This could be explained with the sequestration of the substrate by the active site mutant and its consequent unavailability for the active enzyme. However, bioinformatic search for known motifs that mediate PGN binding in AmiA_Ct did not lead to a positive result. To test if AmiA_Ct binds to PGN *in vitro*, a pulldown experiment was performed. As substrate, commercially available purified PGN of *B. subtilis* was used and incubated together with the purified active site mutant enzyme AmiA_Ct H67A or with wild type AmiA_Ct. The unbound enzyme fraction was found in the

supernatant after a first centrifugation step, the weakly bound protein in the supernatant of a subsequent washing step, and the proteins bound to the precipitated PGN in the pellet. Samples were analyzed by SDS-PAGE and results showed that active site mutant AmiA_Ct H67A was completely bound to the substrate in the pellet (Fig. 8b). Wild type AmiA_Ct was detected in both the supernatant and the pellet, indicating that only a fraction of the enzyme bound to PGN and co-precipitated. To preclude that the rudimentary PBP motif SxN, starting at the serine residue at position 140, is contributing to PGN binding, the expression vector encoding AmiA_Ct was mutagenized by replacing the serine with an alanine. As expected, the AmiA_Ct S140A mutant bound the substrate and no protein was present in the supernatant, indicating that S140A is not conferring PGN binding affinity (Fig. 8b). In addition, amidase activity of AmiA_Ct S140A was only slightly impaired in a dye release assay compared to wild type AmiA_Ct (Fig. 8c). In sum, complete binding of active site mutant AmiA_Ct H67A, that has no activity on PGN in *in vitro* dye release assays, indicates that PGN binding of AmiA_Ct is independent from its enzymatic activity.

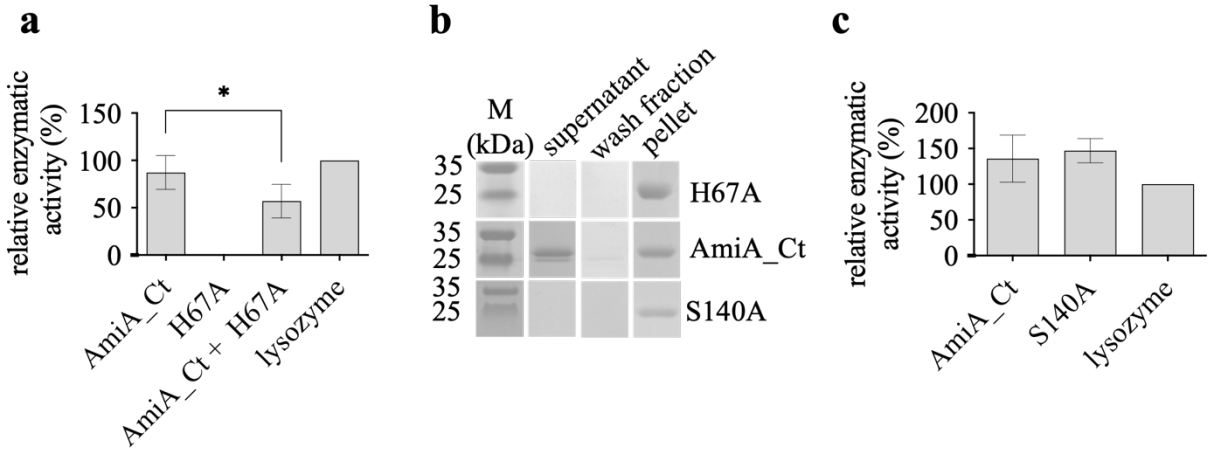

Figure 8: AmiA_Ct binds to PGN *in vitro*. (a) Dye release assays revealed a significant decline in activity of AmiA_Ct when incubated with an active site mutant in an equimolar ratio (unpaired t-test, one-tailed, *p-value ≥ 0.05). (b) To investigate this observation, pulldown assays with PGN as a substrate were performed and analyzed by SDS-PAGE to determine if AmiA_Ct binds to PGN. AmiA_Ct H67A bound to PGN completely, while AmiA_Ct with an intact catalytic center was also present in the unbound fraction. Mutant AmiA_Ct S140A was included to test if PGN binding is mediated by PBP motif SxN, which was not confirmed in pulldown assays. (c) AmiA_Ct S140A still showed activity in dye release assays. Error bars indicate ± s.d. (n=3).

3.1.6. AmiA_Ct can be inhibited by metal chelators *in vitro*

After *in vitro* activity of AmiA_Ct on PGN was demonstrated in this study, ways to inhibit the reaction *in vitro* were investigated. As experiments involving mutagenesis of the active site indicate that AmiA_Ct, like AmiA of *E. coli*, is a zinc-dependent enzyme, chelators of bivalent cations should remove the metal ion from the active site and, thereby, inactivate the enzyme. To investigate this, experiments using chelating agents 1,10-phenanthroline, the antiseptic clioquinol and N,N,N',N'-tetrakis(2-

pyridinyl)-1,2-ethanediamine (TPEN) were performed to determine their inhibitory effect in dye release experiments with AmiA_Ct in a molar ratio of 1:100 (enzyme : inhibitor). Dye release assays were performed in pH conditions ranging from pH 5.5 to pH 9.5 and showed that the chelation agents acted in a pH-dependent manner *in vitro*. Clioquinol significantly inhibited AmiA_Ct at pH 8.5 and pH 9.5 but showed no significant effects at lower pH (Fig. 9a). Conversely, the inhibitory effect of 1,10-phenanthroline was significant in all tested pH conditions but was most profound in acidic conditions at pH 5.5 and pH 6.5 (Fig. 9b). TPEN significantly inhibited the reaction at a neutral pH of 7.5 and in alkaline conditions at pH 8.5 and pH 9.5 (Fig. 9c). Dye release assays with clioquinol and different concentrations of added zinc were performed to test if the inhibitory effect could be attributed to the chelation of zinc through the tested compounds. In these experiments, 2 µM AmiA_Ct were incubated with 200 µM clioquinol at pH 9.5. By the addition of zinc, clioquinol was hypothesized not to withdraw zinc from the active centers of enzymes anymore, as excess zinc was already present. Indeed, at a concentration of 50 µM zinc chloride, which is one quarter in relation to clioquinol, the inhibitory effect was entirely averted and AmiA_Ct activity was rescued (Fig. 9d). In sum, chelation agents of bivalent cations inhibited catalytic activity of AmiA_Ct *in vitro* in a pH-dependent manner. The inhibitory mechanism is hypothesized to rely on the sequestration of the zinc ion from the enzyme's catalytic center.

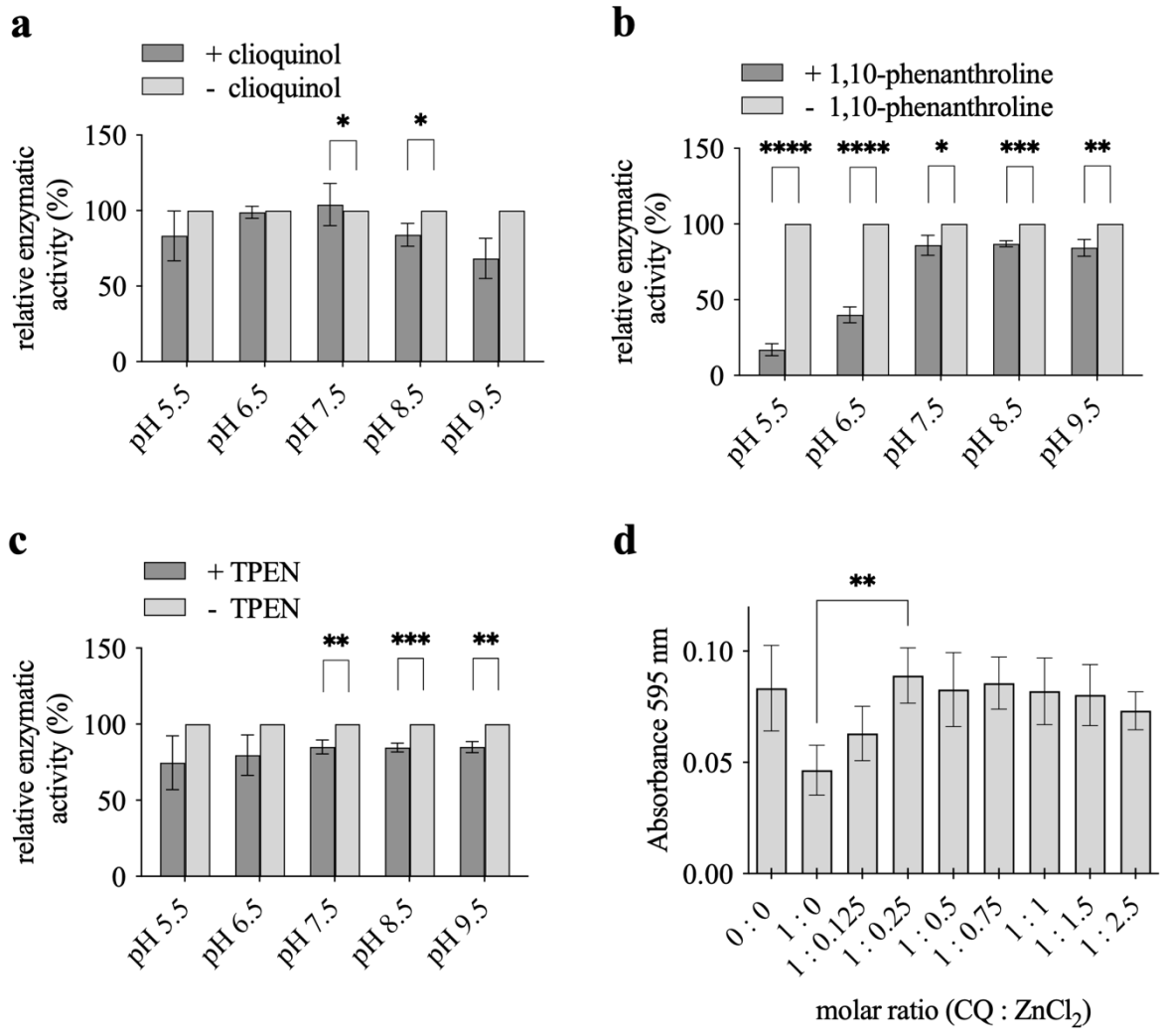

Figure 9: AmiA_Ct is inhibited by chelators of bivalent cations *in vitro*. The antibiotic clioquinol (CQ) (a), 1,10-phenanthroline (b) and TPEN (c) inhibited AmiA_Ct in dye release assays in a pH-dependent manner. (d) Upon addition of excess $ZnCl_2$ to the reaction, the inhibitory effect of CQ was prevented, suggesting that enzyme inhibition relies on the sequestration of the zinc atom by chelators. Error bars indicate ± s.d. (n=3). Unpaired t-test, two-tailed. Significance: * = $p \leq 0.05$, ** = $p \leq 0.01$, *** = $p \leq 0.001$, **** = $p \leq 0.0001$.

3.2. Effects of CRISPRi-induced conditional genetic knockdowns of *amiA* in *C. trachomatis*

CRISPR interference technology (CRISPRi) enables conditional inducible knockdowns of targeted genes. The role of AmiA in chlamydial cell division processes was further investigated by targeting *amiA*_Ct. Therefore, CRISPRi vectors either only targeting *amiA*_Ct or, in addition, simultaneously overexpressing *amiA*_Ct as a complementation were constructed and transformed into *C. trachomatis* (-pL2). The effects on *C. trachomatis* were monitored after transformation into eukaryotic host cells and induction. Clickable D-alanine dipeptides (EDA-DA) were used to detect chlamydial PGN, while immunostaining against chlamydial major outer membrane protein (MOMP) enabled the visualization of chlamydial cells. CRISPRi constructs were established in the group of Dr. Scot Ouellette (University of Nebraska) and experiments validating genetic knockdowns were performed as a part of this work

during a research stay in the lab of Drs. Scot Ouellette and Elizabeth Rucks, funded by the TRR261. Click chemistry and results involving the visualization of chlamydial PGN shown below were established and performed by Dr. George Liechti (Uniformed Services University).

3.2.1. Effects of *amiA* knockdown

To confirm that CRISPRi-mediated genetic knockdowns are functional and result in reduced RNA levels in *C. trachomatis*, RTqPCR was performed using RNA samples isolated from *C. trachomatis* under genetic knockdown conditions. HeLa cells were infected with *C. trachomatis* transformed with the CRISPRi plasmids pLCRia(NT), targeting a random sequence as a negative control, the *amiA* knockdown plasmid pLCRia(*amiA*) or pLCRia-*amiA*_6xH(*amiA*), harboring an inducible *amiA_Ct* copy for overexpression while simultaneously enabling a knockdown of chromosomal *amiA_Ct*. As controls, late gene *omcB,* encoding outer membrane complex protein B, and *euo,* encoding an early transcriptional regulator, were included in addition to *amiA* for amplification as representatives of genes expressed late and early in the chlamydial lifecycle, respectively. As *murE* is encoded downstream proximally to *amiA*, *murE* expression over time during knockdown was also monitored to exclude downstream effects of knockdown.

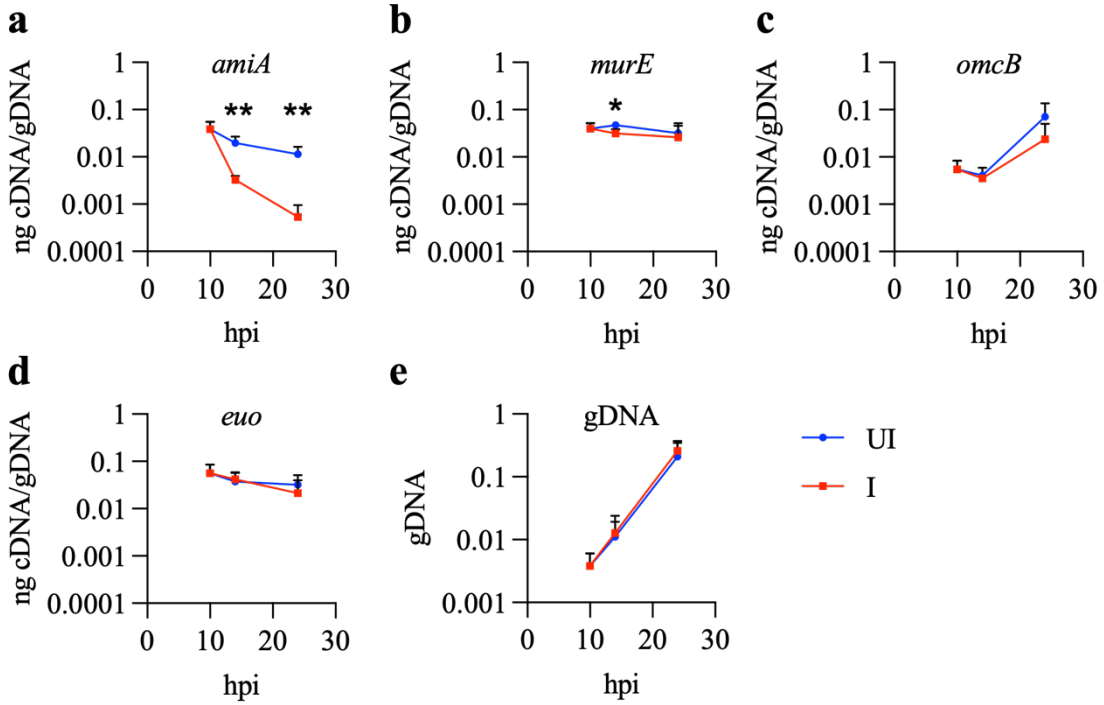

Figure 10: Gene expression during CRISPRi-mediated knockdown over time under uninduced (blue) and induced (red) conditions in *amiA* knockdown strain *C. trachomatis* pLCRia(*amiA*). Cultures were either induced or not at 10 hpi with 5 nM aTc and sampled for RNA and DNA at 10 hpi, 14 hpi, and 24 hpi. Samples for cDNA and gDNA were purified and included in RTqPCR. Levels of respective cDNA were analyzed in relation to gDNA levels and are presented accordingly. (a) Under induced conditions, *amiA* cDNA levels were significantly decreased at 14 hpi and 24 hpi compared to the uninduced control. (b) *murE* expression levels remained constant with minor alterations between induced and uninduced samples. (c) Expression of late gene *omcB* increased while expression levels of

euo decreased (d) over time with no significant differences in between induced and uninduced samples. (e) gDNA levels in both uninduced and induced samples augmented over time and showed no quantitative differences. UI = uninduced, I = induced. Error bars indicate ± s.d. (n=3). Unpaired t-test, two-tailed. Significance: * = $p \leq 0.05$, ** = $p \leq 0.01$.

Analysis of RTqPCR data showed that cDNA levels of *amiA* significantly decreased over time in the knockdown strain *C. trachomatis* pLCRia(*amiA*) under induced conditions, but not in the uninduced samples (Fig. 10a). At 24 hpi, cDNA amounts of *amiA* were decreased more than tenfold compared to the uninduced control. Together with transcript levels of *murE*, *omcB* and *euo*, which were included as controls, these results confirmed *amiA* knockdown on a molecular level. No effects could be observed for *murE* (Fig. 10b), which is encoded downstream of *amiA* in the chlamydial genome, indicating that *murE* expression was not affected by *amiA* knockdown. As controls, late gene *omcB* and early gene *euo* were included in RTqPCR. Levels of *euo* were highest 10 hpi and decreased slightly over the course of sampling (Fig. 10d). Conversely, amounts of *omcB* increased over time and highest amounts were observed 24 hpi (Fig. 10c), as expected. While minor differences were present in *murE* expression between uninduced and induced samples (Fig. 10b), no significant expression alteration was observable for *euo* (Fig. 10d) and *omcB* (Fig. 10c). Over time, gDNA levels were shown to increase (Fig. 10e), as expected.

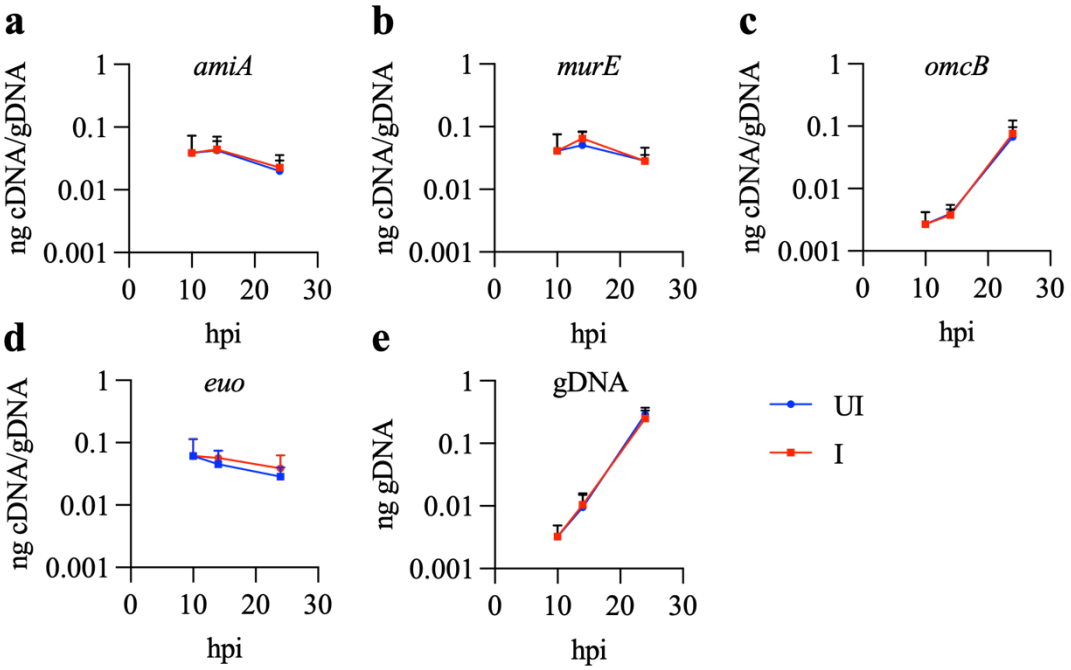

Figure 11: Gene expression during CRISPRi-mediated knockdown over time under uninduced (blue) and induced (red) conditions in *C. trachomatis* pLCRia(NT). Levels of *amiA* (a) and *murE* (b) cDNA are decreased at 24 hpi, but do not differ between uninduced and induced samples. (c) *omcB* cDNA levels increased over time but showed no differences in induced or uninduced conditions. (d) *euo* levels were decreased slightly over time, with no significant differences observable in the induced samples compared to the uninduced samples. (e) gDNA levels in both uninduced and induced samples

elevated over time and showed no quantitative differences. UI = uninduced, I = induced. Error bars indicate ± s.d. (n=3). Unpaired t-test, two-tailed. Significance: * = $p \leq 0.05$, ** = $p \leq 0.01$.

The non-targeting strain *C. trachomatis* pLCRia(NT) was investigated in terms of expression levels to exclude the possibility that decreased levels of cDNA are the result of other effects than targeted knockdown. cDNA levels of *amiA* and *murE* decreased over the course of the experiment and no differences could be observed between uninduced and induced samples (Fig. 11a-b). Like previously shown in the knockdown strain *C. trachomatis* pLCRia(*amiA*), *omcB* levels increased over time (Fig. 11c), while *euo* levels decreased over the course of the experiment (Fig. 11d). Moreover, gDNA levels were shown to increase and highest amounts were measured both for uninduced and induced samples at 24 hpi, as expected (Fig. 11e).

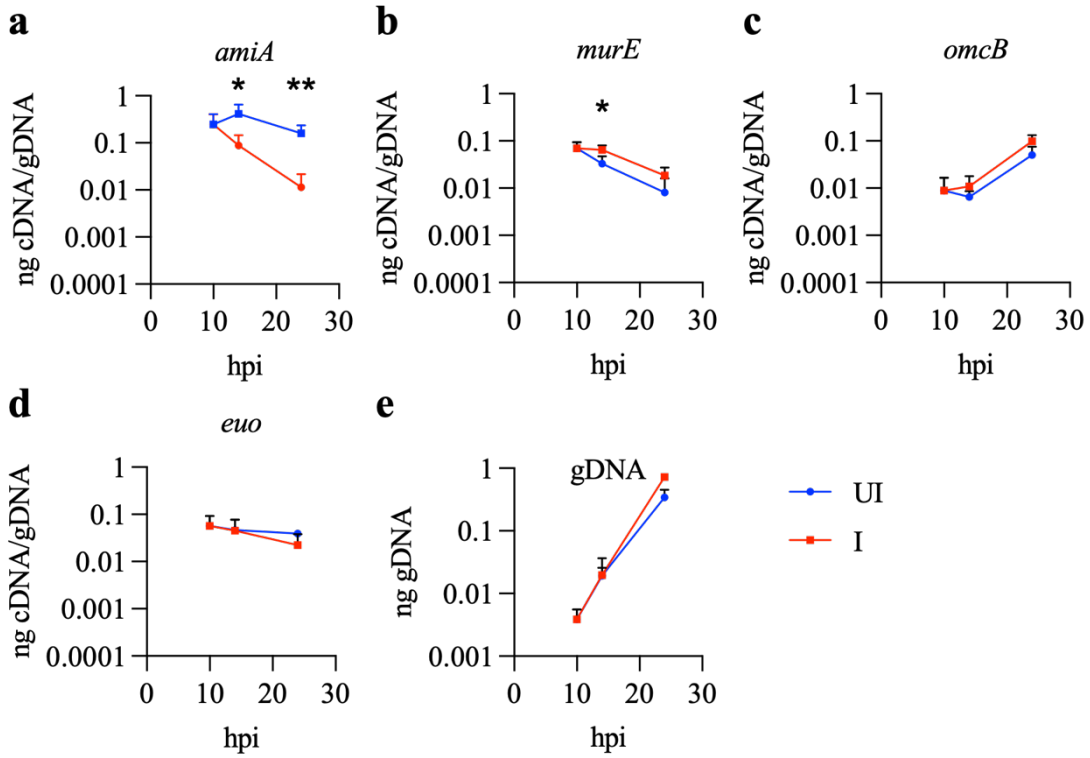

Figure 12: Gene expression during CRISPRi-mediated knockdown over time under uninduced (blue) and induced (red) conditions in *C. trachomatis* pLCRia-*amiA*_6xH(*amiA*). (a) Under induced conditions, *amiA* cDNA levels were significantly decreased at 14 hpi and 24 hpi compared to uninduced samples. (b) Expression of *murE* decreased over time with minor differences between uninduced and induced samples. (c) Levels of *omcB* expression were elevated at in late samples and had no significant differences between induced and uninduced samples. (d) *euo* levels slightly decreased over the course of sampling. (e) gDNA levels in both uninduced and induced samples elevated over time and showed no quantitative differences. UI = uninduced, I = induced. Error bars indicate ± s.d. (n=3). Unpaired t-test, two-tailed. Significance between induced and uninduced samples: * = $p \leq 0.05$, ** = $p \leq 0.01$.

Expression levels were also monitored in the complemented strain *C. trachomatis* pLCRia-*amiA*_6xH(*amiA*). A significant decrease was visible for *amiA* copy numbers over time in the induced strain compared to the uninduced strain. Expression levels of the uninduced sample decreased continuously over time, while they increased at 14 hpi in the induced sample and then decreased until 24 hpi (Fig. 12a). In general, as expected, a higher expression level of *amiA* was observed in the complemented strain, where *amiA* cDNA levels were more than tenfold higher than in the non-targeting strain (Fig. 11a) and in the knockdown strain (Fig. 10a) at 10 hpi. For *murE*, expression levels decreased over the course of the experiment with only slight differences between induced and uninduced samples (Fig. 12b). Like for the non-targeting and knockdown strain, *omcB* levels and gDNA amounts were increased over time (Fig. 12c), while *euo* levels declined slightly (Fig. 12d). For *euo* and *omcB*, no differences between induced and uninduced samples were observed. In sum, results of RTqPCR indicate that targeted knockdown of *amiA* was achieved successfully. Based on these control experiment, further experiments investigating the role of chlamydial AmiA in cell division of *C. trachomatis* and the effects of *amiA* knockdown on a cellular level were enabled.

3.2.2. Knockdown of *amiA* and complementation

The CRISPRi construct pLCRia(*amiA*), used for knockdown of the amidase encoding gene *amiA*_Ct, was transformed into *C. trachomatis* (-pL2), a strain not harboring the native plasmid. After infection of eukaryotic host cells and induction of dCas9 expression by aTc two hours after infection (2 hpi), the effects of *amiA* knockdown were monitored 24 hpi. At this time within the chlamydial infectious cycle, normally, inclusions are filled up with chlamydial RBs on the onset of redifferentiation into infectious EBs. Upon knockdown of *amiA,* chlamydial cells were enlarged and displayed a phenotype alluding to an inhibited cell division as shown by immunostaining directed against MOMP, a highly prevalent chlamydial protein located within the outer membrane (Fig. 13a). Moreover, close-up pictures of chlamydial cells showed that cells were halted in the budding phase of cell division (Fig. 13b), confirming the inhibited cell division phenotype. PGN labeling using EDA-DA showed that PGN seems to be concentrated at the budding poles of chlamydial cells.

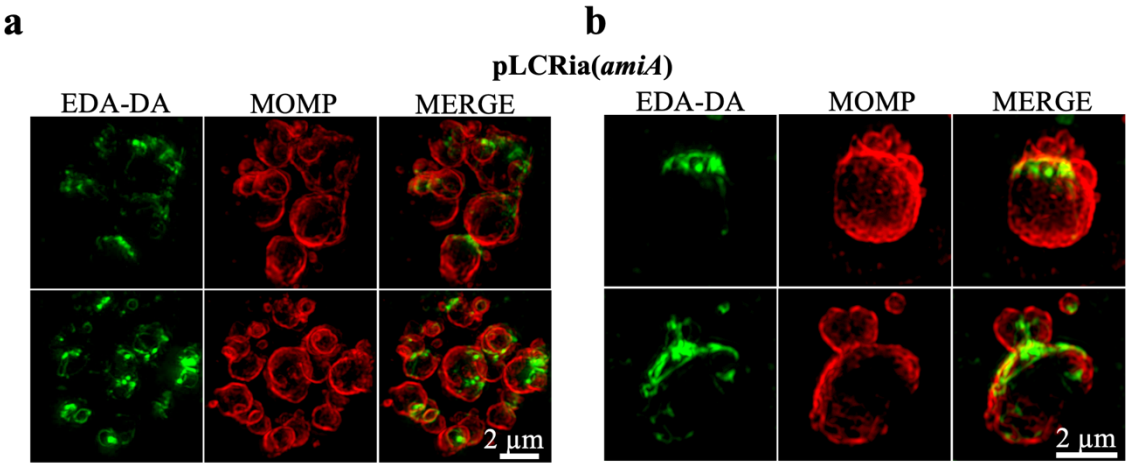

Figure 13: CRISPRi-mediated knockdown of *amiA* leads to chlamydial phenotypes related to impaired cell division in *C. trachomatis*. A construct encoding a CRISPRi system targeting *amiA*_Ct (pLCRia(*amiA*)) was transformed into *C. trachomatis* (-pL2). McCoy cells were infected with the transformants, and expression was induced with 1 nM aTc 2 hpi. Cells were fixed 24 hpi and imaged. Clickable D-alanine dipeptides (EDA-DA) were used for PGN labeling (green) and indirect immunostaining of MOMP (red) was used for visualization of chlamydial cells. (a) Knockdown of *amiA* resulted in enlarged chlamydial cells. (b) Cells displayed a phenotype of inhibited cell division with cells halted in the budding phase and PGN concentrated to the budding poles. Scale bar = 2 µm. EDA-DA = ethynyl-D-alanyl-D-alanine. MOMP = major outer membrane protein.

To investigate if the phenotype observed for *amiA* knockdowns could be complemented, the construct pLCRia-*amiA*_6xH(*amiA*), which leads to *amiA* knockdown while also overexpressing *amiA*_6xH, was transformed into *C. trachomatis* (-pL2). After infection of eukaryotic cells with chlamydial transformants, constructs were induced by aTc. The experiments revealed that the phenotype observed previously can be averted when *amiA* is complemented by overexpression simultaneously to knockdown (Fig. 14). Indeed, normal chlamydial cell size and phenotype was reinstated. PGN localization was no longer restricted to the area around the budding pole and PGN rings at the periphery of dividing cells could be visualized.

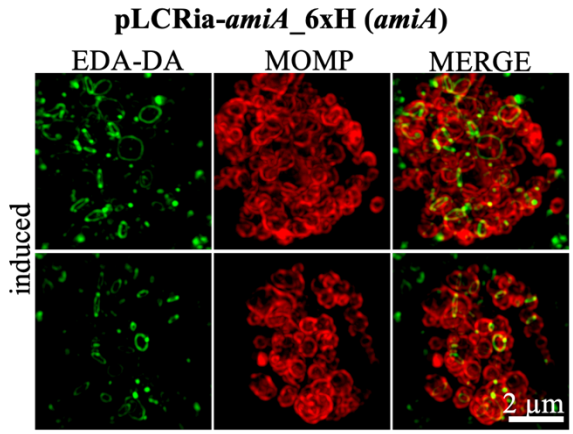

Figure 14: CRISPRi-mediated knockdown of *amiA* is complemented by overexpression of *amiA*. A CRISPRi construct targeted against *amiA*_Ct while simultaneously overexpressing *amiA*_Ct was transformed into *C. trachomatis* (-pL2). McCoy cells were infected with the transformants and expression was induced with 1 nM aTc 2 hpi. Clickable D-alanine peptides (EDA-DA) were used for PGN labeling. Cells were fixed 24 hpi and imaged by fluorescence microscopy. Complementation through *amiA*_Ct overexpression reinstated normal chlamydial phenotype and PGN localization. Scale bar = 2 µm. EDA-DA = ethynyl-D-alanyl-D-alanine. MOMP = major outer membrane protein.

In sum, knockdowns of *amiA* using CRISPRi showed multiple effects in *C. trachomatis*. Upon induction of knockdown, chlamydial cells were enlarged and seemed to be halted in the budding phase of cell division. Together with the phenotype indicating a cell division inhibition, visualization of PGN by click chemistry showed that PGN was located to the budding poles of cells stuck in the budding phase. Abnormal chlamydial growth and PGN localization was reversed by *amiA* overexpression, indicating that the observed effects are due to genetic knockdown of *amiA_Ct.*

3.2.3. Effects of *amiA* knockdown on PGN shown by EDA-DA PGN labeling

The results presented in the previous section indicated that CRISPRi-mediated knockdown of *amiA* affected PGN localization in *C. trachomatis*. Experiments including different CRISPRi constructs, such as pLCRia(*amiA*) and the complemented CRISPRi construct pLCRia-*amiA*_6xH(*amiA*), were performed to determine if genetic knockdowns have further effects on chlamydial PGN. The construct pLCRia(NT) expresses dCas9 targeted against a random sequence and served as a non-targeting (NT) control. Constructs were transformed into *C. trachomatis* (-pL2), induced with 5 nM aTc 23 hpi, and cells were imaged 24 hpi. Like in previous experiments, click-chemistry employing EDA-DA was used to visualize chlamydial PGN and immunostaining was used to detect chlamydial MOMP. While CRISPRi constructs were generated by Dr. Scot Ouellette and colleagues, experiments including click chemistry and quantitative data analysis were performed by Dr. George Liechti and colleagues.

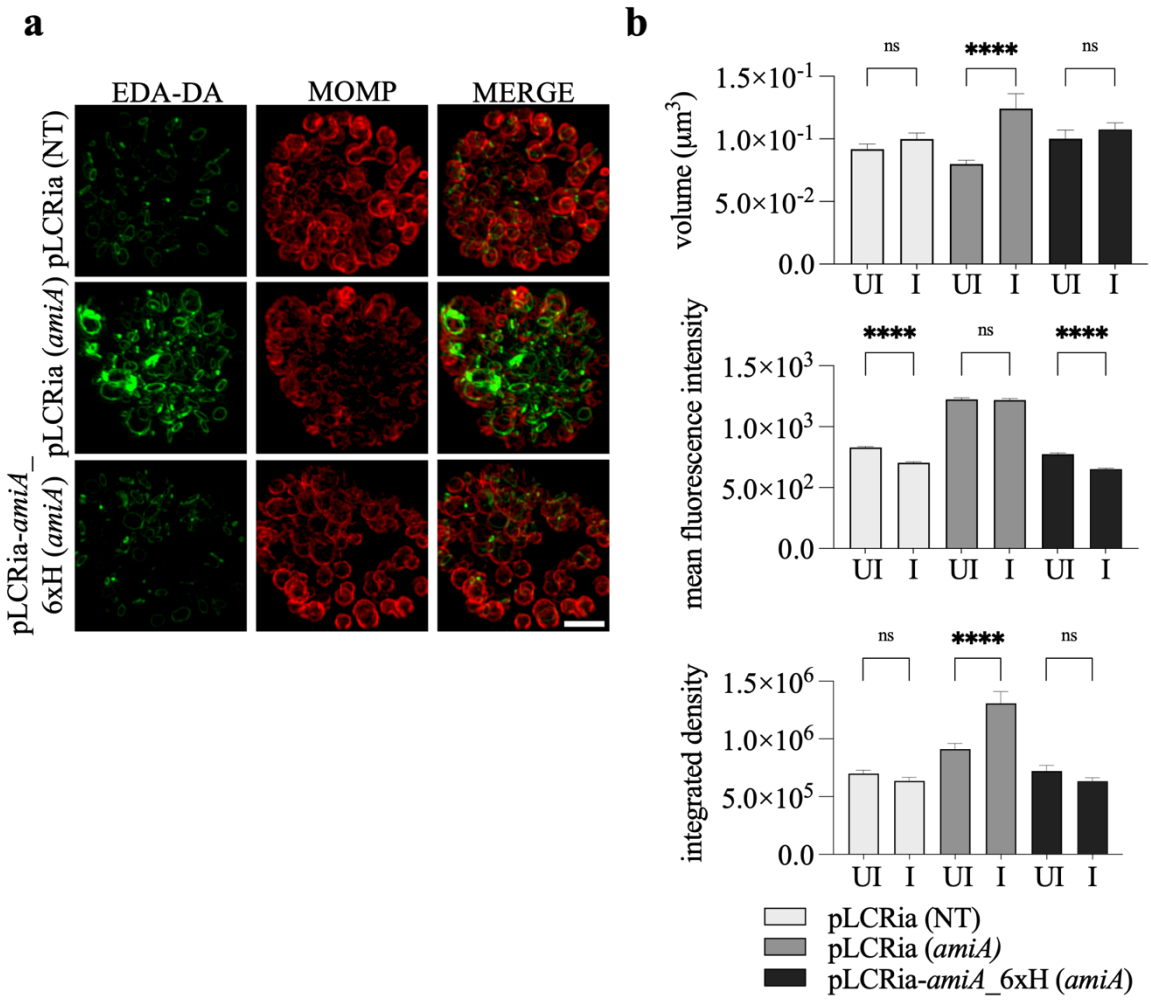

Figure 15: Effects of *amiA* knockdown on PGN in *C. trachomatis*. Constructs pLCRia(NT), pLCRia(*amiA*) and pLCRia-*amiA*_6xH(*amiA*) were transformed into *C. trachomatis* (-pL2). Resulting transformants were used to infect McCoy cells. Induction was performed with 5 nM aTC 23 hpi. After cells were fixed 24 hpi, immunostaining directed against MOMP and click-chemistry for visualization of chlamydial PGN were performed. (a) Fluorescence microscopy images reveal that fluorescence intensity is elevated in *C. trachomatis* transformed with the *amiA* knockdown construct pLCRia(*amiA*) compared to strains bearing the non-targeting (NT) and the complemented knockdown construct. (b) Quantitative analysis revealed that the volumes of imaged PGN structures were larger in the *amiA* knockdown strain under induced conditions compared to the uninduced control (top panels). The mean fluorescence intensity in the strain transformed with pLCRia(*amiA*) on average was higher than in the other two strains but did not differ whether induced or not (middle panel). The integrated density, a result of object volume and fluorescence intensity, is higher in the induced sample of *C. trachomatis* bearing the knockdown construct pLCRia(*amiA*) compared to the uninduced sample (bottom panel). Scale bar = 2 µm. Error bars indicate ± s.d. One-way ANOVA. Significance: * = $p \leq 0.05$, ** = $p \leq 0.01$, *** = $p \leq 0.001$, **** = $p \leq 0.0001$. UI = uninduced. I = induced.

Fluorescence images indicated that fluorescence intensity is elevated in *C. trachomatis* bearing the *amiA* knockdown construct pLCRia(*amiA*) compared to strains with the non-targeting construct (NT) or the complemented construct pLCRia-*amiA*_6xH(*amiA*) (Fig. 15a). Data about volume of PGN structures, fluorescence intensity and integrated density, as a combination of volume and fluorescence intensity, were obtained by quantitative analysis using 3D object counter by ImageJ (Fig. 15b). While PGN object volumes did not differ significantly in strains bearing pLCRia(NT) and pLCRia-*amiA*_6xH(*amiA*) in the induced compared to uninduced conditions, PGN structures were significantly larger for *C. trachomatis* carrying the knockdown plasmids not only under induced conditions compared to the uninduced samples, but also compared to the other two strains included in the experiment. The mean fluorescence intensity in *C. trachomatis* pLCRia(*amiA*) was elevated compared to the non-targeting and complemented strain, reinforcing the qualitative data (Fig. 15a). However, mean fluorescence intensity did not differ significantly between uninduced and induced samples, suggesting a higher background fluorescence intensity within the knockdown strain compared to the control and the complemented knockdown strains. Integrated density values in *C. trachomatis* pLCRia(*amiA*) were elevated compared to the other strains and induced samples within the knockdown strain showed higher values than the uninduced samples. Within the non-targeting and the complemented strain, differences in integrated density were not significant. Taken together, these data suggest that knockdown of *amiA* affects not only PGN localization, as shown in the previous section, but also the volume of imaged PGN structures. Labeling studies showed elevated intensity of labeled PGN under knockdown conditions, providing information about the amount of PGN present within the chlamydial cell at that stage.

3.2.4. Effects of *amiA* knockdown on infectious progeny of *C. trachomatis*

Effects of CRISPRi-mediated knockdown of *amiA*_Ct could be shown in previous experiments. Knockdown of *amiA* led to an inhibited cell division phenotype in *C. trachomatis*. To investigate whether knockdown affects chlamydial proliferation, inclusion forming units (IFU) assays were performed. Therefore, HeLa cells were infected with *C. trachomatis* (-pL2) transformed with either pLCRia(NT), pLCRia(*amiA*) or pLCRia-*amiA*_6xH(*amiA*). Expression was induced 10 hpi with 5 nM aTc, during differentiation from EBs to proliferative RBs. Cells were harvested and used to infect new HeLa monolayers as described in section 2.11.6. Immunostaining was performed to visualize MOMP and MOMP-labeled objects were counted to assess the number of inclusions per infected monolayer. Relative IFU values (%) were calculated in relation to uninduced samples. In parallel, immunofluorescence (IFA) assays were performed as described in 2.11.5. to monitor correct construct expression during the experiment. IFU experiments were performed by Dr. Jeonghoon Lee from the Rucks/Ouellette lab (University of Nebraska).

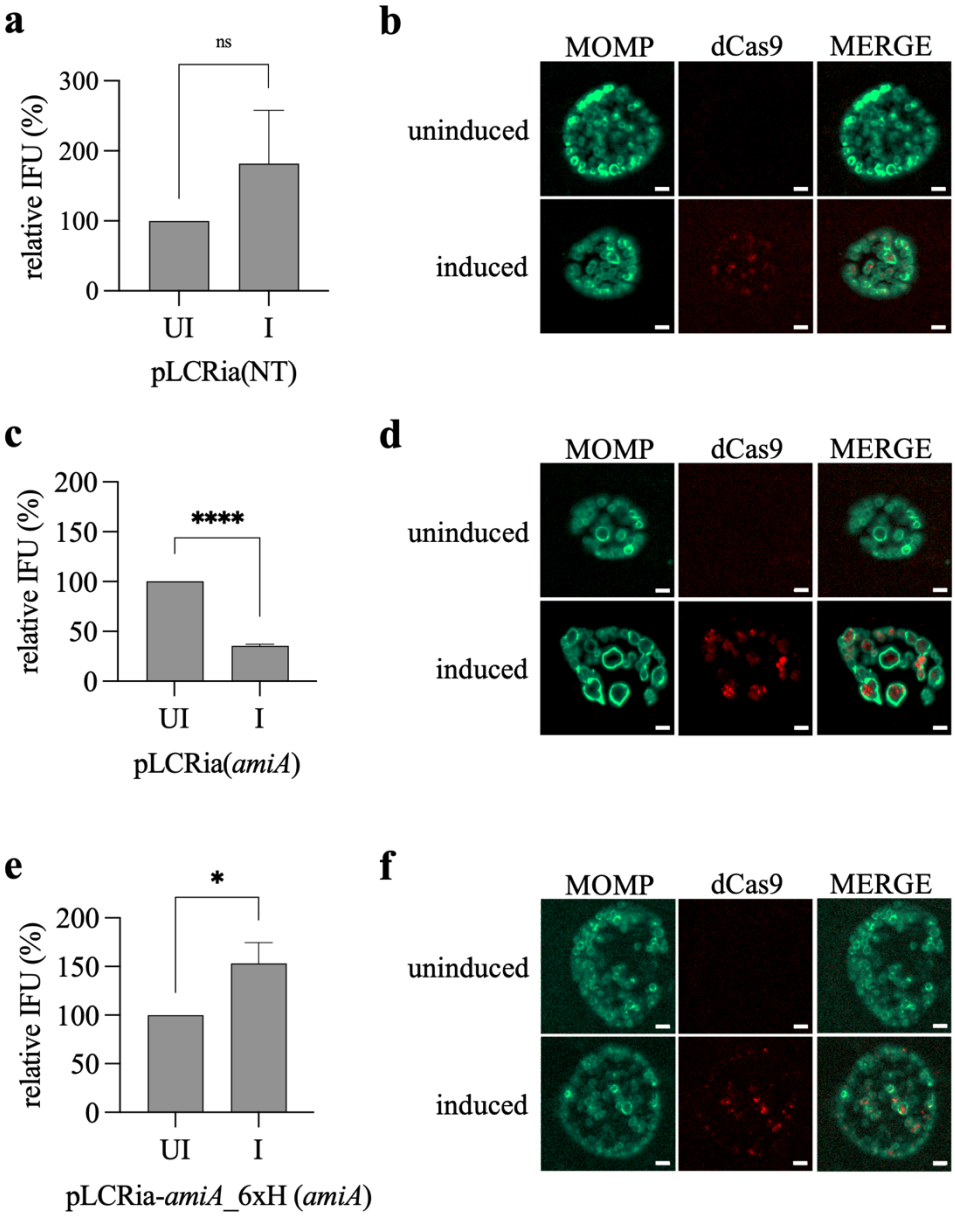

Figure 16: Effects of CRISPRi-mediated knockdown of *amiA* in *C. trachomatis* on proliferation. (a) Relative IFU levels were elevated in samples infected with *C. trachomatis* pLCRia(NT) that had been induced compared to uninduced, but not to a significant extend. (b) IFA controls displayed normal morphology under uninduced and induced conditions and expression of dCas9. (c) Quantitative data for pLCRia(*amiA*) could show a significant decrease of infectious progeny for *C. trachomatis* under induced genetic knockdown of *amiA* compared to the uninduced control. (d) IFA controls verified the enlarged cell phenotype previously observed and the expression of dCas9. (e) The complemented strain produced slightly more infectious progeny upon induction compared to the uninduced control. (f) IFA controls of the strain showed normal morphology and produced dCas9 in the induced samples. Error bars indicate ± s.d. (n=3). Unpaired t-test, two-tailed. Significance: * = $p \leq 0.05$, ** = $p \leq 0.01$, *** = $p \leq 0.001$, **** = $p \leq 0.0001$. UI = uninduced. I = induced.

The experiments unveiled that CRISPRi-mediated knockdown of *amiA* resulted in a significant decrease of infectious progeny (Fig. 16c). Corresponding IFA controls confirmed correct expression of the construct with dCas9 visualized in the induced sample and the inhibited cell division phenotype described in the previous sections (Fig. 16d). In *C. trachomatis* pLCRia(NT), relative IFU levels were slightly increased after induction (Fig. 16a), but not to a significant extend. Construct expression was confirmed by IFA assay by visualization of dCas9 in the induced sample, but cells did not show any morphological anomalies (Fig. 16b). In the complemented strain *C. trachomatis* pLCRia-*amiA*_6xH(*amiA*), relative IFU levels were raised slightly in the induced sample compared to the uninduced strain (Fig. 16e). Correct construct expression was verified by IFA controls that did not show phenotypical peculiarities (Fig. 16f). In sum, knockdown of *amiA* in *C. trachomatis* affected the generation of infectious progeny and thereby chlamydial proliferation, while the non-targeting and the complemented strain did not show a reduction of infectious progeny upon induction of constructs. These results are in line with the hypothesis of *amiA* knockdown negatively affecting chlamydial cell division.

3.3. Overexpression and CRISPRi-mediated knockdown of putatively cell division-associated chlamydial genes affect cell division in *C. trachomatis*

Chlamydia was long considered genetically intractable, but, due to recent advances, tools of genetic manipulation now provide novel possibilities in the assessment of gene functions associated to the cell division and PGN recycling machinery in *C. trachomatis*. CRISPRi-mediated genetic knockdowns could elucidate the effects of absence of the respective proteins, like the previous part of this work showed in case of chlamydial *amiA*. Conversely, overexpression of genes of interest could lead to novel insights on protein localization within the cell, as well as phenotypes associated with an overproduction of the respective protein. The following part focuses on potential glycosyltransferase and SEDS protein RodA and on the putative exo-β-N-acetylmuramidase NamZ in *C. trachomatis*, which have not been mechanistically investigated in *Chlamydia* to date. Constructs for aTc-inducible overexpression and inducible CRISPRi-mediated targeted knockdown of chlamydial *namZ* and *rodA* homologs were established previously in the research group of Drs. Scot Ouellette and Elizabeth Rucks and as a part of this work, respectively, and transformed into *C. trachomatis* (-pL2). Homologs were identified through sequence comparison and show 35 % and 32 % identity to homologous gene products in the model organism *E. coli*, respectively. The transformants were used to infect McCoy cells and construct expression was induced 4 hpi, when EB to RB transition is supposed to take place. Samples for immunofluorescence assays were fixed 11.5 hpi in case of overexpression and 24 hpi in case of both overexpression and knockdown and stained using indirect immunofluorescence. All experiments were performed during a research stay in the group of Drs. Scot Ouellette and Elizabeth Rucks, funded by the TRR261, and analyzed by fluorescence microscopy to gain first insight into the function of NamZ and RodA homologs in chlamydial cells.

3.3.1. CRISPRi-induced knockdown and overexpression of *C. trachomatis rodA*

RodA is a SEDS protein and was shown to interact with cognate class B PBPs in free-living bacteria. Genetic experiments including CRISPRi-mediated knockdown and overexpression in *C. trachomatis* were performed to further elucidate function of the gene product in *Chlamydia*. Evaluation of fluorescence microscopy images showed normal inclusion morphologies under induced conditions of CRISPRi-mediated knockdown of chlamydial *rodA* (Fig. 17). Samples were induced 4 hpi, when EB to RB transition of *Chlamydia* is expected. At 24 hpi, after chlamydial cell division and during redifferentiation of RBs into EBs, cells were fixated. After staining, slightly enlarged inclusions could be observed in the induced samples compared to the uninduced control samples. Within the inclusions, chlamydial cell phenotype alluded to impaired cell division. Compared to the uninduced samples, inclusions were filled with fewer but larger chlamydial cells. While dCas9 could not be detected in the uninduced samples, a red signal could be monitored in the induced samples throughout almost all chlamydial cells that were imaged, confirming dCas9 production. This indicates that genetic knockdown of *rodA* was successful. The resulting phenotype of enlarged chlamydial cells was distinct from uninduced controls and suggests that knockdown of *rodA* influences cell division processes and proliferation in *C. trachomatis*.

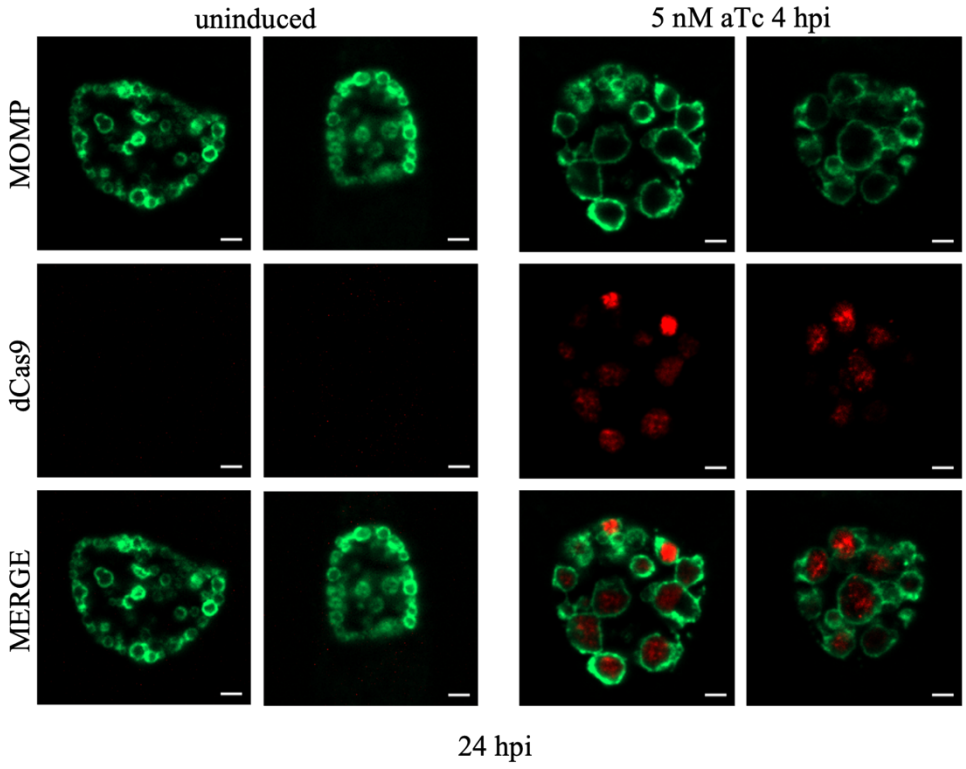

Figure 17: Phenotypic effects of CRISPRi-mediated genetic knockdown of *rodA* in *C. trachomatis.* Expression was either induced or not 4 hpi with 5 nM aTc and infected cells were incubated until 24 hpi. MOMP and dCas9 were visualized by indirect immunostaining. While uninduced samples displayed normal chlamydial phenotypes, enlarged cells were observed when construct expression had been induced. dCas9 was clearly visible in chlamydial cells in induced samples, while no signal was detected in the uninduced samples. Scale bar = 2 µm.

In addition to *rodA* knockdown, the effects of *rodA* overexpression were investigated in *C. trachomatis*. Instead of dCas9, hexahistidine tags indicating presence of overproduced RodA were visualized by indirect immunostaining. In the samples that were fixed 11.5 hpi, during the estimated onset of RB division, small inclusions with only few organisms were imaged for both induced and uninduced conditions (Fig. 18a). No signal indicating hexahistidine tags pointing towards *rodA* overexpression were detected. After additional 12.5 hours of incubation, during which RB division was expected to occur, inclusions in the uninduced samples grew and contained large numbers of chlamydial cells, of which most were regular-sized. In the samples that had been induced 4 hpi, inclusions were significantly smaller, contained fewer cells and some of the cells within were enlarged compared to cells in uninduced controls. The hexahistidine tag was detected in these samples, indicating that *rodA* overproduction was successful. Given the small size of chlamydial cells resulting from this experiment, no statement on the intracellular localization of RodA in *C. trachomatis* could be made. However, these results suggest that overexpression of *rodA* affects inclusion morphology, chlamydial proliferation, and cell division processes. As expected for a *rodA* homolog and in line with results of CRISPRi-mediated knockdown, results suggest a central role of the gene product in the chlamydial cell division machinery and PGN metabolism.

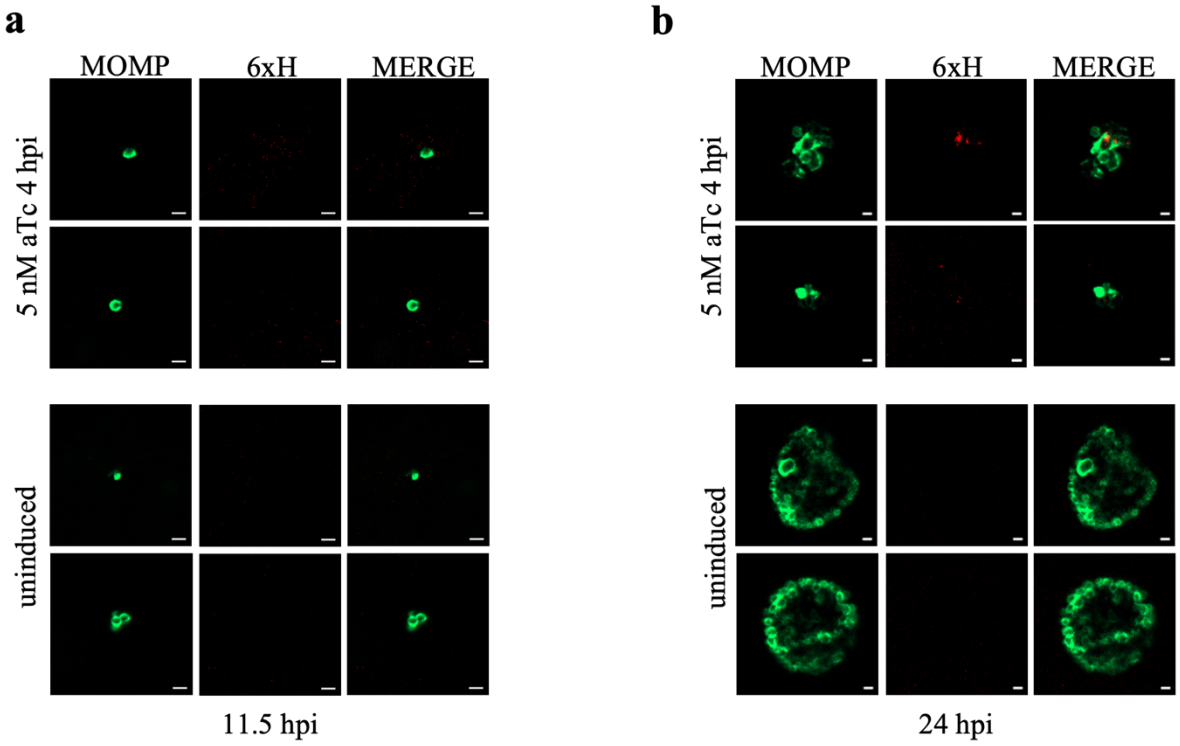

Figure 18: Morphologic effects of *rodA* overexpression in *C. trachomatis*. Expression was either induced or not 4 hpi with 5 nM aTc. MOMP and hexahistidine tags (6xH) were visualized by indirect immunofluorescence. (a) At 11.5 hpi, small inclusions with just few chlamydial cells were present. No signal corresponding to hexahistidine tags was visible. Scale bar = 1 µm. (b) 24 hpi, chlamydial inclusions in induced samples were visibly smaller than in the uninduced controls and contained fewer

chlamydial cells. Some cells were slightly enlarged compared to the uninduced control. While no signal of hexahistidine tags was visible in the uninduced controls, it was detected in the induced samples, indicating RodA overproduction. Scale bar = 2 µm.

3.3.2. CRISPRi-induced knockdown and overexpression of *C. trachomatis namZ*

Like in free-living bacteria, the chlamydial NamZ homolog is suggested to be involved in recycling of PGN-derived fragments. Therefore, knockdown and overexpression of the encoding gene, ct605, was performed to elucidate functioning of the gene product in *C. trachomatis*. Fluorescence microscopy images of inclusions from samples where CRISPRi-knockdown of *namZ* has not been induced showed inclusions with regular sizes filled with chlamydial cells (Fig. 19). Cells were uniformly sized and did not display abnormal morphologies. On the opposite, cells with induced knockdowns showed a non-uniform mix of inclusion sizes. While some were sized as in uninduced controls, parts were smaller and contained few organisms. In addition, parts of the cell population within the inclusions were enlarged compared to cells in uninduced samples. While dCas9 was not detected in the uninduced samples, red signals, indicating intracellular presence of dCas9, were observed in the induced samples. This indicates that dCas9 could be produced and that CRISPRi-mediated knockdown of *namZ* affected *C. trachomatis*, with altered cell and inclusion morphologies post induction.

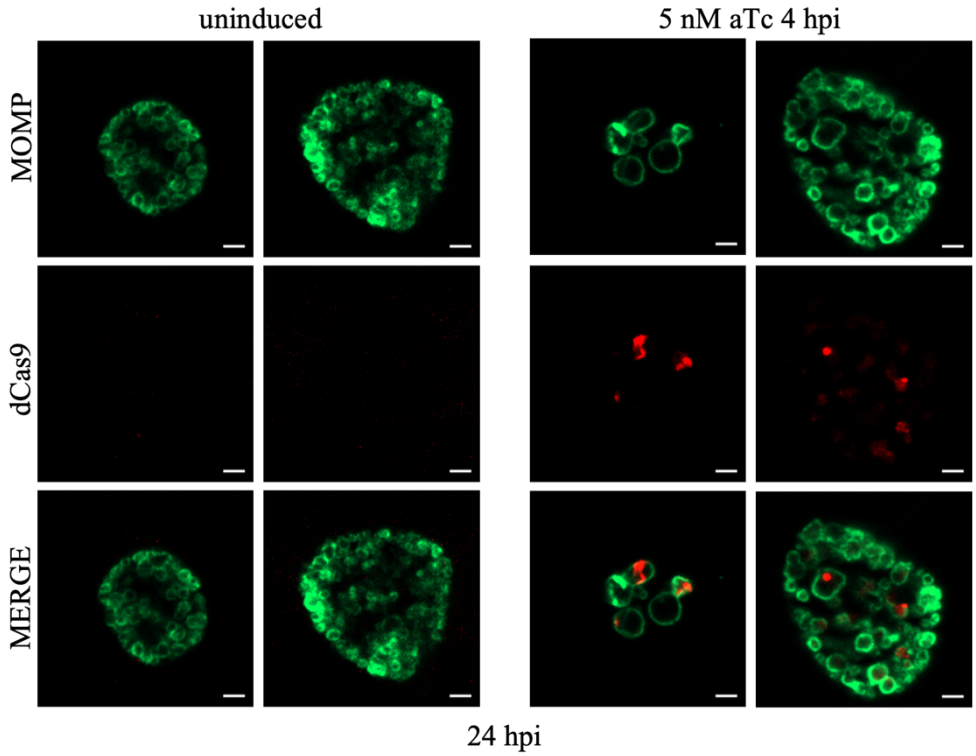

Figure 19: Morphologic effects of CRISPRi-mediated genetic knockdown of *namZ* in *C. trachomatis*. Expression was either induced or not 4 hpi with 5 nM aTc and infected cells were incubated until 24 hpi. MOMP and dCas9 were visualized by indirect immunostaining. While uninduced samples displayed normal chlamydial phenotypes with large inclusions filled with regular-sized chlamydial cells, enlarged cells were observed when construct expression had been induced. Partly, inclusions were

smaller than in uninduced controls. dCas9 was clearly visible in chlamydial cells in induced samples, while no signal was detected in the uninduced samples. Scale bar = 2 µm.

In addition to genetic knockdowns of *namZ*, effects of *namZ* overexpression in *C. trachomatis* were investigated. At 11.5 hpi, both images from uninduced and induced samples show immature small inclusions with few regular-sized organisms within (Fig. 20a). At this timepoint, no signal indicating hexahistidine tags was detectable. At 24 hpi, inclusions in uninduced samples grew and contained significantly more organisms than at the previous timepoint. Organisms were predominantly regular-sized, with few cells that were enlarged compared to the rest of the population. In the samples that were induced 4 hpi, inclusion sizes were significantly decreased compared to the uninduced control and insignificantly larger than at 11.5 hpi (Fig. 20b). Inclusions in induced samples contained very few organisms that were similar in size compared to the samples imaged at 11.5. hpi. Immunofluorescence revealed the presence of the hexahistidine tag, indicating that *namZ* overexpression was successful. However, due to the small inclusion sizes, localization of NamZ could not be determined in this experiment. These data indicate that also *namZ* overexpression has an influence on growth and proliferation in *C. trachomatis*, as it was seen for *rodA.* Together with the results of *namZ* knockdown, a central role of the gene product can be assumed. This is in line with the suggestion of the participation of NamZ in recycling events within the PGN metabolism and the importance of PGN recycling processes in *Chlamydia*.

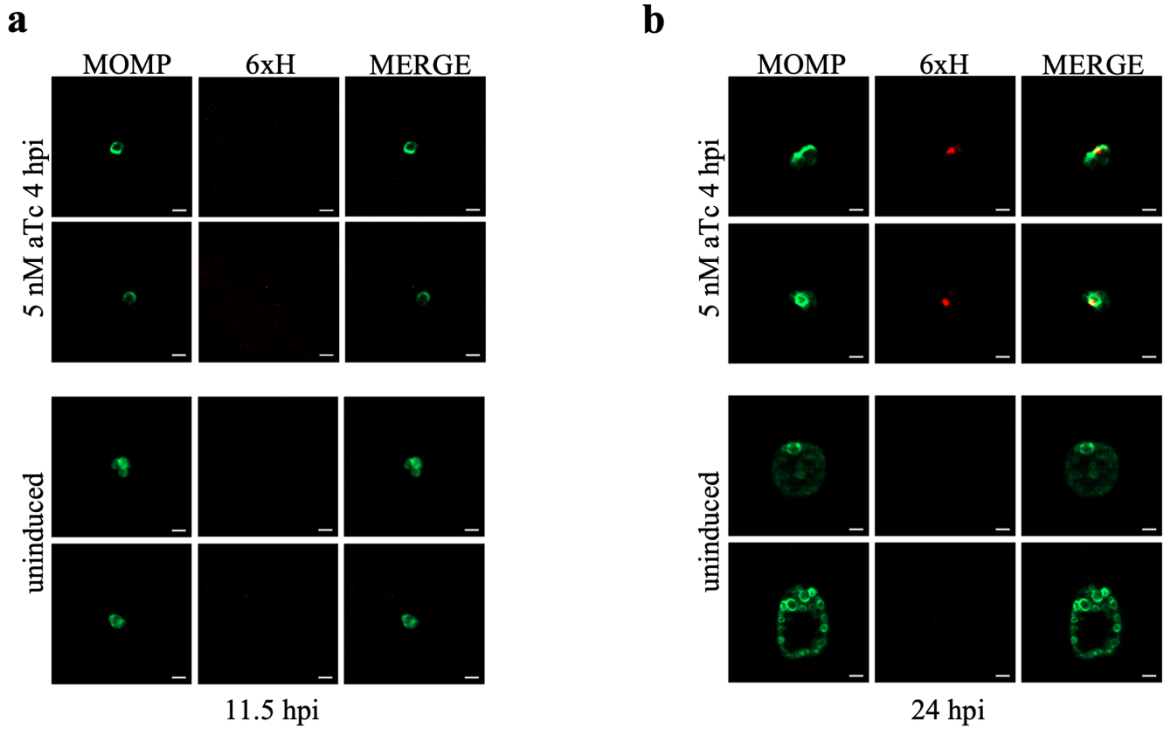

Figure 20: Morphologic effects of *namZ* overexpression in *C. trachomatis.* Expression was either induced or not 4 hpi with 5 nM aTc. MOMP and hexahistidine tags (6xH) were visualized by indirect immunofluorescence. (a) At 11.5 hpi, small inclusions containing few organisms could be observed in both induced and uninduced samples. No signal corresponding to the hexahistidine tag was visible in

induced and uninduced samples. Scale bar = 2 µm. (b) At 24 hpi, chlamydial inclusions post induction were visibly smaller than in the uninduced controls and contained only few chlamydial cells. Cells were partly enlarged compared to the uninduced control. While no signal of the hexahistidine tag was visible in the uninduced controls, it was observed in induced samples. Scale bar = 2 µm.

3.4. New insights into the substrate spectrum of chlamydial recycling enzyme YkfC

To date, little is known about recycling of PGN ring-derived material in *Chlamydia*. We contributed to the elucidation of recycling pathways in the organism by investigating the NlpC/P60-domain containing enzyme YkfC of *C. trachomatis* which has endopeptidase function on PGN-derived peptides (Reuter *et al.*, 2023). Specifically, the enzyme was shown to cleave the non-canonical γ-D-Glu-*m*DAP bond exclusive to peptidoglycan and derivatives and thereby contributes to PGN turnover and recycling processes. This work contributed to the study by characterizing substrate specifity of the enzyme by investigating a set of ten PGN-derived and non-PGN-derived peptides as possible substrates for YkfC. as substrates for YkfC. After incubation with the enzyme, reaction products were analyzed by thin layer chromatography for the detection of peptides.

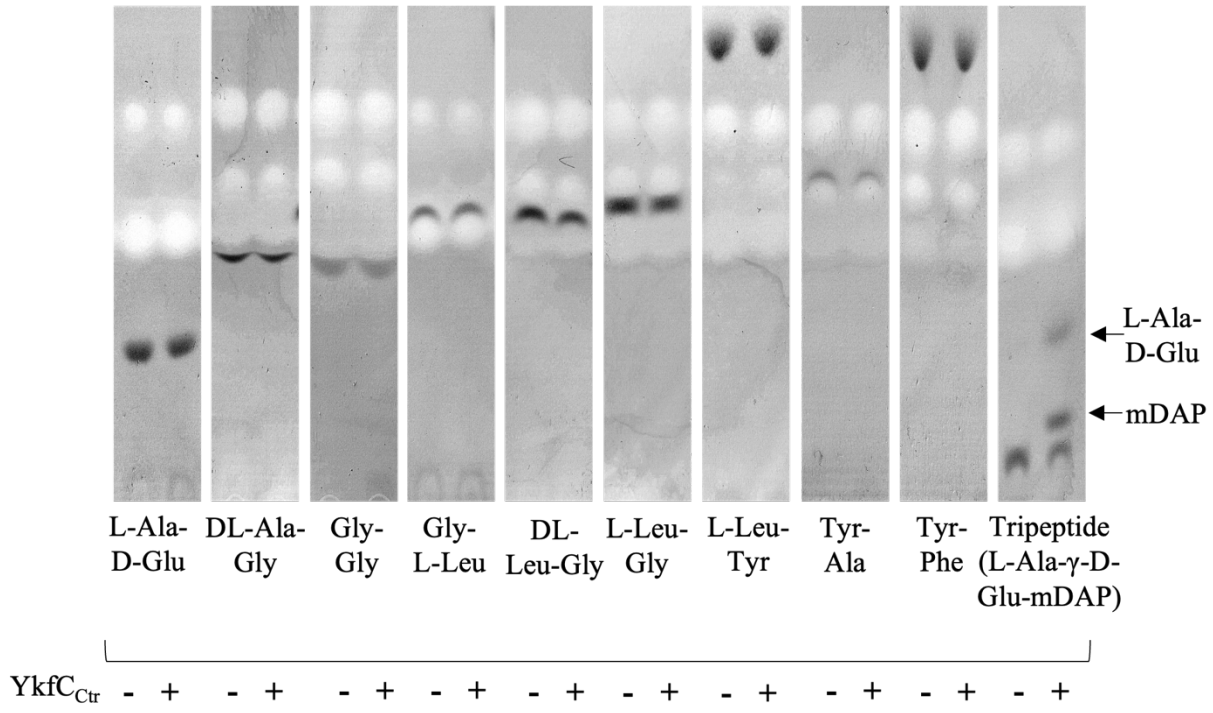

Figure 21: *In vitro* activity of YkfC_Ct on (non)-PGN-derived peptides (adapted from Reuter *et al.*, 2023). *In vitro* peptidase activity towards 10 (non)-PGN-derived peptides was analyzed by TLC. None of the peptides was used as a substrate by YkfC_Ct. PGN-derived tripeptide L-Ala-γ-D-Glu-mDAP was used as a positive control and was cleaved by YkfC_Ct.

Our experiments further corroborated that YkfC_Ct activity was specific to the non-canonical bond between γ-D-Glu-*m*DAP (Fig. 21). In literature, NlpC/P60 domain-containing recycling enzymes were described to require a free L-Ala terminus for substrate recognition (Xu *et al.*, 2015). Consequently,

Reuter *et al*. showed that the enzyme had no activity on dipeptide γ-D-Glu-*m*DAP and also PGN precursor lipid II, UDP-MurNAc tripeptide and MurNAc-tripeptide were not recognized as substrates (Reuter *et al.*, 2023) Other peptides, such as the PGN-derived dipeptide L-Ala-D-Glu or non-PGN-derived peptides, such as Tyr-Phe or Tyr-Ala were not processed by the enzyme either (Fig. 21). This verifies the requirement of a terminal L-Ala residue and the PGN-specific γ-D-Glu-*m*DAP bond for activity of NlpC/P60 enzymes and, therefore, contributed to the investigation of substrate specificity of this enzyme class.

3.5. *C. trachomatis* nutrient starvation and persistence in tissue culture infection models

To broaden the understanding of nutrient starvation-mediated persistence of *C. trachomatis*, we investigated the ability of chelators of bivalent cations to induce persistence in the organism in a cell culture-based infection model. Therefore, the antibiotic clioquinol and the compounds 1,10-phenanthroline and TPEN, which were investigated in terms of *in vitro* inhibition of chlamydial AmiA previously, were considered. As the chelation capacity of the compounds is not limited to zinc, but includes other bivalent cations as well, sequestration of essential micronutrients was investigated as a possible way to induce nutrient starvation-mediated persistence in *C. trachomatis*. This work contributes to broadening the understanding of starvation-induced persistence and investigates possible routes of induction.

3.5.1. Toxicity of metal chelators on mammalian cells

To distinguish between the putative anti-chlamydial effects, the cytotoxicity towards mammalian host cells and the interference among the two effects, compound cytotoxicity on mammalian host cells has to be determined. AlamarBlue assays were performed to determine cytotoxicity. In this resazurin based system, in which non-fluorescent resazurin is reduced to fluorescent resorufin by living mammalian cells, viability of cells is proportional to absorbance levels of resorufin. Cells were treated with compounds of interest in serial dilutions for durations of 18 and 28 hours to simulate treatment durations in our tissue culture-based infection model. After one hour of incubation with alamarBlue reagent, absorbance was measured and cytotoxicity was determined by calculating the cytotoxic concentration (CC_{50}), the concentration that reduces cell viability by 50 %.

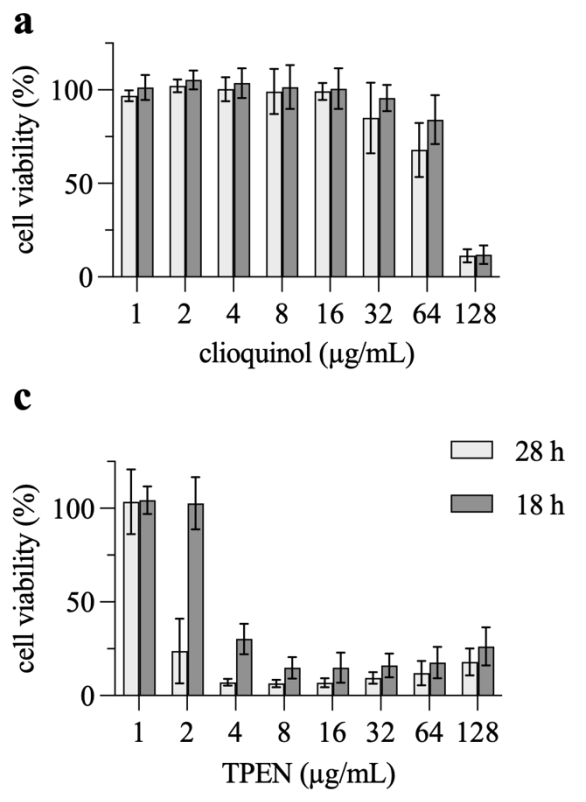

d

compound	CC_{50} 28 h treatment	CC_{50} 18 h treatment
clioquinol	75.21 µg/mL	87.66 µg/mL
1,10-phenanthroline	116.17 µg/mL	> 128 µg/mL
TPEN	1.87 µg/mL	3.62 µg/mL

Figure 22: Cytotoxic effects of metal chelators clioquinol, 1,10-phenanthroline and TPEN on mammalian HEp-2 host cells. HEp-2 cells were treated with serially diluted compounds for 18 h (dark grey) and 28 h (light grey) and absorbance values were measured after one hour of incubation with alamarBlue reagent. (a) Clioquinol showed pronounced cytotoxicity at the highest tested concentration of 128 µg/mL for both treatment durations, whereas concentrations up to 16 µg/mL exhibited almost no cytotoxicity. (b) 1,10-phenanthroline reduced cell viability more than 50 % after 28 h treatment, but otherwise showed almost no cytotoxic effects in this system. (c) Cells that were treated with TPEN for 28 hours in concentrations of 2 µg/mL and higher showed very low viability after treatment. Cytotoxicity was determined by calculating the CC_{50} value using non-linear regression. CC_{50} values represent the compound concentration that is required to reduce cell viability by 50 %. (d) shows the CC_{50} values of clioquinol, 1,10-phenanthroline, and TPEN for both treatment durations. Error bars indicate ± s.d. (n=3).

Evaluation of the experimental data revealed that clioquinol reduced cell viability by approximately 90 % during 18 h and 28 h treatment at the highest tested concentration of 128 µg/mL (Fig. 22a). The lower concentration of 64 µg/mL was less cytotoxic and reduced cell viability by one third during 28 hours of treatment and by approx. 15 % during 18 hours of treatment. Lower concentrations did not lead to more severe cytotoxic effects and calculation of CC_{50} values revealed CC_{50} concentrations of 75.21 µg/mL and 87.66 µg/mL for 28 hours and 18 hours of treatment, respectively (Fig. 22d). 1,10-phenanthroline only showed a cytotoxic effect in the alamarBlue assay at 128 µg/mL after 28 hours with reduced viability of HEp-2 cells by more than half. Lower concentrations and shorter treatment durations did not lead to cytotoxic effects in the alamarBlue assay. The CC_{50} value for cells treated with 1,10-

phenanthroline for 28 hours was determined to be >128 µg/mL and 116.17 µg/mL when applied for 18 hours. TPEN was highly cytotoxic to HEp-2 cells. All concentrations tested, except for 1 µg/mL and 2 µg/mL applied for 18 hours, reduced cell viability by up to 75 %. CC_{50} values were determined at 1.87 µg/mL and 3.62 µg/mL for 28 hours and 18 hours of treatment, respectively. In sum, 1,10-phenanthroline and clioquinol are suitable to be applied in cell culture-based infection models to treat chlamydial infections. As CC_{50} concentrations for these compounds are relatively high, lower concentrations could be used to determine putative effects on *C. trachomatis.* TPEN, on the other hand, did show strong cytotoxic properties towards HEp-2 host cells, making the compound unsuitable for testing it against chlamydial infections and incomparable to clioquinol and 1,10-phenanthroline. Further experiments, therefore, excluded TPEN.

3.5.2. Effects of metal chelators on active chlamydial infections tested in cell culture-based infection models

Metal chelators 1,10-phenanthroline and TPEN and the antibiotic clioquinol inhibited AmiA_Ct activity *in vitro* and, with the exception of TPEN, showed only moderate cytotoxic effects on mammalian HEp-2 cells. To test capacities of the compounds to induce a persistent state of *C. trachomatis* due to nutrient starvation, clioquinol and 1,10-phenanthroline were tested in cell culture-based infection models. Therefore, HEp-2 monolayers were infected with *C. trachomatis* elementary bodies and treated with compounds 2 hpi and 12 hpi for 28 hours and 18 hours, respectively. The early timepoint at 2 hpi represents treatment of chlamydial infections right after entry into the host cell early in the developmental cycle, whereas at 12 hpi, effects on an established chlamydial infection are investigated. As compounds were dissolved in DMSO, it was used as a vehicle control. A treatment diagram for the experiments is presented in Figure 23. After fixation 30 hpi, cells were stained using Pathfinder *Chlamydia* Culture Confirmation system (Bio-Rad) and DAPI and imaged by fluorescence microscopy. Images were analyzed in terms of infection rate, inclusion size, and chlamydial phenotypes. If possible, a minimum inhibitory concentration (MIC) of the compounds was determined. The MIC was defined as the concentration of compound that produced ≥ 90 % reduction of infection rate and/or ≥ 90 % reduction of inclusion size and/or ≥ 90 % alteration of chlamydial phenotype (Donati *et al.*, 1999; Suchland, Geisler and Stamm, 2003).

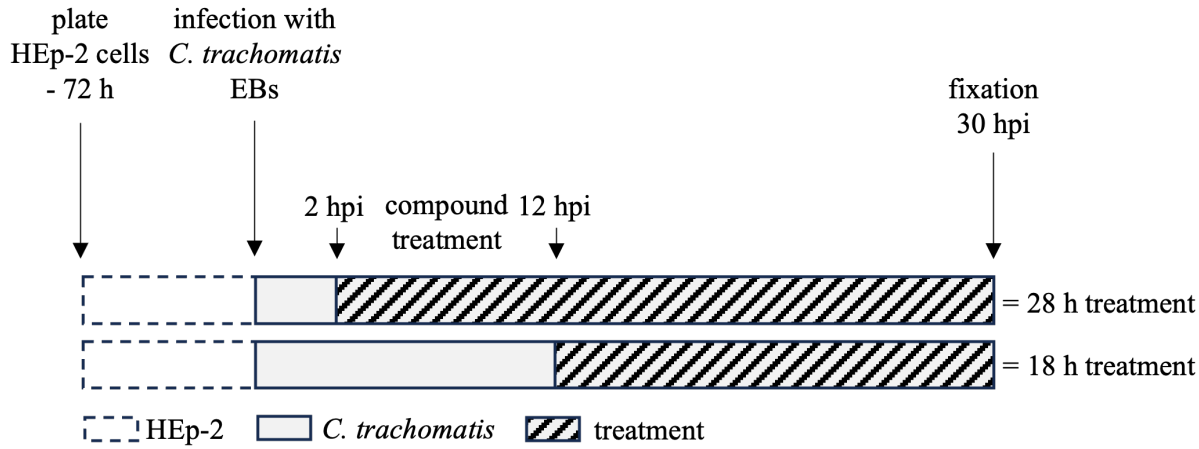

Figure 23: Diagram for the treatment of active chlamydial infections using metal chelators. HEp- 2 cells were grown until monolayer formation and then infected with EBs of *C. trachomatis*. 2 hpi and 12 hpi, compounds were applied and infected cells were incubated for 28 hours and 18 hours, respectively. After methanol fixation 30 hpi, cells were stained and imaged using fluorescence microscopy.

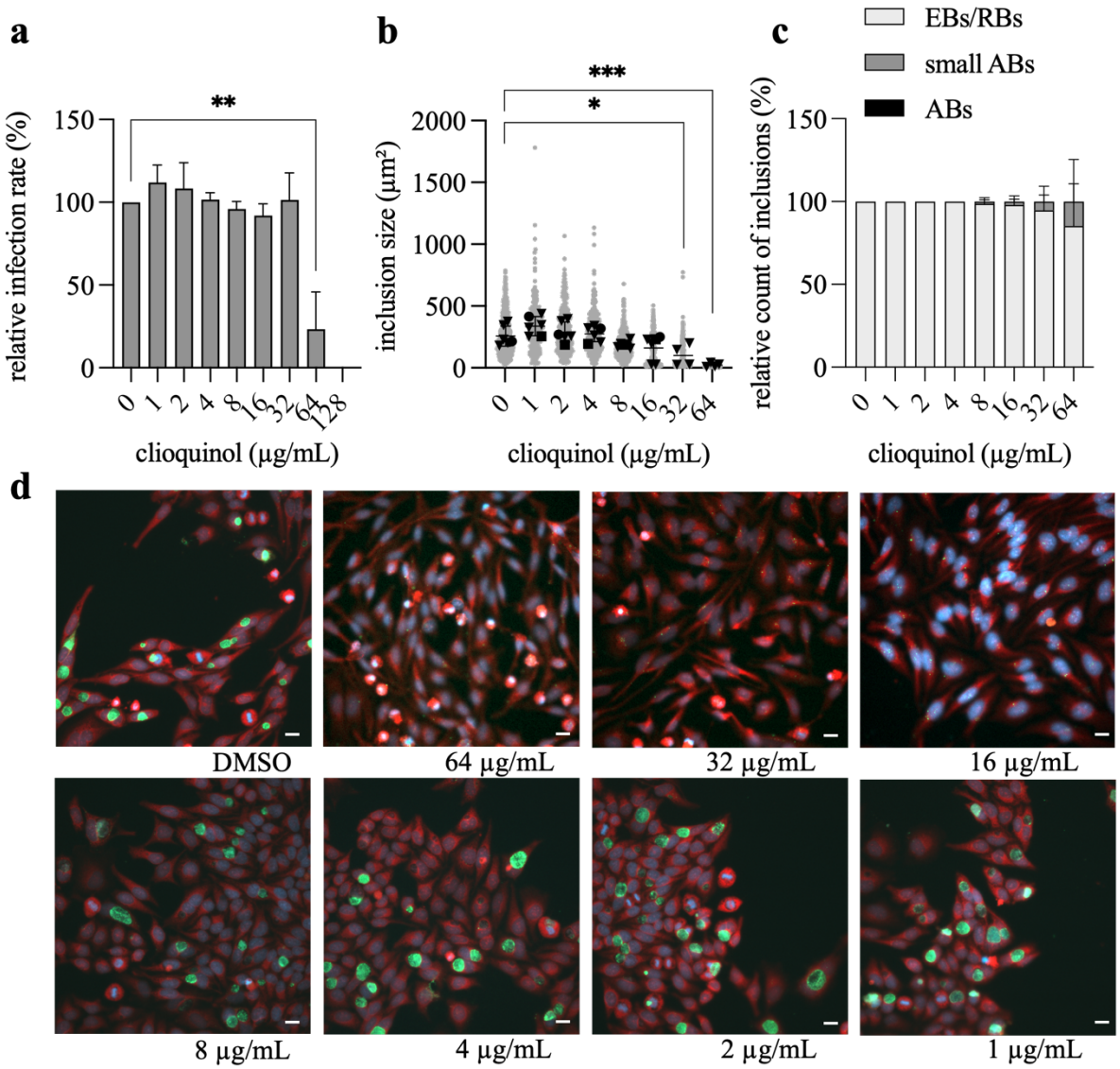

Figure 24: Effects of 28-hour clioquinol treatment on active chlamydial infections (treatment timepoint: 2 hpi). (a) Relative infection rate compared to the DMSO vehicle control (0 µg/mL). At 128 µg/mL clioquinol, no infected cells were observed. 64 µg/mL clioquinol entailed significant reduction of infection rate. (b) Inclusion size was significantly reduced at 32 µg/mL and 64 µg/mL clioquinol. (c) Chlamydial phenotype was altered by 15 % at 64 µg/mL clioquinol treatment applied 2 hours post infection. (d) Fluorescence microscopy images show few and small inclusions resulting from clioquinol treatment at 16 µg/mL to 64 µg/mL, whereas inclusions that were treated with the vehicle control or lower clioquinol concentrations were larger. Scale bar = 20 µm. Error bars indicate ± s.d. (n = 3 biological replicates with 2 technical replicates each). Unpaired t-test, two-tailed. Significance: * = $p \leq 0.05$, ** = $p \leq 0.01$, *** = $p \leq 0.001$, **** = $p \leq 0.0001$.

When treated with the highest clioquinol concentration of 128 µg/mL 2 hpi for 28 hours, no chlamydial infection was detectable (Fig. 24) and, in line with previously determined cytotoxicity of clioquinol (Fig. 23), the host cell monolayer was disrupted. At 64 µg/mL, infection rate was significantly decreased by approx. 75 % (Fig. 24a), which is also reflected in the fluorescence microcopy image (Fig. 24d) showing very few inclusions inside host cells. Inclusion size was significantly reduced when treated with 32 µg/mL and 64 µg/mL clioquinol (Fig. 24b,d). When 16 µg/mL clioquinol were applied, inclusions remained very small. At lower concentrations, inclusion size aligned with the dimensions observed in the DMSO vehicle control. Some chlamydial cells previously treated with higher concentrations of clioquinol were morphologically distinct from the prevailing EB/RB phenotype (Fig. 24d). Up to approx. 15 % of inclusions contained chlamydial cells present as small aberrant bodies (Abs), not as enlarged as ABs observed e.g. in penicillin-induced persistence, but comparable to the size of Abs under IFN-γ or nutrient starvation-induced persistence. The number of chlamydial cells present as small ABs decreased with lower concentrations of clioquinol. Furthermore, the effects of shorter clioquinol treatment starting 12 hpi, representing treatment of an established chlamydial infection, were investigated (Fig. 25). While for 128 µg/mL also no infection was detectable, the effect on infection rate at 64 µg/mL was less profound than for the longer clioquinol treatment (Fig. 25a). Concentrations ranging from 16 to 64 µg/mL clioquinol significantly affected inclusion size (Fig. 25b), which could also be observed in fluorescence microscopy images (Fig. 25d). Like the images shown in Fig. 24d, very small inclusions are present in cells treated with 64 µg/mL and 32 µg/mL, which gain in size at 16 µg/mL clioquinol treatment until they align with vehicle control inclusion sizes at lower clioquinol concentrations. As shown in the previous results, shorter clioquinol treatment also had a phenotypic effect on chlamydial cells, even if they are slightly more developed than in the experiments with earlier clioquinol application. When treated with 64 µg/mL clioquinol, approx. 25 % of inclusions contained chlamydial cells that were visibly enlarged. This portion decreased with diminishing clioquinol concentrations, until regular EB/RB phenotype, as shown in the vehicle control, prevailed.

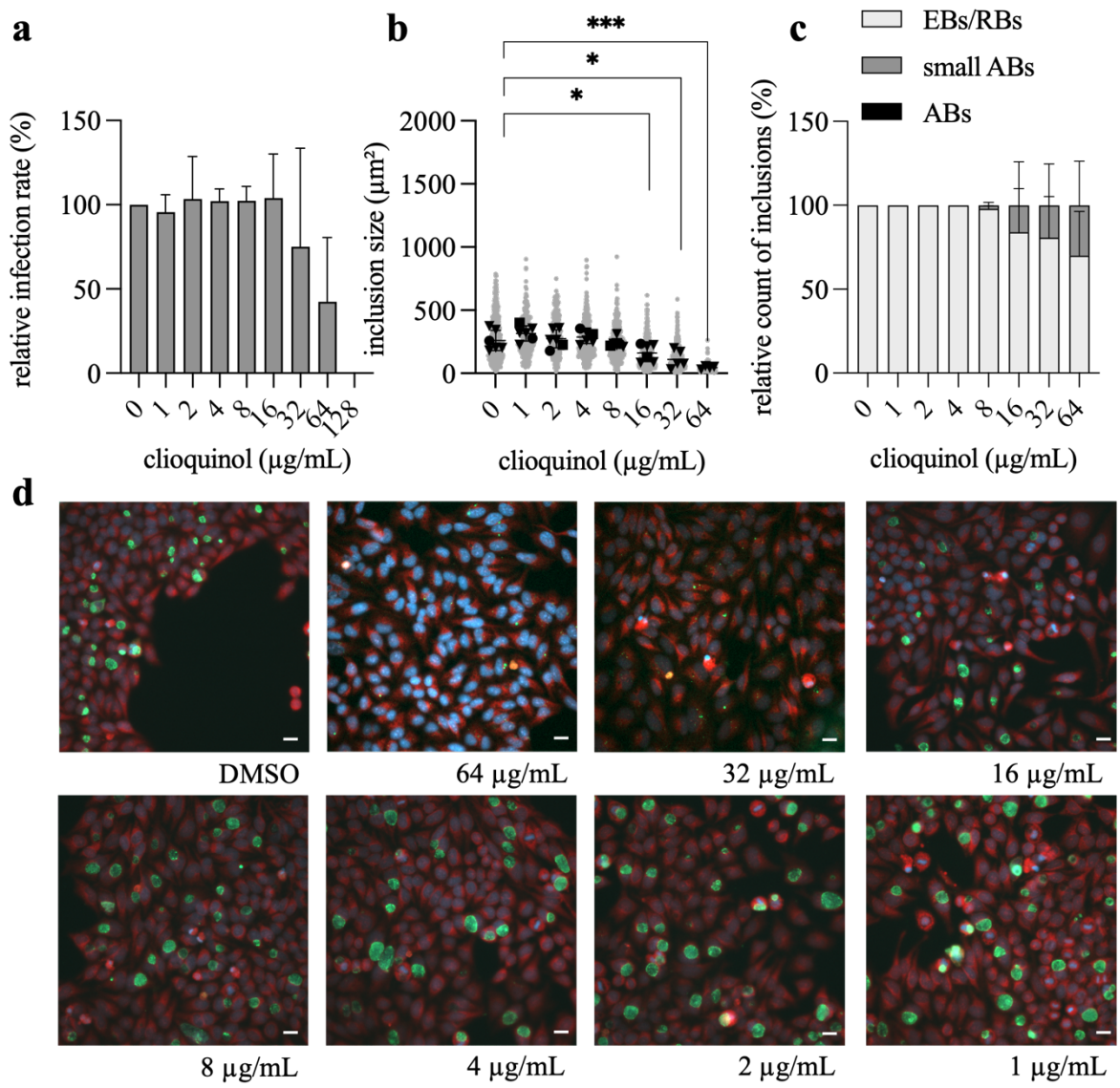

Figure 25: Effects of 18-hour clioquinol treatment on active chlamydial infections (treatment timepoint: 12 hpi). (a) Relative infection rate compared to the DMSO vehicle control (0 µg/mL). At 128 µg/mL clioquinol, no infected cells could be observed, while at 64 µg/mL, approx. 50 % of cells were infected. (b) Inclusion size was significantly reduced from clioquinol concentrations of 16 µg/mL to 64 µg/mL. (c) 25 % of chlamydial cells appear to be present as small aberrant bodies, about the size of aberrant bodies observed in nutrient starvation models induced by the treatment with 2,2-bipyridyl. (d) Fluorescence microscopy images show few and small inclusions resulting from clioquinol treatment at 64 µg/mL and 32 µg/mL, whereas inclusions that were treated with DMSO and lower clioquinol concentrations were larger. Scale bar = 20 µm. Error bars indicate ± s.d. (n = 3 biological replicates with 2 technical replicates each). Unpaired t-test, two-tailed. Significance: * = $p \leq 0.05$, ** = $p \leq 0.01$, *** = $p \leq 0.001$, **** = $p \leq 0.0001$.

Active chlamydial infections were impacted by both treatment regimens of clioquinol. Reductions in infection rate, inclusion sizes and alterations of phenotype could be observed. The highest tested clioquinol concentration of 128 µg/mL was cytotoxic to host cells, 64 µg/mL and all concentrations below were lower than the CC_{50} concentration that was determined previously. Still, results from cytotoxicity data (Fig. 22) indicate that host cells are affected by clioquinol at concentrations below the CC_{50} concentration, e.g. at 32 µg/mL. For both treatment durations, 90 % reduction of infection rate or inclusion size or 90 % alteration of phenotype were not reached by treatment with concentrations up to 64 µg/mL clioquinol. According to these criteria, the MIC for clioquinol on active infections applied 2 hpi or 12 hpi would be considered 128 µg/mL, as infection rate was decreased entirely. However, this concentration was shown to be highly cytotoxic on mammalian host cells, and therefore, a MIC for chlamydial infections could not be determined here.

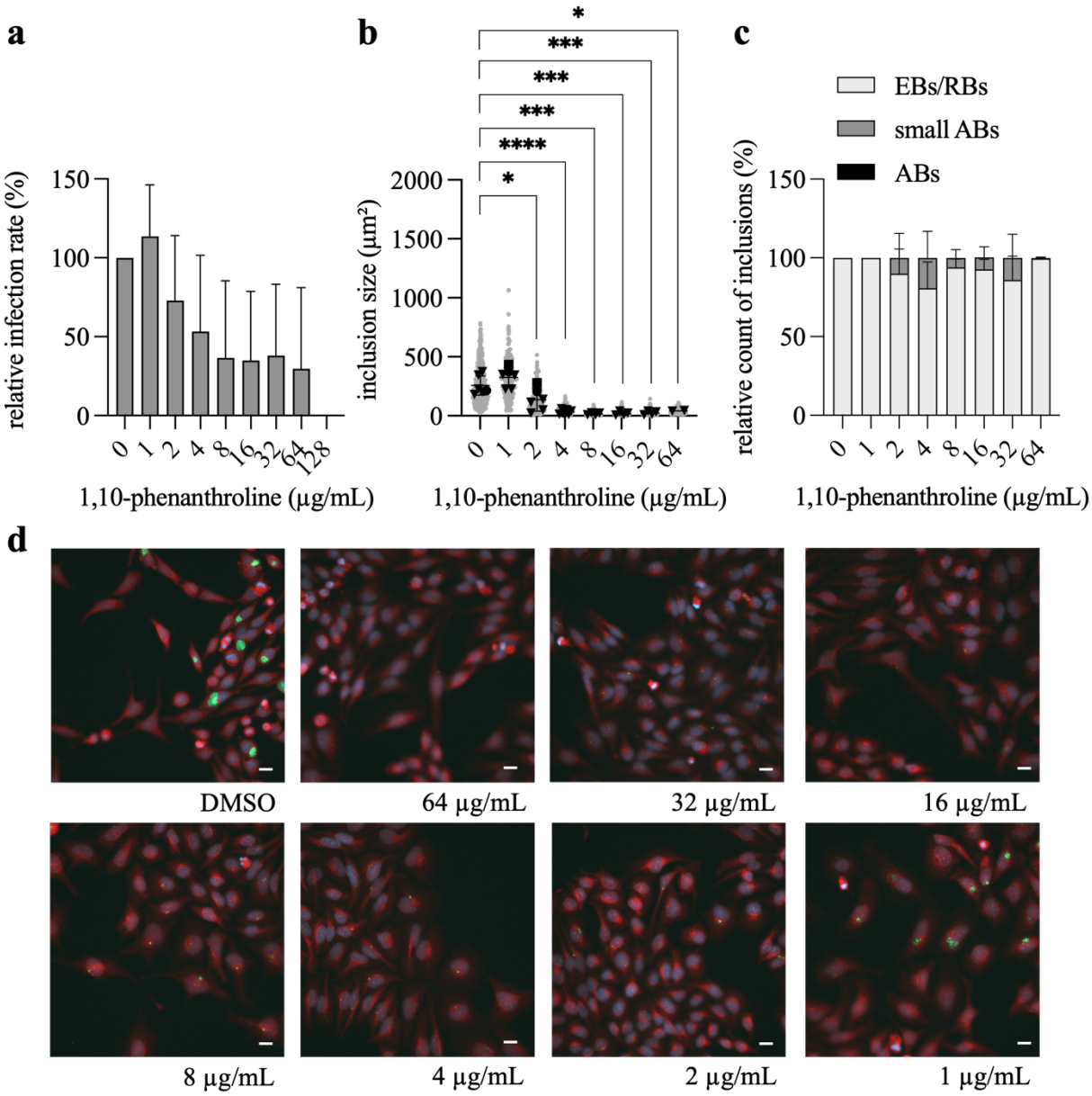

Figure 26: Effects of 28-hour 1,10-phenanthroline treatment on active chlamydial infections (treatment timepoint: 2 hpi). (a) Relative infection rate compared to the DMSO vehicle control (0 µg/mL). At 128 µg/mL clioquinol, no infected host cells could be observed. Concentration down to 2 µg/mL led to at least 25 % reduction of infection rate. (b) Inclusion size was significantly reduced by 2 to 64 µg/mL 1,10-phenanthroline. (c) Chlamydial phenotype was altered by up to 20 % by 1,10-phenanthroline and led to chlamydial cells present as small ABs. (d) On fluorescence microscopy images, small inclusions could be observed for every treatment concentration ranging from 2 to 64 µg/mL, being barely visible at 64 µg/mL, whereas inclusions that were treated with the vehicle control or 1 µg/mL 1,10-phenanthroline were larger. Scale bar = 20 µm. Error bars indicate ± s.d. (n = 3 biological replicates with 2 technical replicates each). Unpaired t-test, two-tailed. Significance: * = $p \leq 0.05$, ** = $p \leq 0.01$, *** = $p \leq 0.001$, **** = $p \leq 0.0001$.

In line with cytotoxicity analyses (Fig. 22), no infected host cells could be observed under treatment conditions with the highest used concentration of 128 µg/mL 1,10-phenanthroline for 28 hours starting at 2 hpi (Fig. 26). At this concentration, also cytotoxic effects of 1,10-phenanthroline were observed, as 128 µg/mL is higher than the CC_{50} concentration that was determined for this treatment duration (Fig. 22d). 8 – 64 µg/mL 1,10-phenanthroline reduced the relative infection rate more than 60 % compared to the DMSO control infection rate (Fig. 26a). All concentrations from 2 to 64 µg/mL entailed a significant reduction of inclusion size in this experiment (Fig. 26b), which is also visible in the fluorescence microscopy images shown in Fig 26d. Predominantly, very small inclusions were visible under these conditions. The small AB phenotype, as described before, was observed when cells were treated with 2 – 32 µg/mL 1,10-phenanthroline (Fig. 26c). At 64 µg/mL, inclusions were too small to determine chlamydial phenotypes, if present. In comparison, a shorter 1,10-phenanthroline treatment starting 12 hpi for further 18 hours, representing treatment of an established infection, was also tested (Fig. 27). While at 128 µg/mL administered compound, no chlamydial infection was observed as well, 4 – 64 µg/mL 1,10-phenanthroline produced reductions of infection rate, however not as profound as observed for the longer treatment (Fig. 27a). Moreover, a significant reduction of inclusion size compared to the DMSO vehicle control was observed under these conditions (Fig. 27b). Microscopy images show predominantly small inclusions when cells were treated with 2 – 32 µg/mL and barely visible inclusions in cells treated with 64 µg/mL 1,10-phenanthroline (Fig. 27d). All tested concentrations led to the formation of small AB phenotypes in chlamydial cells and up to 25 % of inclusions contained these morphological forms at concentrations between 4 and 32 µg/mL (Fig. 27c).

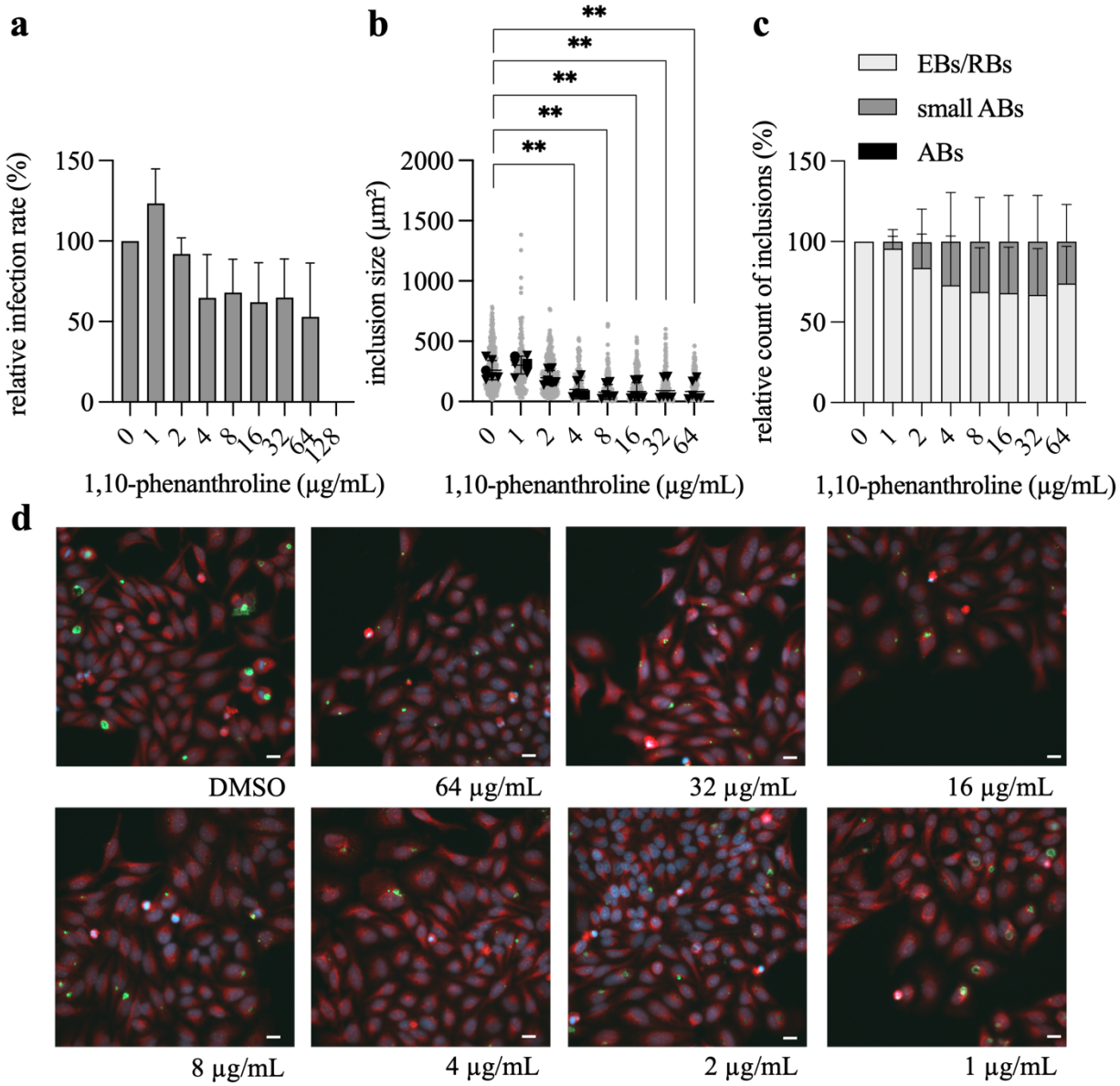

Figure 27: Effects of 18-hour 1,10-phenanthroline treatment on active chlamydial infections (treatment timepoint: 12 hpi). (a) Relative infection rate compared to the DMSO vehicle control (0 µg/mL). When treated with 128 µg/mL 1,10-phenanthroline, no chlamydial infection was observed. Infection rates were reduced up to 40 % by 4 µg/mL 1,10-phenanthroline and higher concentrations. (b) Inclusion size was significantly reduced by 4 - 64 µg/mL 1,10-phenanthroline. (c) Chlamydial phenotype was altered by up to 25 % by 1,10-phenanthroline and led to chlamydial cells being as small ABs. (d) On fluorescence microscopy images, inclusions that were significantly smaller than those in the infection treated with DMSO were observed. Scale bar = 20 µm. Error bars indicate ± s.d. (n = 3 biological replicates with 2 technical replicates each). Unpaired t-test, two-tailed. Significance: * = $p \leq 0.05$, ** = $p \leq 0.01$, *** = $p \leq 0.001$, **** = $p \leq 0.0001$.

Like clioquinol, both treatment regimens with 1,10-phenanthroline impacted chlamydial infections in their infection rates, inclusion sizes and in terms of phenotype of chlamydial cells. However, criteria for the determinations of MIC were not met except for 128 µg/mL 1,10-phenanthroline for the 18-hour

treatment, that produced a 100 % reduction of infection rate. However, as this concentration displayed pronounced cytotoxic properties in the longer treatment regimen lasting 28 hours, toxicity towards host cells in the 28 hour treatment as well as in the shorter treatment cannot be excluded. Therefore, like for clioquinol, a MIC towards chlamydial cells cannot be determined within this framework.

3.5.3. Effects of metal chelators on penicillin G-induced persistent chlamydial infections in cell culture-based infection models

The effects of metal chelators clioquinol and 1,10-phenanthroline on penicillin G-induced persistent chlamydial infections were investigated as described in section 3.4.2., with the only exception of the addition of penicillin G being added 2 hpi in both treatment models (Fig. 28). By adding chelators and penicillin G simultaneously, putative additive or synergistic effects were investigated at the onset of chlamydial infections. The effects of chelators on established persistent chlamydial infections were tested when penicillin G was administered 2 hpi followed by the chelator 12 hpi.

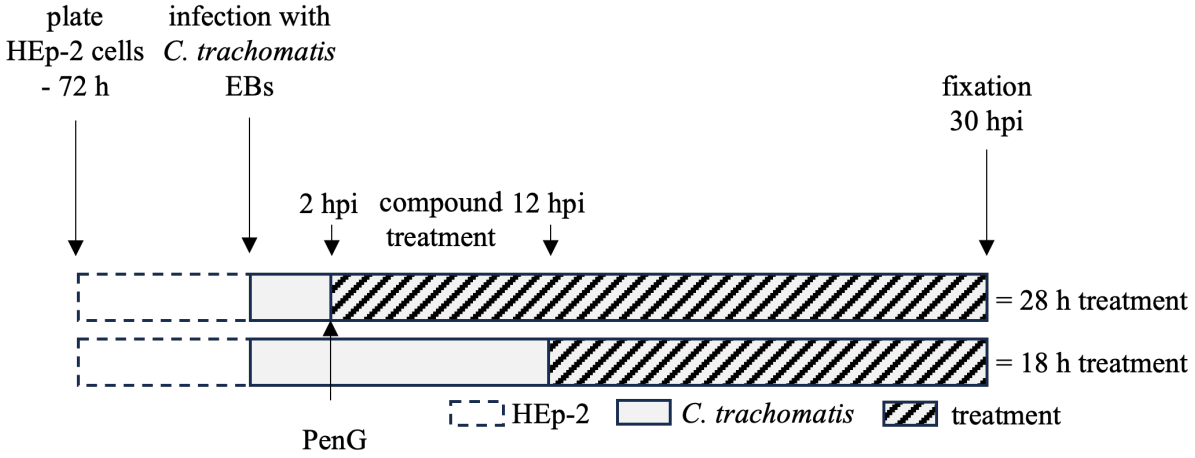

Figure 28: Diagram for the treatment of penicillin G-induced persistent chlamydial infections using metal chelators. HEp-2 cells were grown until monolayer formation and then infected with EBs of *C. trachomatis*. In both experimental setups, 100 U/mL penicillin G was added 2 hpi to induce chlamydial persistence. Chelators were added 2 hpi and 12 hpi and infected cells were incubated for 28 hours and 18 hours, respectively. Simultaneous chelator and penicillin G treatment 2 hpi represents a control experiment to test, if administered together, penicillin G and chelators have additive or synergistic effects on chlamydial infection. When compounds were added 12 hpi within this setup, chlamydial persistence was already established due to penicillin G treatment 2 hpi. Therefore, this setup investigates the effects of chelators on established persistent infections. After methanol fixation 30 hpi, cells were stained and imaged using fluorescence microscopy.

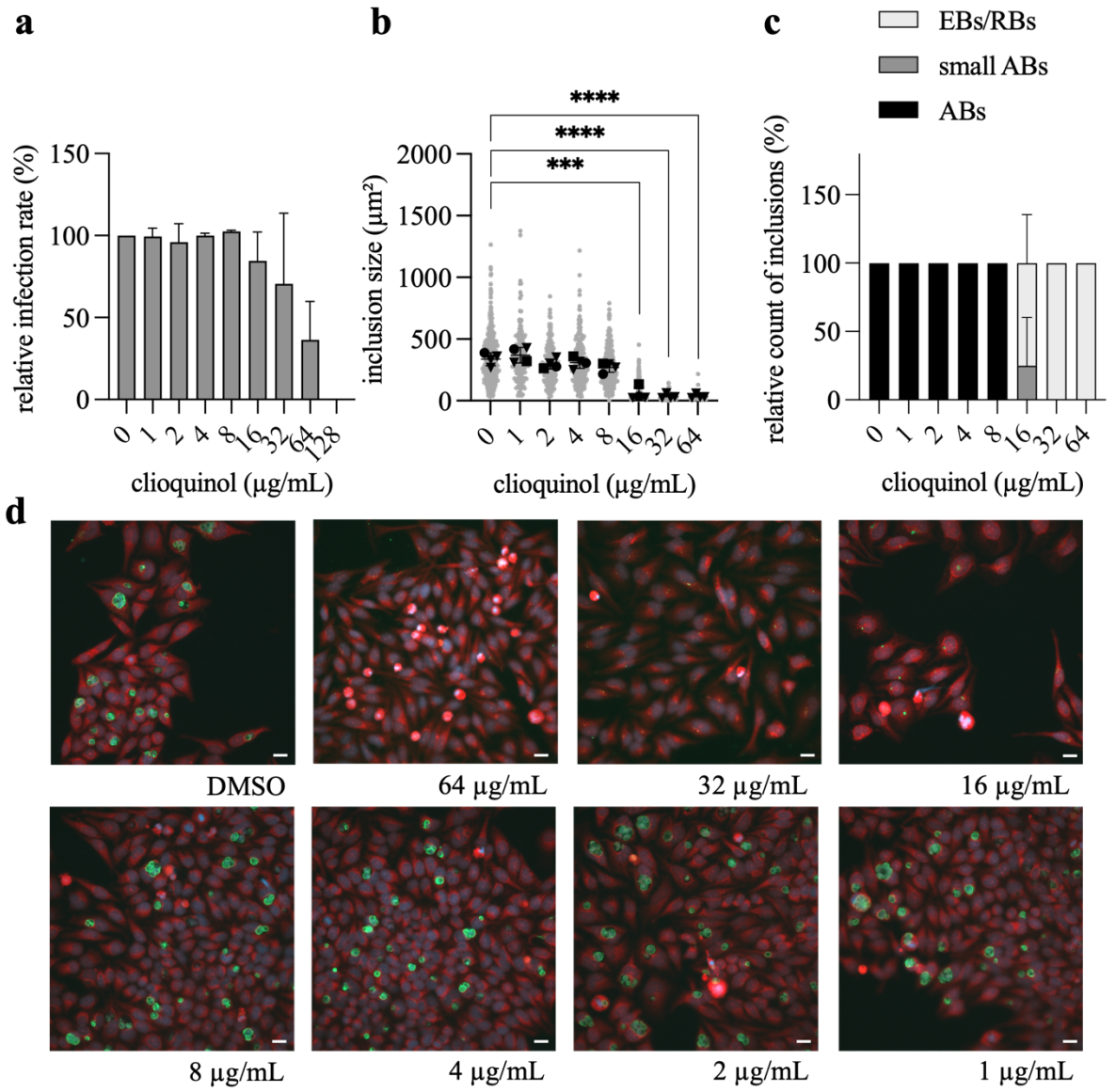

Figure 29: Effects of simultaneous clioquinol and penicillin G treatment on chlamydial infections (treatment timepoint: 2 hpi). (a) Relative infection rate compared to the DMSO vehicle control (0 µg/mL). When treated with 128 µg/mL clioquinol, none of the host cells was infected. Relative infection rates were reduced more than 50 % by 64 µg/mL clioquinol. (b) Inclusion sizes were significantly reduced at 16 - 64 µg/mL clioquinol. (c) While treatment with the vehicle control and 1 – 8 µg/mL clioquinol did not affect the penicillin-induced aberrant phenotype, no enlarged chlamydial cells were observed when treated with 16 – 64 µg/mL clioquinol. (d) Fluorescence microscopy images show inclusions with aberrant bodies when infections were treated with 1 – 8 µg/mL clioquinol, whereas very small inclusions were observed for infections treated with higher concentrations. Scale bar = 20 µm. Error bars indicate ± s.d. (n = 3 biological replicates with 2 technical replicates each). Unpaired t-test, two-tailed. Significance: * = $p \leq 0.05$, ** = $p \leq 0.01$, *** = $p \leq 0.001$, **** = $p \leq 0.0001$.

When *C. trachomatis* infections were treated with penicillin G and 128 µg/mL clioquionol for 28 hours starting 2 hpi simultaneously, no chlamydial infection could be detected in host cells (Fig. 29a,d). At 64

µg/mL, relative infection rate was reduced by more than 50 % (Fig. 29a). A significant reduction of inclusion sizes was observed in cells treated with 16 – 64 µg/mL (Fig. 29b,d), with inclusions being barely visible. At lower concentrations and in the vehicle control, aberrant bodies were present as expected from penicillin G-induced persistence (Fig. 29c,d). At 16 – 64 µg/mL clioquinol, no aberrant bodies were present within chlamydial inclusions. At 16 µg/mL, some inclusions contained chlamydial cells showing small ABs, but, for the most part, the EB/RB phenotype was prevailing in very small inclusions (Fig. 29c). Shorter clioquinol treatment, starting at 12 hpi until 30 hpi represents treatment of established persistent chlamydial infections and led to eradication of chlamydial infection when treated with 128 µg/mL clioquinol (Fig. 30a). At all lower concentrations, however, relative infection rate was not reduced compared to the vehicle control. Inclusions sizes decreased with rising clioquinol concentrations and differences compared to the control were significant when cells were treated with 16 - 64 µg/mL (Fig. 30b). Microscopy images revealed that, at these concentrations, inclusions were very small (Fig. 30d). Inclusions at 16 µg/mL were larger than those in the previous experiment, where they were treated with clioquinol for longer. While also here aberrant bodies were observed in the vehicle control and at concentrations 1 – 8 µg/mL, up to 50 % of chlamydial cells were present as small ABs at the highest concentration of clioquinol and approx. 30 % at 8 µg/mL (Fig. 30c). In contrast to the experiment with the longer treatment duration, the EB/RB phenotype did not occur in this experiment and a larger proportion of chlamydial cells was present as small ABs. Like in active infections, clioquinol impacted penicillin G-induced persistent chlamydial infections in this experiment in terms of infection rate, inclusion size and phenotype. Analogously to the previous experiment, 128 µg/mL reduced the infection rate by 100 % and lower concentrations were not sufficient to reduce infection rate or inclusion size by 90 % or alter chlamydial phenotype by 90 %. With sole regard to chlamydial infections, the MIC would be determined to be 128 µg/mL due to clearance effects, but, as this concentration exceeds the CC_{50}, cytotoxic effects on mammalian host cells are highly likely to interfere with the anti-chlamydial effect. This makes it impossible to distinguish between anti-chlamydial effects and cytotoxicity towards host cells, so that in this setup a MIC could not be determined.

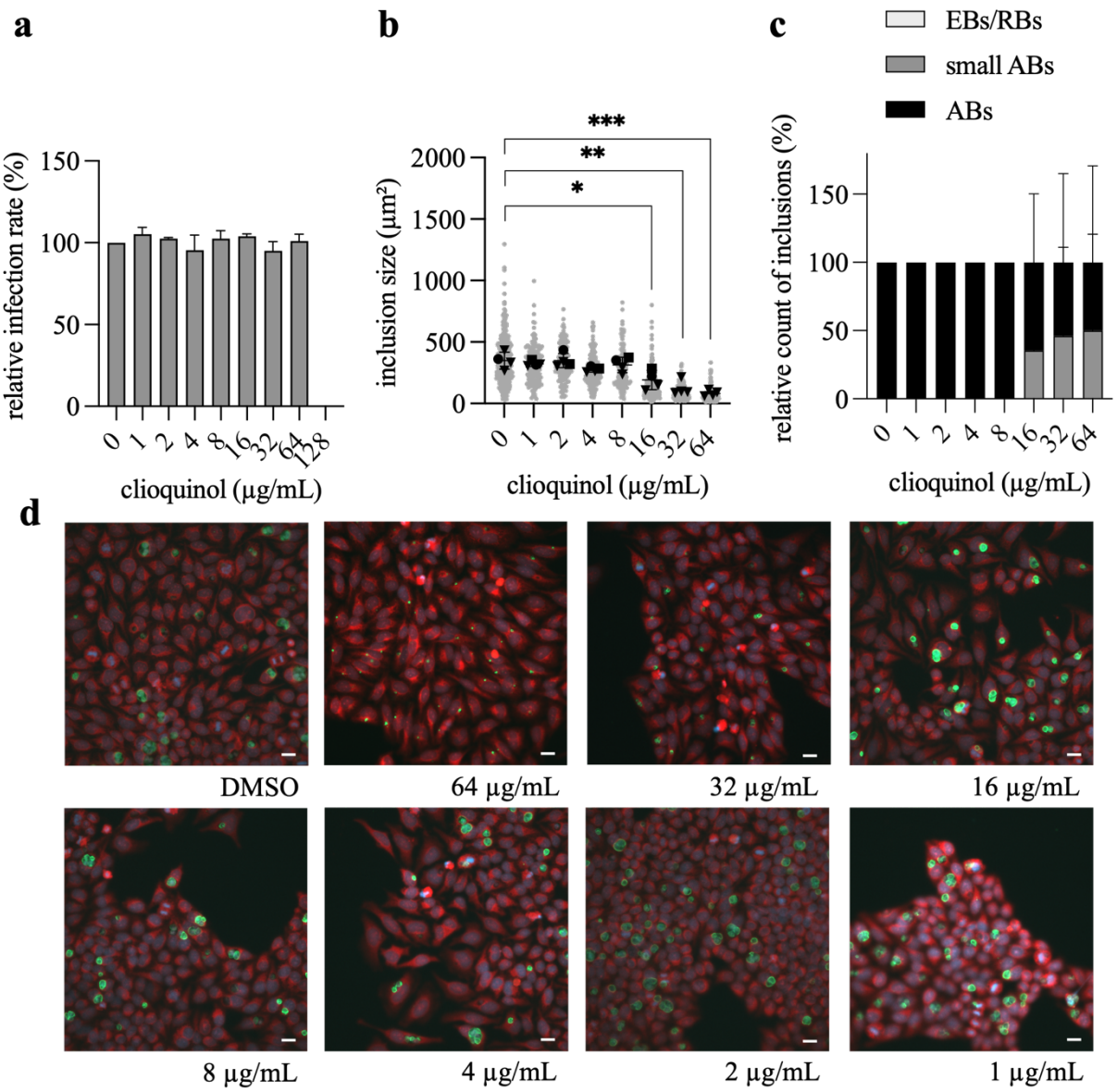

Figure 30: Effects of 18-hour clioquinol treatment on penicillin-induced persistent chlamydial infections (treatment timepoint: 12 hpi). (a) Relative infection rate compared to the DMSO vehicle control (0 µg/mL). 18-hour clioquinol treatment using concentrations 1 – 64 µg/mL did not affect the infection rate. No infection of host cells could be monitored after treatment with 128 µg/mL clioquinol (b). Inclusion sizes were significantly reduced at 16 - 64 µg/mL clioquinol. (c) While treatment with the vehicle control and 1 – 8 µg/mL clioquinol did not affect the penicillin-induced aberrant phenotype, treatment with 16 – 64 µg/mL clioquinol caused up to 50 % of chlamydial cells to form small ABs. (d) Fluorescence microscopy images show inclusions with aberrant bodies when infections were treated with 1 – 8 µg/mL clioquinol, whereas smaller inclusions were observed for infections treated with higher concentrations. Scale bar = 20 µm. Error bars indicate ± s.d. (n = 3 biological replicates with 2 technical replicates each). Unpaired t-test, two-tailed. Significance: * = $p \leq 0.05$, ** = $p \leq 0.01$, *** = $p \leq 0.001$, **** = $p \leq 0.0001$.

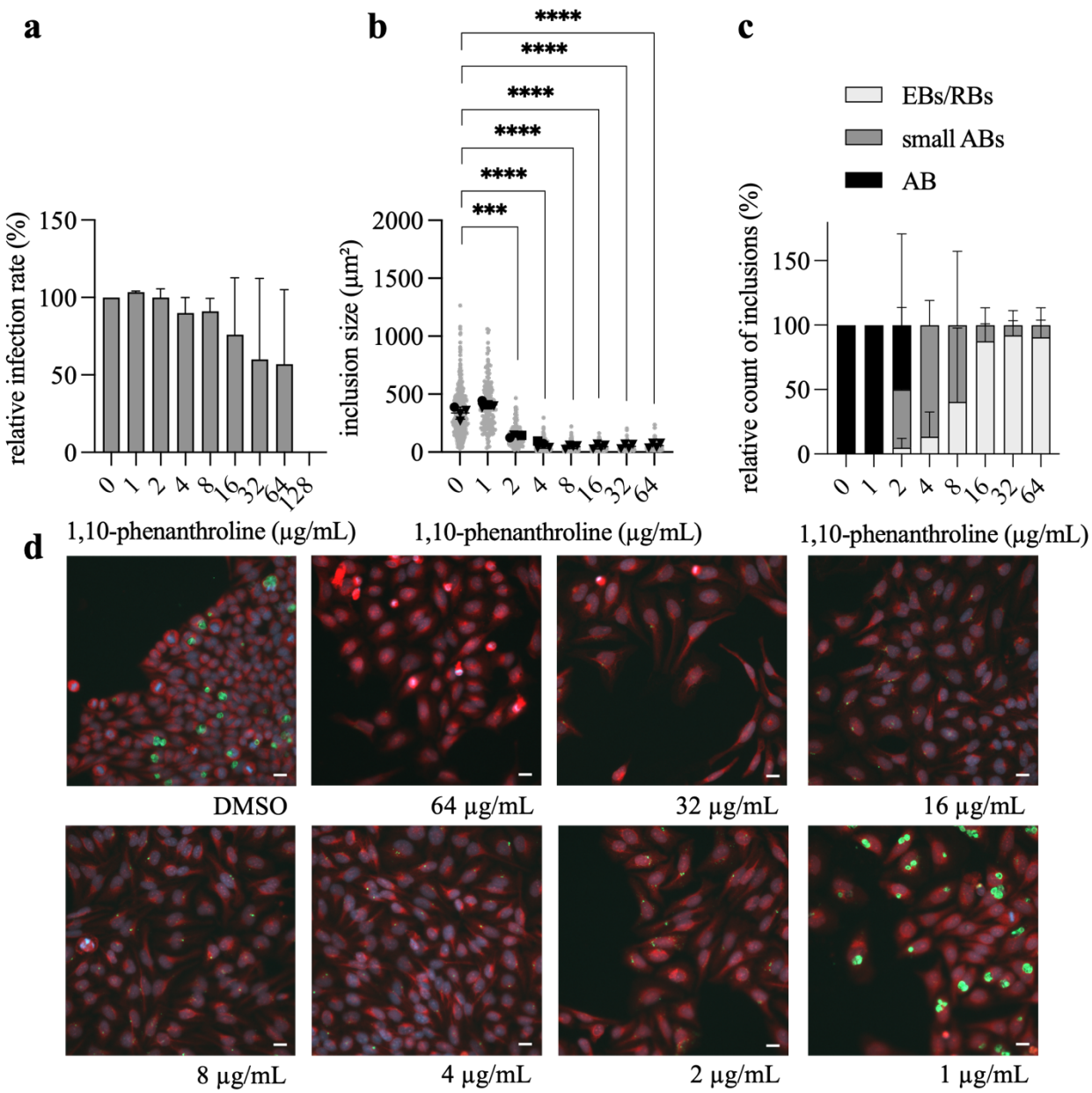

Figure 31: Effects of simultaneous 1,10-phenanthroline and penicillin G treatment on chlamydial infections (treatment timepoint: 2 hpi). (a) Relative infection rate compared to the DMSO vehicle control (0 µg/mL). No chlamydial infection was monitored under treatment with 128 µg/mL 1,10-phenanthroline. (b) Infection rates were reduced by almost 50 % by 64 µg/mL 1,10-phenanthroline and inclusion sizes were significantly reduced at 2 - 64 µg/mL 1,10-phenanthroline. (c) While treatment with the vehicle control and 1 µg/mL 1,10-phenanthroline did not affect the penicillin-induced aberrant phenotype, almost half of chlamydial cells were present as small ABs when treated with 2 µg/mL 1,10-phenanthroline and the percentage rised to almost 80 % under 4 µg/mL 1,10-phenanthroline treatment. (d) Fluorescence microscopy images show inclusions with aberrant bodies when infections were treated with 1 µg/mL 1,10-phenanthroline, whereas very small inclusions with chlamydial cells present as small ABs were visible for the higher treatment concentrations tested. Scale bar = 20 µm. Error bars indicate ± s.d. (n = 3 biological replicates with 2 technical replicates each). Unpaired t-test, two-tailed. Significance: * = $p \leq 0.05$, ** = $p \leq 0.01$, *** = $p \leq 0.001$, **** = $p \leq 0.0001$.

Like in previous experiments and in line with cytotoxicity experiments, no infection could be detected after 28-hour treatment of penicillin G-induced persistent chlamydial infections with 128 µg/mL 1,10-phenanthroline (Fig. 31a) and relative infection rates were reduced by almost 50 % at 64 µg/mL (Fig. 31b). The treatment impacted inclusion size to a larger extend than the clioquinol treatment, but comparably to 1,10-phenanthroline treatment of active infections: 2 – 64 µg/mL significantly reduced inclusion size in this experiment. Fluorescence microscopy images show very small inclusion sizes confirming these data (Fig. 31d). While the EB/RB phenotype prevailed in very small inclusions in samples treated with 16 – 64 µg/mL, some inclusions containing chlamydial cells present as small ABs were visible in cells treated with 2 – 64 µg/mL (Fig. 31c,d). Also an 18-hour treatment with 1,10-phenanthroline affected chlamydial cells during established persistence (Fig. 32). While no infection occurred at 128 µg/mL treatment, lower concentrations did not affect the infection rate (Fig. 32a), like already seen for 18-hour clioquinol treatment of persistent cells. Inclusion size was affected to a lesser extend compared to longer treatment, but still entailed significant reduction at 8 – 64 µg/mL (Fig. 32b). Fluorescence microscopy images show inclusions to be slightly larger than in the previous experiment and small ABs were observed in up to 50 % of inclusions treated with 16 – 64 µg/mL 1,10-phenanthroline (Fig. 32c,d). Interestingly, chlamydial cells present as small ABs were more abundant when cells were treated with chelating compounds 12 hpi. All in all, 1,10-phenanthroline treatment affected chlamydial infection rate, inclusion size and phenotype. Like for clioquinol, the only concentration producing effects meeting the definition criteria for an MIC is 128 µg/mL, as lower concentrations did not lead to reductions or alterations of 90 % or higher. While for a 28-hour treatment the CC_{50} is exceeded by 128 µg/ml 1,10-phenanthroline, the MIC could be determined at 128 µg/mL for an 18-hour treatment regimen, as the CC_{50} is not exceeded.

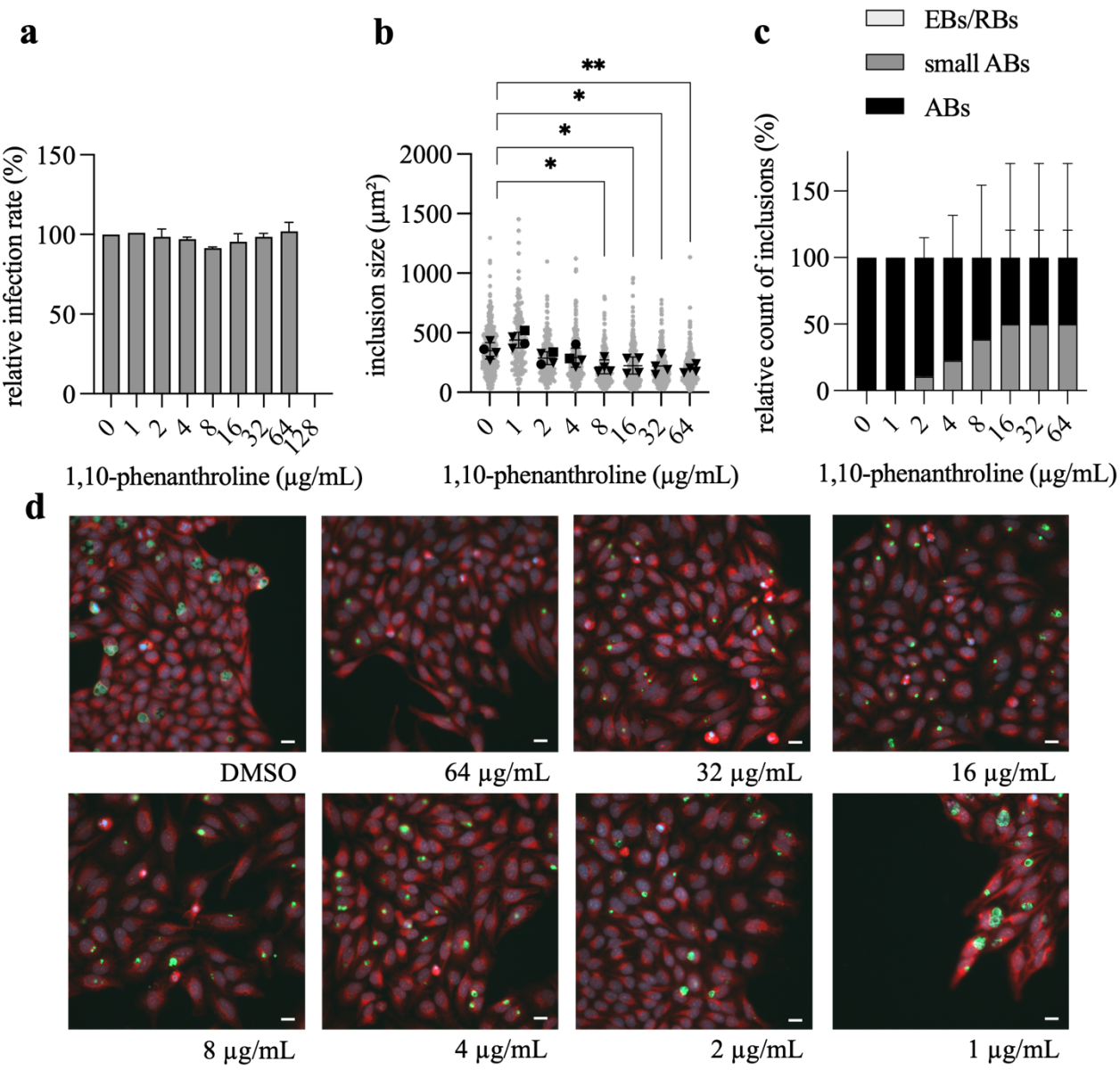

Figure 32: Effects of 18-hour 1,10-phenanthroline treatment on penicillin-induced persistent chlamydial infections (treatment timepoint: 12 hpi). (a) Relative infection rate compared to the DMSO vehicle control (0 µg/mL). No chlamydial infection was monitored under treatment with 128 µg/mL 1,10-phenanthroline, while lower concentrations of 1,10-phenanthroline did not affect infection rates. (b) Inclusion sizes were significantly reduced at 8 - 64 µg/mL 1,10-phenanthroline. (c) While treatment with the vehicle control and 1 µg/mL 1,10-phenanthroline did not affect the penicillin-induced aberrant phenotype, almost half of chlamydial cells were present as small ABs when treated with 16 - 64 µg/mL 1,10-phenanthroline. (d) Fluorescence microscopy images show inclusions with predominantly aberrant bodies. With rising concentrations, the inclusion sizes decreased, and the aberrant phenotype was partly changed towards small ABs. Scale bar = 20 µm. Error bars indicate ± s.d. (n = 3 biological replicates with 2 technical replicates each). Unpaired t-test, two-tailed. Significance: * = $p \leq 0.05$, ** = $p \leq 0.01$, *** = $p \leq 0.001$, **** = $p \leq 0.0001$.

3.5.4. Effects of metal chelators on interferon-γ induced persistent chlamydial infections tested in cell culture-based infection models

The effects of metal chelators clioquinol and 1,10-phenanthroline on interferon-γ (IFN-γ)-induced persistent chlamydial infections were investigated in the same way that active infections have been and like described in section 3.5.2. with the only exception of cells being pretreated with interferon-γ 24 hours prior to infection and 2 hpi. IFN-γ-induced persistence is mechanistically different from penicillin G-induced persistence, as instead of inhibition of cell division proteins, a tryptophane starvation is induced by IFN-γ. By including this model, a comparative approach of effects of metal chelators on two different persistence models is enabled. The experimental setup is depicted in Figure 33. Due to the pretreatment of host cells with IFN-γ 24 h prior to infection, tryptophane starvation is already induced at the onset of chlamydial infection.

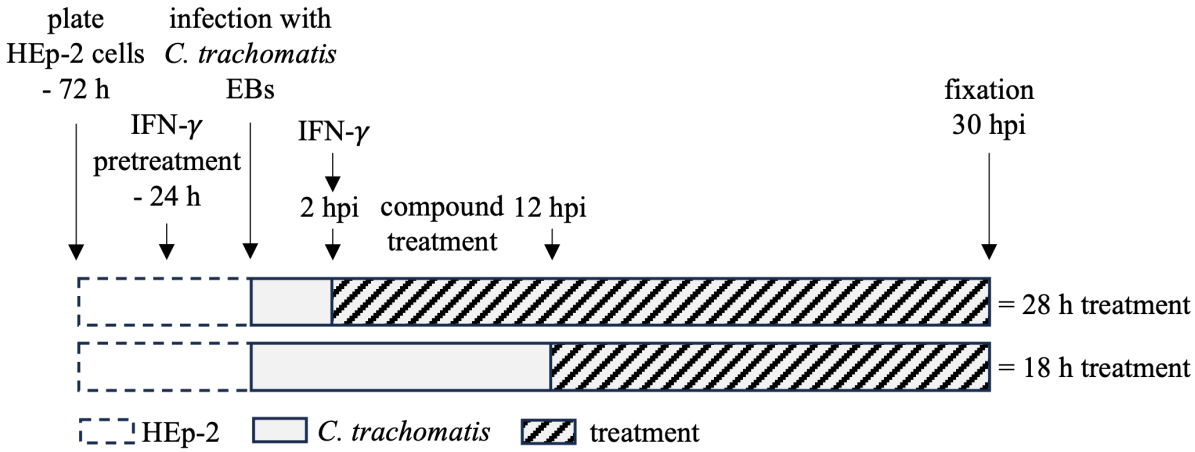

Figure 33: Diagram for the treatment of interferon-γ-induced persistent chlamydial infections using metal chelators. HEp-2 cells were grown until monolayer formation and pre-treated with 40 U/mL interferon-γ 24 hours prior to infection with EBs of *C. trachomatis*. Compounds were added 2 hpi and 12 hpi to media containing 40 U/mL interferon-γ and infected cells were incubated for 28 hours and 18 hours, respectively. After methanol fixation 30 hpi, cells were stained and imaged using fluorescence microscopy.

64 – 128 µg/mL clioquinol eradicated chlamydial infection entirely in this model, in which infected cells were treated with clioquinol for 28 hours starting 2 hpi (Fig. 34). 16 – 32 µg/mL clioquinol reduced relative infection rates, however not to a significant extend (Fig. 34a). Lower concentrations did not have a negative effect on chlamydial infection rates. Inclusion sizes were visibly smaller when treated with 32 µg/mL clioquinol, but not to a significant extend (Fig. 34b). This is also reflected in the fluorescence microscopy images, where 32 µg/mL clioquinol treatment produced smaller inclusions compared to the other conditions (Fig. 34d). Lower concentrations did not lead to any effects and, on average, mean values were similar compared to the vehicle control (Fig. 34b). Phenotype classification revealed that the expected interferon-γ induced phenotype of aberrant bodies was not altered by either concentration of clioquinol (Fig. 34c). Analysis of fluorescence microscopy images showed that

inclusion sizes were comparable to the vehicle control upon treatment of 1- 16 µg/mL, while 32 µg/ml clioquinol produced inclusions that were mostly smaller (Fig. 34d). Concentrations of 64 µg/mL and higher eradicated chlamydial infection, so that inclusion sizes could not be determined.

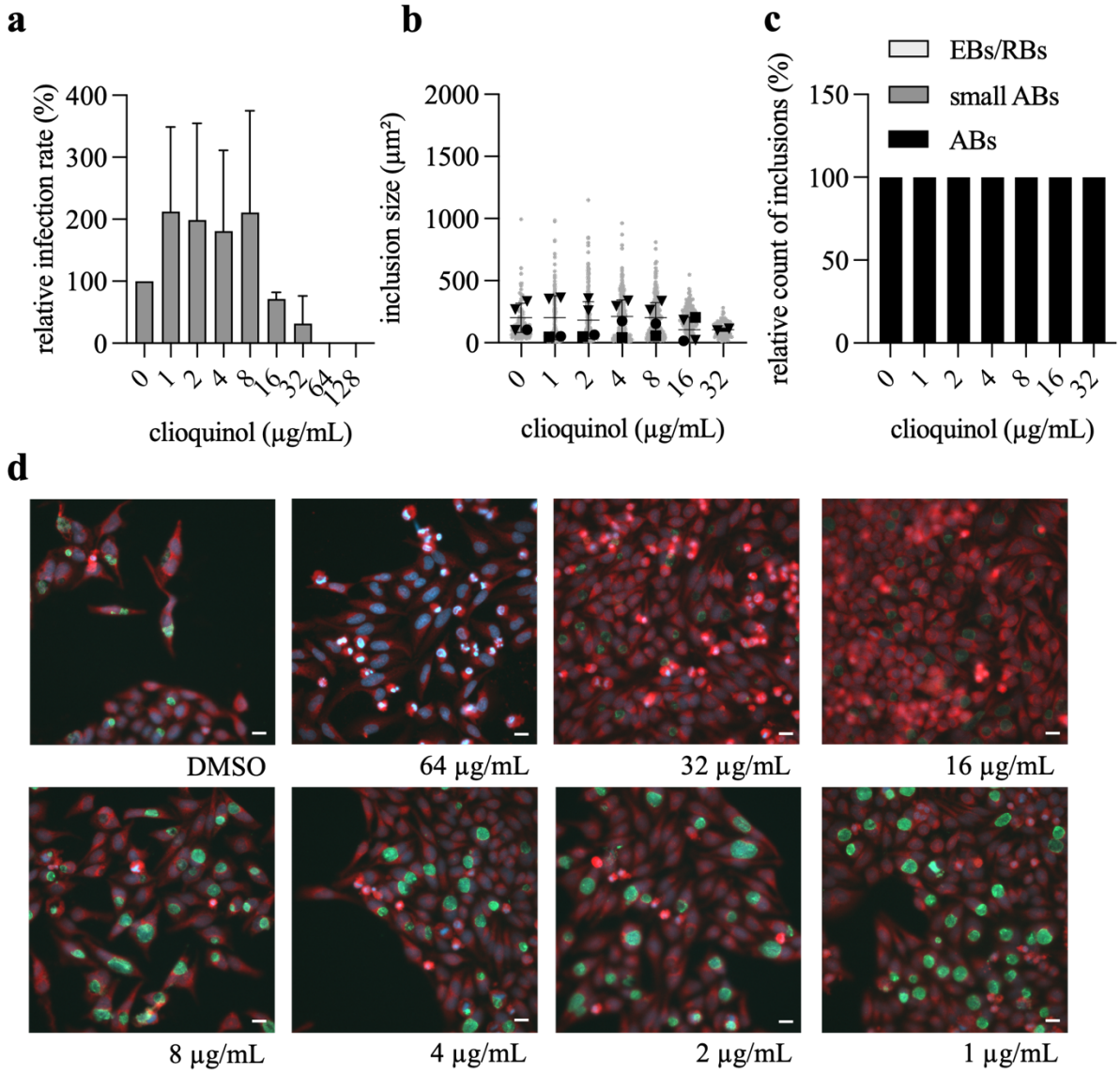

Figure 34: Effects of 28-hour clioquinol treatment on interferon-γ-induced persistent chlamydial infections (treatment timepoint: 2 hpi). (a) Relative infection rate compared to the DMSO vehicle control (0 µg/mL). When treated with 128 - 64 µg/mL clioquinol, none of the host cells was infected. Relative infection rates were reduced more than 50 % by 32 µg/mL clioquinol and 16 µg/mL did not produce significant effects on infection rates compared to the vehicle control. (b) Inclusion sizes were visibly smaller at 32 µg/mL clioquinol compared to the vehicle control, but overall, effects were not significant. (c) The aberrant phenotype induced by IFN-γ treatment was not altered by clioquinol application at either concentration and aberrant bodies, sized as expected for IFN-γ-treated cells, were observed throughout. (d) Fluorescence microscopy images show inclusions with small aberrant bodies in all conditions independent from the concentration of clioquinol. Scale bar = 20 µm. Error bars indicate ± s.d. (n = 2 biological replicates with 2 technical replicates each). Unpaired t-test, two-tailed.

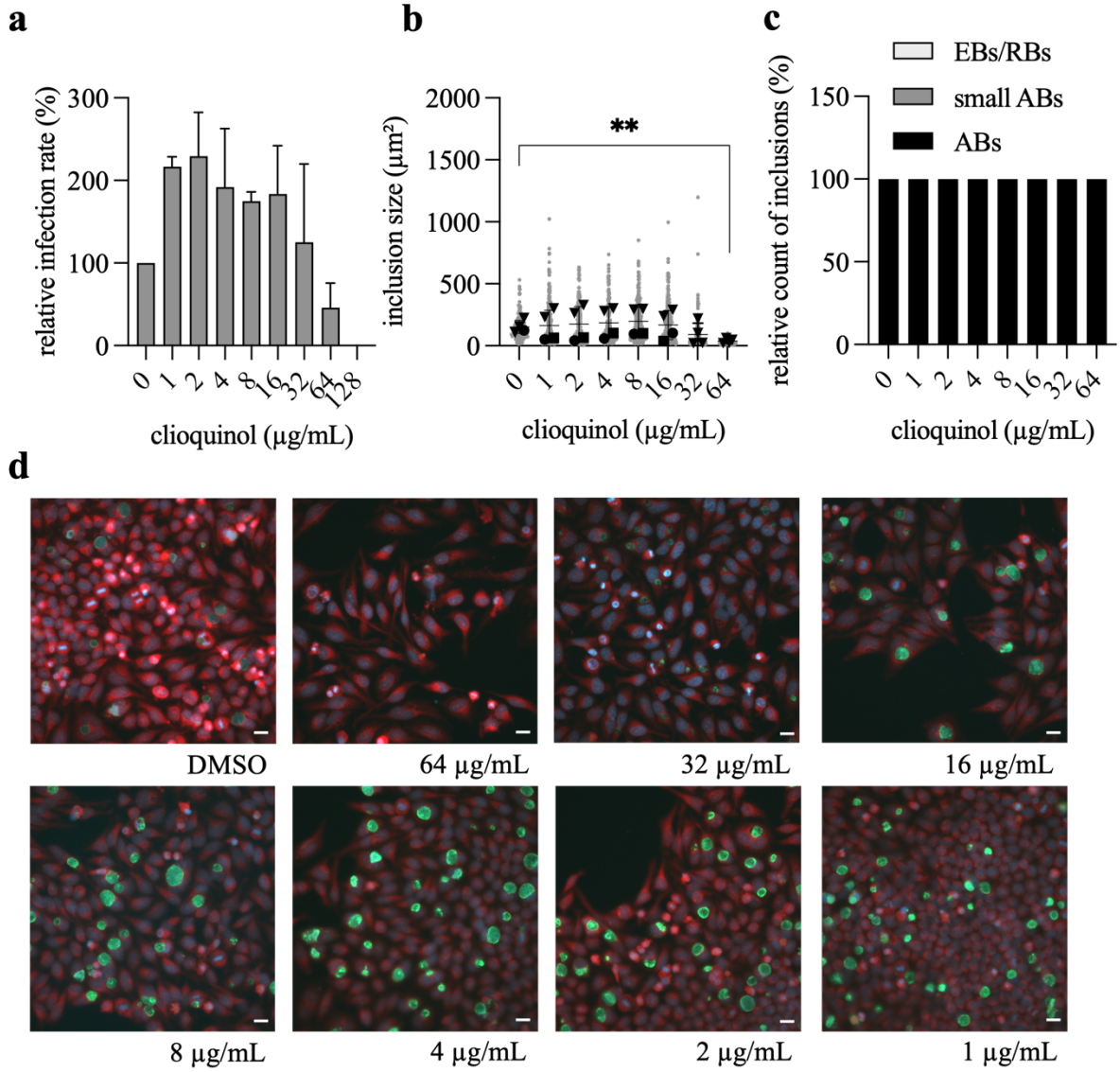

Figure 35: Effects of 18-hour clioquinol treatment on interferon-γ-induced persistent chlamydial infections (treatment timepoint: 12 hpi). (a) Relative infection rate compared to the DMSO vehicle control (0 µg/mL). When treated with 128 µg/mL clioquinol, none of the host cells was infected. Relative infection rates were reduced approx. 50 % by 64 µg/mL clioquinol. Overall, effects on relative infection rates were not significant. (b) Inclusion sizes were visibly and significantly reduced at 64 µg/mL clioquinol compared to the verhicle control. Lower concentrations did not lead to significant effects. (c) The aberrant phenotype induced by IFN-γ treatment was not altered by clioquinol application at either concentration and aberrant bodies, sized as expected in IFN-γ treatment were observed throughout. (d) Fluorescence microscopy images show inclusions with small aberrant bodies in all conditions independent from the concentration of clioquinol. Concentrations of 64 µg/mL and 32 µg/mL produced very small inclusions. Scale bar = 20 µm. Error bars indicate ± s.d. (n = 2 biological replicates with 2 technical replicates each). Unpaired t-test, two-tailed. Significance: * = $p \leq 0.05$, ** = $p \leq 0.01$.

In comparison, the effects of 18-hour clioquinol treatment on interferon-γ induced persistent chlamydial infections were assessed (Fig. 35). The highest clioquinol concentration applied led to clearance of

chlamydial infection. While the same effect was observed for 64 µg/mL in the 28-hour treatment model, here, 64 µg/mL clioquinol led to an approx. 50 % reduction of infection rate (Fig. 35a). Treatment with 64 µg/mL clioquinol led to a significant reduction of inclusion size, whereas lower concentrations had no significant effects (Fig. 35b). Like in the previous experiment with the longer treatment duration, the aberrant body phenotype as induced by interferon-γ-treatment prevailed throughout the experiment and was not altered by any clioquinol concentration applied (Fig. 35c). Fluorescence microscopy images showed barely visible inclusions in infection models treated with 64 µg/mL clioquinol (Fig. 35d). At lower concentrations, inclusions were visible and approx. equal in size.

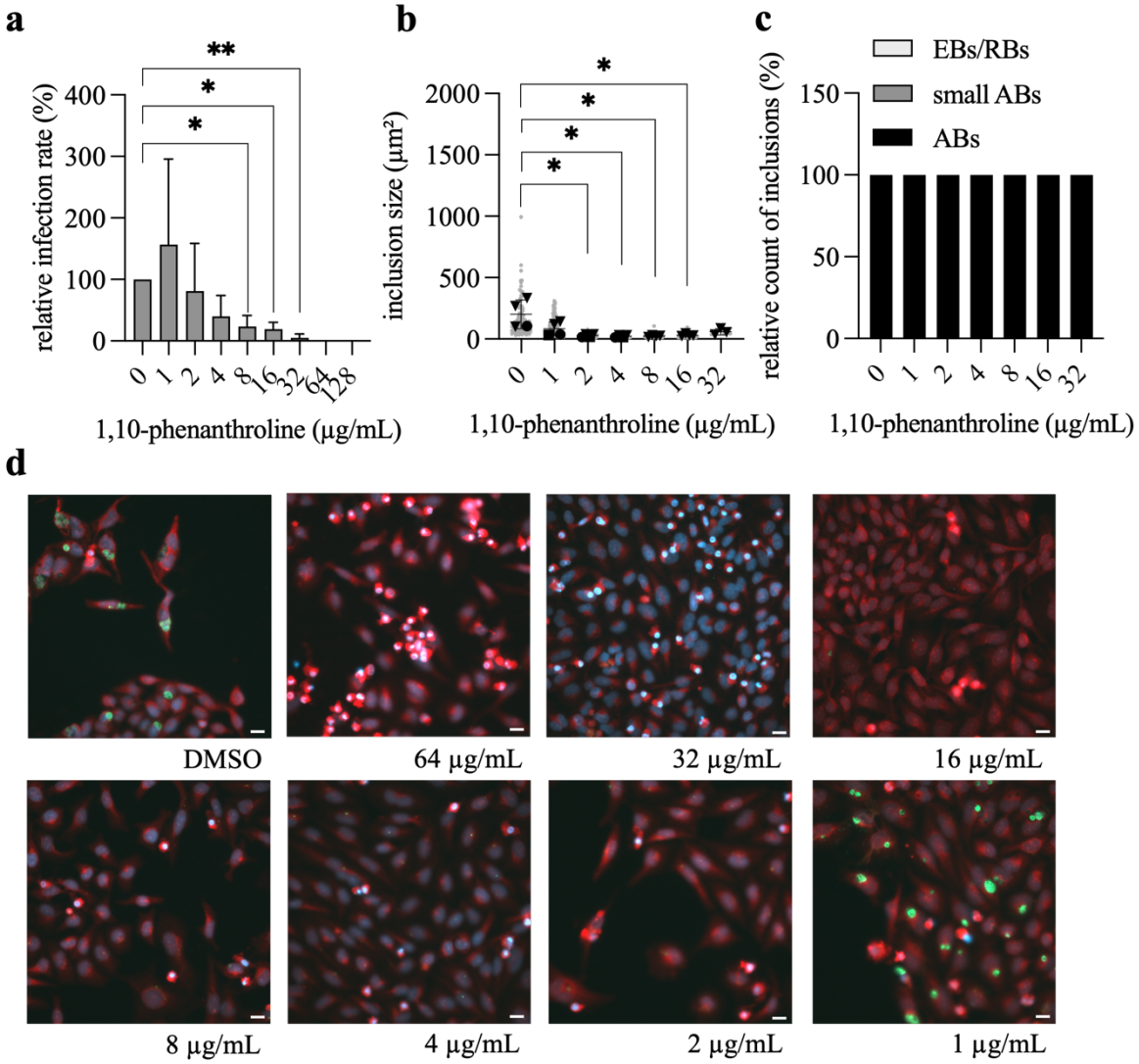

Figure 36: Effects of 28-hour 1,10-phenanthroline treatment on interferon-γ-induced persistent chlamydial infections (treatment timepoint: 2 hpi). (a) Relative infection rate compared to the DMSO vehicle control (0 µg/mL). When treated with 64 - 128 µg/mL 1,10-phenanthroline, none of the host cells was infected. Relative infection rates were reduced significantly by 8 – 32 µg/mL 1,10-phenanthroline and 4 µg/mL led to a reduction of approx. 50 %. (b) Inclusion sizes were visibly reduced by all concentrations except 1 µg/mL compared to the vehicle control and effects were significant at 2

– 16 µg/mL. (c) The aberrant phenotype induced by interferon-γ treatment was not altered by 1,10-phenanthroline application at either concentration and ABs sized as expected were observed throughout. (d) Fluorescence microscopy images show very small inclusions that were barely visible at 2 – 32 µg/mL with ABs in all conditions independent from the concentration of 1,10-phenanthroline. Scale bar = 20 µm. Error bars indicate ± s.d. (n = 2 biological replicates with 2 technical replicates each). Unpaired t-test, two-tailed. Significance: * = $p \leq 0.05$, ** = $p \leq 0.01$.

As previously observed for clioquinol, 64 - 128 µg/mL 1,10-phenanthroline led to a clearance of chlamydial infection in this model when applied on interferon-γ-induced persistent chlamydial infections for 28 hours (Fig. 36a). Concentrations of 8 – 32 µg/mL led to a significant reduction of inclusion size, whereas lower concentrations did not. All concentrations except for 1 µg/mL and 32 µg/mL led significant decreases of inclusion sizes (Fig. 36b). This is also shown in fluorescence microscopy images, where no inclusions were present at 64 µg/mL and upon treatment of 32 – 2 µg/mL, inclusions were mostly barely visible and very small (Fig. 36d). Like in all other experiment within the interferon-γ- induced persistence models, no alteration of phenoytypes could be observed in this experiment either (Fig. 36c). Analogously to the same treatment duration model with clioquinol, only 128 µg/mL 1,10-phenanthroline applied 12 hpi for 18 hours led to eradication of chlamydial infection, but not 64 µg/mL like in the 28-hour treatment model (Fig. 37a). While 64 µg/mL led to a reduction of relative infection rate of approx. 75 %, effects were not significant at either concentration. Treatment with 1,10-phenanthroline also entailed reduction of inclusion sizes, which was significant at 4 – 64 µg/mL (Fig. 37b). On average, inclusions were larger than in the model with the 28-hour treatment duration shown in the previous figure, so that inclusion visibility was better in fluorescence microscopy images compared to the previous experiment (Fig. 37d). This finding was according to expectations, as the onset of starvation putatively induced by chelators was later and therefore led to a shorter exposure. Under these conditions, no alteration of the typical interferon-γ induced persistent phenotype of chlamydial cells could be observed here either (Fig. 37c). As observed in previous experiment, neither clioquinol nor 1,10-phenanthroline treatment below 128 µg/mL met the criteria set for the determination of the MIC in *Chlamydia*. As cytotoxicity has been observed for both compounds at this concentration, effects on *Chlamydia* and effects on host cells cannot be distinguished from each other. Therefore, an MIC cannot be determined here either.

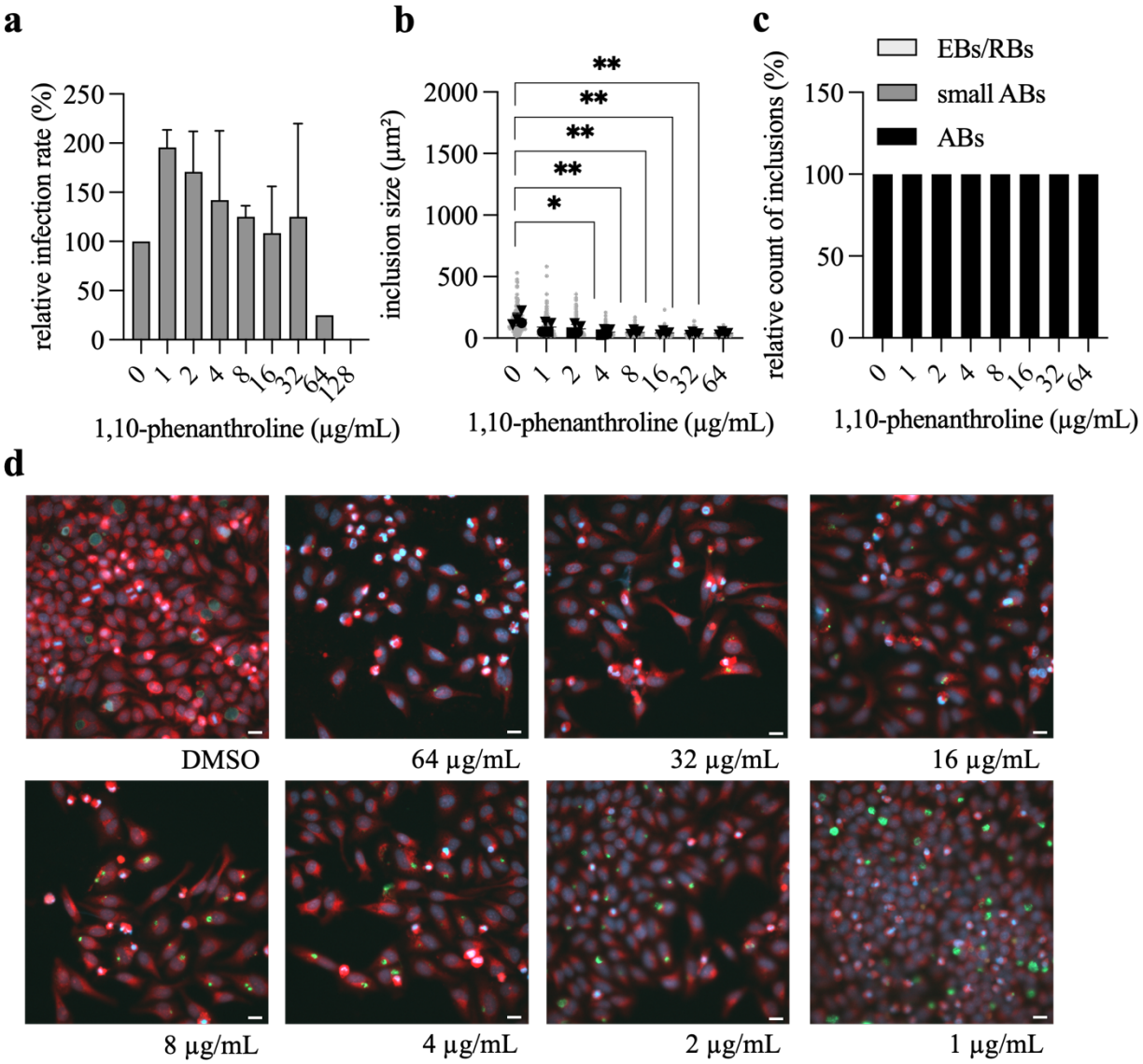

Figure 37: Effects of 18-hour 1,10-phenanthroline treatment on interferon-γ-induced persistent chlamydial infections (treatment timepoint: 12 hpi). (a) Relative infection rate compared to the DMSO vehicle control (0 µg/mL). When treated with 128 µg/mL 1,10-phenanthroline, none of the host cells was infected. Relative infection rates were reduced by 64 µg/mL clioquinol, but effects were not significant. (b) Inclusion sizes were visibly reduced by all concentrations compared to the vehicle control and effects were significant at 4 – 64 µg/mL. (c) The aberrant phenotype induced by interferon-γ treatment was not altered by clioquinol application at either concentration and ABs were observed throughout. (d) Fluorescence microscopy images show very small inclusions that were barely visible at 2 – 64 µg/mL with ABs in all conditions independent from the concentration of 1,10-phenanthroline. Scale bar = 20 µm. Error bars indicate ± s.d. (n = 2 biological replicates with 2 technical replicates each). Unpaired t-test, two-tailed. Significance: * = $p \leq 0.05$, ** = $p \leq 0.01$.

3.5.5. Rescue of chelator-treated chlamydial infections

The results of previous experiments showed that the chelating compounds clioquinol and 1,10-phenanthroline affected growth, morphology, and proliferation of chlamydial infections (see 3.5.2-3.5.4). Originally, clioquinol and 1,10-phenanthroline were included in this work to test *in vitro* inhibition of purified AmiA_Ct. However, the effects of these inhibitors in tissue culture, a more complex system, cannot only be attributed to one specific action such as the withdrawal of a zinc atom from AmiA. Instead, these compounds were included in cell culture-based infection models to test if treatment with metal chelators can induce nutrient starvation-mediated persistence in *Chlamydia*. Clioquinol and 1,10-phenanthroline are known to form complexes with bivalent cations, such as Zn^{2+} but also Fe^{2+}. It was, therefore, investigated if the observed effects might have been mediated by iron starvation by adding $FeSO_4$ to clioquinol and 1,10-phenanthroline-treated cells. Yet, $ZnSO_4$ was utilized in the experiment as well to determine if effects were zinc-specific. To perform the experiment, cytotoxic effects of metal compounds $ZnSO_4$ and $FeSO_4$ had to be excluded. As a control, $ZnSO_4$, $FeSO_4$, and a combination of both were applied to infected eukaryotic cells together with DMSO as a vehicle control, 2 hpi or 12 hpi (Fig. 38). Experiments were stopped 30 hpi, corresponding to treatment durations of 28 hours and 18 hours, respectively. After staining, cells were imaged by fluorescence microscopy. Neither 40 µg/mL $FeSO_4$, 20 µg/mL $ZnSO_4$ nor the combination of both metal compounds exhibited any visible damage on the host cell monolayer or *C. trachomatis.* In addition, 2,2-bipyridyl, as a commonly used iron starvation agent in *Chlamydia,* was applied to an active chlamydial infection. Fluorescence microscopy images revealed that 2,2-bipyridyl treatment starting 2 hpi allowed the formation of single small inclusions with few chlamydial cells visible. When treated for a shorter time starting 12 hpi, inclusions were slightly larger, but an abnormal phenotype of chlamydial cells within the inclusions was still visible. The control experiment showed, in this model, that controlled iron starvation induced a similar phenotype to what was observed in previous experiments with clioquinol and 1,10-phenanthroline. Moreover, $FeSO_4$ and $ZnSO_4$ were shown not to be cytotoxic to both host cells and *C. trachomatis* at the employed concentrations. Therefore, they could be tested together with chelation agents as a next step.

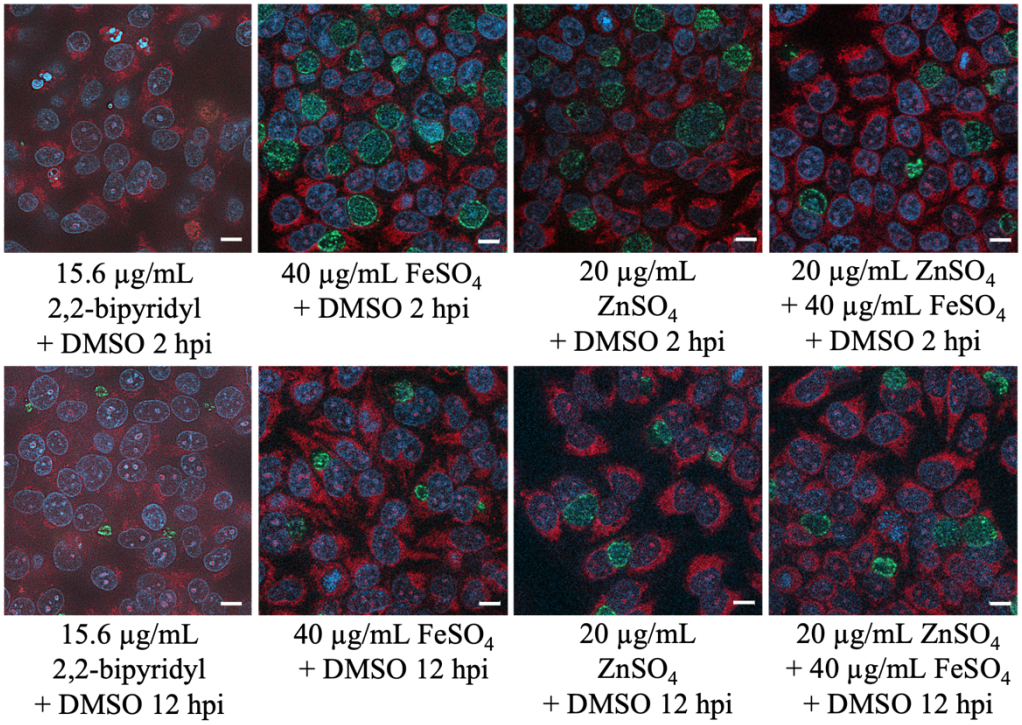

Figure 38: 2,2-bipyridyl treatment led to small inclusions filled with slightly enlarged chlamydial cells. Inclusion and cell morphology were normal when $FeSO_4$, $ZnSO_4$ or a combination of both was applied 2 hpi and 12 hpi. At any condition, DMSO was also applied to cells to serve as a vehicle control for following experiments, as chelators were dissolved in DMSO. Scale bar = 10 µm.

A rescue attempt of chlamydial infections treated with clioquinol or 1,10-phenanthroline for either 18 or 28 hours was performed by supplementing either $ZnSO_4$, $FeSO_4$ or a combination of both 2 hpi (Fig. 39). Treatment with both metal chelators at either timepoint resulted in the phenotype described previously, marked by small inclusions and an abnormal phenotype of chlamydial cells. When $FeSO_4$ was added 2 hpi, chlamydial cells treated with chelators, either simultaneously or 12 hpi, displayed no unusual phenotypes in terms of inclusion size and cell morphology. The same outcome was visible when 1,10-phenanthroline-treated cells were treated with $ZnSO_4$ or a combination of $FeSO_4$ and $ZnSO_4$. Clioquinol-treated cells were entirely eradicated when supplemented with $ZnSO_4$ or the combination of both metal compounds, so that images for these conditions were not obtained. These results indicate that the chlamydial phenotype induced by 1,10-phenanthroline can be averted by the addition of $FeSO_4$ alone or $ZnSO_4$ alone. The combination of both metal compounds did not change the resulting chlamydial phenotype or cell morphology and rescued chlamydial phenotype as well. Clioquinol-treated cells did not tolerate the addition of $ZnSO_4$ or the combination of both metal compounds combined. However, they were rescued by the addition of $FeSO_4$ alone. As results of control experiments (Fig. 38) proved, both metal compounds in combination did not show any toxic properties on either host cells or chlamydial infections, indicating a synergistic effect of clioquinol and zinc-containing compounds that leads towards cell death.

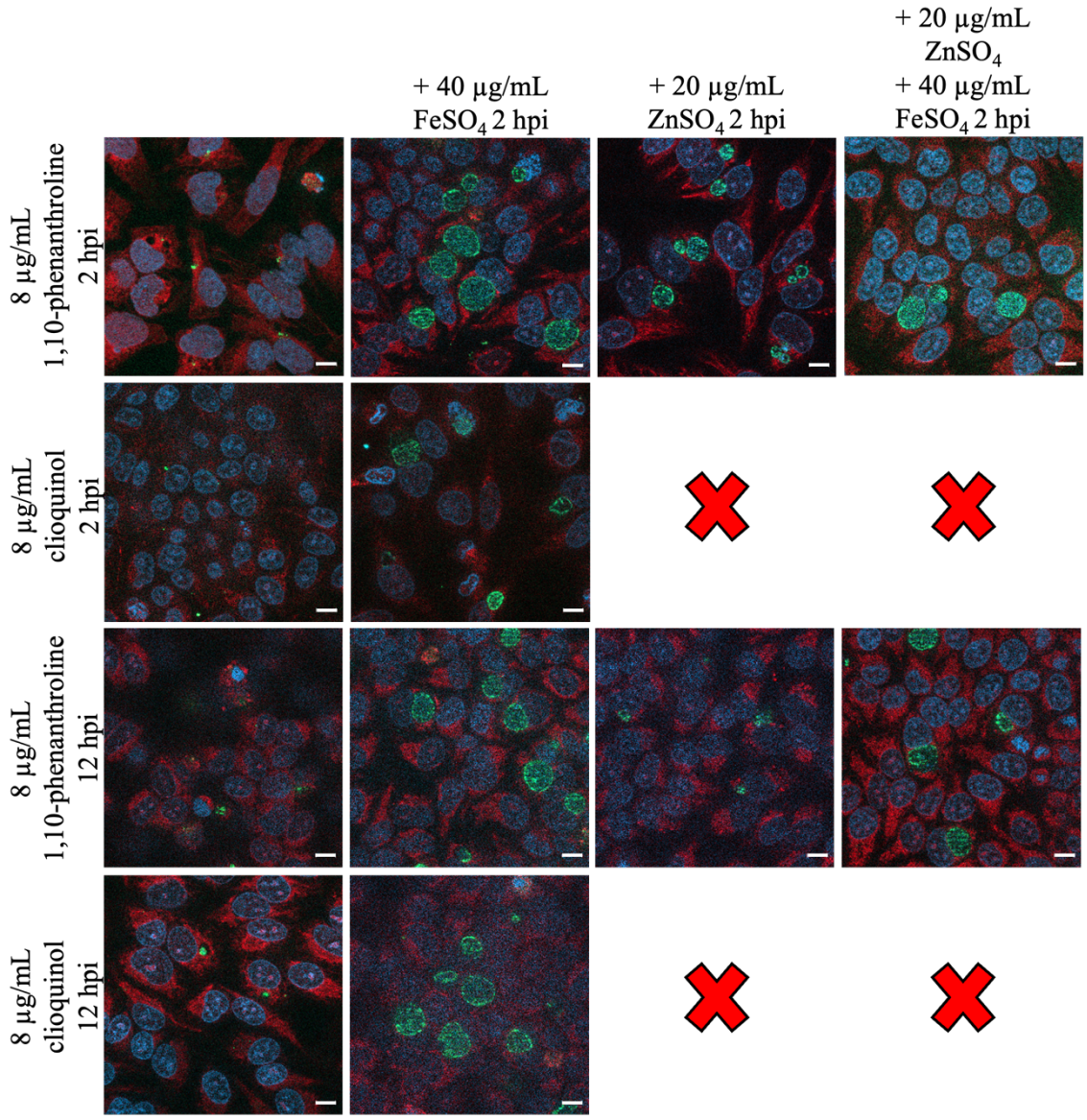

Figure 39: Rescue of 1,10-phenanthroline and clioquinol-induced phenotypes by iron and zinc compounds applied 2 hpi. Clioquinol and 1,10-phenanthroline induced the formation of very small inclusions filled with abnormal looking chlamydial cells when applied either 2 hpi or 12 hpi. When $FeSO_4$ was added 2 hpi, chlamydial cell morphologies normalized and regular inclusion sizes were observed in all conditions. The same applied to $ZnSO_4$ addition to 1,10-phenanthroline-treated cells. Also, a combination of $ZnSO_4$ and $FeSO_4$ was able to rescue 1,10-phenanthroline-induced chlamydial phenotypes. $ZnSO_4$ alone and the combination of $ZnSO_4$ and $FeSO_4$ however killed infected host cells treated with clioquinol entirely. Scale bar = 10 µm.

In a different approach, chelator-treated cells were supplemented with $FeSO_4$, $ZnSO_4$ or a combination of both 12 hpi. This way, metals were added to infected and chelator-treated cells either 10 hours after the addition of clioquinol or 1,10-phenanthroline or simultaneously. Fluorescence images show that 2 hpi and 12 hpi 1,10-phenanthroline-treated cells were rescued by the addition of $FeSO_4$, $ZnSO_4$ and the

combination of both metal compounds (Fig. 40). Also, supplementation of $FeSO_4$ to clioquinol-treated cells led to normalization of inclusion size and chlamydial phenotype in comparison to cells that had been treated with clioquinol alone. Like in the previous experiment, images for clioquinol-treated cells supplemented with $ZnSO_4$ or the combination of $FeSO_4$ and $ZnSO_4$ at either timepoint could not be obtained, as cells did not tolerate clioquinol in combination with $ZnSO_4$, likely due to ionophoric properties of clioquinol, and died. In sum, 1,10-phenanthroline-treated cells could be rescued also when metal compounds were added 12 hpi. This also applied for clioquinol-treated chlamydial infections, but only for iron and not zinc supplementation. These results indicate that the phenotype observed after clioquinol and 1,10-phenanthroline treatment is not zinc-specific, as it could be averted by the addition of iron. These results match expectations towards chelation agents that are not specific, but instead confer affinity towards a set of bivalent cations.

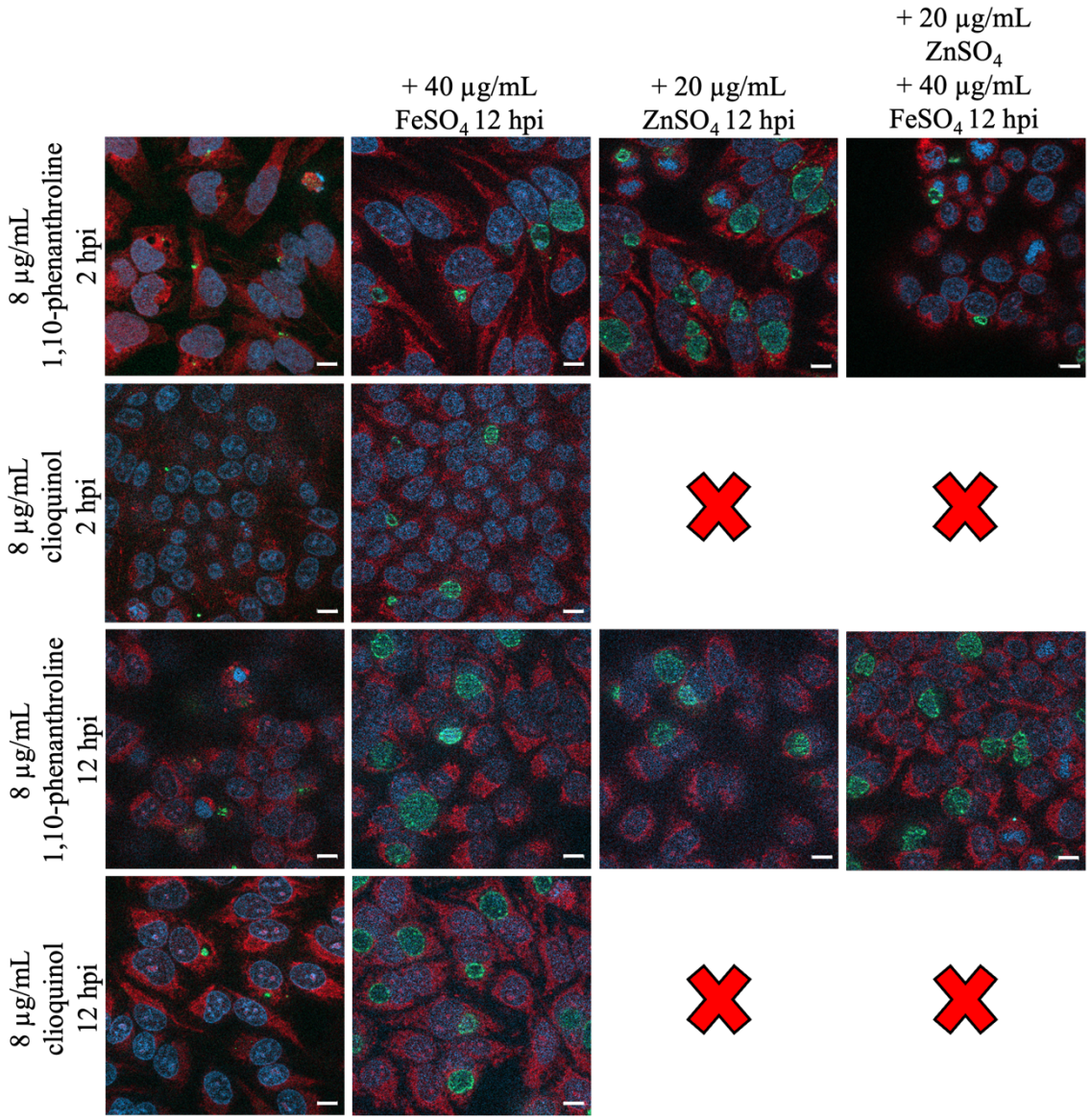

Figure 40: Rescue of 1,10-phenanthroline and clioquinol-induced phenotypes by iron and zinc compounds applied on an established *C. trachomatis* infection 12 hpi. Application of $FeSO_4$ on cells

treated with clioquinol or 1,10-phenanthroline 2 hpi and 12 hpi led to a normalization of inclusion size and chlamydial cell morphology. The same applied for cells treated with 1,10-phenanthroline 2 hpi or 12 hpi supplied with $ZnSO_4$ and a combination of $FeSO_4$ and $ZnSO_4$. Like in the previous experiment, clioquinol-treated infected host cells were eradicated by the addition of $ZnSO_4$ and the combination of both metal compounds. Scale bar = 10 µm.

3.5.6. Recovery of active and penicillin G-induced persistent chlamydial infections treated with metal chelators

In the previous experiments, the effect of metal chelators clioquinol and 1,10-phenanthroline was investigated mechanistically. The observed chlamydial phenotypes could be attributed to chelation of bivalent cations, which are needed in chlamydial development. The observed phenotype of small aberrant bodies under chelator treatment alluded to persistence and nutrient starvation-induced persistence has been described for *Chlamydia*. To verify if treatment with metal chelators induces nutrient starvation-mediated persistence in *Chlamydia*, it was necessary to test if the hallmark of persistence, reversibility, was met. Therefore, recovery assays were performed to determine if the effects of the tested metal chelators on chlamydial infections, shown in the previous section, affect the generation of infectious progeny after infections were allowed to recover from the compound treatment. If not, effects evoked by chelator treatment could be considered reversible and therefore meet the criteria of chlamydial persistence. Mammalian cells were infected with *C. trachomatis* and treated with tested compounds 2 hpi and 12 hpi. Analogously to previous experiments and corresponding to treatment durations of 18 hours when applied 12 hpi and 28 hours when applied 2 hpi, cells were treated and incubated until media and compounds were removed 30 hpi. For both compounds, only concentrations that did not lead to cytotoxic effects on the host cells, according to cytotoxicity data, were tested. DMSO was used as a vehicle control and was applied for 28 hours, corresponding to the longer treatment regimen that was applied for clioquinol and 1,10-phenanthroline. After fresh medium was supplied, active infections were allowed to recover for further 48 hours, while PenG-induced persistent infections recovered for 72 hours. The infected cells were harvested and supernatants containing chlamydial EBs were stored in phosphate-sucrose buffer at –80 ° C until usage as new inocula on fresh host cell monolayers. Consequently, infectious progeny of treated and recovered chlamydial infections could be determined by fluorescence microscopy and counting of inclusions.

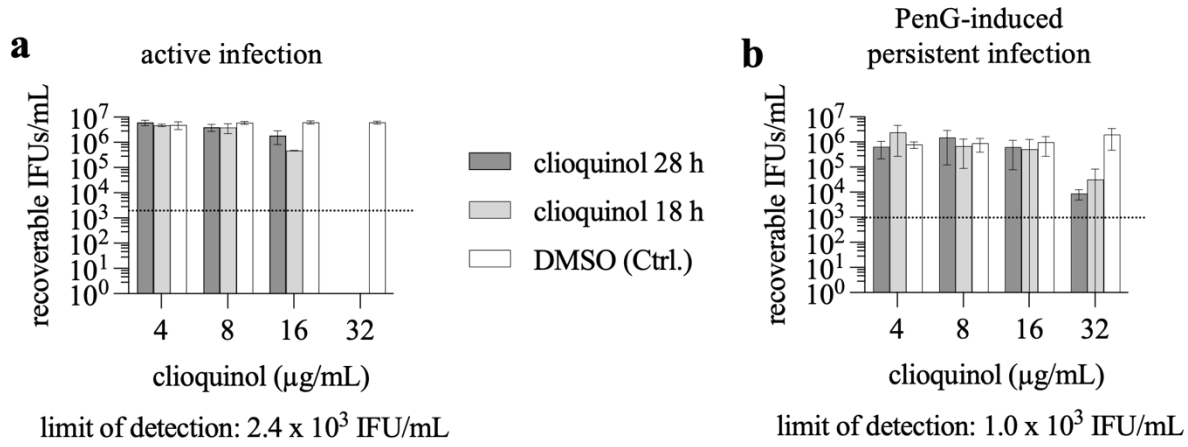

Figure 41: Recovery clioquinol-treated infections. (a) Active chlamydial infections were treated with clioquinol for 18 hours (12 hpi) and 28 hours (2 hpi) and were allowed to recover for 48 hours after removal of the compound. While clioquinol at 4 µg/mL to 16 µg/mL did not have an impact on infectious progeny, chlamydial infections treated with 32 µg/mL clioquinol did not produce infectious progeny. (b) PenG-induced persistent chlamydial infections treated with 4 – 16 µg/mL clioquinol for 18 hours and 28 hours were not impaired in proliferation after 72 hours of recovery. 32 µg/mL slightly impaired generation of infectious progeny. Error bars indicate ± s.d. (n=3).

Active and PenG-induced persistent infections were treated with different concentrations of clioquinol ranging from 4 µg/mL to 32 µg/mL. In active infections, clioquinol did not lead to a decrease of infectious progeny at 4 – 16 µg/mL compared to the vehicle control, except for 16 µg/mL treated for 28 hours, where a slight decrease of IFUs/mL was observable (Fig. 41a). When treated with 32 µg/mL clioquinol, *C. trachomatis* was unable to generate infectious progeny during recovery, even though small inclusions could still be observed under these conditions in the previous experiment (Fig. 25). In PenG-induced persistent infections treated with 4 – 16 µg/mL clioquinol, no decrease of IFUs/mL after recovery compared to the vehicle control was observed. Treatment with 32 µg/mL clioquinol affected production of EBs during lifecycle progression in both the 18 hour and 28 hour treatment, with more profound effects during 28 hour treatment, where no infectious progeny could be generated anymore (Fig. 41b). Except for the treatment of active infections with 32 µg/mL, effects of clioquinol treatment were reversible. Due to its reversibility, in this model, clioquinol was shown to induce nutrient starvation-mediated persistence at concentrations below 32 µg/mL.

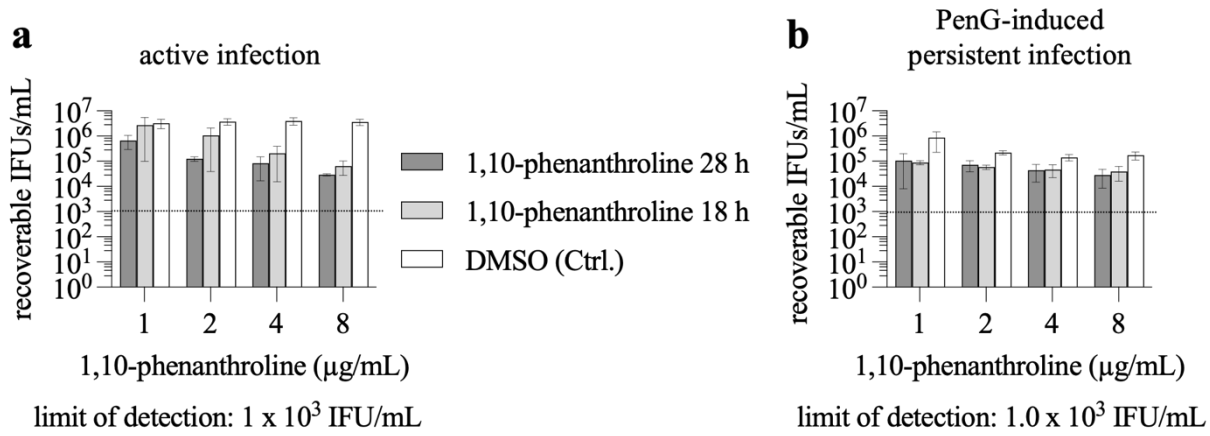

Figure 42: Recovery of 1,10-phenanthroline-treated infections. (a) Active chlamydial infections were treated with 1,10-phenanthroline for 18 hours (12 hpi) and 28 hours (2 hpi) and were allowed to recover for 48 hours after removal of the compound. While 1 µg/mL did not lead to severe impairment of infectious progeny generation, 2 - 4 µg/mL application impaired chlamydial proliferation. In general, a longer treatment duration led to a decrease of recoverable IFUs/mL compared to a shorter treatment duration. (b) PenG-induced persistent chlamydial infections were recovered for 72 hours after removal of the compound. 1 – 8 µg/mL 1,10-phenanthroline only led to a slight decrease of infectious progeny compared to the DMSO vehicle control, that was uniform at all applied concentrations. Error bars indicate ± s.d. (n=3).

Metal chelator 1,10-phenanthroline was applied in a concentration range of 1 – 8 µg/mL. No effects were observed for active infections treated with 1 µg/mL 1,10-phenanthroline, but higher concentrations led to a gradual decrease of IFUs/mL compared to the vehicle control. Effects were more pronounced in the samples treated for 28 hours than for 18 hours (Fig. 42a). Penicillin G-induced persistent infections treated with 1,10-phenanthroline showed a slight decrease in generation of infectious progeny compared to the vehicle control at all tested concentrations. Both treatment durations produced highly comparable amounts of IFUs/mL. In general, 1,10-phenanthroline treatment affected proliferation more strongly when applied on active infections than on penicillin G-induced persistent infections (Fig. 42b). This is in accordance with data resulting from previous treatment experiments, as effects on active chlamydial infections were more pronounced than in the penicillin G-persistence models, which was especially reflected in inclusion sizes. All in all, effects evoked by treatment of 1,10-phenanthroline were reversible upon removal of the compound and recovery. This indicates that 1,10-phenanthroline induces nutrient starvation-mediated persistence. Both clioquinol and 1,10-phenanthroline are therefore suitable for the introduction of persistence induced by nutrient starvation in *Chlamydia.*

4. Discussion

Infections with the intracellular pathogen *Chlamydia* cause various health issues and socioeconomic consequences worldwide. Infections with serovars A-C of *C. trachomatis* are the world's most prevalent cause of preventable blindness, while serovars D-K elicit the world's most widespread sexually transmitted disease caused by bacteria (WHO, 2021). Further members of the genus mainly provoke respiratory or multi-organ diseases in humans and animals (Gregory and Schaffner, 1997; Andersen and Vanrompay, 2000; Shima, Kuhlenbäumer and Rupp, 2010). The so called environmental chlamydiae or *Chlamydia*-related bacteria comprise various endosymbionts of amoebae and other protists and play for a long time an underestimated role as emerging pathogens in humans and animals (Greub and Raoult, 2002b; Greub, 2009). A common characteristic of all chlamydiae is their unique and obligate intracellular, biphasic lifecycle, in which the organisms alternate between two distinct morphological forms. Extracellularly, chlamydiae are present as rigid EBs and are able to endure various environmental stressors. Chlamydial replication requires a eukaryotic host cell. Therefore, after endocytosis-mediated entry, organisms change into RBs that are specialized for the acquisition of nutrients and replication and proliferate within a membrane-enclosed compartment termed inclusion.

A distinct temporal gene regulation pattern allows *Chlamydia* to sequentially express genes needed for the different phases of the chlamydial lifecycle. After multiple rounds of RB replication, organisms adopt an EB conformation again and late gene expression, yielding entry-mediating pre-packed inclusion membrane proteins (Incs), enables chlamydial EBs to reenter a new infectious cycle after exit of the host cell (Saka *et al.*, 2011). Upon adverse environmental conditions like nutrient starvation, co-infection with viruses or other intracellular bacteria or exposure to host cell cytokines elicited by the host's immune system, organisms can enter a persistent state that allows them to outlast the influence of external stressors and to reenter their lifecycle after tolerable conditions are restored (Skilton *et al.*, 2009). Persistence is characterized by a third morphological shape, in which RBs enlarge significantly and form ABs that are unable to undergo division. Depending on the stressor and the persistence-underlying mechanism, AB sizes differ from each other. Typically, persistent chlamydial cells that form upon exposure to host cell cytokines produces smaller ABs compared to persistent cells following treatment with antibiotics, e.g. penicillin (Kozusnik, Adams and Greub, 2024). Penicillin-induced persistence in *Chlamydia* was enigmatic for a long time, as, contrary to free-living bacteria, the organism does not have a PGN sacculus. Instead, only a minimal amount of PGN is synthesized by the organism and, instead of a cell wall, the organisms synthesize a narrow PGN ring (Liechti *et al.*, 2014; Liechti, Kuru, Packiam, Hsu, Tekkam, Hall, Jonathan T. Rittichier, *et al.*, 2016). *Chlamydia* divide via a budding mechanism and the PGN structure forming at the site of bud formation is required for septum formation and cell division. Penicillin targets the transpeptidase domain of PBPs, of which *Chlamydia* retained the homologs PBP2 and PBP3. Additionally, carboxypeptidase function of PBP6 and bifunctional enzyme AmiA in *C. pneumoniae* is inhibited (Klöckner *et al.*, 2014). Disruptions of the PGN precursor incorporation are suggested to trigger the formation of non-dividing persisting *Chlamydia* cells, as the

entire PGN metabolism in the organism is proposed to be interconnected with cell division to such a degree that, upon interference with one part of the PGN cycle, the entire process and thus, also cell division, comes to a standstill (Reuter *et al.*, 2023). Besides other persistence-evoking mechanisms, the PGN metabolism offers various points of attack and areas that are sensitive towards interruptions. Especially sensitive steps involve PGN remodeling and recycling. During the division process, the PGN ring is subject to constant remodeling involving not only biosynthetic, but also degradation steps that are required for the ring to expand and constrict. Therefore, the activity of lytic enzymes needs to be tightly regulated in *Chlamydia*. In free-living bacteria, uncontrolled degradation of the stability determining PGN sacculus would lead to cell lysis in free-living bacteria. Regulatory strategies can involve the modulation of hydrolase-encoding gene expression, the global control of hydrolase activity through production of inhibitors, or production of cell wall-modifying enzymes that block PGN cleavage (Vollmer *et al.*, 2008b; Yamamoto *et al.*, 2008; Clarke, Scheurwater and Clarke, 2010; Moynihan and Clarke, 2011; Yang *et al.*, 2012). To date, no regulatory mechanism for enzymatic activity is known for chlamydial amidases, hinting towards a fundamental difference compared to cell division amidases of *E. coli*, which underlie a multi-enzyme regulation machinery that is spatiotemporally distinct. In free-living bacteria, cell division amidases cleave septal PGN layers that are initially shared by the nascent daughter cells. In Gram-negative bacteria like *E. coli*, splitting of the septum and invagination of the membranes happen simultaneously, also highlighting the need for regulation of hydrolytic enzymes during the process (Vollmer *et al.*, 2008b). *E. coli* encodes three periplasmic cell division amidases: AmiA, AmiB and AmiC. Of the three, AmiA is the smallest and does not contain the amiN domain, thought to anchor amidases onto PGN material and for recruitment to the division site (Rocaboy *et al.*, 2013; Cook *et al.*, 2023). Deletion mutants of *amiA*, *amiC* and triple mutants showed chain-forming phenotypes, showing that cells are not able to separate anymore (Heidrich, Templin, Ursinus, Merdanovic, Berger, Schwarz, De Pedro and J. Höltje, 2001; Heidrich, Ursinus, Jürgen Berger, *et al.*, 2002). Cell division amidases of *E. coli* can adopt a resting state with an autoinhibited conformation. A blocking helix which is part of a larger regulatory domain was shown to occlude the active site (Yang *et al.*, 2012; Rocaboy *et al.*, 2013; Cook *et al.*, 2023). The autoinhibition theory is supported by evidence of additional inhibitory domains present in PGN hydrolases from various organisms, including *Listeria monocytogenes* (Bublitz *et al.*, 2009; Pérez-Dorado *et al.*, 2010). *In vitro*, removal of the inhibitory domain was sometimes shown to result in an active protein (Yang *et al.*, 2012). In AmiA of *E. coli*, a conserved glutamate residue in the blocking helix was shown to co-coordinate the zinc atom in the active center of the enzyme and to be the main factor that holds the blocking helix in place (Cook *et al.*, 2023). Removal of the blocking helix from the active center can only be achieved by exogenous activation by LytM-domain containing proteins. In *E. coli*, AmiA and AmiB are activated by LytM-protein EnvC, while AmiC is activated by NlpD (Uehara, Dinh and Bernhardt, 2009; Uehara *et al.*, 2010). Proteins containing LytM domains are often involved in cell division processes, cell elongation along the longitudinal axis during cell growth or sporulation events (Firczuk, Mucha and Bochtler, 2005; Uehara,

Dinh and Bernhardt, 2009; Bonis *et al.*, 2010; Meisner and Moran, 2011; Singh *et al.*, 2012). The majority of these proteins are metallo-endopeptidases and EnvC and NlpD are among the few exceptions of LytM-containing proteins not to have hydrolytic activity themselves (Uehara *et al.*, 2010). In *E. coli*, deletions of *nlpD* and *envC* lead to the formation of cell chains, similar to what was observed in amidase deletion mutants (Uehara, Dinh and Bernhardt, 2009). Activators EnvC and NlpD localize at the division septum earlier than their cognate amidases. While they are not needed for their recruitment, their presence is required for amidase activation (Peters, Dinh and Bernhardt, 2011). Recruitment of AmiB and AmiC to the septum is likely mediated through their N-terminal amiN-domains, that confer affinity towards PGN (Rocaboy *et al.*, 2013). AmiA, however, was not shown to localize to the division site distinctly, but to be dispersed across the periplasm (Bernhardt and De Boer, 2003). Lacking an amiN-domain, septal recruitment of this amidase is suggested to function through another, yet unknown mechanism. Like cell division amidases in *E. coli*, NlpD and EnvC are also not active by default, but display a similar autoinhibitory mechanism. A domain referred to as "restraining arm" occludes the LytM domain binding grove (Cook *et al.*, 2020). This binding grove is intended for another part of the regulatory domain of cell division amidases, the interaction helix, to bind (Cook *et al.*, 2023). According to molecular dynamics data, the interaction helix of cell division amidase AmiA in *E. coli* is more dynamic than the rest of the protein and stands out spatially. The solvent-facing residues of the helix are hydrophobic, and, given the fact that the lining of the LytM-domain containing binding grove of EnvC is also lined with hydrophobic residues, hydrophobic interaction between EnvC and the interaction helix of amidases is suggested. Mutations in the interaction helix diminishing its hydrophobic character led to a weakened interaction of the proteins, supporting this theory (Cook *et al.*, 2023). Cook *et al.* co-crystallized AmiB and its cognate activator protein EnvC and could show that the interaction helix of AmiB binds to the LytM-binding grove in EnvC that is previously occluded by the inherent restraining arm (Yang *et al.*, 2012). This indicates that prior to amidase activation by EnvC, the restraining arm must be withdrawn from the binding grove. Yang *et al*. proposed a model where LytM-protein activation is dependent on ATP hydrolysis by ABC transporter-like protein complex FtsEX in *E. coli*, that is part of the divisome, arriving to the prospective division site before onset of constriction (Schmidt *et al.*, 2004; Corbin *et al.*, 2007; Yang *et al.*, 2011). FtsE is an ATPase associated with transmembrane protein FtsX and FtsZ. FtsX is thought to interact with LytM proteins on the periplasmic side (Yang *et al.*, 2011). According to the model by Yang *et al*., ATP hydrolysis in the cytoplasm induces FtsX to trigger a conformational switch in the associated EnvC in the periplasm of *E. coli*, withdrawing the restraining arm from the LytM binding grove. Subsequently, binding of the interaction helix of a cell division amidase is enabled, through which in turn the blocking helix is retrieved from its active site. Thereby, the cell division amidase is switched on until ATP hydrolysis is completed in *E. coli*. Reset of the system renders the enzyme inactive again, until further ATP is hydrolyzed by FtsE (Yang *et al.*, 2012). Interestingly, an FtsEX complex deficient in ATPase activity was shown to still recruit LytM activator proteins, but failed to actually promote cell separation, suggesting that ATP hydrolysis is inevitable for

function (Yang *et al.*, 2011). With EnvC localizing close to the inner membrane due to its interaction with transmembrane protein FtsX and the other LytM activator NlpD being an outer membrane lipoprotein, the hypothesis that a concerted splitting of septal PGN with simultaneous invagination of both membranes at the same time is supported (Peters, Dinh and Bernhardt, 2011). Part of the mechanistic process of amidase activation is also temporal coordination of cell division amidase and activator interaction. Activator proteins EnvC and NlpD are recruited prior to their cognate cell division amidases, but EnvC and AmiA/AmiB and NlpD and AmiC are all recruited independently from each other and have different requirements concerning divisome composition (Hale and de Boer, 2002; Peters, Dinh and Bernhardt, 2011). FtsN, the final essential protein of divisome assembly, is not only needed for activity of e.g. PBP3, but also for AmiB, NlpD and AmiC localization to the septum, while EnvC localizes independently (Peters, Dinh and Bernhardt, 2011). Interestingly, inhibition of septal PGN biosynthesis causes cell division amidases not to localize at the putative division site, while activators still localize (Peters, Dinh and Bernhardt, 2011). Similarly, inhibition of Z-ring formation causes AmiB to be dispersed across the periplasm, while, normally, the enzyme displays distinct localization at the division site (Bi and Lutkenhaus, 1993). Relatively to each other, EnvC was shown to localize at the future septum first, followed by AmiB and NlpD. AmiC was suggested to localize last and was shown to be distinct in deeply constricted, late septa. The authors proposing this model suggest that such late septa require additional action of AmiC, as AmiA and AmiB, at this point, might not be active anymore (Peters, Dinh and Bernhardt, 2011). The observation of Heidrich *et al*. that *amiC* deletion mutants produce the most prevalent cell chain forming phenotype of all the single amidase deletion mutants tested in *E. coli* is in favor of this theory (Heidrich, Ursinus, Jürgen Berger, *et al.*, 2002). These regulatory events are likely to ensure that septal PGN biosynthesis always precedes hydrolytic activity (Peters, Dinh and Bernhardt, 2011). Peters *et al.* proposed that weak association of FtsN with the Z-ring triggers low-level PGN biosynthesis at the prospective septum (Peters, Dinh and Bernhardt, 2011). As amidase activators are most likely already present at this stage, action of diffusing amidase encountering their cognate activators at the septum are thought to hydrolyze newly synthesized PGN. Denuded glycans originating from this action are proposed to serve as a scaffold for FtsN, now interacting with PGN via its SPOR domain and initiating further PGN synthesis. Cell division amidases are then recruited to the septal region by amiN domains in case of AmiB and AmiC (de Souza *et al.*, 2008b; Peters, Dinh and Bernhardt, 2011; Rocaboy *et al.*, 2013). The mechanism that causes AmiA to localize at the division site is still unknown, as it lacks the N-terminal amiN domain. However, the enzyme plays an important role in lysis of cells exposed to a high dose of β-lactams, that originates from the septal region and is thought to be dependent on AmiA (Schwarz, Asmus and Frank, 1969; Chung *et al.*, 2009; Uehara, Dinh and Bernhardt, 2009).

For *Chlamydia*, that retained AmiA as the only cell division amidase, no regulatory mechanism as described above is known. Though there is no crystal structure of either AmiA from *C. pneumoniae* or *C. trachomatis*, the sequence assigned to the regulatory domain of AmiA_Ec could not be aligned with

any part of the sequence of chlamydial amidases (Fig. 4) (Klöckner *et al.*, 2014). This indicates that the regulatory domain is missing in AmiA_Ct and AmiA_Cp. While also structure predictions of AmiA_Ec depict the regulatory domain with two alpha helices forming its core, no such structure is observable in predictions of chlamydial amidases. According to structure predictions, the active centers of chlamydial amidases are constantly exposed. LytM-factor containing activator proteins NlpD or EnvC are not encoded in chlamydial genomes. LysM protein Cpn0902 from *C. pneumoniae* was falsely annotated as NlpD but was shown to be a carboxypeptidase likely participating in chlamydial PGN remodeling processes (Klöckner *et al.*, 2014). While in *E. coli* FtsEX was shown to regulate LytM-domain containing activators and is associated with the Z-ring, in *Chlamydia* FtsEX is not encoded. Also, as FtsZ is missing in *Chlamydia* entirely and was likely replaced functionally by MreB in organizing the divisome (Gaballah *et al.*, 2011; Ranjit, Liechti and Maurelli, 2020), processes of chlamydial divisome assembly and amidase regulation without FtsEX remain unknown. Differences in regulation mechanisms comparing AmiA_Ec and chlamydial amidases also become apparent regarding *in vitro* activity. Lupoli *et al.* showed that purified AmiA_Ec is active *in vitro* and requires at least a tetrasaccharide-containing PGN substrate for activity (Lupoli *et al.*, 2009). Dye release assays performed in this work similar to the experiments performed by Uehara *et al.* showed that *in vitro* activity of *E. coli* amidases requires activation by cognate LytM-containing activator proteins (Uehara, Dinh and Bernhardt, 2009). Klöckner *et al.* performed dye release assays with AmiA_Cp, the homolog from *C. pneumoniae,* and showed that the enzyme is active by default and degraded PGN *in vitro* without any protein activation required (Klöckner *et al.*, 2014). The same was shown for AmiA_Ct in this work. The enzyme had highest activity in alkaline conditions, which was also shown for the *E. coli* homolog previously (Tomioka *et al.*, 1983; Holtje and Tuomanen, 1991). *E. coli* is known to maintain a cytosolic pH between pH 7.4-7.7, while periplasmic pH equals external conditions (Wilks and Slonczewski, 2007; Reyes-Fernández and Schuldiner, 2020). Despite of different attempts to measure the intracellular and periplasmic pH of *Chlamydia*, conditions within the EB, RB or even AB remain largely unknown. However, data about pH conditions inside the inclusion have been obtained by Grieshaber *et al*. and Schramm *et al*. Using pH-sensitive probes, the pH inside the inclusion was reported not to fall below pH 6 over the course of infection (Schramm, Bagnell and Wyrick, 1996). In line with the fact that *Chlamydia* avoid fusion with the acidic phagolysosomes of the host cell at the beginning of the infection, a general avoidance of the organism of acidic conditions can be assumed. Upon entry of *Chlamydia* into the host cell, disulfide bonds in the envelope layer of EBs are reduced, likely accompanied by a lower pH value compared to extracellular environments. After escape of the lysosomal pathway, the pH within the inclusion is suggested to be neutral, around pH 7.25, which is almost equivalent to pH conditions inside host cell cytoplasm (Grieshaber, Swanson and Hackstadt, 2002). The authors suggest that the inclusion membrane can be permeated freely by ions, resulting in a pH equilibrium. Moreover, pH within inclusions is regulated by Na^+-K^+ ATPase, that is acquired via fusion with membrane-enclosed intracellular compartments. After fusion, *Chlamydia* uses this ion pump

to maintain favorable conditions within the inclusion and prevent acidification. This was shown by Schramm *et al.*, who could also demonstrate impaired chlamydial inclusion development by specific inhibition of the ion transporter within the inclusion membrane (Schramm, Bagnell and Wyrick, 1996). Although the pH conditions within chlamydial cells are still unknown, the efforts of the organism to avoid acidification indicate that, intracellularly, neutral pH conditions are favorable for the organism. Most likely, intracellular pH is maintained strictly, as deviations might result in unwanted protein reduction or oxidation, possibly entailing detrimental effects for the intracellular organism. The reaction optimum of AmiA for PGN cleavage in neutral to alkaline conditions, that was investigated in *in vitro* experiments in this work, are in line with the present data about pH within chlamydial inclusions.

Moreover, chlamydial amidases do not only cleave polymeric PGN but also the precursor molecule lipid II, which was shown for AmiA_Cp by Klöckner *et al*. (Klöckner *et al.*, 2014) and in this work for AmiA_Ct. While AmiA_Cp has dual activity acting as amidase and carboxypeptidase, interestingly, AmiA_Ct was shown to be a monofunctional amidase. This indicates that functional properties differ between these closely related enzymes and that carboxypeptidase activity, that is an important part of PGN remodeling, might have been dispensed in AmiA_Ct. As *C. trachomatis* encodes for both a PBP6 and Cpn0902 homolog, carboxypeptidase activity is likely executed by these enzymes. Besides the lack of the regulatory domain of AmiA_Ec in chlamydial amidases, also active site architectures are different from each other. Cook *et al.* showed that, in the active conformation of *E. coli* AmiA, the zinc atom in the active center is coordinated by three residues: H65, H133 and E80. Two extra residues located in the regulatory domain co-coordinate the zinc atom in the inactivated conformation, with E167 likely being the most important and forming a latch that holds the blocking helix in place (Cook et al., 2023). These two residues are not conserved in *Chlamydia*, concomitant to the fact that the enzyme lacks the regulatory domain entirely. In chlamydial amidases, the zinc atom is likely coordinated by homologous residues H67, H136 and E83. E242 in AmiA_Ec is supposed to act as a base catalyst (Lupoli *et al.*, 2009) and this residue is conserved in AmiA_Ct and AmiA_Cp as E205/E207, respectively. Whether this residue is involved in zinc coordination remains unknown, as crystal structures for these enzymes are not yet available. *In vitro* activity assays with purified AmiA_Ec active site mutants, in which residues H65, H133, E80 and E242 were replaced, revealed that, except for the replacement of E80, all mutations resulted in full loss of *in vitro* activity (Lupoli *et al.*, 2009). As this residue did not seem to be as essential as the other residues involved in zinc coordination, functionality of mutants affecting E80 was not considered in the following experiments. An *E. coli* overexpression strain overproducing AmiA_Ct and its active site mutants was lysed by activity of the heterologously overproduced chlamydial enzyme. The same experimental setup was part of the research published by Klöckner *et al.,* who included AmiA_Cp, the homolog from *C. pneumoniae*. Findings about AmiA_Ct in this work showed that each tested residue considered to be part of the active site was equally important for lysis of the host strain and enzymatic activity. Mutations of either active site residue abolished lytic activity of AmiA_Ct. Conversely, in AmiA_Cp, not all residues were equally important for enzymatic function,

as upon mutation of E207, AmiA_Cp was still able to lyze the *E. coli* host upon overproduction. This indicates a different function of this residue in AmiA_Ct and a potentially modified functional architecture of the active site between the closely related chlamydial protein homologs, also shown in the fact that AmiA_Ct, in contrast to AmiA_Cp, is a monofunctional amidase lacking carboxypeptidase activity (Klöckner *et al.*, 2014).

As the comparison in this work showed and the data published by Klöckner *et al.* (2014) indicate, another difference between chlamydial amidases relates to periplasmic export. Generally speaking, while in *E. coli* AmiA is exported tat-dependently, chlamydial amidases must be exported via an alternative pathway given that the tat-pathway is absent in *Chlamydia*. Klöckner *et al.* showed that AmiA_Cp is likely exported via the sec-pathway (Klöckner *et al.*, 2014), and AmiA_Ct, considering the sequence of the predicted signal peptide, likely is as well. The consensus sequence of sec signal peptides is subdivided into a positively charged N-terminal region, a hydrophobic core region and a C-terminus containing polar amino acids. Comparison of the amino acids in both predicted signal peptide sequences of AmiA_Cp and AmiA_Ct (Fig. 4d) showed that the putative sec signal peptide of AmiA_Ct matches these criteria to a higher degree than AmiA_Cp. Residues in the sequence match these criteria to 28 %, 74 % and 50 %, while residues in the predicted AmiA_Cp signal peptide sequence match to 27 %, 50 % and 20 %, respectively. Additionally, the sequence from AmiA_Ct includes the signal peptide cleavage consensus motif A-X-A, which is missing from the signal peptide of AmiA_Cp (Fig. 4d). This could be a possible explanation for the recognition of the native signal peptide of AmiA_Ct by the *E. coli* overexpression host, whereas overproduction of AmiA_Cp required expression within pASK-IBA2, in which the protein is fused to an OmpA leader peptide mediating periplasmic export (Klöckner *et al.*, 2014).

Another *in vivo* experiment performed in this work with AmiA_Ct further confirmed functional conservation of the enzyme in cell division. AmiA_Ct rescued cell division in an amidase-deficient *E. coli* strain that was not able to perform septal cleavage and was, therefore, growing in cell chains. Previously, the experiment was also performed with AmiA_Cp by Klöckner *et al.*, yielding the same result and proving that these chlamydial enzymes exert the assigned functions even in heterologous host systems (Klöckner *et al.*, 2014). An interesting difference between AmiA in *E. coli* and the two other periplasmic cell division amidases of the organism is the lack of an amiN-domain conferring binding towards PGN in AmiA. In contrast to the other two periplasmic cell division amidases of *E. coli*, AmiA_Ec consists of a single globular domain, while in AmiB and AmiC, an amiN domain is attached to the N-termini of the *E. coli* proteins. AmiA of *C. trachomatis* and *C. pneumoniae* also does not contain an amiN domain. Bioinformatic analysis of the amino acid sequence also did not reveal the presence of any known PGN binding domains previously identified in hydrolases such as SPOR, CHAPS, SHb3 or LysM. Zoll *et al.* investigated substrate binding of AmiE, a subunit of autolysin AtlA in *Staphylococcus epidermidis*, that also coordinates a zinc atom within its catalytic center (Zoll *et al.*, 2010). Upon mutagenesis of active site residues, the enzyme was catalytically inactive. However, PGN binding was

not impaired by catalytic inactivation, but instead, substrate affinity increased. One of the residues, H177, is not thought to be involved in zinc coordination, but in the stabilization of the enzyme-substrate transition state during the catalytic process. Proposed to enable a water-mediated nucleophilic attack, a stabilizing function of the transition state within the catalytic process is attributed to the enzyme. According to the authors, this increase in binding affinity could be mediated by the smaller structure that results from the replacement of histidine by alanine. In pulldown experiments presented in this work, binding affinity of purified AmiA_Ct and active site mutant AmiA_Ct H67A towards PGN was assessed. While the active enzyme was bound to the substrate only partly, the catalytically inactive active site mutant was co-pelleted with PGN entirely. In analogy to the hypothesis proposed by Zoll *et al.*, replacement of histidine by alanine might result in a smaller structure that stabilizes the transition state of catalysis and might lead to permanent binding of the substrate to the enzyme. The replacement of highly conserved residues of the catalytic center can lead to the construction of a substrate trap, as described by Flint *et al.* for protein tyrosine phosphatases (Flint *et al.*, 1997). As histidine residues in the catalytic centers of PGN amidases are highly conserved, this could be a possible explanation. Also, substrate association, catalysis and dissociation are highly dynamic processes. The observation that the active enzyme AmiA_Ct binds to the substrate only in parts, with the rest of the enzyme being unbound could be explained by this. According to this hypothesis, the observation that parts of the enzyme are bound to the substrate might represent a momentary glance on the actual situation. To further assess how PGN binding is conferred, another residue in AmiA_Ct was considered. Carboxypeptidase activity in AmiA_Cp relies on the presence of an active site serine (S96) located within the PBP motif SxxK. Group 1 PBPs can be independent or fused to another enzyme and invariably contain the motifs SxxK, SxN and KTG (Goffin and Ghuysen, 2002). Besides the active SxxK motif in AmiA_Cp, the enzyme also contains an SxN motif. AmiA_Ct does not have carboxypeptidase activity but is a monofunctional amidase. Still, the SxN motif was positionally conserved. According to structure predictions of AmiA_Cp, it is not located closely to the SxxK motif, but on the opposite site of the protein close to the predicted active center region. A role of the SxN motif related to PBP activity can be excluded in case of AmiA_Ct, and this work also confirmed that the motif is not involved in PGN binding. Therefore, the serine residue was replaced by alanine and the purified protein was included in pulldown assays. Like the active site mutant, the S140A mutant co-pelleted with PGN completely. In contrast to the active site mutant, however, amidase activity was not impaired by the amino acid substitution. This fact also met expectations, as an involvement of serine-containing motifs in amidase activity was not anticipated. However, like in the active site mutant, a replacement of a residue within or close to the active site is hypothesized to modulate binding affinity. When replacing serine by alanine, the affected region within the enzyme has less polar characteristics and could be speculated to confer increased binding affinity towards PGN. To verify this speculation, however, crystal structures of the enzyme bound to PGN as a substrate are necessary.

Although the exact mode of substrate recognition and binding remains to be fully clarified in chlamydial amidases, the coordinated zinc in the enzyme's active center is conserved across this enzyme class and most likely plays an important role. To further investigate this, experiments with the compounds clioquinol, 1,10-phenanthroline and TPEN were performed. These compounds are known chelators of bivalent cations *in vitro* and *in vivo* and are applied in various settings. 1,10-phenanthroline is a membrane-permeable compound and a chelator of bivalent cations like zinc, iron, and copper. Here, three molecules of 1,10-phenanthroline chelate one metal ion. In analytical chemistry, ferroin, a complex formed by 1,10-phenanthroline and iron, is used as a redox indicator (Sriramam, 1972). Antibiotic action against some Gram-positive, Gram-negative and acid-fast bacteria has been demonstrated, and also antifungal activity is known (Dwyer *et al.*, 1969). The latter is suggested to be due to damage of the mitochondrial membrane and subsequent impairment of respiration and DNA cleavage inducing cell death or distorted cell morphologies (McCann *et al.*, 2000; MacPherson, Larochelle and Turcotte, 2006; Kilah and Meggers, 2012). On *Candida albicans*, a MIC of 1.25 µg/mL 1,10-phenanthroline was determined (McCann *et al.*, 2000). *In vitro*, the compound was shown to inhibit zinc-dependent pancreatic carboxypeptidase A by removing the zinc atom from its active center (Vallee and Neurath, 1955; Vallee *et al.*, 1960). Brul *et al.* also demonstrated antifungal activity due to zinc chelation (Brul *et al.*, 1997). AmiC, the only amidase homolog retained in the pathogen *Neisseria gonorrhoeae,* showed a decrease in *in vitro* activity upon application of 1,10-phenanthroline at pH 8.5 (Lenz *et al.*, 2016). Also, a purified amidase of *Ochrobactrum anthropi* was inhibited by the compound at pH 8.0 and activity could be restored by adding zinc, manganese, or magnesium to the reaction (Sonke *et al.*, 2005). The reaction being rescued by also transition metals other than zinc indicates that complex formation is a dynamic process. By supplying e.g. manganese, chelators forming complexes could release previously bound zinc, which then can be bound by an apoenzyme that changes into a holoenzyme upon metal binding. While studying the substrate spectrum of AmiA of *E. coli*, Lupoli *et al.* successfully inhibited the *in vitro* reaction by application of 1,10-phenanthroline at pH 7.5 (Lupoli *et al.*, 2009). In this work, activity of AmiA_Ct on a PGN substrate was also inhibited by 1,10-phenanthroline in a pH-dependent manner. In general, metal complex formation depends on pH conditions, as known for EDTA, which has increased affinity for metal complexes with augmenting pH values (Scholz and Kahlert, 2019). 1,10-phenanthroline inhibited AmiA_Ct dye release reactions in all tested pH conditions ranging from pH 5.5 to pH 9.5. In this case, inhibition was most profound at lower pH values around 5.5 to 6.5. However, at these pH values, AmiA_Ct was less active on PGN compared to alkaline conditions, as determined by experiments investigating the enzyme's pH optimum in this work. Nevertheless, by determining relative enzymatic activities in relation to the uninhibited positive control, inhibitory action could also be shown under these conditions. Trace metal sequestration also entails consequences for eukaryotic cells, as impairment of e.g. metal-dependent transcription factors and metallopeptidases can possibly lead to metabolic dysfunction (Chen *et al.*, 2024). Due to this, metal complexes of 1,10-phenanthroline and its derivatives are investigated in cancer research as potential novel chemotherapeutic drugs. In cell

culture models, the compound exhibits higher toxicity towards cancer cell lines compared to human keratinocytes (McCann *et al.*, 2012). Like 1,10-phenanthroline, clioquinol binds not only to zinc, but also to other transition metals and is membrane-permeable. Two clioquinol molecules form a complex with one metal ion. Formerly, the antimicrobial substance was used to treat severe intestinal diseases such as lambliasis, shigellosis or amoebal infections of the intestinal tract (Bareggi and Cornelli, 2012). Clioquinol was also used as a drug in non-infectious disease. The skin disease acrodermatitis enteropathica, caused by zinc malabsorption in the human gut, leads to skin rashes and inflammation. Treatment with clioquinol relieves the symptoms due to its zinc-binding and membrane-permeable properties, that enable zinc enrichment in intestinal tissues (Hanakago and Uono, 1981). However, clioquinol was suspected to lead to subacute myelo-optic neuropathy, affecting vision and motoric function, in the 1970s and was withdrawn from the market for consumer safety reasons (Arbiser *et al.*, 1998). Likely, complexation of zinc and enrichment of the complex in tissue caused cytotoxicity in surrounding cells. In low concentrations, clioquinol is still available and in use as a topic antiseptic used on mild skin infections. Recently, its potential role in the treatment of Alzheimer's disease (AD) was investigated. In AD, function of the central nervous system is impaired due to the formation of protein aggregates, also referred to as β-amyloid plaques. Transition metals play a role in stabilization of plaques by binding β-amyloid peptides (Atwood *et al.*, 2000). The chelation of metals within the brain tissue is thought to reduce β-amyloid aggregation and, therefore, to mitigate and delay AD symptoms, as demonstrated in a mouse model system (Cherny *et al.*, 1999). Clioquinol also has possible implications in chemotherapy by various putative mechanisms. Bound to a metal ion, clioquinol was shown to have an inhibitory effect on the proteasome in eukaryotic cells and, in higher concentrations, clioquinol exerted this function on its own, thereby suppressing the NF-κB-pathway (Yu, Lou and Ding, 2010). Alternatively, the ionophore activity of clioquinol is thought to be applicable in cancer therapy, as elevated levels of e.g. zinc in tissues can mediate cytotoxicity and were shown to induce apoptosis in cancer cell lines (Ding *et al.*, 2005; Khan *et al.*, 2020). Copper ionophores were shown to act selectively against rapidly proliferating cells that depend on a high level of mitochondrial respiration, which is especially elevated in cancer cell lines. This process is referred to as cuproptosis (Xie *et al.*, 2023). In some breast and pancreatic cancer cell lines, also depletion of transition metals playing roles in respiratory chains, such as zinc, is discussed as a putative inhibitory mechanism that can be achieved through chelation (Hoang *et al.*, 2016). Lastly, also superoxide dismutase is discussed as a putative target. Inhibition of the enzyme through metal chelation is thought to induce oxidative stress in some cell lines that lead to apoptosis through formation of reactive oxygen species (Ding *et al.*, 2005; Kawamura *et al.*, 2014). Like for 1,10-phenanthroline, zinc chelation could be demonstrated for clioquinol in a pH-dependent manner. By determining relative enzymatic activity compared to AmiA_Ct reactions in the absence of clioquinol, inhibitory effects on the enzyme's amidase activity could be determined under alkaline pH conditions. Effects were significant at pH 8.5 and pH 7.5, close to the AmiA_Ct reaction optimum, and still clearly visible at pH 9.5. The experiment performed by Sonke *et*

al. for an amidase of *Ochrobactrum anthropi* was reproduced with attempts to rescue the inhibited reaction by adding excess concentrations of zinc (Sonke *et al.*, 2005). By adding zinc in a 1:4 molar ratio in relation to clioquinol, an inhibitory effect could be averted. As two clioquinol molecules are known to form complexes with one metal ion, theoretically, the added amount in the rescue experiment would compensate for half of the zinc bound to clioquinol. Ultimately, this was sufficient to reinstate enzymatic activity compared to uninhibited conditions and indicated that the observed inhibitory effects are likely due to zinc chelation. Tetrakis(2-pyridylmethyl)ethylenediamine (TPEN), like clioquinol and 1,10-phenanthroline, is membrane-permeable and chelates bivalent cations, specifically zinc (Mendivil-Perez, Velez-Pardo and Jimenez-Del-Rio, 2012). Due to the high cytotoxicity exhibited by TPEN, the compound is also investigated in cancer therapy. It had time- and dose-dependent toxic effects on human breast cancer cell lines and zinc depletion is discussed as a possible mode of cytotoxicity (Hashemi *et al.*, 2007). An antifungal and antibacterial action has also been suggested. In a mouse model, TPEN treatment improved survival rates of mice infected with *Aspergillus fumigatus* (Laskaris *et al.*, 2016). In carbapenem-resistant *Enterobacteriaceae*, reduction of *in vitro* activity of metal-dependent carbapenemase has been observed, possibly conferring increased sensitivity towards meropenem treatment (Azumah *et al.*, 2016). *In vitro*, the compound also exerted an effect on AmiA_Ct dye release assays and inhibited the reaction in alkaline reaction conditions to a significant extend. These tested compounds represent an opportunity to further characterize the role of metal coordination in enzymatic functions of chlamydial amidases, but also experiments with e.g. *E. coli* AmiA could be considered in the future. Most likely, the compounds exert an inhibitory function on other chlamydial metal-dependent enzymes as well. Due to high affinity towards other transition metals and toxic implications dependent and independent from these properties, the compounds are probably not suited for treatment of chlamydial infections comparable to the use of antibiotics.

However, as metal chelators were proven to be effective against fungal infections in various settings, and topic preparations of clioquinol are available for the treatment of uncomplicated skin infections (Tschachler *et al.*, 2007), non-toxic chelating compounds could be investigated in terms of treatment options for bacterial infections. Especially iron chelators could be feasible options. In medical settings, compounds like deferiprone or deferasirox are employed for the treatment of iron overload conditions of the liver or the heart (Lehmann, 2020; Scott *et al.*, 2021). As binding affinities of metal chelators are often not restricted to just iron, zinc deficiencies can occur as a consequence of their use in treatment (Vermylen, 2008). Bacteria use oligopeptides with iron-chelating properties, termed siderophores, for iron acquisition. A possibility to restrict iron availability and control infectious processes is to use recombinant or synthetic siderophores that cannot be taken up by bacteria (Eto *et al.*, 2013; Parquet *et al.*, 2019; Lehmann, 2020; Scott *et al.*, 2021). However, using bacterial siderophores conjugated to antibiotics proved to be a promising strategy that may help reaching target structures in bacteria, as shown for *Pseudomonas aeruginosa*, with a siderophore conjugated to ampicillin (Kinzel *et al.*, 1998). These conjugates exploit the uptake pathway bacteria use for the readmission of siderophores and

facilitate the uptake of antibiotics. As the inner membrane likely cannot be crossed by the conjugate, an antibiotic targeting periplasmic structures in Gram-negative bacteria is recommended for establishment of these conjugates (Mislin and Schalk, 2014). Moreover, also novel antibiotics designed to mimic siderophores are investigated as a possible strategy to treat infections (Ribeiro, Sousa and Simões, 2022). In therapeutic settings, high toxicity levels of TPEN are most likely disadvantageous and application of clioquinol was linked to serious health issues after application, causing the withdrawal of orally-administered medications from the market decades ago (Mao and Schimmer, 2008). 1,10-phenanthroline to date has never been applied in a clinical context. Nevertheless, effective metal-chelating properties could qualify these compounds as possible lead structures for drug development for chelation therapy for topical application. For instance, clioquinol is a derivate of the heterocyclic compound chinoline, which was already investigated as a therapeutic agent in infectious skin diseases in the 1960s (Wanic, 1967). Most likely, topical application, like in case of clioquinol-containing skin formulations, would serve as the preferred mode of administration. Moreover, eye drops containing metal chelators such as clioquinol could be considered. In systemic application, adverse effects of metal chelation divergent from the target could not be excluded. As not only bacterial enzymes, but also many enzymatic processes in mammals are dependent on transition metals, the prerequisite of selective toxicity (Ehrlich and Gonder, 1913), often applied in the search of treatment options for infectious diseases, does not comply with in the case of metal chelators. Leveraging metal chelators in the treatment of chlamydial infections has not been tested so far.

Usually, bacterial genital and ocular infections can be treated successfully with antibiotics targeting protein or DNA synthesis machineries. Among the most prevalently administered antibiotics for the treatment of these infections are doxycycline, azithromycine and moxifloxacin (Kohlhoff and Hammerschlag, 2015; Wolle and West, 2019). Even though penicillin or cell-wall targeting antibiotics in general are the most frequently administered antibacterial medication (Bush and Bradford, 2016), their use is inappropriate for the treatment of chlamydial infections, since, upon treatment with e.g. penicillin G, *Chlamydia* enter a persistent state. Persistence is generally defined as an alternative stage that bacteria, intracellular and free-living, can adopt as a survival strategy to outlast adverse environmental conditions. Persistence as a response on adverse environmental stimuli was also observed in the *Chlamydia*-related bacteria *Estrella*, *Simkania* and *Waddlia* (Scaioli *et al.*, 2019; Scherler *et al.*, 2020; Rovero, Kebbi-Beghdadi and Greub, 2023). Among other stressors, drug concentrations that normally would be bactericidal can result inefficient (Riffaud, Rucks and Ouellette, 2023a). Main hallmarks of true persistence in bacteria include its reversibility, lack of generation of infectious progeny during persistent states and its non-hereditary nature (Balaban *et al.*, 2019; Riffaud, Rucks and Ouellette, 2023a). Once the environmental stressor is removed, the normal bacterial lifecycle can be resumed and replication can reoccur. In *Chlamydia*, persistence can be induced by exposure to pro-inflammatory cytokines like interferon-γ, heat shock, antibiotics, and coinfection of the host cell with a virus or with other intracellular bacteria (A. Matsumoto and Manire, 1970; Kahane and Friedman, 1992; Beatty,

Byrne and Morrison, 1993; Deka *et al.*, 2006; Huston *et al.*, 2008). Interestingly, transcriptional responses of persistence types induced in *Chlamydia* differ from each other, indicating different mechanisms inducing the processes (Beatty *et al.*, 1994; LaRue *et al.*, 2007). Also, persistent phenotypes in *Chlamydia* and *Chlamydia*-related bacteria occurred spontaneously upon infection of non-optimal hosts without any further treatment. This indicates the high level of adaptation chlamydiae have undergone in the process of co-evolution with the host (Kozusnik, Adams and Greub, 2024). For the first time, chlamydial persistence was observed upon treatment with β-lactam antibiotics like penicillin. This was first discovered by Weiss *et al.* in 1950, who observed aberrantly enlarged cells of *C. muridarum* and *C. felis* upon exposure to penicillin (Weiss, 1950). It is still unclear to which degree penicillin-induced persistence in *Chlamydia* plays a role in natural settings. However, persistent chlamydial infections have been detected in post-gonococcal patients treated with penicillin that simultaneously carried infections with *C. trachomatis* (Richmond, Hilton and Clarke, 1972). Also, *C. pneumoniae* aberrant bodies have been detected in patient-derived atherosclerotic tissue samples (Borel *et al.*, 2008). Also *C. muridarum* was shown to maintain persistent infections in mouse models after amoxicillin treatment (Phillips Campbell *et al.*, 2012). Penicillin targets the crosslinking processes of nascent PGN by inhibiting transpeptidation performed by PBPs (Kraus and Höltje, 1987). Free-living bacteria depend on an intact PGN sacculus for osmotic protection and rigidity of this protective layer is also dependent on crosslinking of PGN macromolecules with each other. Therefore, lysis of cells as a consequence of high cell turgor in combination with defective crosslinking of PGN is a result of interference with PGN biosynthesis through antibiotics (Panzetta, Valdivia and Saka, 2018). However, in free-living bacteria, cellular mechanisms leading to cell lysis after antibiotic treatment targeting cell-envelope-associated mechanisms are not entirely understood to date and require further investigation. *Chlamydia* do not depend on a PGN sacculus for osmotic protection due to their residence within a relatively homeostatic intracellular environment. However, chlamydial cell division depends on the presence of septal PGN and drugs targeting the PGN biosynthesis machinery disrupt the ability of *Chlamydia* to divide (Jacquier *et al.*, 2014b). While exposure to β-lactam antibiotics fails to block EB to RB transition in *Chlamydia*, proliferation of RBs and downstream steps within the chlamydial developmental cycle are impaired (Jacquier *et al.*, 2014b; Cox, Abdelrahman and Ouellette, 2020; Brockett and Liechti, 2021). As the targets for β-lactams, transpeptidase domains of monofunctional transpeptidases PBP2 and PBP3 and carboxypeptidase domains of PBP6 and AmiA of *C. pneumoniae,* are present in *Chlamydia* (Klöckner *et al.*, 2014; Otten *et al.*, 2015), chlamydial septal PGN biosynthesis is affected, leading to an arrest of cell division (Barbour *et al.*, 1982; Ouellette *et al.*, 2012). Through this, entry into a persistent state is induced by a mechanism that is not entirely elucidated yet. At the same time, replication of 16s rRNA, plasmid and genomic DNA is continued, causing chlamydial cells to accumulate genetic material and enlarge, forming ABs while entering persistence (Lambden, Pickett and Clarke, 2006; Ouellette *et al.*, 2006; Skilton *et al.*, 2009; Kintner *et al.*, 2014). Formation of aberrant chlamydial phenotypes is thus suggested to be a result of inhibited division while bacterial growth

processes in general are continued (Kozusnik, Adams and Greub, 2024). Transcription of late genes, among them *omcB* and *hctB*, that are involved in secondary differentiation, are downregulated while genes related to chlamydial stress responses are upregulated (Goellner *et al.*, 2006; Ouellette *et al.*, 2006). Although the exact mechanisms are not entirely understood, presumably the stress originating from inhibited cell division in *Chlamydia* contributes to enter the observed persistence phenotype until the antibiotic is removed.

As mentioned earlier, starvation of essential nutrients and trace elements can trigger persistence in *Chlamydia*. In contrast to other bacteria, *Chlamydia* do not have siderophores or heme capture mechanisms, but still require to scavenge iron from the host (Stephens *et al.*, 1998b; Pokorzynski, Thompson and Carabeo, 2017). Eukaryotic cells acquire iron via the transferrin pathway (Luck and Mason, 2012; Winter, Bazydlo and Harris, 2014). In the serum, iron (Fe^{3+}) is bound by the serum carrier protein transferrin. Transferrin receptors on the surface of host cells bind loaded transferrin and internalize the transferrin-bound ferric iron, together with the transferrin-receptor-complex. Inside the cell, the internalized vesicles are transported and acidify in the process, which causes ferric iron to dissociate from the receptor. In the cytoplasm, ferric iron is reduced to ferrous iron (Fe^{2+}). Ferrous iron can be stored within the cell or is oxidized again and bound by ferritine (Greenberg and Wintrobe, 1946; Jacobs, 1977). The unloaded apotransferrin stays bound to the receptor molecule and is transported back to the membrane. The exact mechanism through which *Chlamydia* acquire iron from the host is not completely understood yet, but, likely, iron is scavenged by exploiting the slow transferrin recycling pathway (Ouellette and Carabeo, 2010). The majority of transferrin is recycled travelling through vesicular compartments that are positive for Rab4 or Rab5 GTPases, or both. This route is comparably quick and transferrin molecules are processed within 30 minutes after internalization. Approx. 10-20 % of transferrin is recycled through a slower pathway, in which transferrin is internalized into Rab5 positive early endosomes that develop into Rab11 positive endosomes (Ouellette and Carabeo, 2010). After Rab4 positive endosomal compartments fuse with Rab11 endosomes, transferrin-containing vesicles are likely transported to the membrane for transferrin release and recycling. Rab11 and Rab4 containing vesicles were observed to localize near the chlamydial inclusion and a “kiss and run” mechanism facilitating entry of free iron into the chlamydial inclusion was proposed (Rzomp *et al.*, 2003; Rzomp, Moorhead and Scidmore, 2006; Cortes *et al.*, 2007; Ouellette and Carabeo, 2010). While the transport mechanism of iron across the outer membrane is unknown in *Chlamydia* (Pokorzynski, Thompson and Carabeo, 2017), YtgA was identified as a periplasmic protein that likely traffics ferric and ferrous iron alike to inner membrane ABC transporter YtgCD, which is then thought to transport iron into chlamydial cells (Raulston *et al.*, 2007; Miller *et al.*, 2009; Thompson *et al.*, 2012).

Iron acquisition and metabolism are interesting aspects considering the genital biovars of *C. trachomatis*, as the natural environment, especially since the female genital tract does not offer constant iron supply. Production of iron-binding glycoprotein lactoferrin in the genital tract is regulated by estrogen levels, that are varying over the course of the menstrual cycle (Cohen *et al.*, 1987; Kelver

et al., 1996). Available iron is sequestered by lactoferrin and, thereby, unavailable for *Chlamydia*. Secondly, during bacterial vaginosis, which often coincides with chlamydial infection (Gallo *et al.*, 2012), interleukine levels are increased (Bellmann-Weiler *et al.*, 2013). As part of the innate immune system, neutrophile granulocytes are recruited and release lactoferrin into the environment (Lepanto *et al.*, 2019). Similarly to lactoferrin released during the menstrual cycle dependent on estrogen levels, elevated lactoferrin levels as part of an immune response contribute to the unavailability of iron. Moreover, release of pro-inflammatory cytokines like IFN-γ contributes to the downregulation of transferrin receptor production (Bourgeade *et al.*, 1988). This limits host cells in their iron intake and simultaneously leads to iron starvation in intracellular *Chlamydia*. In order to circumvent iron starvation, the pathogen makes use of a regulatory mechanism affecting the production of probable iron transporter YtgABCD. Expression of the encoding gene is negatively regulated by YtgR (Akers *et al.*, 2011). In favorable conditions, YtgR binds iron-dependently to an operator sequence upstream of *ytgABCD* and represses transcription. If iron is limited, YtgR dissociates from the operator sequence and YtgABCD production is upregulated as an effort to accelerate iron import through more import possibilities. If this mechanism does not lead to sufficient iron supply, *Chlamydia* enters nutrient starvation-mediated persistence (Brinkworth, Wildung and Carabeo, 2018). In this state, *Chlamydia* adopt an aberrant phenotype and cells reside within small inclusions. Generation of infectious progeny is stalled, as survival is prioritized over replication (Brinkworth, Wildung and Carabeo, 2018). Due to the reversibility of this state, meeting the definition of persistence in *Chlamydia*, nutrient-starvation mediated persistence is considered true persistence (Pokorzynski, Thompson and Carabeo, 2017). Iron starvation-mediated persistence could be speculated to be of relevance in clinical settings, as persistent chlamydial infections might require persistence-breaking treatment. Recently, MraY inhibitor muraymycin was shown to break the persistence phenotype in *Chlamydia* (Löckener *et al.*, 2024). However, evidence of iron starvation-induced chlamydial persistence *in vivo* and data on antibiotic susceptibility of *C. trachomatis* under iron-starved conditions is still required (Pokorzynski, Thompson and Carabeo, 2017).

Besides the general need of iron as a trace element, a direct link between iron starvation and inhibited cell division in *Chlamydia,* that is mechanistically different from other inductors, e.g. β-lactam antibiotics*,* is suggested: proteins IspG and IspH are involved in the MEP-pathway in *Chlamydia*, ultimately yielding membrane carrier bactoprenol needed in chlamydial PGN synthesis for flipping precursor molecule lipid II across the inner membrane. IspG and IspH contain iron sulfur clusters, with iron acquired from cytosolic pools. During iron starvation, these proteins lose functionality, ultimately leading to a lack of bactoprenol carrier molecules, negatively affecting the entire PGN metabolism (Slade *et al.*, 2019; Kozusnik, Adams and Greub, 2024). Interestingly, persistent states caused by iron starvation and by pro-inflammatory cytokine IFN-γ share certain links and mechanisms. IFN-γ induces tryptophane starvation in *C. trachomatis* and also in other intracellular pathogens like e.g. *Toxoplasma gondii*, by inducing the enzyme indoleamine-2,3-dioxygenase (IDO), which degrades tryptophane

(MacKenzie *et al.*, 1999). An alternative mechanism suggested for IFN-γ to induce persistence in *Chlamydia* is the inhibition of host cell transcription factor c-Myc, which is known to positively regulate translation of glutamine transporters and glutaminases essential for chlamydial proliferation (Rajeeve *et al.*, 2020; Vollmuth *et al.*, 2022). IFN-γ is suggested to decrease levels of c-Myc, ultimately inducing *Chlamydia* to enter persistence. The aberrant phenotype however is not only thought to be mediated by starvation of an essential nutrient but can also be seen in a mechanistic perspective: cell division enzymes PBP2, RodA, PBP3 and MraY are proteins rich in tryptophane. During tryptophane shortage, translation of these enzyme is suggested to be impaired (Riffaud, Rucks and Ouellette, 2023b), ultimately leading to an arrest of cell division and persistence. The regulatory protein YtgR is also rich in tryptophane and its translation is, therefore, also thought to be influenced negatively by tryptophane unavailability (Pokorzynski *et al.*, 2020). However, this is not uniform in *Chlamydia* and *Chlamydia*-related bacteria: *S. negevensis* encodes for a YtgR homolog that does not contain a triple tryptophane motif, indicating a different response compared to the mechanism described for *C. trachomatis* (Pillonel *et al.*, 2019; Kozusnik, Adams and Greub, 2024). To restock intracellular tryptophane pools, chlamydial proteins like YtgR that are rich in tryptophane can also be degraded in the event of starvation and are not within reach for tryptophane-degrading IDO (Kozusnik, Adams and Greub, 2024). Moreover, YtgR does not only regulate the expression of *ytgABCD*, but also of *trpB* and *trpA*, genes which encode for both subunits of tryptophane synthase within the Trp-operon (Wood *et al.*, 2003; Pokorzynski *et al.*, 2020). The operon is not uniformly distributed among *Chlamydia* and *Chlamydia*-related bacteria (Kozusnik, Adams and Greub, 2024). The only member within the *Chlamydiales* that retained the entire operon necessary for synthesis of tryptophane is *S. negevensis*, while *C. trachomatis* encodes for proteins that partially execute the pathway. Others like *W. chondrophila* and ocular strains of *C. trachomatis* have reduced the pathway completely and are auxotrophic for tryptophane (Banerjee and Nelson, 2019; Kozusnik, Adams and Greub, 2024). Due to the connection of iron and tryptophane-related pathways, lack of tryptophane would simultaneously entail upregulation of an iron transporter and tryptophane synthase, as both genetic regions would not be negatively regulated by YtgR anymore. Likewise, with YtgR regulation being dependent on iron, iron limitation alleviates mechanisms leading to elevated iron import and tryptophane synthesis at the same time.

On a transcriptional level, iron starvation, IFN-γ exposure and penicillin treatment each induce upregulation of *euo* and downregulation of *omcB* (Timms *et al.*, 2009; Shima *et al.*, 2021). The developmental regulator *euo* represses late gene transcription and *omcB* encodes an outer membrane complex protein involved in secondary differentiation. These factors indicate that chlamydial development is stalled by both adverse environmental conditions and also by β-lactam treatment. *Waddlia* also enters a persistent state and forms aberrant cells during iron starvation. Transcriptome analysis revealed a decreased expression of genes correlated with cell envelope biosynthesis, turnover and degradation (Ardissone *et al.*, 2020). Consequently, also *amiA* was shown to be downregulated under these conditions, underlining the hypothesis that iron starvation is associated with stalled

chlamydial late stage development. However, *amiA* transcripts were shown to be upregulated under penicillin-induced persistence (Shima *et al.*, 2021). Curiously, Brinkworth *et al*. demonstrated that, under iron-starved conditions, synthesis of nucleotides, charged tRNAs, amino acids and other macromolecular precursors in *Chlamydia* is upregulated, while protein synthesis itself is downregulated. The authors propose this mechanism to be part of a "stock the pantry"-mechanism, in which cells prepare to quickly restart metabolism once favorable environmental conditions are reestablished (Brinkworth, Wildung and Carabeo, 2018). In IFN-γ-induced persistence, curiously, Ouellette *et al*. found genes encoding proteins low in tryptophane to be downregulated, while tryptophane codon-rich genes are upregulated (Ouellette, Rueden and Rucks, 2016). Globally, transcription is increased, while translation is stalled compared to regular chlamydial infections (Ouellette *et al.*, 2006; Ouellette, Rueden and Rucks, 2016). Either, upregulated transcription is suggested to be a product of misregulation, or, as an advantage once the developmental cycle can be resumed normally. The abundance of transcripts could then confer a metabolic head start and could enable *Chlamydia* to resume development more quickly, analogous to the mechanism Brinkworth *et al.* suggested (Brinkworth, Wildung and Carabeo, 2018; Ouellette *et al.*, 2018).

Under laboratory conditions, different strategies have been employed to induce iron starvation in *Chlamydia*. Salicylaldehyde isonicotinoyl hydrazone (SIH) chelates iron, but also interferes with type 3 secretion system (T3SS) in *Chlamydia*, and therefore should be avoided (Simunek *et al.*, 2005; Thompson and Carabeo, 2011). Deferoxamin (DFO) was long considered state of the art. However, the compound proved to be largely ineffective, as, due to its hydrophilic nature, its membrane permeability was low, so that DFO pretreatment of the host cells was required prior to infection with *Chlamydia* (Martell and Smith R.M., 1974; Al-Younes *et al.*, 2001; Thompson and Carabeo, 2011). The bipyridine compound 2,2-bipyridyl proved to be more effective. Due to its hydrophobicity, the compound is highly membrane-permeable (Romeo *et al.*, 2001). It sequesters Fe^{2+} and Fe^{3+} alike, and therefore is suited to deplete both extracellular and intracellular iron pools and might even reach chlamydial cells (Thompson and Carabeo, 2011). Furthermore, the compound is only weakly cytotoxic (Thompson and Carabeo, 2011). Here, 2,2-bipyridyl was used as a positive control to demonstrate micronutrient starvation of chlamydial infection, like already shown for *Chlamydia* by Brinkworth *et al*. and by Ardissone *et al*. for *Waddlia* (Thompson and Carabeo, 2011; Brinkworth, Wildung and Carabeo, 2018; Ardissone *et al.*, 2020).

In this work, the compounds 1,10-phenanthroline, TPEN and clioquinol were shown to chelate zinc in enzymatic *in vitro* assays with AmiA_Cp, but their ability to chelate bivalent cations also includes ferrous iron. Cytotoxicity assays performed in this work indicated that clioquinol and 1,10-phenanthroline are applicable in cell culture settings at concentrations that do not evoke cytotoxic effects. However, TPEN displayed a high cytotoxicity towards host cells, and as it is a zinc-specific chelator with low affinity towards iron, it was not included in iron starvation models discussed in the following. Additionally, cytotoxicity data determined in this work indicated high toxicity towards the

employed mammalian cell lines. In a pH-dependent manner, chelating compounds that form complexes with transition metals have different affinities towards ligands, which change along with pH values. According to Irving-Williams series, general complexation affinities for iron and zinc are comparable (Irving and Williams, 1948). Besides zinc, chelation of iron by clioquinol and 1,10-phenanthroline has been demonstrated in various settings (Eizric *et al.*, 1986; Zhu *et al.*, 2021). In this work, when applied onto active chlamydial infections, formation of small aberrant bodies within small inclusions was observed for both clioquinol and 1,10-phenanthroline. Morphologically, chlamydial cells were comparable to cells after 2,2-bipyridyl treatment. In case of clioquinol and 1,10-phenanthroline, the inhibitory effects could be averted by the addition of $FeSO_4$. However, 1,10-phenanthroline-treated cells could also be rescued from persistence by the addition of $ZnSO_4$. Still, the effect of 1,10-phenanthroline on *Chlamydia* might be attributed to iron starvation, at least partially. As complex formation is a dynamic process, iron could have been sequestered before by chelating agents, but, when supplied with $ZnSO_4$, dissociation and reassociation of complexes might have also included available zinc, releasing iron, which would now be available for chlamydial infections. Changing affinities towards metal ions also affect complex formation with 2,2-bipyridyl, which was shown to chelate not only iron, but also other transition metals like zinc and copper (Fei *et al.*, 2013; Dianov *et al.*, 2018; Li *et al.*, 2021; Nisbet, Hiralal and Poeppelmeier, 2021), suggesting that membrane-permeable 2,2-bipyridyl is not necessarily a superior compound for iron chelation compared to clioquinol and 1,10-phenanthroline, both of which permeate membranes as well. Clioquinol-treated infections could not be rescued by the addition of zinc, likely because clioquinol functions as an ionophore and transports metal ions across membranes (Freedman, 2012; Seo *et al.*, 2015). This way, intracellular transition metal levels can become enriched and, in the case of zinc, have a cytotoxic effect on eukaryotic cells (Kriedt *et al.*, 2010; Akbaba, 2020; Salesa, Sabater i Serra and Serrano-Aroca, 2021). This effect has been extensively studied in cancer research and in *in vivo* models of several neurodegenerative diseases and cancer (Nguyen, Hamby and Massa, 2005; Perez, Sklar and Chigaev, 2019; Khan *et al.*, 2020; Teil *et al.*, 2022). Zinc combined with clioquinol led to host cell death within the experiments performed in this work, even though the employed concentrations of clioquinol and $ZnSO_4$ alone did not have cytotoxic effects in preparatory experiments. In recovery experiments performed in this work, effects of chelating agents on active and PenG-induced persistent chlamydial infections was reversible except for the highest tested concentration of clioquinol, which is also in line with the trace element starvation hypothesis inducing a persistent state which can be reverted.

PenG-induced persistent chlamydial infections were also altered phenotypically by chelating compound treatment in this work. Not only infection rates were affected negatively, but also inclusion sizes were reduced when higher concentrations of either clioquinol or 1,10-phenanthroline were applied. While chlamydial cells were present as ABs due to penicillin treatment, additional chelator treatment led to the formation of small aberrant bodies or cells resembling EBs and/or RBs. Treatment of IFN-γ-induced persistent chlamydial infections led to the same outcome, except for effects on chlamydial phenotypes,

which did not change from small aberrant bodies already described in IFN-γ-induced persistence. Given the hypothesis that persistence, especially in the case of IFN-γ-induced models, stalls development of *Chlamydia* before redifferentiation from RBs to EBs, induction of possible iron starvation through chelating agents adds to this effect. Also given the link between iron starvation and tryptophan starvation induced by IFN-γ, both effects can be hypothesized to refuel one another.

While cell culture-based infection models are frequently used to assess novel treatment options and gain insight into several metabolic processes that do not exclusive surround the PGN metabolism, novel techniques allow genetic manipulations of chlamydial genomes. Chlamydiae were long considered genetically intractable organisms, which made novel discoveries regarding chlamydial genomes challenging and introducing mutations, knockouts and deletions has been impossible for a long time (Heuer *et al.*, 2007). The discovery that, in fact, horizontal gene transfer had occurred in evolution of *Chlamydia* by identification of genetic recombinants changed this status. Although the mechanism was unknown, natural transformation events between individual chlamydial cells was suggested as the underlying mechanism (DeMars *et al.*, 2007). This discovery, however, did not change anything about the unavailability of genetic manipulation methods in *Chlamydia*. Transport of genetic material into chlamydial cells within the host cells was hard to achieve, as polar nucleic acids would have to pass various membranes: the cell membrane of the eukaryotic host, the inclusion membrane and both the outer and inner chlamydial membrane (Ölander and Sixt, 2022). A leap forward leading to genetic manipulation of *Chlamydia* was achieved by Binet & Maurelli, who introduced a method of allelic exchange in *C. psittaci* by electroporation (Binet and Maurelli, 2009). Analysis of single gene function was enabled by chemical mutagenesis and subsequent screening for single nucleotide polymorphisms, which was introduced by Kari *et al.* (Kari *et al.*, 2011). By generating a shuttle vector consisting of the native chlamydial plasmid and an origin of replication of *E. coli*, Wang *et al*. introduced a major success in genetic tractability of *Chlamydia* and introduced the first method of chemical $CaCl_2$-dependent transformation and the first stable transformation system in *Chlamydia* to that point (Wang *et al.*, 2011). Since then, the method has been modified for several other chlamydial species (Shima *et al.*, 2018) and conditional and inducible expression vectors have been generated (Wickstrum *et al.*, 2013). Further genetic advances include the TargeTron technology (Johnson and Fisher, 2013), which functions via self-splicing group II introns that insert into specific DNA loci, enabling mutations and deletions. A most recent technology in chlamydial genome manipulation is CRISPR interference (CRISPRi), which is based on the CRISPR system. CRISPR is an acronym for clustered regularly interspaced short palindromic repeats and can be described as an immune system bacteria employ to protect themselves against phages integrating DNA into bacterial genomes (Bhaya, Davison and Barrangou, 2011; Terns and Terns, 2011; Wiedenheft, Sternberg and Doudna, 2012). It relies on an endonuclease, e.g. Cas9, associated to two RNA molecules. The crRNA sequence is complementary to a target DNA sequence and enables binding of the complex in this region. crRNA maturation and guidance of the complex towards the target region can only be achieved if crRNA is bound to the tracrRNA molecule via repeat

sequences. Endonuclease Cas9 introduces double-stranded breaks into the target DNA when crRNA is bound to a complementary sequence and is close to the protospacer adjacent motif sequence (PAM). Leveraging this system enables the introduction of target-specific mutations into bacterial genomes. The RNA duplex consisting of crRNA and tracrRNA can be replaced by an engineered single guide RNA (sgRNA) molecule exerting both functions: binding to a complementary sequence and association to Cas9 (Jiang and Doudna, 2017). Beyond introducing breaks within the target DNA, also genomic sequences can be introduced simultaneously into a targeted region. Within CRISPRi technology, a catalytically inactive version of Cas9 is employed and is termed dCas9 (dead Cas9) (Qi *et al.*, 2013). Employing the same mechanism as described previously for DNA sequence targeting, the catalytic inactivity causes dCas9-sgRNA complexes to bind to, but not to cleave target DNA. This way, transcription is blocked through a proposed mechanism of the RNA polymerase and the dCas9 complex colliding with each other and terminating transcription of the specific DNA sequence with high efficiency (Qi *et al.*, 2013). In chlamydial research, the method was first applied by Scot Ouellette, who developed a single plasmid system for conditional expression of a dCas9 variant associated to guide RNA, which could introduce conditional and reversible knockdowns in *Chlamydia* (Ouellette, 2018b). Meanwhile, alterations and ameliorations have been introduced, e.g. by introducing dCas12 instead of dCas9, which broadens the repertoire for putative target sequences (Ouellette *et al.*, 2021). In this work, the effects of *amiA* knockdown in *C. trachomatis* were investigated in active chlamydial infections. Therefore, a plasmid based on the pLCRia vector (Ouellette *et al.*, 2021) was constructed by Ouellette *et al*., harboring the possibility of aTc-inducible dCas9 expression targeted against *amiA*. The experiment including staining was performed by Liechti *et al*. After transformation of the construct into *C. trachomatis* elementary bodies and infection of mammalian cells, dCas9 production was induced two hours after infection. Imaging 24 hpi and indirect immunofluorescence staining of MOMP revealed that chlamydial cells were significantly enlarged. As shown in this work, cells displayed an inhibited cell division phenotype, which became more apparent when looking at single cells. Results of this work specifically depict cells that seem to be stuck within the budding phase. The experiment was performed again using a construct that besides *amiA* knockdown also facilitates overproduction of His-tagged AmiA upon aTc-induction. Results revealed that phenotypes evoked by *amiA* knockdown were averted by simultaneous overexpression of *amiA* on the same plasmid upon induction with aTc and normal chlamydial cell size and morphology could be reinstated.

To test if knockdown of *amiA* is reflected on a transcriptional level, it was necessary to perform RT-qPCR to quantify *amiA* transcripts, as otherwise, the observed effects could not be attributed to *amiA* knockdown securely. Therefore, these experiments were part of the research conducted during the TRR261-funded research stay at University of Nebraska Medical Center. As transcription levels are subject to variation over the course of the chlamydial developmental cycle, no gene within the chlamydial genome is constantly expressed at the same level. This requires a different method of normalization for RT-qPCR-derived transcriptomic data other than the frequently used method of 16s

rRNA quantification (Ouellette *et al.*, 2005). As Ouellette *et al.* proposed, genomic DNA was used to quantify and normalize the data resulting from RT-qPCR. Infected cells were sampled at three different time points: 10 hpi, samples were drawn from tissue culture after induction of dCas9 expression, if performed, to obtain data from a time point where expression levels under both induced and uninduced conditions should be constant. This time point was also representative of an early point of gene expression, while samples drawn 14 hpi reflect the phase in which mid-cycle genes are expressed. When sampling 24 hpi, changes within the phase of late gene expression during differentiation from RBs to EBs are monitored (Shaw *et al.*, 2000; Belland *et al.*, 2003). Besides *amiA*, also transcriptional levels for *murE* were determined, as the gene is located directly downstream of *amiA* and therefore enabled exclusion of polar effects of *amiA* knockdown (Stephens *et al.*, 1998b; Patin *et al.*, 2009). Moreover, as a developmental cycle control, *euo* and *omcB* were also quantified. Developmental regulator *euo* is expressed early and is involved in repression of late gene transcription (Rosario, Hanson and Tan, 2014; Hakiem *et al.*, 2023). The late gene *omcB* encodes for the large periplasmic cysteine-rich protein, which is part of the outer envelope of chlamydial EBs (Allen and Stephens, 1989; Moelleken and Hegemann, 2008). As expected, only transcripts of *amiA* decreased over time. Transcript number decline was significant at 14 hpi and became more apparent at 24 hpi, and knockdown had no polar effects on *murE*. As expected, transcript levels of *euo* decreased over the course of the experiment, while *omcB* levels and genomic DNA levels raised over the experimental time course. These data show that knockdown of *amiA* was successful and did not affect adjacent genes. Interestingly, transcription of *omcB*, which, under penicillin-induced persistence (Goellner *et al.*, 2006), is downregulated, is not affected under *amiA* knockdown, which produces a persistence-resembling phenotype. This indicates that the mechanisms underlying chlamydial phenotype following *amiA* knockdown and persistence induced by penicillin are different from each other.

Besides the knockdown strain producing dCas9 targeting *amiA*, also the non-targeting strain (NT) directed against a random sequence and serving as a negative control was included. Results showed that production of the non-targeting dCas9 did not affect any of the tested genes, nor general proliferation as reflected in gDNA levels, proving that the construct serves as a negative control. The complemented construct pLCRia-*amiA*-6xH(*amiA*) which simultaneously produces a knockdown of *amiA* while overproducing a His-tagged version of the protein upon induction of construct expression was also included in this experiment. Not only to verify that the observed phenotype after *amiA* knockdown was could be complemented, but mainly, that the observed effects of knockdown are a direct consequence of amiA knockdown, including of this construct was essential. While all tested genes except for *murE* at mid-replication timepoint 14 hpi and gDNA levels turned out to be as expected, *amiA* transcript levels were significantly decreased in the induced samples compared to the uninduced samples. Upon comparison of *amiA* transcript quantification in the knockdown strain, however, a key difference became apparent: in the knockdown strain, *amiA* levels in the induced sample were 20-fold lower than in the complemented strain under identical conditions. This observation can probably be explained by the

mechanism of complementation. While *amiA* expression is suppressed by dCas9, simultaneously, *amiA* is overexpressed from the same plasmid. Hypothetically, this explains the generally higher level of *amiA* expression shown in the transcription data. Furthermore, knockdown of *amiA* will most likely not only affect chromosome-encoded *amiA*, but also plasmid-encoded *amiA*. While *amiA* is transcribed from the plasmid, it is simultaneously knocked down by dCas9, resulting in an apparent decrease of transcripts compared to the samples where dCas9 had not been induced. At 10 hpi, early in the RB-replicating stage, also the amount of *amiA* transcripts is 8-fold higher in the complemented strain compared to the knockdown strain. Possibly, this could be due to tet-promotor leakage, inducing transcription even without intended induction.

Besides chlamydial phenotype as visualized by outer membrane protein MOMP imaging, the experiments also focused on the amount and localization of PGN within chlamydial cells during knockdown of *amiA*. As this work showed that AmiA_Ct hydrolyzed PGN *in vitro*, an impairment of PGN ring remodeling processes after *amiA* knockdown was hypothesized. PGN was visualized via labeled D-Ala-D-Ala analogs and click chemistry-based reactions, which were used to elucidate the existence of PGN in *Chlamydia* using a previously established methodology (Liechti *et al.*, 2014). Through genetic analyses proving that a lipid II biosynthetic pathway has been retained in *Chlamydia*, proof of *in vitro* function of successfully purified proteins and susceptibility towards cell wall-targeting antibiotics, the existence of PGN was suspected and the inability to purify it was debated extensively. As both Ddl, ligating two D-Ala moieties to each other, and MurF, ligating D-Ala-D-Ala to MurNAc-tripeptide during lipid II biosynthesis in the cytoplasm, have been functionally conserved in *Chlamydia* (McCoy and Maurelli, 2005; Patin *et al.*, 2012), a method for incorporation of fluorescently labeled D-Ala analogs was developed (Kuru *et al.*, 2012). However, despite the ability of *C. trachomatis* to take up D-Ala analogs (Moulder, Novosel and Officer, 1963; McCoy and Maurelli, 2005), attempts to incorporate them into PGN failed (Kuru *et al.*, 2012; Siegrist *et al.*, 2013; G. W. Liechti *et al.*, 2014). Liechti *et al*. introduced a method based on the uptake of modified D-Ala-D-Ala analogs, such as alkyl-coupled ethynyl-D-alanyl-D-alanine, thereby bypassing Ddl (G. W. Liechti *et al.*, 2014). Click chemistry enables the coupling of an alkyl moiety to an azide moiety, which, in this case, was conjugated to fluorophore AlexaFluor 488 (Breinbauer and Köhn, 2003). After fixation, fluorescence microscopy cannot only reveal the presence of PGN, but also its localization. The results provided by Liechti *et al.* as part of a collaborative research project of the Liechti, Ouellette and Henrichfreise labs and shown in this work demonstrated that, during *amiA* knockdown, PGN is localized in discrete patches at the budding poles of chlamydial cells stuck in the initial phase of cell division. Upon complementation by *amiA* overexpression, normal PGN distribution was reinstated and even PGN rings present during chlamydial cell division could be observed. PGN during knockdown of *amiA* was also investigated quantitatively regarding PGN quantity by determining object volumes and fluorescence intensities. Liechti *et al.* performed the experiments, which, besides the *amiA* knockdown strain and the complemented strain referred to, also contained a negative control strain targeting a random sequence

(NT). Results revealed, that mean object volumes of PGN structures were significantly larger in the knockdown strain under induced conditions than under uninduced conditions. That fits the observation made in the experiment performed previously, which showed significantly enlarged chlamydial cells. Concomitantly, also the PGN object volumes can be hypothesized to be larger than under induced conditions. At the same time, no significant increase was detected between uninduced and induced samples of the non-targeting negative control and the complemented strain, indicating that, here, the constructs exerted no effect on PGN, as expected. The integrated density, quotient of PGN object volume and fluorescence intensity, is significantly elevated compared to the uninduced control and higher compared to the non-targeting negative control and the complemented strain under induced conditions of the *amiA* knockdown strain. Hypothetically, this could be due to the impairment of PGN degradation. While the PGN biosynthesis machinery itself is not impaired by knockdown of *amiA*, the degradation machinery relies on AmiA activity to a large extend. Besides a putative SpoIID homolog acting as a lytic glycosyltransferase (Jacquier *et al.*, 2019), AmiA is the only known PGN-degrading enzyme in *Chlamydia* to date. Upon knockdown of *amiA*, the degradation of PGN by *Chlamydia* is suggested to be significantly impaired, while PGN biosynthesis is not, potentially leading to an accumulation of PGN without further processing. Due to significant enlargement of chlamydial cells, inhibition of the cell division process is suggested as a possible mechanism. Presumably, this should also affect the generation of infectious progeny. To test this, IFU assays were performed with the *amiA* knockdown strain, the complemented strain and the non-targeting negative control strain. Previously, this experimental setup was employed to test the effects of CRISPRi-mediated knockdowns of protease Tsp, which is important for developmental regulation of proteome components in *Chlamydia* and of components of the proteasome complex Clp (Wood *et al.*, 2020; Swoboda *et al.*, 2023). IFU data resulting from the induced samples were normalized to the strains in which construct expression was not induced. To verify correct construct expression, immunofluorescence assays were performed simultaneously. This work was in parts performed during the research collaboration of the Henrichfreise lab with the Ouellette lab, which was funded by the TRR261. In all strains, dCas9 production could be detected after induction of construct expression. Also, the previously observed phenotype of enlarged chlamydial cells could be verified again in this experiment. IFU assays revealed that the non-targeting (NT) strain was not impaired in proliferation. This shows that, in general, dCas9 production does not impair *Chlamydia* regarding EB production. Also, dCas9 targeting a random sequence did not have an effect regarding chlamydial phenotype. Knockdown of *amiA* entailed a significant reduction of infectious progeny by approx. 70 %, while EB production in the complemented strain was slightly increased in the induced sample compared to uninduced conditions. The hypothesis suggesting that inhibited cell division due to *amiA* knockdown is causing the enlarged cell phenotype and that the limited generation of infectious progeny is supported by the role AmiA is assigned within the chlamydial PGN metabolism. In lysis experiments and complementation in a triple-amidase mutant incapable of separating daughter cells, chlamydial AmiA was shown to degrade PGN material and, thereby, lyse its host strain or rescue cell

separation, respectively. The PGN ring which is only present in *Chlamydia* during cell division requires constant remodeling in order to dilate and constrict (Liechti *et al.*, 2014; Liechti *et al.*, 2016). Klöckner *et al.* postulated a sustaining function of chlamydial AmiA within the cycle, that most likely connects biosynthesis, processing and recycling of PGN (Klöckner *et al.*, 2014). Liechti *et al*. hypothesized that aberrant phenotypes observed during chlamydial persistence do not divide anymore because of inhibited PGN synthesis or failure of PGN ring assembly (Brockett and Liechti, 2021). Likewise, absence or inactivity of chlamydial AmiA, the only PGN amidase retained within the organism, could lead to disruptions in PGN metabolism. Increased PGN object volumes, as observed in the experiments presented in this work, are likely a result of *amiA* knockdown. According to Liechti (2021), PGN object volumes are a result of balance between interconnected processes of PGN degradation and synthesis (Liechti, 2021). Upon shift of the balance between those processes, PGN object volumes either increase or decrease. In regular chlamydial cell division, PGN objects form as a disc at the future site of the division septum. Outward synthesis is suggested to be reliant on PBP2 and RodA activity, while inward-facing PGN material is subject to degradation. Conversely, constriction of the ring in the final phases of chlamydial cell division is proposed to be mediated through inward PGN synthesis through PBP3 and FtsW activity, eventually leading to disc formation, while outward-facing PGN is degraded. Upon finalization of cell division, balance is thought to shift towards degradative processes, until PGN material is fully disassembled. Likewise, increased PGN labeling intensity is suggested to be a result of a high level of PGN synthesis, outweighing degradative processes. The effects of *amiA* knockdown presented in this work are matching this theory because chlamydial AmiA, besides a probable SpoIID homolog acting as a lytic transglycosylase, is the only known PGN-degrading enzyme in *Chlamydia* to date. Impairment of PGN degradation prevents correct PGN ring assembly, growth and constriction, and, thereby, causes inhibited cell division, to which the observed phenotype alludes to. In *Chlamydia*, AmiA plays a key role in cell division early in the process through the enzyme's involvement in PGN-remodeling and recycling processes, enabling correct formation of septal PGN rings. In contrast, cell division amidases of free-living bacteria such as model organism *E. coli* achieve highest relevance towards the final stages of bacterial cell division. Here, activity of cell division amidases is required to cleave shared layers of peptidoglycan between nascent daughter cells, enabling their separation (Heidrich, Templin, Ursinus, Merdanovic, Berger, Schwarz, De Pedro and J. Höltje, 2001). Although hydrolytic reactions catalyzed by both amidases are identical and chlamydial amidases can substitute in amidase-deficient *E. coli* mutants by cleaving shared PGN layers (Klöckner *et al.*, 2014), cell division amidases of *Chlamydia* and free-living bacteria are assigned distinct functions within cellular environments, highlighting and interesting spatiotemporal difference between them.

In this work, besides AmiA, also RodA and a putative NamZ homolog were investigated using recent genetic methods. Besides CRISPRi knockdowns, both genes were also used in an overexpression screening to learn about resulting effects and about protein localization. RodA, member of the SEDS proteins (shape, elongation, division, sporulation), was first suggested to be involved in PGN

biosynthetic processes by Meeske *et al.,* who investigated RodA in *Bacillus subtilis* (Meeske *et al.*, 2016). Recently, the RodA-PBP2 complex was shown to be functional in Gram-negative bacteria as well, as Nygaard *et al.* investigated the function of the complex in model organism *E. coli* (Nygaard *et al.*, 2023). RodA is also conserved in *Chlamydia* and is suggested to act as transglycosylase in PGN ring expansion together with cognate transpeptidase PBP2 during chlamydial cell division (Henrichfreise, Brunke and Patrick H Viollier, 2016; Liechti, 2021). NamZ is an exo-β-N-acetylmuramidase that cleaves off the MurNAc moiety from the minimal PGN-derived substrate MurNAc-GlcNAc from the non-reducing end in free-living bacteria (Müller *et al.*, 2021). The enzyme was characterized in *B. subtilis* and *Tannerella forsythia* and is suggested to play a role in PGN recycling, as mutants lacking NamZ were shown to accumulate PGN fragments (Müller *et al.*, 2021; Borisova *et al.*, 2022). Sequence comparisons revealed that a chlamydial protein encoded by *ct605* had 35 % identity with the amino acid sequence of NamZ from *B. subtilis*. Therefore, in this work, *ct605* was suggested to encode for a NamZ homolog in *C. trachomatis* and was investigated regarding potential involvement in PGN recycling in *Chlamydia*. Analogously to the experiments performed with AmiA, aTc-inducible CRISPRi vectors were created with dCas9 targeting *rodA* or *namZ*. Subsequent fluorescence microscopy and imaging of dCas9 indicated that knockdowns were successful. When induced 4 hpi, during primary differentiation from EBs to RBs, and imaged 24 hpi, during redifferentitation, knockdown of *rodA* revealed significantly enlarged chlamydial cells compared to the uninduced control. This resembled the inhibited cell division phenotype, that previously has been observed also in knockdowns of *amiA*. RodA is proposed to function as a glycosyltransferase acting together with cognate monofunctional transpeptidase PBP2 in synthesis of PGN, as *Chlamydia* lacks all known class A PBPs conferring both glycosyltransferase and transpeptidase activity (Packiam *et al.*, 2015; Meeske *et al.*, 2016). Due to the fact that homologs of SEDS proteins and class B PBPs are more widely conserved in bacteria than bifunctional class A PBPs, the mechanism combining glycosyltransferase activity and monofunctional transpeptidase PBPs is proposed to be ancestral (Egan *et al.*, 2015; Van der Ploeg, Goudelis and Den Blaauwen, 2015; Henrichfreise, Brunke and Patrick H. Viollier, 2016). Emami *et al.* observed growth arrest upon inhibition of RodA in a *B. subtilis* mutant lacking all class A PBPs, indicating its role in cell proliferation processes (Emami *et al.*, 2017). In *Chlamydia*, the RodA-PBP2 complex is suggested to perform the final steps of outward PGN synthesis of the PGN ring, contributing to its expansion (Liechti, 2021). Interestingly, treatment with the mostly PBP2-specific antibiotic mecillinam (Spratt, 1977) resulted in chlamydial cells reduced in size (Liechti, 2021). Conversely, interfering with the complex by genetic knockdown of *rodA* resulted in the opposite outcome, with cells being significantly enlarged. As PGN biosynthesis and processing are exclusive to cell division-related processes in *Chlamydia* and interfering with these processes results in halting of the developmental cycle (Brockett and Liechti, 2021), effects of *rodA* knockdown could be explained by the organism's inability to progress synthesis of the PGN ring needed for division. Similarly, knockdown of *ct605*, presumed to encode a functionally conserved NamZ homolog putatively involved in PGN recycling, yielded significantly enlarged

chlamydial cells. In *B. subtilis*, NamZ was characterized by Müller *et al*. and was identified as the founding member of a novel family of exolytic PGN hexosaminidases (Müller *et al.*, 2021). While enzymes degrading the PGN glycan backbone or glycosidic linkages of muropeptides, e.g. endo-β-N-acetylglucosaminidases like NagZ, are well characterized, nothing was known about exo-β-N-acetylmuramidases, that cleave off MurNAc-residues from the non-reducing end of muropeptides, resulting from e.g. NagZ activity (Litzinger *et al.*, 2010; Müller *et al.*, 2021). Litzinger *et al*. could show that NagZ is involved in PGN recycling in *B. subtilis* (Litzinger *et al.*, 2010). Amidase AmiE and previously uncharacterized NamZ are encoded within the same operon in *B. subtilis* and sequential digest of PGN by NagZ, NamZ and AmiE was shown by Müller *et al*. (Müller *et al.*, 2021). Within this process, AmiE requires previous NagZ digest of PGN, because only MurNAc peptides can serve as a substrate. However, while the presence of NamZ is usually coupled to NagZ, NagZ does not require NamZ (Müller *et al.*, 2021). Activity of these enzymes yields anhydro-MurNAc and GlcNAc moieties, which can be transported to the cytoplasm by phosphotransferase system transporters such as MurNAc transporter MurP in *E. coli* and GlcNAc-transporter NagP of *B. subtilis* (Dahl *et al.*, 2004; Gaugué *et al.*, 2013). After phosphorylation, a reentry into a new cycle of PGN biosynthesis is possible. If, hypothetically, the gene product encoded by *ct605* is a functional NamZ homolog, it could be involved in PGN recycling in *Chlamydia*. Likely, a SpoIID homolog performs cleavage of glycosidic linkages within the PGN glycan backbone in *Chlamydia*, yielding GlcNAc-anhydroMurNAc-tetrapeptide and GlcNAc-anhydroMurNAc-tetrapeptide in *Chlamydia*-related bacterium *Waddlia,* as shown by Jacquier *et al.* (Jacquier *et al.*, 2019). According to the characterization of NamZ performed by Müller *et al.*, the minimal substrate for NamZ is a disaccharide with MurNAc at the non-reducing end (Müller *et al.*, 2021). Likely, products of putative SpoIID activity would therefore not yield suitable substrate for putative NamZ. However, NamZ activity preceding SpoIID activity is possible and it would cleave off MurNAc moieties from the reducing end of glycan strands whenever exposed. As recycling of PGN material is essential for *Chlamydia* in terms of energy efficiency and immune evasion aspects, detrimental effects of *namZ* knockdown could be considered. Although free-living bacteria, like model organism *E. coli,* recycle a large part of PGN material as well (Goodell and Schwarz, 1985; Park and Uehara, 2008), they do not depend on recycling of PGN to the same extent like *Chlamydia*. Amino acid *m*DAP at position three of the stem peptide in PGN and precursor molecules cannot be scavenged from the host (Reuter *et al.*, 2023). *De novo* synthesis requires six energy-intense biosynthetic steps (McCoy *et al.*, 2006; Klöckner *et al.*, 2018). Therefore, recycling of this molecule is favorable for *Chlamydia*. Recently, NlpC/P60 domain containing enzyme YkfC in *C. trachomatis* was characterized to be a part of chlamydial PGN recycling processes and to be conserved in *Chlamydia*-related bacteria as well. YkfC was shown to cleave the γ-D-Glu-*m*DAP bond from PGN-derived peptides specifically, thereby providing *m*DAP (Reuter *et al.*, 2023). By determining substrate specificity, this work contributed to the characterization of YkfC. The non-canonical amino acid *m*DAP is proposed to reenter a novel cycle of PGN biosynthesis after reentry into the chlamydial cell, presumably through peptide transporter

complex homolog OppABCDF (Singh, Liechti, *et al.*, 2020). Moreover, YkfC activity probably plays a role in immune evasion, as its substrate, tripeptide L-Ala-γ-D-Glu-mDAP, is recognized as a pathogen-associated molecular pattern (PAMP) by the eukaryotic host's innate immune system (Girardin *et al.*, 2003). Formation of aberrant phenotypes and stalling of PGN biosynthesis is thought to be a mechanism that helps avoiding the shed of PGN material into the surroundings (G W Liechti *et al.*, 2014; Kozusnik, Adams and Greub, 2024). Cytoplasmic pattern recognition receptors (PRR) like NOD (nucleotide binding oligomerization domain) activate pathways like NFκB leading to an inflammatory response or activate stress response-associated JNK (Chamaillard *et al.*, 2003; Inohara *et al.*, 2003; Welter-Stahl *et al.*, 2006). NOD1 consists of an N-terminal caspase recruiting domain, the central NOD domain and a C-terminal leucine repeat and senses mDAP-containing PGN fragments. While NOD1 is ubiquitous in all cell types, NOD2 is more limited to e.g. monocytes, but reacts less specifically, e.g. to PGN-derived peptides in general (Inohara *et al.*, 2003; Girardin, Boneca, Carneiro, *et al.*, 2003; Girardin, Boneca, Viala, *et al.*, 2003). By minimizing the shedding of immunogenic material into the surroundings, e.g. through activity of YkfC cleaving the innate immune system recognition motif, *Chlamydia* adopts measures to remain undetected within its intracellular niche (Reuter *et al.*, 2023). Besides, *Chlamydia* is suggested to rely on the maintenance of a full cycle of PGN ring biosynthesis, including remodeling and recycling aspects. With limited resources of *de novo* synthesis and not all necessary constituents being provided by the host, Reuter *et al*. suggested a closed-loop system ensuring constant ability of PGN synthesis (Reuter *et al.*, 2023). In this context, presuming that the putative NamZ homolog is also part of the chlamydial PGN recycling machinery, effects of *ct605* knockdown can be explained. By knockdown of an enzyme involved in recycling of PGN constituents, the tightly interlinked processes involved in chlamydial cell division can be affected. Like shown in knockdown of *rodA*, interference and impairment of chlamydial cell division can lead to a phenotype resembling aberrance. Besides the introduction of genetic knockdowns of *rodA* and *ct605*, both genes were cloned into overexpression plasmids to test effects of protein overproduction and to learn about protein localization within the chlamydial cell. Therefore, proteins of interest were genetically tagged with hexahistidines to allow for indirect immunofluorescence detection of RodA and putative NamZ. In both experiments, that were part of the research collaboration between the Henrichfreise and the Ouellette lab funded by the TRR261, construct expression was induced 4 hpi and cells were imaged 11.5 hpi and 24 hpi. The earlier timepoint reflects an early stage of chlamydial proliferation phase when RBs likely begin division (Belland *et al.*, 2003; Abdelrahman and Belland, 2005). For both RodA and NamZ, no particular phenotype was expected at this point, which was confirmed by fluorescence microscopy data. At 24 hpi, overproduction yielded visible effects. Overexpression of *rodA* could be confirmed by detection of hexahistidine tags by indirect immunofluorescence, while the signal was not present in uninduced control samples. Inclusion morphology was visibly smaller when *rodA* overexpression was induced compared to the uninduced samples. Fewer organisms within the inclusions indicated that chlamydial proliferation was impaired. While chlamydial cells did not display an aberrance-like phenotype like in knockdowns of

rodA, some of the cells were enlarged, possibly hinting towards an inhibited cell division process. From the images obtained in this experiment, it was difficult assessing the proteins localization within the cell. SEDS protein RodA is suggested to work in conjunction with PBP2 in expanding the PGN ring during chlamydial cell division by performing outward PGN biosynthesis (Liechti, 2021). Therefore, chlamydial RodA, like other known RodA homologs, is expected to localize as a transmembrane protein within the inner membrane, where the enzyme's glycosyltransferase activity incorporates new PGN building blocks into existing PGN material to extend the PGN ring at the septum. According to predictions, the protein harbors eight transmembrane domains, additionally supporting this theory. This hypothesis is in line with the hypothesis that chlamydial cell division proceeds through a polarized budding mechanism, where the budding site is predetermined by the presence of MOMP and Hsp60 on the opposite cell pole (Abdelrahman *et al.*, 2016). Therefore, a similar localization pattern could be assumed for RodA, as its function is needed at the prospective site of cell division. Profiling of temporal gene expression revealed that *rodA* expression is slightly elevated at 8 hpi and is suggested to peak at 16 hpi where chlamydial cell division is expected to occur (Belland *et al.*, 2003). In the experiment presented in this work, imaging of infected cells at 11.5 hpi could potentially already have shown *rodA* overexpression, but depending on cell line, chlamydial serovar, various environmental conditions and the delay between transcription and translation process could be considered reasons why *rodA* could not be imaged until 24 hpi. Likely, a timepoint in between would have depicted *rodA* expression as well. Localization experiments have been performed in free-living bacteria such as *Corynebacterium glutamicum*, where RodA was shown to localize at the cell pole in the uninduced samples of an overexpression experiment, however, with a leaky promotor that still allowed RodA production. Upon induction of the overexpression construct, RodA delocalized and dispersed across the cell near the membrane (Sieger *et al.*, 2013). In the experiments performed in this work, localization of *rodA* could not be determined clearly and a strict membrane-association of the protein according to expectations could not be observed. Also, RodA did not localize distinctly to the prospective division site. In contrast, cytoplasmic protein YkfC, involved in recycling of PGN material, was shown to localize near the septum in late stages of cell division, while in early stages, the protein was not produced at the prospective division site, which is the MOMP-enriched pole of the cell (Reuter *et al.*, 2023). Cytoplasmic localization of YkfC could also be confirmed. Overexpression experiments with putative *namZ* homolog were analyzed in a similar fashion and results revealed effects on chlamydial infections as well. As shown in this work, inclusion sizes at 24 hpi, after division and on the onset of redifferentiation of RBs into EBs, were significantly smaller than in the uninduced control and contained very few chlamydial cells. Overexpression of *namZ* was successful, as indicated by a well-visible immunofluorescent signal representing hexahistidine tags. The inclusion size at 24 hpi, which almost did not progress in the induced samples compared to the samples imaged at 11.5 hpi, during EB to RB transition, indicates that *namZ* overexpression influenced inclusion development and chlamydial proliferation, as cell numbers increased only insignificantly compared to the earlier timepoint. In the uninduced samples, an increase

in inclusion size was observed between 11.5 hpi and 24 hpi, showing that, in general, inclusion maturation and chlamydial proliferation are not impaired by the presence of the overexpression construct as such. In this experiment, exact localization of putative NamZ was unclear, as only few small cells were present within an inclusion.

For both NamZ from *B. subtilis* and the predicted NamZ homolog from *C. trachomatis*, encoded by *ct605*, a signal peptide-dependent export is predicted. According to sequence predictions, the protein is suggested to be exported sec-dependently in both organisms, however, likelihood of the presence of a sec signal peptide was relatively low for the *B. subtilis* protein with 63 % compared to 93 % probability for putative NamZ in *C. trachomatis*. For the putative *C. trachomatis* protein, export into the periplasm is in line with its predicted function, as cleavage of the PGN glycan backbone occurs in the periplasm during PGN remodeling and recycling processes in the context of chlamydial cell division. In the images obtained during the experiment, a localization proximal to the membrane is indicated, which is in favor of the hypothesis of periplasmic localization of the protein. However, as chlamydial cells are visibly impaired in terms of cell growth and proliferation, further testing is required to confirm protein localization to better characterize this putative new recycling enzyme in *Chlamydia*.

According to transcriptional profiling, *ct605* expression is low at 8 hpi and 24 hpi and further reduced at 40 hpi, while it peaks at 16 hpi with moderate expression levels (Belland *et al.*, 2003). This is also in accordance with the gene product's predicted function as an exo-β-N-acetylmuramidase during PGN recycling, which occurs subsequently to chlamydial cell division. The highest rate of chlamydial cell division and PGN turnover is expected at 16 hpi, when PGN rings required for cell division are subject to turnover processes. Both overexpression and knockdown experiments with chlamydial *rodA* and putative *namZ* require further replicates to gain insight into the consequences of either knockdown or overexpression of both genes. In case of CRISPRi knockdowns, as an additional measure, transcriptional analysis of knockdown strains is recommended to verify decrease of transcripts of either *rodA* and putative *namZ* and to exclude polar effects. Analysis of transcripts could also serve as an additional method in overexpression experiments, as not only overexpression of genes of interest could be confirmed, but also transcripts of late gene *omcB* and early gene *euo* could be quantified. In light of visibly impaired chlamydial development, which was observed after overexpression of *rodA* and *ct605*, quantification of these transcripts could shed light on the underlying transcriptional and developmental processes. IFU assays that revealed impaired generation of infectious progeny should also be performed in case of overexpression and knockdown of both *ct605* and *rodA*. Likely, proliferation ability of *rodA* and *namZ* knockdown strains is impaired, as phenotypes observed in fluorescence microscopy suggested cell division defects. In this case, redifferentiation of RBs into EBs is thought to be halted, resulting in arrest of the developmental cycle. For overexpression of these genes, a decrease of infectious progeny can also be assumed, as chlamydial cells and inclusion morphology was severely set back compared to uninduced controls. Likely, impaired chlamydial development would also result in the inability of the organism to generate sufficient infectious progeny.

Moreover, further *in vitro* analyses could be feasible to characterize enzymatic functioning of the chlamydial NamZ homolog. NamZ is likely involved in PGN recycling processes, as is NlpC/P60 domain containing protein YkfC from *C. trachomatis*, of which the substrate spectrum was further specified as a part of this work (Reuter *et al.*, 2023). Therefore, *in vitro* characterization as performed for NamZ in *B. subtilis* by Müller *et al.* (Müller *et al.*, 2021) should be considered after purification of the *C. trachomatis* homolog in the future. To assess if the enzyme has conserved function as an exo-β-N-acetylmuramidase, substrate spectrum analyses with denuded glycans as a substrate could be feasible. Moreover, pH spectrum analyses could provide first insight about the largely unknown physiologic conditions within chlamydial cells, an issue also tackled by the determination of the pH optimum of chlamydial AmiA in this work.

This work contributed to the understanding of the PGN metabolism in *Chlamydia*, not only by characterization of the only cell division amidase of major human pathogen *C. trachomatis*, but also by comparative analyses with its closest homolog from *C. pneumoniae*, revealing remarkable differences in enzymatic functioning and active site architecture. Using CRISPRi-mediated knockdown as a novel tool of genetic manipulation in *C. trachomatis*, this work showed that knockdown of *amiA* not only affects chlamydial proliferation, but also demonstrated that AmiA in *Chlamydia* is important at an early stage of cell division and not only in the late stage of cell separation as in the free-living model organism *E. coli.* For the first time, chlamydial homologs of RodA and NamZ were investigated using genetic tools as part of this work, yielding results that indicate major importance of these enzymes within the tightly interconnected processes of PGN synthesis and cell division. Like AmiA, these enzymes could be considered attractive targets not only for therapeutic interventions, but also for further elucidation of PGN-related processes in *Chlamydia*. Additionally, investigations concerning chlamydial persistence in this work led to the identification of potent novel inducers of nutrient-starvation mediated persistence that could be leveraged to gain further insight into different persistence mechanisms.

5. Summary

The obligate intracellular pathogen *C. trachomatis* is an important human pathogen and retained only a minimal, yet sufficient biosynthetic pathway needed for peptidoglycan biosynthesis. The genome-reduced organism divides by a unique mechanism which depends on the synthesis of a PGN ring at the division site and requires constant remodeling and recycling of the PGN structure. This work aimed to provide novel insights on the role that PGN amidase AmiA plays in the tightly connected interplay of PGN synthesis, cell division, PGN turnover and recycling in the major human pathogen *C. trachomatis*. Functional conservation of AmiA activity in *C. trachomatis* was confirmed by means of cell lysis and complementation experiments employing surrogate host systems. Moreover, amidase activity on PGN and precursor molecule lipid II could be validated in *in vitro* analyses with the purified enzyme. Experiments revealed a differential active site functional composition compared to the AmiA homolog of the closely related organism *C. pneumoniae* and, in contrast to *C. pneumoniae* AmiA, only monofunctional amidase activity. PGN binding affinity of *C. trachomatis* AmiA was shown to be independent of enzymatic activity. *In vitro*, as expected for a zinc-coordinating enzyme, the enzyme was shown to be inhibited by chelators of bivalent cations such as the antibiotic clioquinol in a pH dependent manner. Reaction products of amidase activity are likely recycled by the chlamydial homolog of NlpC/P60 domain-containing enzyme YkfC, for which the substrate spectrum was further specified as a part of this work.

Chelators were also used in tissue culture-based infection models and proved to induce nutrient starvation-induced persistence in *C. trachomatis*. Thereby, novel opportunities of inducing nutrient starvation and concomitant persistence in *Chlamydia*, equal to state of the art compound 2,2-bipyridyl, were identified.

Leveraging CRISPRi as a novel tool of genetic manipulation of *Chlamydia*, knockdown of *amiA* led to an impaired cell division phenotype and visibly distorted PGN localization and metabolism. These results highlight the role AmiA plays in the closed-loop system of PGN biosynthesis, remodeling and recycling in *Chlamydia* already in the early stages of cell division. In contrast, the cell division amidase AmiA of organism *E. coli* mediates cell separation in the final stages.

Furthermore, CRISPRi was employed to investigate RodA and NamZ homologs in *Chlamydia*, providing first evidence on the important role of SEDS protein RodA within chlamydial cell division. Knockdown of *namZ* yielded a phenotype alluding to inhibited cell division and indicated that *C. trachomatis* NamZ, the homolog of a exo-β-N-acetylmuramidase in *B. subtilis* is contributing to the interconnected chlamydial PGN metabolism, likely by performing recycling processes. Also overexpression of *rodA* and *namZ* in *C. trachomatis* led to distinct phenotypes with chlamydial development and division processes being severely impaired, emphasizing the impact these enzymes have on *Chlamydia*.

All in all, this work provides new insights into the tightly interlinked processes comprised within the chlamydial PGN metabolism and contributes to the characterization of enzymes involved in PGN ring biosynthesis and degradation and cell division in a genetically streamlined and optimized organism.

References

Aaron, M. *et al.* (2007) 'The tubulin homologue FtsZ contributes to cell elongation by guiding cell wall precursor synthesis in *Caulobacter crescentus*', *Molecular Microbiology*, 64(4), pp. 938–952. Available at: https://doi.org/10.1111/j.1365-2958.2007.05720.x.

Aarsman, M.E.G. *et al.* (2005) 'Maturation of the *Escherichia coli* divisome occurs in two steps', *Molecular Microbiology*, 55(6), pp. 1631–1645. Available at: https://doi.org/10.1111/j.1365-2958.2005.04502.x.

Abdelrahman, Y. *et al.* (2016a) 'Polarized Cell Division of Chlamydia trachomatis', *PLOS Pathogens*, 12(8), p. e1005822. Available at: https://doi.org/10.1371/journal.ppat.1005822.

Abdelrahman, Y. *et al.* (2016b) 'Polarized Cell Division of Chlamydia trachomatis', *PLOS Pathogens*, 12(8), p. e1005822. Available at: https://doi.org/10.1371/journal.ppat.1005822.

Abdelrahman, Y.M. and Belland, R.J. (2005) 'The chlamydial developmental cycle.', *FEMS microbiology reviews*, 29(5), pp. 949–59. Available at: https://doi.org/10.1016/j.femsre.2005.03.002.

AbdelRahman, Y.M. and Belland, R.J. (2005) 'The chlamydial developmental cycle: Figure 1', *FEMS Microbiology Reviews*, 29(5), pp. 949–959. Available at: https://doi.org/10.1016/j.femsre.2005.03.002.

Ajonuma, C.L. *et al.* (2010) 'CFTR is required for cellular entry and internalization of *Chlamydia trachomatis*', *Cell Biology International*, 34(6), pp. 593–600. Available at: https://doi.org/10.1042/CBI20090227.

Akbaba, G.B. (2020) 'Toxicity assessment of zinc sulfate: A commonly used compound', *Toxicology and Industrial Health*, 36(10), pp. 779–787. Available at: https://doi.org/10.1177/0748233720944771.

Akers, J.C. *et al.* (2011) 'Identification and Functional Analysis of CT069 as a Novel Transcriptional Regulator in Chlamydia', *Journal of Bacteriology*, 193(22), pp. 6123–6131. Available at: https://doi.org/10.1128/JB.05976-11.

Allen, J.E. and Stephens, R.S. (1989) 'Identification by sequence analysis of two-site posttranslational processing of the cysteine-rich outer membrane protein 2 of Chlamydia trachomatis serovar L2', *Journal of Bacteriology*, 171(1), pp. 285–291. Available at: https://doi.org/10.1128/jb.171.1.285-291.1989.

Altschul, S.F. *et al.* (1990) 'Basic local alignment search tool', *Journal of Molecular Biology*, 215(3), pp. 403–410. Available at: https://doi.org/10.1016/S0022-2836(05)80360-2.

Alvarez, L. *et al.* (2014) 'Peptidoglycan Remodeling by the Coordinated Action of Multispecific Enzymes', *Microbial Drug Resistance*, 20(3), pp. 190–198. Available at: https://doi.org/10.1089/mdr.2014.0047.

Al-Younes, H.M. *et al.* (2001) 'Low iron availability modulates the course of *Chlamydia pneumoniae* infection', *Cellular Microbiology*, 3(6), pp. 427–437. Available at: https://doi.org/10.1046/j.1462-5822.2001.00125.x.

Ames, G.F., Mimura, C.S. and Shyamala, V. (1990) 'Bacterial periplasmic permeases belong to a family of transport proteins operating from Escherichia coli to human: Traffic ATPases.', *FEMS microbiology reviews*, 6(4), pp. 429–46. Available at: https://doi.org/10.1111/j.1574-6968.1990.tb04110.x.

Andersen, A.A. and Vanrompay, D. (2000) 'Avian chlamydiosis.', *Revue scientifique et technique (International Office of Epizootics)*, 19(2), pp. 396–404.

Angert, E.R. (2005) 'Alternatives to binary fission in bacteria', *Nature Reviews Microbiology*, 3(3), pp. 214–224. Available at: https://doi.org/10.1038/nrmicro1096.

Arbiser, J.L. *et al.* (1998) 'Clioquinol-Zinc Chelate: A Candidate Causative Agent of Subacute Myelo-Optic Neuropathy', *Molecular Medicine*, 4(10), pp. 665–670. Available at: https://doi.org/10.1007/BF03401927.

Arcia Franchini, A.P. *et al.* (2022) 'The Role of Chlamydia Trachomatis in the Pathogenesis of Cervical Cancer', *Cureus* [Preprint]. Available at: https://doi.org/10.7759/cureus.21331.

Ardissone, S. *et al.* (2020) 'Transcriptional Landscape of Waddlia chondrophila Aberrant Bodies Induced by Iron Starvation', *Microorganisms*, 8(12), p. 1848. Available at: https://doi.org/10.3390/microorganisms8121848.

Atwood, C.S. *et al.* (2000) 'Characterization of Copper Interactions with Alzheimer Amyloid β Peptides', *Journal of Neurochemistry*, 75(3), pp. 1219–1233. Available at: https://doi.org/10.1046/j.1471-4159.2000.0751219.x.

Aussel, L. *et al.* (2002) 'FtsK Is a DNA Motor Protein that Activates Chromosome Dimer Resolution by Switching the Catalytic State of the XerC and XerD Recombinases', *Cell*, 108(2), pp. 195–205. Available at: https://doi.org/10.1016/S0092-8674(02)00624-4.

Azumah, R. *et al.* (2016) '*In vitro* evaluation of metal chelators as potential metallo- β -lactamase inhibitors', *Journal of Applied Microbiology*, 120(4), pp. 860–867. Available at: https://doi.org/10.1111/jam.13085.

Balaban, N.Q. *et al.* (2019) 'Definitions and guidelines for research on antibiotic persistence', *Nature Reviews Microbiology*, 17(7), pp. 441–448. Available at: https://doi.org/10.1038/s41579-019-0196-3.

Banerjee, A. and Nelson, D.E. (2019) 'How *Chlamydia trachomatis* conquered gut microbiome-derived antimicrobial compounds and found a new home in the eye', *Proceedings of the National Academy of Sciences*, 116(25), pp. 12136–12138. Available at: https://doi.org/10.1073/pnas.1907647116.

Barbour, A.G. *et al.* (1982a) 'Chlamydia trachomatis has penicillin-binding proteins but not detectable muramic acid', *Journal of Bacteriology*, 151(1), pp. 420–428. Available at: https://doi.org/10.1128/jb.151.1.420-428.1982.

Barbour, A.G. *et al.* (1982b) 'Chlamydia trachomatis has penicillin-binding proteins but not detectable muramic acid', *Journal of Bacteriology*, 151(1), pp. 420–428. Available at: https://doi.org/10.1128/jb.151.1.420-428.1982.

Bareggi, S.R. and Cornelli, U. (2012) 'Clioquinol: Review of its Mechanisms of Action and Clinical Uses in Neurodegenerative Disorders', *CNS Neuroscience & Therapeutics*, 18(1), pp. 41–46. Available at: https://doi.org/10.1111/j.1755-5949.2010.00231.x.

de Barsy, M. and Greub, G. (2013) 'Waddlia chondrophila: from biology to pathogenicity', *Microbes and Infection*, 15(14–15), pp. 1033–1041. Available at: https://doi.org/10.1016/j.micinf.2013.09.010.

Barton, B., Grinnell, A. and Morgenstein, R.M. (2021) 'Disruption of the MreB Elongasome Is Overcome by Mutations in the Tricarboxylic Acid Cycle', *Frontiers in Microbiology*, 12. Available at: https://doi.org/10.3389/fmicb.2021.664281.

Bastidas, R.J. *et al.* (2013) 'Chlamydial Intracellular Survival Strategies', *Cold Spring Harbor Perspectives in Medicine*, 3(5), pp. a010256–a010256. Available at: https://doi.org/10.1101/cshperspect.a010256.

Bateman, A. *et al.* (2023) 'UniProt: the Universal Protein Knowledgebase in 2023', *Nucleic Acids Research*, 51(D1), pp. D523–D531. Available at: https://doi.org/10.1093/nar/gkac1052.

Baud, D. *et al.* (2011) 'Waddlia chondrophila: From Bovine Abortion to Human Miscarriage', *Clinical Infectious Diseases*, 52(12), pp. 1469–1471. Available at: https://doi.org/10.1093/cid/cir205.

Beatty, W.L. *et al.* (1994) 'Tryptophan depletion as a mechanism of gamma interferon-mediated chlamydial persistence', *Infection and Immunity*, 62(9), pp. 3705–3711. Available at: https://doi.org/10.1128/iai.62.9.3705-3711.1994.

Beatty, W.L., Byrne, G.I. and Morrison, R.P. (1993) 'Morphologic and antigenic characterization of interferon gamma-mediated persistent Chlamydia trachomatis infection in vitro.', *Proceedings of the National Academy of Sciences*, 90(9), pp. 3998–4002. Available at: https://doi.org/10.1073/pnas.90.9.3998.

Beatty, W.L., Morrison, R.P. and Byrne, G.I. (1994) 'Persistent chlamydiae: from cell culture to a paradigm for chlamydial pathogenesis.', *Microbiological reviews*, 58(4), pp. 686–99. Available at: https://doi.org/10.1128/mr.58.4.686-699.1994.

Becker, E. and Hegemann, J.H. (2014) 'All subtypes of the Pmp adhesin family are implicated in chlamydial virulence and show species-specific function', *MicrobiologyOpen*, 3(4), pp. 544–556. Available at: https://doi.org/10.1002/mbo3.186.

Bedson, S.P. and Bland, J.O.W. (1932) 'A Morphological Study of Psittacosis Virus, with the Description of a Developmental Cycle', *Br J Exp Pathol*, 13(5), pp. 461–466.

Belland, R.J. *et al.* (2003a) 'Genomic transcriptional profiling of the developmental cycle of *Chlamydia trachomatis*', *Proceedings of the National Academy of Sciences*, 100(14), pp. 8478–8483. Available at: https://doi.org/10.1073/pnas.1331135100.

Belland, R.J. *et al.* (2003b) 'Genomic transcriptional profiling of the developmental cycle of *Chlamydia trachomatis*', *Proceedings of the National Academy of Sciences*, 100(14), pp. 8478–8483. Available at: https://doi.org/10.1073/pnas.1331135100.

Bellmann-Weiler, R. *et al.* (2013) 'Neutrophil gelatinase-associated lipocalin and interleukin-10 regulate intramacrophage Chlamydia pneumoniae replication by modulating intracellular iron homeostasis', *Immunobiology*, 218(7), pp. 969–978. Available at: https://doi.org/10.1016/j.imbio.2012.11.004.

De Benedetti, S. *et al.* (2014) 'Characterization of serine hydroxymethyltransferase GlyA as a potential source of D-alanine in Chlamydia pneumoniae', *Frontiers in Cellular and Infection Microbiology*, 4. Available at: https://doi.org/10.3389/fcimb.2014.00019.

Bernadac, A. *et al.* (1998) '*Escherichia coli tol-pal* Mutants Form Outer Membrane Vesicles', *Journal of Bacteriology*, 180(18), pp. 4872–4878. Available at: https://doi.org/10.1128/JB.180.18.4872-4878.1998.

Bernhardt, T.G. and De Boer, P.A.J. (2003) 'The *Escherichia coli* amidase AmiC is a periplasmic septal ring component exported via the twin-arginine transport pathway', *Molecular Microbiology*, 48(5), pp. 1171–1182. Available at: https://doi.org/10.1046/j.1365-2958.2003.03511.x.

Bernhardt, T.G. and De Boer, P.A.J. (2004) 'Screening for synthetic lethal mutants in *Escherichia coli* and identification of EnvC (YibP) as a periplasmic septal ring factor with murein hydrolase activity', *Molecular Microbiology*, 52(5), pp. 1255–1269. Available at: https://doi.org/10.1111/j.1365-2958.2004.04063.x.

Bernhardt, T.G. and de Boer, P.A.J. (2005) 'SlmA, a Nucleoid-Associated, FtsZ Binding Protein Required for Blocking Septal Ring Assembly over Chromosomes in E. coli', *Molecular Cell*, 18(5), pp. 555–564. Available at: https://doi.org/10.1016/j.molcel.2005.04.012.

Bertani, G. (1951) 'STUDIES ON LYSOGENESIS I', *Journal of Bacteriology*, 62(3), pp. 293–300. Available at: https://doi.org/10.1128/jb.62.3.293-300.1951.

Bertelli, C. *et al.* (2018) 'Reduced Chlorine in Drinking Water Distribution Systems Impacts Bacterial Biodiversity in Biofilms', *Frontiers in Microbiology*, 9. Available at: https://doi.org/10.3389/fmicb.2018.02520.

Bhaya, D., Davison, M. and Barrangou, R. (2011) 'CRISPR-Cas Systems in Bacteria and Archaea: Versatile Small RNAs for Adaptive Defense and Regulation', *Annual Review of Genetics*, 45(1), pp. 273–297. Available at: https://doi.org/10.1146/annurev-genet-110410-132430.

Bi, E. and Lutkenhaus, J. (1993) 'Cell division inhibitors SulA and MinCD prevent formation of the FtsZ ring', *Journal of Bacteriology*, 175(4), pp. 1118–1125. Available at: https://doi.org/10.1128/jb.175.4.1118-1125.1993.

Billaudeau, C. *et al.* (2019) 'MreB Forms Subdiffraction Nanofilaments during Active Growth in Bacillus subtilis', *mBio*, 10(1). Available at: https://doi.org/10.1128/mBio.01879-18.

Binet, R. and Maurelli, A.T. (2009) 'Transformation and isolation of allelic exchange mutants of *Chlamydia psittaci* using recombinant DNA introduced by electroporation', *Proceedings of the National Academy of Sciences*, 106(1), pp. 292–297. Available at: https://doi.org/10.1073/pnas.0806768106.

Bisson-Filho, A.W. *et al.* (2017) 'Treadmilling by FtsZ filaments drives peptidoglycan synthesis and bacterial cell division', *Science*, 355(6326), pp. 739–743. Available at: https://doi.org/10.1126/science.aak9973.

Blanchard, T.J. and Mabey, D.C. (1994) 'Chlamydial infections.', *The British journal of clinical practice*, 48(4), pp. 201–5.

Blasi, F., Tarsia, P. and Aliberti, S. (2009) 'Chlamydophila pneumoniae', *Clinical Microbiology and Infection*, 15(1), pp. 29–35. Available at: https://doi.org/10.1111/j.1469-0691.2008.02130.x.

Block, S.L. *et al.* (1997) 'Chlamydia pneumoniae in acute otitis media', *The Pediatric Infectious Disease Journal*, 16(9), pp. 858–862. Available at: https://doi.org/10.1097/00006454-199709000-00008.

Bonis, M. *et al.* (2010) 'A M23B family metallopeptidase of Helicobacter pylori required for cell shape, pole formation and virulence', *Molecular Microbiology*, 78(4), pp. 809–819. Available at: https://doi.org/10.1111/j.1365-2958.2010.07383.x.

Borel, N. *et al.* (2008) 'Evidence for persistent Chlamydia pneumoniae infection of human coronary atheromas', *Atherosclerosis*, 199(1), pp. 154–161. Available at: https://doi.org/10.1016/j.atherosclerosis.2007.09.026.

Borisova, M. *et al.* (2022) 'NamZ1 and NamZ2 from the Oral Pathogen Tannerella forsythia Are Peptidoglycan Processing Exo-β- *N* -Acetylmuramidases with Distinct Substrate Specificities', *Journal of Bacteriology*, 204(3). Available at: https://doi.org/10.1128/jb.00597-21.

Bourgeade, M.-F. *et al.* (1988) 'Reduction of transferrin receptor expression by interferon γ in a human cell line sensitive to its antiproliferative effect', *Biochemical and Biophysical Research Communications*, 153(3), pp. 897–903. Available at: https://doi.org/10.1016/S0006-291X(88)81312-3.

Bradford, M.M. (1976) 'A rapid and sensitive method for the quantitation of microgram quantities of protein utilizing the principle of protein-dye binding.', *Analytical biochemistry*, 72, pp. 248–54. Available at: https://doi.org/10.1006/abio.1976.9999.

Breinbauer, R. and Köhn, M. (2003) 'Azide–Alkyne Coupling: A Powerful Reaction for Bioconjugate Chemistry', *ChemBioChem*, 4(11), pp. 1147–1149. Available at: https://doi.org/10.1002/cbic.200300705.

Brinkworth, A.J., Wildung, M.R. and Carabeo, R.A. (2018) 'Genomewide Transcriptional Responses of Iron-Starved Chlamydia trachomatis Reveal Prioritization of Metabolic Precursor Synthesis over Protein Translation', *mSystems*, 3(1). Available at: https://doi.org/10.1128/mSystems.00184-17.

Brockett, M.R. and Liechti, G.W. (2021) 'Persistence Alters the Interaction between Chlamydia trachomatis and Its Host Cell', *Infection and Immunity*, 89(8). Available at: https://doi.org/10.1128/IAI.00685-20.

Brul, S. *et al.* (1997) 'The antifungal action of 1,10-o-phenanthroline and EDTA is mediated through zinc chelation and involves cell wall construction', *Food technology and biotechnology*, 35(4), pp. 267–274.

Bublitz, M. *et al.* (2009) 'Structural basis for autoinhibition and activation of Auto, a virulence-associated peptidoglycan hydrolase of *Listeria monocytogenes*', *Molecular Microbiology*, 71(6), pp. 1509–1522. Available at: https://doi.org/10.1111/j.1365-2958.2009.06619.x.

Bush, K. and Bradford, P.A. (2016) 'β-Lactams and β-Lactamase Inhibitors: An Overview', *Cold Spring Harbor Perspectives in Medicine*, 6(8), p. a025247. Available at: https://doi.org/10.1101/cshperspect.a025247.

Carballido-López, R. (2006) 'The Bacterial Actin-Like Cytoskeleton', *Microbiology and Molecular Biology Reviews*, 70(4), pp. 888–909. Available at: https://doi.org/10.1128/MMBR.00014-06.

Carpenter, A.E. *et al.* (2006) 'CellProfiler: image analysis software for identifying and quantifying cell phenotypes.', *Genome biology*, 7(10), p. R100. Available at: https://doi.org/10.1186/gb-2006-7-10-r100.

Cascales, E. *et al.* (2002) 'Pal Lipoprotein of *Escherichia coli* Plays a Major Role in Outer Membrane Integrity', *Journal of Bacteriology*, 184(3), pp. 754–759. Available at: https://doi.org/10.1128/JB.184.3.754-759.2002.

Casson, N. *et al.* (2008) '*Protochlamydia naegleriophila* as Etiologic Agent of Pneumonia', *Emerging Infectious Diseases*, 14(1), pp. 168–172. Available at: https://doi.org/10.3201/eid1401.070980.

Chamaillard, M. *et al.* (2003) 'Nods, Nalps and Naip: intracellular regulators of bacterial-induced inflammation', *Cellular Microbiology*, 5(9), pp. 581–592. Available at: https://doi.org/10.1046/j.1462-5822.2003.00304.x.

Chen, B. *et al.* (2024) 'Cellular zinc metabolism and zinc signaling: from biological functions to diseases and therapeutic targets', *Signal Transduction and Targeted Therapy*, 9(1), p. 6. Available at: https://doi.org/10.1038/s41392-023-01679-y.

Cheng, Q. and Park, J.T. (2002) 'Substrate Specificity of the AmpG Permease Required for Recycling of Cell Wall Anhydro-Muropeptides', *Journal of Bacteriology*, 184(23), pp. 6434–6436. Available at: https://doi.org/10.1128/JB.184.23.6434-6436.2002.

Cherny, R.A. *et al.* (1999) 'Aqueous Dissolution of Alzheimer's Disease Aβ Amyloid Deposits by Biometal Depletion', *Journal of Biological Chemistry*, 274(33), pp. 23223–23228. Available at: https://doi.org/10.1074/jbc.274.33.23223.

Chopra, I. *et al.* (1998) 'Antibiotics, peptidoglycan synthesis and genomics: the chlamydial anomaly revisited', *Microbiology*, 144(10), pp. 2673–2678. Available at: https://doi.org/10.1099/00221287-144-10-2673.

Chung, H.S. *et al.* (2009) 'Rapid β-lactam-induced lysis requires successful assembly of the cell division machinery', *Proceedings of the National Academy of Sciences*, 106(51), pp. 21872–21877. Available at: https://doi.org/10.1073/pnas.0911674106.

Clarke, C.A., Scheurwater, E.M. and Clarke, A.J. (2010) 'The Vertebrate Lysozyme Inhibitor Ivy Functions to Inhibit the Activity of Lytic Transglycosylase', *Journal of Biological Chemistry*, 285(20), pp. 14843–14847. Available at: https://doi.org/10.1074/jbc.C110.120931.

Clausen, J.D. *et al.* (1997) '*Chlamydia trachomatis* utilizes the host cell microtubule network during early events of infection', *Molecular Microbiology*, 25(3), pp. 441–449. Available at: https://doi.org/10.1046/j.1365-2958.1997.4591832.x.

Cohen, M.S. *et al.* (1987) 'Preliminary observations on lactoferrin secretion in human vaginal mucus: Variation during the menstrual cycle, evidence of hormonal regulation, and implications for infection with Neisseria gonorrhoeae', *American Journal of Obstetrics and Gynecology*, 157(5), pp. 1122–1125. Available at: https://doi.org/10.1016/S0002-9378(87)80274-0.

Coles, A. (1993) 'Low-nutrient induction of abnormal chlamydial development: A novel component of chlamydial pathogenesis?', *FEMS Microbiology Letters*, 106(2), pp. 193–200. Available at: https://doi.org/10.1016/0378-1097(93)90080-L.

Collingro, A. *et al.* (2011) 'Unity in Variety--The Pan-Genome of the Chlamydiae', *Molecular Biology and Evolution*, 28(12), pp. 3253–3270. Available at: https://doi.org/10.1093/molbev/msr161.

Collingro, A., Köstlbacher, S. and Horn, M. (2020) 'Chlamydiae in the Environment', *Trends in Microbiology*, 28(11), pp. 877–888. Available at: https://doi.org/10.1016/j.tim.2020.05.020.

Cook, J. *et al.* (2020) 'Insights into bacterial cell division from a structure of EnvC bound to the FtsX periplasmic domain', *Proceedings of the National Academy of Sciences*, 117(45), pp. 28355–28365. Available at: https://doi.org/10.1073/pnas.2017134117.

Cook, J. *et al.* (2023a) 'Activator-induced conformational changes regulate division-associated peptidoglycan amidases', *Proceedings of the National Academy of Sciences*, 120(24). Available at: https://doi.org/10.1073/pnas.2302580120.

Cook, J. *et al.* (2023b) 'Activator-induced conformational changes regulate division-associated peptidoglycan amidases', *Proceedings of the National Academy of Sciences*, 120(24). Available at: https://doi.org/10.1073/pnas.2302580120.

Cook, J.A. (2008) 'Eliminating Blinding Trachoma', *New England Journal of Medicine*, 358(17), pp. 1777–1779. Available at: https://doi.org/10.1056/NEJMp0708546.

Corbin, B.D. *et al.* (2007) 'Interaction between Cell Division Proteins FtsE and FtsZ', *Journal of Bacteriology*, 189(8), pp. 3026–3035. Available at: https://doi.org/10.1128/JB.01581-06.

Corsaro, D. and Venditti, D. (2009) 'Detection of Chlamydiae from freshwater environments by PCR, amoeba coculture and mixed coculture', *Research in Microbiology*, 160(8), pp. 547–552. Available at: https://doi.org/10.1016/j.resmic.2009.08.001.

Cortes, C. *et al.* (2007) '*Chlamydia pneumoniae* Inclusion Membrane Protein Cpn0585 Interacts with Multiple Rab GTPases', *Infection and Immunity*, 75(12), pp. 5586–5596. Available at: https://doi.org/10.1128/IAI.01020-07.

Cox, J. V., Abdelrahman, Y.M. and Ouellette, S.P. (2020) 'Penicillin-binding proteins regulate multiple steps in the polarized cell division process of Chlamydia', *Scientific Reports*, 10(1), p. 12588. Available at: https://doi.org/10.1038/s41598-020-69397-x.

Dahl, U. *et al.* (2004) 'Identification of a Phosphotransferase System of *Escherichia coli* Required for Growth on *N* -Acetylmuramic Acid', *Journal of Bacteriology*, 186(8), pp. 2385–2392. Available at: https://doi.org/10.1128/JB.186.8.2385-2392.2004.

Darville, T. (2005) 'Chlamydia trachomatis infections in neonates and young children.', *Seminars in pediatric infectious diseases*, 16(4), pp. 235–44. Available at: https://doi.org/10.1053/j.spid.2005.06.004.

Deka, S. *et al.* (2006a) 'Chlamydia trachomatis enters a viable but non-cultivable (persistent) state within herpes simplex virus type 2 (HSV-2) co-infected host cells', *Cellular Microbiology*, 8(1), pp. 149–162. Available at: https://doi.org/10.1111/j.1462-5822.2005.00608.x.

Deka, S. *et al.* (2006b) 'Chlamydia trachomatis enters a viable but non-cultivable (persistent) state within herpes simplex virus type 2 (HSV-2) co-infected host cells', *Cellular Microbiology*, 8(1), pp. 149–162. Available at: https://doi.org/10.1111/j.1462-5822.2005.00608.x.

DeMars, R. *et al.* (2007) 'Lateral Gene Transfer In Vitro in the Intracellular Pathogen *Chlamydia trachomatis*', *Journal of Bacteriology*, 189(3), pp. 991–1003. Available at: https://doi.org/10.1128/JB.00845-06.

Dharamshi, J.E. *et al.* (2020) 'Marine Sediments Illuminate Chlamydiae Diversity and Evolution', *Current Biology*, 30(6), pp. 1032-1048.e7. Available at: https://doi.org/10.1016/j.cub.2020.02.016.

Dianov, E.B. *et al.* (2018) 'Synthesis and Structure of Zinc(II) Complexes with 2,2'-Bipyridine', *Russian Journal of General Chemistry*, 88(4), pp. 843–845. Available at: https://doi.org/10.1134/S1070363218040357.

Ding, W.-Q. *et al.* (2005) 'Anticancer Activity of the Antibiotic Clioquinol', *Cancer Research*, 65(8), pp. 3389–3395. Available at: https://doi.org/10.1158/0008-5472.CAN-04-3577.

Donati, M. *et al.* (1999) 'Comparative in-vitro activity of moxifloxacin, minocycline and azithromycin against Chlamydia spp.', *Journal of Antimicrobial Chemotherapy*, 43(6), pp. 825–827. Available at: https://doi.org/10.1093/jac/43.6.825.

Doublet, P. *et al.* (1993) 'The murI gene of Escherichia coli is an essential gene that encodes a glutamate racemase activity', *Journal of Bacteriology*, 175(10), pp. 2970–2979. Available at: https://doi.org/10.1128/jb.175.10.2970-2979.1993.

Dwyer, F. *et al.* (1969) 'The Biological Actions of 1,10-Phenanthroline and 2,2′-Bipyridine Hydrochlorides, Quaternary Salts and Metal Chelates and Related Compounds', *Australian Journal of Experimental Biology and Medical Science*, 47(2), pp. 203–218. Available at: https://doi.org/10.1038/icb.1969.21.

Dzakah, E.E. *et al.* (2022) 'Chlamydia trachomatis Stimulation Enhances HIV-1 Susceptibility through the Modulation of a Member of the Macrophage Inflammatory Proteins', *Journal of Investigative Dermatology*, 142(5), pp. 1338-1348.e6. Available at: https://doi.org/10.1016/j.jid.2021.09.020.

Egan, A.J.F. *et al.* (2015) 'Activities and regulation of peptidoglycan synthases', *Philosophical Transactions of the Royal Society B: Biological Sciences*, 370(1679), p. 20150031. Available at: https://doi.org/10.1098/rstb.2015.0031.

Egan, A.J.F. and Vollmer, W. (2013) 'The physiology of bacterial cell division.', *Annals of the New York Academy of Sciences*, 1277, pp. 8–28. Available at: https://doi.org/10.1111/j.1749-6632.2012.06818.x.

Ehlert, K., Höitje, J.-V. and Templin, M.F. (1995) 'Cloning and expression of a murein hydrolase lipoprotein from Escherichia coli', *Molecular Microbiology*, 16(4), pp. 761–768. Available at: https://doi.org/10.1111/j.1365-2958.1995.tb02437.x.

Ehrlich, P. and Gonder, R. (1913) 'Chemotherapie', *Handbuch der pathogenen Mikroorganismen*, pp. 752–779.

Eizric, D.L. *et al.* (1986) '1, 10 Phenanthroline, a metal chelator, protects against alloxan- but not streptozotocin-induced diabetes', *Journal of Free Radicals in Biology & Medicine*, 2(3), pp. 189–192. Available at: https://doi.org/10.1016/S0748-5514(86)80069-1.

Elwell, C., Mirrashidi, K. and Engel, J. (2016) 'Chlamydia cell biology and pathogenesis', *Nature Reviews Microbiology*, 14(6), pp. 385–400. Available at: https://doi.org/10.1038/nrmicro.2016.30.

Emami, K. *et al.* (2017) 'RodA as the missing glycosyltransferase in Bacillus subtilis and antibiotic discovery for the peptidoglycan polymerase pathway', *Nature Microbiology*, 2(3), p. 16253. Available at: https://doi.org/10.1038/nmicrobiol.2016.253.

Erickson, H.P., Anderson, D.E. and Osawa, M. (2010) 'FtsZ in Bacterial Cytokinesis: Cytoskeleton and Force Generator All in One', *Microbiology and Molecular Biology Reviews*, 74(4), pp. 504–528. Available at: https://doi.org/10.1128/MMBR.00021-10.

Eto, D. *et al.* (2013) 'Divergent effects of desferrioxamine on bacterial growth and characteristics', *The Journal of Antibiotics*, 66(4), pp. 199–203. Available at: https://doi.org/10.1038/ja.2012.111.

Everett, K.D. and Hatch, T.P. (1995) 'Architecture of the cell envelope of Chlamydia psittaci 6BC', *Journal of Bacteriology*, 177(4), pp. 877–882. Available at: https://doi.org/10.1128/jb.177.4.877-882.1995.

Fei, B.-L. *et al.* (2013) 'Two novel copper complexes of 2,2′-bipyridine: Evaluation of the DNA binding and cytotoxic activity', *Journal of Photochemistry and Photobiology B: Biology*, 125, pp. 32–41. Available at: https://doi.org/10.1016/j.jphotobiol.2013.04.011.

Firczuk, M., Mucha, A. and Bochtler, M. (2005) 'Crystal Structures of Active LytM', *Journal of Molecular Biology*, 354(3), pp. 578–590. Available at: https://doi.org/10.1016/j.jmb.2005.09.082.

Flint, A.J. *et al.* (1997) 'Development of "substrate-trapping" mutants to identify physiological substrates of protein tyrosine phosphatases', *Proceedings of the National Academy of Sciences*, 94(5), pp. 1680–1685. Available at: https://doi.org/10.1073/pnas.94.5.1680.

Frandi, A. *et al.* (2014) 'FtsZ-independent septal recruitment and function of cell wall remodelling enzymes in chlamydial pathogens', *Nature Communications*, 5(1), p. 4200. Available at: https://doi.org/10.1038/ncomms5200.

Freedman, J.C. (2012) 'Ionophores in Planar Lipid Bilayers', in *Cell Physiology Source Book*. Elsevier, pp. 61–66. Available at: https://doi.org/10.1016/B978-0-12-387738-3.00004-4.

Gaballah, A. *et al.* (2011) 'Functional analysis of the cytoskeleton protein MreB from Chlamydophila pneumoniae.', *PloS one*, 6(10), p. e25129. Available at: https://doi.org/10.1371/journal.pone.0025129.

Gallo, M.F. *et al.* (2012) 'Bacterial Vaginosis, Gonorrhea, and Chlamydial Infection Among Women Attending a Sexually Transmitted Disease Clinic: A Longitudinal Analysis of Possible Causal Links',

Annals of Epidemiology, 22(3), pp. 213–220. Available at: https://doi.org/10.1016/j.annepidem.2011.11.005.

Gaugué, I. *et al.* (2013) 'The Use of Amino Sugars by Bacillus subtilis: Presence of a Unique Operon for the Catabolism of Glucosamine', *PLoS ONE*, 8(5), p. e63025. Available at: https://doi.org/10.1371/journal.pone.0063025.

Gerding, M.A. *et al.* (2007) 'The *trans* -envelope Tol–Pal complex is part of the cell division machinery and required for proper outer-membrane invagination during cell constriction in *E. coli*', *Molecular Microbiology*, 63(4), pp. 1008–1025. Available at: https://doi.org/10.1111/j.1365-2958.2006.05571.x.

Girardin, Stephen E *et al.* (2003) 'Nod1 detects a unique muropeptide from gram-negative bacterial peptidoglycan.', *Science (New York, N.Y.)*, 300(5625), pp. 1584–7. Available at: https://doi.org/10.1126/science.1084677.

Girardin, Stephen E., Boneca, I.G., Carneiro, L.A.M., *et al.* (2003) 'Nod1 Detects a Unique Muropeptide from Gram-Negative Bacterial Peptidoglycan', *Science*, 300(5625), pp. 1584–1587. Available at: https://doi.org/10.1126/science.1084677.

Girardin, Stephen E., Boneca, I.G., Viala, J., *et al.* (2003) 'Nod2 Is a General Sensor of Peptidoglycan through Muramyl Dipeptide (MDP) Detection', *Journal of Biological Chemistry*, 278(11), pp. 8869–8872. Available at: https://doi.org/10.1074/jbc.C200651200.

Goellner, S. *et al.* (2006) 'Transcriptional Response Patterns of *Chlamydophila psittaci* in Different In Vitro Models of Persistent Infection', *Infection and Immunity*, 74(8), pp. 4801–4808. Available at: https://doi.org/10.1128/IAI.01487-05.

Goffin, C. and Ghuysen, J.-M. (2002) 'Biochemistry and Comparative Genomics of SxxK Superfamily Acyltransferases Offer a Clue to the Mycobacterial Paradox: Presence of Penicillin-Susceptible Target Proteins versus Lack of Efficiency of Penicillin as Therapeutic Agent', *Microbiology and Molecular Biology Reviews*, 66(4), pp. 702–738. Available at: https://doi.org/10.1128/MMBR.66.4.702-738.2002.

Goodell, E.W. and Schwarz, U. (1985) 'Release of cell wall peptides into culture medium by exponentially growing Escherichia coli', *Journal of Bacteriology*, 162(1), pp. 391–397. Available at: https://doi.org/10.1128/jb.162.1.391-397.1985.

Goujon, M. *et al.* (2010) 'A new bioinformatics analysis tools framework at EMBL-EBI.', *Nucleic acids research*, 38(Web Server issue), pp. W695-9. Available at: https://doi.org/10.1093/nar/gkq313.

Greenberg, D. *et al.* (2003) 'High Rate of Simkania negevensis among Canadian Inuit Infants Hospitalized with Lower Respiratory Tract Infections', *Scandinavian Journal of Infectious Diseases*, 35(8), pp. 506–508. Available at: https://doi.org/10.1080/00365540310014648.

Greenberg, G.R. and Wintrobe, M.M. (1946) 'A LABILE IRON POOL', *Journal of Biological Chemistry*, 165(1), pp. 397–398. Available at: https://doi.org/10.1016/S0021-9258(17)41250-6.

Gregory, D.W. and Schaffner, W. (1997) 'Psittacosis.', *Seminars in respiratory infections*, 12(1), pp. 7–11.

Grenga, L. *et al.* (2008) 'The *Escherichia coli* FtsK functional domains involved in its interaction with its divisome protein partners', *FEMS Microbiology Letters*, 287(2), pp. 163–167. Available at: https://doi.org/10.1111/j.1574-6968.2008.01317.x.

Greub, G. *et al.* (2003) '*Parachlamydiaceae* as Rare Agents of Pneumonia', *Emerging Infectious Diseases*, 9(6), pp. 755–756. Available at: https://doi.org/10.3201/eid0906.020613.

Greub, G. (2009) 'Parachlamydia acanthamoebae, an emerging agent of pneumonia', *Clinical Microbiology and Infection*, 15(1), pp. 18–28. Available at: https://doi.org/10.1111/j.1469-0691.2008.02633.x.

Greub, G. and Raoult, D. (2002a) 'Crescent Bodies of *Parachlamydia acanthamoeba* and Its Life Cycle within *Acanthamoeba polyphaga* : an Electron Micrograph Study', *Applied and Environmental Microbiology*, 68(6), pp. 3076–3084. Available at: https://doi.org/10.1128/AEM.68.6.3076-3084.2002.

Greub, G. and Raoult, D. (2002b) '*Parachlamydiaceae*: Potential Emerging Pathogens', *Emerging Infectious Diseases*, 8(6), pp. 626–630. Available at: https://doi.org/10.3201/eid0806.010210.

Grieshaber, S., Swanson, J.A. and Hackstadt, T. (2002) 'Determination of the physical environment within the Chlamydia trachomatis inclusion using ion-selective ratiometric probes', *Cellular Microbiology*, 4(5), pp. 273–283. Available at: https://doi.org/10.1046/j.1462-5822.2002.00191.x.

Grieshaber, S.S. *et al.* (2006) '*Chlamydia trachomatis* Causes Centrosomal Defects Resulting in Chromosomal Segregation Abnormalities', *Traffic*, 7(8), pp. 940–949. Available at: https://doi.org/10.1111/j.1600-0854.2006.00439.x.

Grieshaber, S.S., Grieshaber, N.A. and Hackstadt, T. (2003) '*Chlamydia trachomatis* uses host cell dynein to traffic to the microtubule-organizing center in a p50 dynamitin-independent process', *Journal of Cell Science*, 116(18), pp. 3793–3802. Available at: https://doi.org/10.1242/jcs.00695.

Habtamu, E. *et al.* (2015) 'Trachoma and Relative Poverty: A Case-Control Study', *PLOS Neglected Tropical Diseases*, 9(11), p. e0004228. Available at: https://doi.org/10.1371/journal.pntd.0004228.

Hackstadt, T. (2000) 'Redirection of Host Vesicle Trafficking Pathways by Intracellular Parasites', *Traffic*, 1(2), pp. 93–99. Available at: https://doi.org/10.1034/j.1600-0854.2000.010201.x.

Hackstadt, T., Todd, W.J. and Caldwell, H.D. (1985) 'Disulfide-mediated interactions of the chlamydial major outer membrane protein: role in the differentiation of chlamydiae?', *Journal of Bacteriology*, 161(1), pp. 25–31. Available at: https://doi.org/10.1128/jb.161.1.25-31.1985.

Hakiem, O.R. *et al.* (2023) 'Euo is a developmental regulator that represses late genes and activates midcycle genes in *Chlamydia trachomatis*', *mBio*, 14(5). Available at: https://doi.org/10.1128/mbio.00465-23.

Hale, C.A. (2001) 'Dynamic localization cycle of the cell division regulator MinE in Escherichia coli', *The EMBO Journal*, 20(7), pp. 1563–1572. Available at: https://doi.org/10.1093/emboj/20.7.1563.

Hale, C.A. and de Boer, P.A.J. (2002) 'ZipA Is Required for Recruitment of FtsK, FtsQ, FtsL, and FtsN to the Septal Ring in *Escherichia coli*', *Journal of Bacteriology*, 184(9), pp. 2552–2556. Available at: https://doi.org/10.1128/JB.184.9.2552-2556.2002.

Hanakago, R. and Uono, M. (1981) 'Clioquinol Intoxication Occurring in the Treatment of Acrodermatitis Enteropathica with Reference to SMON Outside of Japan', *Clinical Toxicology*, 18(12), pp. 1427–1434. Available at: https://doi.org/10.3109/15563658108990351.

Hantke, K. and Braun, V. (1973) 'Covalent Binding of Lipid to Protein', *European Journal of Biochemistry*, 34(2), pp. 284–296. Available at: https://doi.org/10.1111/j.1432-1033.1973.tb02757.x.

Hashemi, M. *et al.* (2007) 'Cytotoxic effects of intra and extracellular zinc chelation on human breast cancer cells', *European Journal of Pharmacology*, 557(1), pp. 9–19. Available at: https://doi.org/10.1016/j.ejphar.2006.11.010.

Hatch, T.P. (1996) 'Disulfide cross-linked envelope proteins: the functional equivalent of peptidoglycan in chlamydiae?', *Journal of Bacteriology*, 178(1), pp. 1–5. Available at: https://doi.org/10.1128/jb.178.1.1-5.1996.

Hatch, T.P., Miceli, M. and Sublett, J.E. (1986) 'Synthesis of disulfide-bonded outer membrane proteins during the developmental cycle of Chlamydia psittaci and Chlamydia trachomatis', *Journal of Bacteriology*, 165(2), pp. 379–385. Available at: https://doi.org/10.1128/jb.165.2.379-385.1986.

Heidrich, C., Templin, M.F., Ursinus, A., Merdanovic, M., Berger, J., Schwarz, H., De Pedro, M.A. and Höltje, J. (2001) 'Involvement of *N* -acetylmuramyl- <scp>l</scp> -alanine amidases in cell separation and antibiotic-induced autolysis of *Escherichia coli*', *Molecular Microbiology*, 41(1), pp. 167–178. Available at: https://doi.org/10.1046/j.1365-2958.2001.02499.x.

Heidrich, C., Templin, M.F., Ursinus, A., Merdanovic, M., Berger, J., Schwarz, H., De Pedro, M.A. and Höltje, J.-V. (2001) 'Involvement of N-acetylmuramyl-l-alanine amidases in cell separation and antibiotic-induced autolysis of Escherichia coli', *Molecular Microbiology*, 41(1), pp. 167–178. Available at: https://doi.org/10.1046/j.1365-2958.2001.02499.x.

Heidrich, C., Ursinus, A., Berger, Jürgen, *et al.* (2002) 'Effects of multiple deletions of murein hydrolases on viability, septum cleavage, and sensitivity to large toxic molecules in Escherichia coli.', *Journal of bacteriology*, 184(22), pp. 6093–9. Available at: https://doi.org/10.1128/JB.184.22.6093-6099.2002.

Heidrich, C., Ursinus, A., Berger, Jürgen, *et al.* (2002) 'Effects of Multiple Deletions of Murein Hydrolases on Viability, Septum Cleavage, and Sensitivity to Large Toxic Molecules in *Escherichia coli*', *Journal of Bacteriology*, 184(22), pp. 6093–6099. Available at: https://doi.org/10.1128/JB.184.22.6093-6099.2002.

Heijenoort, J. van (2001) 'Recent advances in the formation of the bacterial peptidoglycan monomer unit (1985 to 2000)', *Natural Product Reports*, 18(5), pp. 503–519. Available at: https://doi.org/10.1039/a804532a.

Henrichfreise, B., Schiefer, A., Schneider, T., Nzukou, E., Poellinger, C., Hoffmann, T., *et al.* (2009) 'Functional conservation of the lipid II biosynthesis pathway in the cell wall-less bacteria *Chlamydia* and *Wolbachia* : why is lipid II needed?', *Molecular Microbiology*, 73(5), pp. 913–923. Available at: https://doi.org/10.1111/j.1365-2958.2009.06815.x.

Henrichfreise, B., Schiefer, A., Schneider, T., Nzukou, E., Poellinger, C., Hoffmann, T.-J., *et al.* (2009) 'Functional conservation of the lipid II biosynthesis pathway in the cell wall-less bacteria Chlamydia and Wolbachia: why is lipid II needed?', *Molecular microbiology*, 73(5), pp. 913–23. Available at: https://doi.org/10.1111/j.1365-2958.2009.06815.x.

Henrichfreise, B., Brunke, M. and Viollier, Patrick H (2016) 'Bacterial Surfaces: The Wall that SEDS Built.', *Current biology : CB*, 26(21), pp. R1158–R1160. Available at: https://doi.org/10.1016/j.cub.2016.09.028.

Henrichfreise, B., Brunke, M. and Viollier, Patrick H. (2016) 'Bacterial Surfaces: The Wall that SEDS Built', *Current Biology*, 26(21), pp. R1158–R1160. Available at: https://doi.org/10.1016/j.cub.2016.09.028.

Hepler, R.W. *et al.* (2018) 'Spectroscopic analysis of chlamydial major outer membrane protein in support of structure elucidation', *Protein Science*, 27(11), pp. 1923–1941. Available at: https://doi.org/10.1002/pro.3501.

Hervé, M. *et al.* (2007) 'Biochemical characterization and physiological properties of Escherichia coli UDP-N-acetylmuramate:L-alanyl-γ-D-glutamyl-meso-diaminopimelate ligase', *Journal of Bacteriology*, 189(11), pp. 3987–3995. Available at: https://doi.org/10.1128/JB.00087-07.

Hesse, L. *et al.* (2003) 'Functional and Biochemical Analysis of *Chlamydia trachomatis* MurC, an Enzyme Displaying UDP- *N* -Acetylmuramate:Amino Acid Ligase Activity', *Journal of Bacteriology*, 185(22), pp. 6507–6512. Available at: https://doi.org/10.1128/JB.185.22.6507-6512.2003.

Heuer, D. *et al.* (2007) 'Tackling the intractable – Approaching the genetics of Chlamydiales', *International Journal of Medical Microbiology*, 297(7–8), pp. 569–576. Available at: https://doi.org/10.1016/j.ijmm.2007.03.011.

Hoang, B.X. *et al.* (2016) 'Zinc as a possible preventive and therapeutic agent in pancreatic, prostate, and breast cancer', *European Journal of Cancer Prevention*, 25(5), pp. 457–461. Available at: https://doi.org/10.1097/CEJ.0000000000000194.

Höltje, J. V *et al.* (1994) 'The negative regulator of beta-lactamase induction AmpD is a N-acetyl-anhydromuramyl-L-alanine amidase.', *FEMS microbiology letters*, 122(1–2), pp. 159–64. Available at: https://doi.org/10.1111/j.1574-6968.1994.tb07159.x.

Höltje, J.-V. (1995) 'From growth to autolysis: the murein hydrolases inEscherichia coli', *Archives of Microbiology*, 164(4), pp. 243–254. Available at: https://doi.org/10.1007/BF02529958.

Holtje, J.-V. and Tuomanen, E.I. (1991) 'The murein hydrolases of Escherichia coli: properties, functions and impact on the course of infections in vivo', *Journal of General Microbiology*, 137(3), pp. 441–454. Available at: https://doi.org/10.1099/00221287-137-3-441.

Honkila, M. *et al.* (2017) 'Probability of vertical transmission of *Chlamydia trachomatis* estimated from national registry data', *Sexually Transmitted Infections*, 93(6), pp. 416–420. Available at: https://doi.org/10.1136/sextrans-2016-052884.

Horn, M. *et al.* (2004) 'Illuminating the Evolutionary History of Chlamydiae', *Science*, 304(5671), pp. 728–730. Available at: https://doi.org/10.1126/science.1096330.

Huang, J., Yang, S. and Zhang, S. (2016) 'Performance and diversity of polyvinyl alcohol-degrading bacteria under aerobic and anaerobic conditions', *Biotechnology Letters*, 38(11), pp. 1875–1880. Available at: https://doi.org/10.1007/s10529-016-2174-4.

Huston, W.M. *et al.* (2008) 'Chlamydia trachomatis responds to heat shock, penicillin induced persistence, and IFN-gamma persistence by altering levels of the extracytoplasmic stress response protease HtrA', *BMC Microbiology*, 8(1), p. 190. Available at: https://doi.org/10.1186/1471-2180-8-190.

Hybiske, K. and Stephens, R.S. (2007) 'Mechanisms of host cell exit by the intracellular bacterium *Chlamydia*', *Proceedings of the National Academy of Sciences*, 104(27), pp. 11430–11435. Available at: https://doi.org/10.1073/pnas.0703218104.

Inohara, N. *et al.* (2003) 'Host Recognition of Bacterial Muramyl Dipeptide Mediated through NOD2', *Journal of Biological Chemistry*, 278(8), pp. 5509–5512. Available at: https://doi.org/10.1074/jbc.C200673200.

Irving, H. and Williams, R.J.P. (1948) 'Order of Stability of Metal Complexes', *Nature*, 162(4123), pp. 746–747. Available at: https://doi.org/10.1038/162746a0.

Jackson, M. *et al.* (1999) 'Epizootiology of Chlamydia infections in two free-range koala populations', *Veterinary Microbiology*, 65(4), pp. 255–264. Available at: https://doi.org/10.1016/S0378-1135(98)00302-2.

Jacobs, A. (1977) 'An Intracellular Transit Iron Pool', in, pp. 91–106. Available at: https://doi.org/10.1002/9780470720325.ch5.

Jacobs, C. *et al.* (1995) 'AmpD, essential for both β-lactamase regulation and cell wall recycling, is a novel cytosolic *N* -acetylmuramyl-L-alanine amidase', *Molecular Microbiology*, 15(3), pp. 553–559. Available at: https://doi.org/10.1111/j.1365-2958.1995.tb02268.x.

Jacquier, N. *et al.* (2014a) 'Cell wall precursors are required to organize the chlamydial division septum', *Nature Communications*, 5(1), p. 3578. Available at: https://doi.org/10.1038/ncomms4578.

Jacquier, N. *et al.* (2014b) 'Cell wall precursors are required to organize the chlamydial division septum', *Nature Communications*, 5(1), p. 3578. Available at: https://doi.org/10.1038/ncomms4578.

Jacquier, N. *et al.* (2015) 'Disassembly of a Medial Transenvelope Structure by Antibiotics during Intracellular Division', *Chemistry & Biology*, 22(9), pp. 1217–1227. Available at: https://doi.org/10.1016/j.chembiol.2015.08.009.

Jacquier, N. *et al.* (2019) 'A SpoIID Homolog Cleaves Glycan Strands at the Chlamydial Division Septum', *mBio*, 10(4). Available at: https://doi.org/10.1128/mBio.01128-19.

Jacquier, N., Viollier, P.H. and Greub, G. (2015) 'The role of peptidoglycan in chlamydial cell division: towards resolving the chlamydial anomaly', *FEMS Microbiology Reviews*, 39(2), pp. 262–275. Available at: https://doi.org/10.1093/femsre/fuv001.

Jaeger, T., Arsic, M. and Mayer, C. (2005) 'Scission of the Lactyl Ether Bond of N-Acetylmuramic Acid by Escherichia coli "Etherase"', *Journal of Biological Chemistry*, 280(34), pp. 30100–30106. Available at: https://doi.org/10.1074/jbc.M502208200.

Jenkin, H.M. (1960) 'Preparation and properties of cell walls of the agent of meningopneumonitis.', *Journal of bacteriology*, 80(5), pp. 639–47. Available at: https://doi.org/10.1128/jb.80.5.639-647.1960.

Jiang, F. and Doudna, J.A. (2017) 'CRISPR–Cas9 Structures and Mechanisms', *Annual Review of Biophysics*, 46(1), pp. 505–529. Available at: https://doi.org/10.1146/annurev-biophys-062215-010822.

Johnson, C.M. and Fisher, D.J. (2013) 'Site-Specific, Insertional Inactivation of incA in Chlamydia trachomatis Using a Group II Intron', *PLoS ONE*, 8(12), p. e83989. Available at: https://doi.org/10.1371/journal.pone.0083989.

Kahane, S. (1993) 'Description and partial characterization of a new chlamydia-like microorganism', *FEMS Microbiology Letters*, 109(2–3), pp. 329–333. Available at: https://doi.org/10.1016/0378-1097(93)90041-Y.

Kahane, S. and Friedman, M.G. (1992) 'Reversibility of heat shock in *Chlamydia trachomatis*', *FEMS Microbiology Letters*, 97(1–2), pp. 25–30. Available at: https://doi.org/10.1111/j.1574-6968.1992.tb05434.x.

Kamneva, O.K. *et al.* (2012) 'Analysis of Genome Content Evolution in PVC Bacterial Super-Phylum: Assessment of Candidate Genes Associated with Cellular Organization and Lifestyle', *Genome Biology and Evolution*, 4(12), pp. 1375–1390. Available at: https://doi.org/10.1093/gbe/evs113.

Kanehisa, M. and Goto, S. (2000) 'KEGG: kyoto encyclopedia of genes and genomes.', *Nucleic acids research*, 28(1), pp. 27–30. Available at: https://doi.org/10.1093/nar/28.1.27.

Kari, L. *et al.* (2011) 'Generation of targeted *Chlamydia trachomatis* null mutants', *Proceedings of the National Academy of Sciences*, 108(17), pp. 7189–7193. Available at: https://doi.org/10.1073/pnas.1102229108.

Kawamura, K. *et al.* (2014) 'Superoxide dismutase as a target of clioquinol-induced neurotoxicity', *Biochemical and Biophysical Research Communications*, 452(1), pp. 181–185. Available at: https://doi.org/10.1016/j.bbrc.2014.04.067.

Kazar, J., Gillmore, J.D. and Gordon, F.B. (1971) 'Effect of Interferon and Interferon Inducers on Infections with a Nonviral Intracellular Microorganism, *Chlamydia trachomatis*', *Infection and Immunity*, 3(6), pp. 825–832. Available at: https://doi.org/10.1128/iai.3.6.825-832.1971.

Kelley, L.A. *et al.* (2015) 'The Phyre2 web portal for protein modeling, prediction and analysis.', *Nature protocols*, 10(6), pp. 845–58. Available at: https://doi.org/10.1038/nprot.2015.053.

Kelver, M.E. *et al.* (1996) 'Estrogen Regulation of Lactoferrin Expression in Human Endometrium', *American Journal of Reproductive Immunology*, 36(5), pp. 243–247. Available at: https://doi.org/10.1111/j.1600-0897.1996.tb00171.x.

Kemege, K.E. *et al.* (2015) '*Chlamydia trachomatis* protein <scp>CT</scp> 009 is a structural and functional homolog to the key morphogenesis component <scp>RodZ</scp> and interacts with division septal plane localized <scp>MreB</scp>', *Molecular Microbiology*, 95(3), pp. 365–382. Available at: https://doi.org/10.1111/mmi.12855.

Khan, R. *et al.* (2020) 'Feasibility of Repurposing Clioquinol for Cancer Therapy', *Recent Patents on Anti-Cancer Drug Discovery*, 15(1), pp. 14–31. Available at: https://doi.org/10.2174/1574892815666200227090259.

Khoshbayan, A. *et al.* (2021) 'The association of Chlamydia pneumoniae infection with atherosclerosis: Review and update of in vitro and animal studies', *Microbial Pathogenesis*, 154, p. 104803. Available at: https://doi.org/10.1016/j.micpath.2021.104803.

Kilah, N.L. and Meggers, E. (2012) 'Sixty Years Young: The Diverse Biological Activities of Metal Polypyridyl Complexes Pioneered by Francis P. Dwyer', *Australian Journal of Chemistry*, 65(9), p. 1325. Available at: https://doi.org/10.1071/CH12275.

Kintner, J. *et al.* (2014) 'Commonly prescribed Î²-lactam antibiotics induce C. trachomatis persistence/stress in culture at physiologically relevant concentrations', *Frontiers in Cellular and Infection Microbiology*, 4. Available at: https://doi.org/10.3389/fcimb.2014.00044.

Kinzel, O. *et al.* (1998) 'The Synthesis and Antibacterial Activity of two Pyoverdin-ampicillin Conjugates, Entering Pseudomonas aeruginosa via the Pyoverdin-mediated Iron Uptake Pathway.', *The Journal of Antibiotics*, 51(5), pp. 499–507. Available at: https://doi.org/10.7164/antibiotics.51.499.

Klöckner, A. *et al.* (2014) 'AmiA is a penicillin target enzyme with dual activity in the intracellular pathogen Chlamydia pneumoniae', *Nature Communications*, 5(1), p. 4201. Available at: https://doi.org/10.1038/ncomms5201.

Klöckner, A. *et al.* (2018) 'Deconstructing the Chlamydial Cell Wall.', *Current topics in microbiology and immunology*, 412, pp. 1–33. Available at: https://doi.org/10.1007/82_2016_34.

Kohlhoff, S.A. and Hammerschlag, M.R. (2015) 'Treatment of chlamydial infections: 2014 update', *Expert Opinion on Pharmacotherapy*, 16(2), pp. 205–212. Available at: https://doi.org/10.1517/14656566.2015.999041.

Kosma, P. (1999) 'Chlamydial lipopolysaccharide', *Biochimica et Biophysica Acta (BBA) - Molecular Basis of Disease*, 1455(2–3), pp. 387–402. Available at: https://doi.org/10.1016/S0925-4439(99)00061-7.

Kozusnik, T., Adams, S.E. and Greub, G. (2024) 'Aberrant Bodies: An Alternative Metabolic Homeostasis Allowing Survivability?', *Microorganisms*, 12(3), p. 495. Available at: https://doi.org/10.3390/microorganisms12030495.

Kraus, W. and Höltje, J. V (1987) 'Two distinct transpeptidation reactions during murein synthesis in Escherichia coli', *Journal of Bacteriology*, 169(7), pp. 3099–3103. Available at: https://doi.org/10.1128/jb.169.7.3099-3103.1987.

Kriedt, C.L. *et al.* (2010) 'Zinc functions as a cytotoxic agent for prostate cancer cells independent of culture and growth conditions.', *Journal of experimental therapeutics & oncology*, 8(4), pp. 287–95.

Kuru, E. *et al.* (2012) 'In Situ Probing of Newly Synthesized Peptidoglycan in Live Bacteria with Fluorescent <scp>D</scp> -Amino Acids', *Angewandte Chemie International Edition*, 51(50), pp. 12519–12523. Available at: https://doi.org/10.1002/anie.201206749.

Lagkouvardos, I. *et al.* (2014) 'Integrating metagenomic and amplicon databases to resolve the phylogenetic and ecological diversity of the Chlamydiae', *The ISME Journal*, 8(1), pp. 115–125. Available at: https://doi.org/10.1038/ismej.2013.142.

Di Lallo, G. *et al.* (2003) 'Use of a two-hybrid assay to study the assembly of a complex multicomponent protein machinery: bacterial septosome differentiation', *Microbiology*, 149(12), pp. 3353–3359. Available at: https://doi.org/10.1099/mic.0.26580-0.

Lambden, P.R., Pickett, M.A. and Clarke, I.N. (2006) 'The effect of penicillin on Chlamydia trachomatis DNA replication', *Microbiology*, 152(9), pp. 2573–2578. Available at: https://doi.org/10.1099/mic.0.29032-0.

LaRue, R.W. *et al.* (2007) 'Chlamydial Hsp60-2 Is Iron Responsive in *Chlamydia trachomatis* Serovar E-Infected Human Endometrial Epithelial Cells In Vitro', *Infection and Immunity*, 75(5), pp. 2374–2380. Available at: https://doi.org/10.1128/IAI.01465-06.

Laskaris, P. *et al.* (2016) 'Administration of Zinc Chelators Improves Survival of Mice Infected with Aspergillus fumigatus both in Monotherapy and in Combination with Caspofungin', *Antimicrobial Agents and Chemotherapy*, 60(10), pp. 5631–5639. Available at: https://doi.org/10.1128/AAC.00324-16.

Last, A. *et al.* (2020) 'Detecting extra-ocular Chlamydia trachomatis in a trachoma-endemic community in Ethiopia: Identifying potential routes of transmission', *PLOS Neglected Tropical Diseases*, 14(3), p. e0008120. Available at: https://doi.org/10.1371/journal.pntd.0008120.

Lee, J., Cox, J. V. and Ouellette, S.P. (2020) 'Critical Role for the Extended N Terminus of Chlamydial MreB in Directing Its Membrane Association and Potential Interaction with Divisome Proteins', *Journal of Bacteriology*, 202(9). Available at: https://doi.org/10.1128/JB.00034-20.

Lee, J.K. *et al.* (2018) 'Replication-dependent size reduction precedes differentiation in Chlamydia trachomatis', *Nature Communications*, 9(1), p. 45. Available at: https://doi.org/10.1038/s41467-017-02432-0.

Lehmann, C.D. (2020) ‘Iron should be restricted in acute infection’, *Frontiers in Bioscience*, 25(4), p. 4827. Available at: https://doi.org/10.2741/4827.

Lenz, J.D. *et al.* (2016) ‘Amidase Activity of AmiC Controls Cell Separation and Stem Peptide Release and Is Enhanced by NlpD in Neisseria gonorrhoeae’, *Journal of Biological Chemistry*, 291(20), pp. 10916–10933. Available at: https://doi.org/10.1074/jbc.M116.715573.

Lepanto, M.S. *et al.* (2019) ‘Lactoferrin in Aseptic and Septic Inflammation’, *Molecules*, 24(7), p. 1323. Available at: https://doi.org/10.3390/molecules24071323.

Li, B. *et al.* (2021) ‘Redox Activity of Noninnocent 2,2′-Bipyridine in Zinc Complexes: An Experimental and Theoretical Study’, *ACS Omega*, 6(28), pp. 18325–18332. Available at: https://doi.org/10.1021/acsomega.1c02201.

Li, Z. *et al.* (2007) ‘The structure of FtsZ filaments in vivo suggests a force-generating role in cell division’, *The EMBO Journal*, 26(22), pp. 4694–4708. Available at: https://doi.org/10.1038/sj.emboj.7601895.

Liechti, G., Kuru, E., Packiam, M., Hsu, Y.-P., Tekkam, S., Hall, E., Rittichier, Jonathan T., *et al.* (2016) ‘Pathogenic Chlamydia Lack a Classical Sacculus but Synthesize a Narrow, Mid-cell Peptidoglycan Ring, Regulated by MreB, for Cell Division’, *PLOS Pathogens*, 12(5), p. e1005590. Available at: https://doi.org/10.1371/journal.ppat.1005590.

Liechti, G., Kuru, E., Packiam, M., Hsu, Y.-P., Tekkam, S., Hall, E., Rittichier, Jonathan T, *et al.* (2016) ‘Pathogenic Chlamydia Lack a Classical Sacculus but Synthesize a Narrow, Mid-cell Peptidoglycan Ring, Regulated by MreB, for Cell Division.’, *PLoS pathogens*, 12(5), p. e1005590. Available at: https://doi.org/10.1371/journal.ppat.1005590.

Liechti, G., Singh, R., Rossi, Patricia L., *et al.* (2018) ‘*Chlamydia trachomatis dapF* Encodes a Bifunctional Enzyme Capable of Both <scp>d</scp> -Glutamate Racemase and Diaminopimelate Epimerase Activities’, *mBio*, 9(2). Available at: https://doi.org/10.1128/mBio.00204-18.

Liechti, G., Singh, R., Rossi, Patricia L, *et al.* (2018) ‘Chlamydia trachomatis dapF Encodes a Bifunctional Enzyme Capable of Both d-Glutamate Racemase and Diaminopimelate Epimerase Activities.’, *mBio*, 9(2). Available at: https://doi.org/10.1128/mBio.00204-18.

Liechti, G. W. *et al.* (2014) ‘A new metabolic cell-wall labelling method reveals peptidoglycan in Chlamydia trachomatis’, *Nature*, 506(7489), pp. 507–510. Available at: https://doi.org/10.1038/nature12892.

Liechti, G W *et al.* (2014) ‘A new metabolic cell-wall labelling method reveals peptidoglycan in Chlamydia trachomatis.’, *Nature*, 506(7489), pp. 507–10. Available at: https://doi.org/10.1038/nature12892.

Liechti, G.W. (2021) ‘Localized Peptidoglycan Biosynthesis in Chlamydia trachomatis Conforms to the Polarized Division and Cell Size Reduction Developmental Models’, *Frontiers in Microbiology*, 12. Available at: https://doi.org/10.3389/fmicb.2021.733850.

Litzinger, S. *et al.* (2010) ‘Muropeptide Rescue in *Bacillus subtilis* Involves Sequential Hydrolysis by β- *N* -Acetylglucosaminidase and *N* -Acetylmuramyl- <scp>l</scp> -Alanine Amidase’, *Journal of Bacteriology*, 192(12), pp. 3132–3143. Available at: https://doi.org/10.1128/JB.01256-09.

Löckener, I. *et al.* (2024) ‘The MraY Inhibitor Muraymycin D2 and Its Derivatives Induce Enlarged Cells in Obligate Intracellular Chlamydia and Wolbachia and Break the Persistence Phenotype in Chlamydia’, *Antibiotics*, 13(5), p. 421. Available at: https://doi.org/10.3390/antibiotics13050421.

Lommatzsch, J. *et al.* (1997) ‘Outer membrane localization of murein hydrolases: MltA, a third lipoprotein lytic transglycosylase in Escherichia coli’, *Journal of Bacteriology*, 179(17), pp. 5465–5470. Available at: https://doi.org/10.1128/jb.179.17.5465-5470.1997.

Luck, A.N. and Mason, A.B. (2012) ‘Transferrin-Mediated Cellular Iron Delivery’, in, pp. 3–35. Available at: https://doi.org/10.1016/B978-0-12-394390-3.00001-X.

Lupoli, T.J. *et al.* (2009) 'Studying a Cell Division Amidase Using Defined Peptidoglycan Substrates', *Journal of the American Chemical Society*, 131(51), pp. 18230–18231. Available at: https://doi.org/10.1021/ja908916z.

Mabey, D.C., Solomon, A.W. and Foster, A. (2003) 'Trachoma', *The Lancet*, 362(9379), pp. 223–229. Available at: https://doi.org/10.1016/S0140-6736(03)13914-1.

Mabonga, E. *et al.* (2021) 'Prevalence and predictors of asymptomatic *Chlamydia trachomatis* and *Neisseria gonorrhoeae* in a Ugandan population most at risk of HIV transmission', *International Journal of STD & AIDS*, 32(6), pp. 510–516. Available at: https://doi.org/10.1177/0956462420979799.

MacKenzie, C.R. *et al.* (1999) 'Inhibition of indoleamine 2,3-dioxygenase in human macrophages inhibits interferon-γ-induced bacteriostasis but does not abrogate toxoplasmastasis', *European Journal of Immunology*, 29(10), pp. 3254–3261. Available at: https://doi.org/10.1002/(SICI)1521-4141(199910)29:10<3254::AID-IMMU3254>3.0.CO;2-0.

MacPherson, S., Larochelle, M. and Turcotte, B. (2006) 'A Fungal Family of Transcriptional Regulators: the Zinc Cluster Proteins', *Microbiology and Molecular Biology Reviews*, 70(3), pp. 583–604. Available at: https://doi.org/10.1128/MMBR.00015-06.

Mao, X. and Schimmer, A. (2008) 'The toxicology of Clioquinol☆', *Toxicology Letters*, 182(1–3), pp. 1–6. Available at: https://doi.org/10.1016/j.toxlet.2008.08.015.

Martell, A.E. and Smith R.M. (1974) *Critical stability constants*. New York: Plenum Press.

Martin-Iguacel, R. *et al.* (2010) 'Lymphogranuloma venereum proctocolitis: a silent endemic disease in men who have sex with men in industrialised countries', *European Journal of Clinical Microbiology & Infectious Diseases*, 29(8), pp. 917–925. Available at: https://doi.org/10.1007/s10096-010-0959-2.

Matsumoto, A. (1973) 'Fine Structures of Cell Envelopes of *Chlamydia* Organisms as Revealed by Freeze-Etching and Negative Staining Techniques', *Journal of Bacteriology*, 116(3), pp. 1355–1363. Available at: https://doi.org/10.1128/jb.116.3.1355-1363.1973.

Matsumoto, A and Manire, G.P. (1970) 'Electron microscopic observations on the effects of penicillin on the morphology of Chlamydia psittaci.', *Journal of bacteriology*, 101(1), pp. 278–85. Available at: https://doi.org/10.1128/jb.101.1.278-285.1970.

Matsumoto, A. and Manire, G.P. (1970) 'Electron Microscopic Observations on the Effects of Penicillin on the Morphology of *Chlamydia psittaci*', *Journal of Bacteriology*, 101(1), pp. 278–285. Available at: https://doi.org/10.1128/jb.101.1.278-285.1970.

Matthiesen, S. *et al.* (2021) 'Wie gut ist das Wissen über sexuell übertragbare Infektionen in Deutschland?', *Bundesgesundheitsblatt - Gesundheitsforschung - Gesundheitsschutz*, 64(11), pp. 1355–1363. Available at: https://doi.org/10.1007/s00103-021-03319-8.

McCann, M. *et al.* (2000) 'Insights Into the Mode of Action of the Anti-Candida Activity of 1,10-Phenanthroline and its Metal Chelates', *Metal-Based Drugs*, 7(4), pp. 185–193. Available at: https://doi.org/10.1155/MBD.2000.185.

McCann, M. *et al.* (2012) 'Deciphering the Antimicrobial Activity of Phenanthroline Chelators', *Current Medicinal Chemistry*, 19(17), pp. 2703–2714. Available at: https://doi.org/10.2174/092986712800609733.

McClarty, G. (1994) 'Chlamydiae and the biochemistry of intracellular parasitism', *Trends in Microbiology*, 2(5), pp. 157–164. Available at: https://doi.org/10.1016/0966-842X(94)90665-3.

McCoy, A.J. *et al.* (2006) '<scp>l</scp> , <scp>l</scp> -diaminopimelate aminotransferase, a trans-kingdom enzyme shared by *Chlamydia* and plants for synthesis of diaminopimelate/lysine', *Proceedings of the National Academy of Sciences*, 103(47), pp. 17909–17914. Available at: https://doi.org/10.1073/pnas.0608643103.

McCoy, A.J. and Maurelli, A.T. (2005) 'Characterization of *Chlamydia* MurC-Ddl, a fusion protein exhibiting D-alanyl-D-alanine ligase activity involved in peptidoglycan synthesis and D-cycloserine

sensitivity', *Molecular Microbiology*, 57(1), pp. 41–52. Available at: https://doi.org/10.1111/j.1365-2958.2005.04661.x.

McCoy, A.J., Sandlin, R.C. and Maurelli, A.T. (2003) 'In Vitro and In Vivo Functional Activity of *Chlamydia* MurA, a UDP- *N* -Acetylglucosamine Enolpyruvyl Transferase Involved in Peptidoglycan Synthesis and Fosfomycin Resistance', *Journal of Bacteriology*, 185(4), pp. 1218–1228. Available at: https://doi.org/10.1128/JB.185.4.1218-1228.2003.

McGuffin, L.J., Bryson, K. and Jones, D.T. (2000) 'The PSIPRED protein structure prediction server.', *Bioinformatics (Oxford, England)*, 16(4), pp. 404–5. Available at: https://doi.org/10.1093/bioinformatics/16.4.404.

Meeske, A.J. *et al.* (2016) 'SEDS proteins are a widespread family of bacterial cell wall polymerases', *Nature*, 537(7622), pp. 634–638. Available at: https://doi.org/10.1038/nature19331.

Mehlitz, A. and Rudel, T. (2013) 'Modulation of host signaling and cellular responses by Chlamydia', *Cell Communication and Signaling*, 11(1), p. 90. Available at: https://doi.org/10.1186/1478-811X-11-90.

Meisner, J. and Moran, C.P. (2011) 'A LytM Domain Dictates the Localization of Proteins to the Mother Cell-Forespore Interface during Bacterial Endospore Formation', *Journal of Bacteriology*, 193(3), pp. 591–598. Available at: https://doi.org/10.1128/JB.01270-10.

Mendivil-Perez, M., Velez-Pardo, C. and Jimenez-Del-Rio, M. (2012) 'TPEN Induces Apoptosis Independently of Zinc Chelator Activity in a Model of Acute Lymphoblastic Leukemia and *Ex Vivo* Acute Leukemia Cells through Oxidative Stress and Mitochondria Caspase-3- and AIF-Dependent Pathways', *Oxidative Medicine and Cellular Longevity*, 2012, pp. 1–14. Available at: https://doi.org/10.1155/2012/313275.

Mengin-Lecreulx, D., van Heijenoort, J. and Park, J.T. (1996) 'Identification of the mpl gene encoding UDP-N-acetylmuramate: L-alanyl-gamma-D-glutamyl-meso-diaminopimelate ligase in Escherichia coli and its role in recycling of cell wall peptidoglycan.', *Journal of bacteriology*, 178(18), pp. 5347–52. Available at: https://doi.org/10.1128/jb.178.18.5347-5352.1996.

Miller, J.D. *et al.* (2009) 'Chlamydia trachomatis YtgA is an iron-binding periplasmic protein induced by iron restriction', *Microbiology*, 155(9), pp. 2884–2894. Available at: https://doi.org/10.1099/mic.0.030247-0.

Mislin, G.L.A. and Schalk, I.J. (2014) 'Siderophore-dependent iron uptake systems as gates for antibiotic Trojan horse strategies against Pseudomonas aeruginosa', *Metallomics*, 6(3), pp. 408–420. Available at: https://doi.org/10.1039/C3MT00359K.

Mitchell, C.M. *et al.* (2010) 'Chlamydia pneumoniae Is Genetically Diverse in Animals and Appears to Have Crossed the Host Barrier to Humans on (At Least) Two Occasions', *PLoS Pathogens*, 6(5), p. e1000903. Available at: https://doi.org/10.1371/journal.ppat.1000903.

Moelleken, K. and Hegemann, J.H. (2008) 'The *Chlamydia* outer membrane protein OmcB is required for adhesion and exhibits biovar-specific differences in glycosaminoglycan binding', *Molecular Microbiology*, 67(2), pp. 403–419. Available at: https://doi.org/10.1111/j.1365-2958.2007.06050.x.

Moore, E.R. and Ouellette, S.P. (2014) 'Reconceptualizing the chlamydial inclusion as a pathogen-specified parasitic organelle: an expanded role for Inc proteins', *Frontiers in Cellular and Infection Microbiology*, 4. Available at: https://doi.org/10.3389/fcimb.2014.00157.

Morgenstein, R.M. *et al.* (2015) 'RodZ links MreB to cell wall synthesis to mediate MreB rotation and robust morphogenesis', *Proceedings of the National Academy of Sciences*, 112(40), pp. 12510–12515. Available at: https://doi.org/10.1073/pnas.1509610112.

Moulder, J.W. (1966) 'The Relation of the Psittacosis Group (Chlamydiae) to Bacteria and Viruses', *Annual Review of Microbiology*, 20(1), pp. 107–130. Available at: https://doi.org/10.1146/annurev.mi.20.100166.000543.

Moulder, J.W. (1968) 'The Life and Death of the Psittacosis Virus', *Hospital Practice*, 3(6), pp. 35–45. Available at: https://doi.org/10.1080/21548331.1968.11706659.

Moulder, J.W. (1983) ‘Inhibition of onset of overt multiplication of Chlamydia psittaci in persistently infected mouse fibroblasts (L cells)’, *Infection and Immunity*, 39(2), pp. 898–907. Available at: https://doi.org/10.1128/iai.39.2.898-907.1983.

Moulder, J.W. (1991) ‘Interaction of chlamydiae and host cells in vitro’, *Microbiological Reviews*, 55(1), pp. 143–190. Available at: https://doi.org/10.1128/mr.55.1.143-190.1991.

Moulder, J.W., Novosel, D.L. and Officer, J.E. (1963) ‘INHIBITION OF THE GROWTH OF AGENTS OF THE PSITTACOSIS GROUP BY <scp>d</scp> -CYCLOSERINE AND ITS SPECIFIC REVERSAL BY <scp>d</scp> -ALANINE’, *Journal of Bacteriology*, 85(3), pp. 707–711. Available at: https://doi.org/10.1128/jb.85.3.707-711.1963.

Moynihan, P.J. and Clarke, A.J. (2011) ‘O-Acetylated peptidoglycan: Controlling the activity of bacterial autolysins and lytic enzymes of innate immune systems’, *The International Journal of Biochemistry & Cell Biology*, 43(12), pp. 1655–1659. Available at: https://doi.org/10.1016/j.biocel.2011.08.007.

Müller, M. *et al.* (2021a) ‘The exo-β-N-acetylmuramidase NamZ from Bacillus subtilis is the founding member of a family of exo-lytic peptidoglycan hexosaminidases’, *Journal of Biological Chemistry*, 296, p. 100519. Available at: https://doi.org/10.1016/j.jbc.2021.100519.

Müller, M. *et al.* (2021b) ‘The exo-β-N-acetylmuramidase NamZ from Bacillus subtilis is the founding member of a family of exo-lytic peptidoglycan hexosaminidases’, *Journal of Biological Chemistry*, 296, p. 100519. Available at: https://doi.org/10.1016/j.jbc.2021.100519.

Mullis, K. *et al.* (1986) ‘Specific enzymatic amplification of DNA in vitro: the polymerase chain reaction.’, *Cold Spring Harbor symposia on quantitative biology*, 51 Pt 1, pp. 263–73. Available at: https://doi.org/10.1101/sqb.1986.051.01.032.

Nelson, D. (2012) *Intracellular Pathogens I*. Edited by M. Tan and P.M. Bavoil. Washington, DC, USA: ASM Press. Available at: https://doi.org/10.1128/9781555817329.

Nguyen, T., Hamby, A. and Massa, S.M. (2005) ‘Clioquinol down-regulates mutant huntingtin expression *in vitro* and mitigates pathology in a Huntington’s disease mouse model’, *Proceedings of the National Academy of Sciences*, 102(33), pp. 11840–11845. Available at: https://doi.org/10.1073/pnas.0502177102.

Nicholson, T.L. *et al.* (2003) ‘Global Stage-Specific Gene Regulation during the Developmental Cycle of *Chlamydia trachomatis*’, *Journal of Bacteriology*, 185(10), pp. 3179–3189. Available at: https://doi.org/10.1128/JB.185.10.3179-3189.2003.

Nisbet, M.L., Hiralal, E. and Poeppelmeier, K.R. (2021) ‘Crystal structures of three copper(II)–2,2′-bipyridine (bpy) compounds, $[Cu(bpy)_2(H_2O)][SiF_6]\cdot 4H_2O$, $[Cu(bpy)_2(TaF_6)_2]$ and $[Cu(bpy)_3][TaF_6]_2$ and a related coordination polymer, $[Cu(bpy)(H_2O)_2SnF_6]_n$’, *Acta Crystallographica Section E Crystallographic Communications*, 77(2), pp. 158–164. Available at: https://doi.org/10.1107/S2056989021000633.

Nygaard, R. *et al.* (2023) ‘Structural basis of peptidoglycan synthesis by E. coli RodA-PBP2 complex’, *Nature Communications*, 14(1), p. 5151. Available at: https://doi.org/10.1038/s41467-023-40483-8.

Ölander, M. and Sixt, B.S. (2022) ‘Bringing genetics to heretofore intractable obligate intracellular bacterial pathogens: Chlamydia and beyond’, *PLOS Pathogens*, 18(7), p. e1010669. Available at: https://doi.org/10.1371/journal.ppat.1010669.

Omsland, A. *et al.* (2014a) ‘Chlamydial metabolism revisited: interspecies metabolic variability and developmental stage-specific physiologic activities’, *FEMS Microbiology Reviews*, 38(4), pp. 779–801. Available at: https://doi.org/10.1111/1574-6976.12059.

Omsland, A. *et al.* (2014b) ‘Chlamydial metabolism revisited: interspecies metabolic variability and developmental stage-specific physiologic activities’, *FEMS Microbiology Reviews*, 38(4), pp. 779–801. Available at: https://doi.org/10.1111/1574-6976.12059.

Otten, C. *et al.* (2015) 'Co-Solvents as Stabilizing Agents during Heterologous Overexpression in Escherichia coli – Application to Chlamydial Penicillin-Binding Protein 6', *PLOS ONE*, 10(4), p. e0122110. Available at: https://doi.org/10.1371/journal.pone.0122110.

Ouellette, S.P. *et al.* (2005) 'The *Chlamydia pneumoniae* Type III Secretion-Related *lcrH* Gene Clusters Are Developmentally Expressed Operons', *Journal of Bacteriology*, 187(22), pp. 7853–7856. Available at: https://doi.org/10.1128/JB.187.22.7853-7856.2005.

Ouellette, S.P. *et al.* (2006) 'Global transcriptional upregulation in the absence of increased translation in *Chlamydia* during IFNγ-mediated host cell tryptophan starvation', *Molecular Microbiology*, 62(5), pp. 1387–1401. Available at: https://doi.org/10.1111/j.1365-2958.2006.05465.x.

Ouellette, S.P. *et al.* (2012) 'Chlamydia co-opts the rod shape-determining proteins MreB and Pbp2 for cell division.', *Molecular microbiology*, 85(1), pp. 164–78. Available at: https://doi.org/10.1111/j.1365-2958.2012.08100.x.

Ouellette, S.P. *et al.* (2018) 'Characterization of Chlamydial Rho and the Role of Rho-Mediated Transcriptional Polarity during Interferon Gamma-Mediated Tryptophan Limitation', *Infection and Immunity*, 86(7). Available at: https://doi.org/10.1128/IAI.00240-18.

Ouellette, S.P. (2018a) 'Feasibility of a Conditional Knockout System for Chlamydia Based on CRISPR Interference.', *Frontiers in cellular and infection microbiology*, 8, p. 59. Available at: https://doi.org/10.3389/fcimb.2018.00059.

Ouellette, S.P. (2018b) 'Feasibility of a Conditional Knockout System for Chlamydia Based on CRISPR Interference.', *Frontiers in cellular and infection microbiology*, 8, p. 59. Available at: https://doi.org/10.3389/fcimb.2018.00059.

Ouellette, S.P. *et al.* (2021a) 'CRISPR Interference To Inducibly Repress Gene Expression in Chlamydia trachomatis', *Infection and Immunity*, 89(7). Available at: https://doi.org/10.1128/IAI.00108-21.

Ouellette, S.P. *et al.* (2021b) 'CRISPR Interference To Inducibly Repress Gene Expression in Chlamydia trachomatis', *Infection and Immunity*, 89(7). Available at: https://doi.org/10.1128/IAI.00108-21.

Ouellette, S.P. *et al.* (2021c) 'CRISPR Interference To Inducibly Repress Gene Expression in Chlamydia trachomatis', *Infection and Immunity*, 89(7). Available at: https://doi.org/10.1128/IAI.00108-21.

Ouellette, S.P. *et al.* (2022) 'Localized cardiolipin synthesis is required for the assembly of MreB during the polarized cell division of Chlamydia trachomatis', *PLOS Pathogens*, 18(9), p. e1010836. Available at: https://doi.org/10.1371/journal.ppat.1010836.

Ouellette, S.P. and Carabeo, R.A. (2010) 'A Functional Slow Recycling Pathway of Transferrin is Required for Growth of Chlamydia', *Frontiers in Microbiology*, 1. Available at: https://doi.org/10.3389/fmicb.2010.00112.

Ouellette, Scot P, Lee, J. and Cox, J. V (2020) 'Division without Binary Fission: Cell Division in the FtsZ-Less Chlamydia.', *Journal of bacteriology*, 202(17). Available at: https://doi.org/10.1128/JB.00252-20.

Ouellette, Scot P., Lee, J. and Cox, J. V. (2020) 'Division without Binary Fission: Cell Division in the FtsZ-Less *Chlamydia*', *Journal of Bacteriology*, 202(17). Available at: https://doi.org/10.1128/JB.00252-20.

Ouellette, S.P., Rueden, K.J. and Rucks, E.A. (2016) 'Tryptophan Codon-Dependent Transcription in Chlamydia pneumoniae during Gamma Interferon-Mediated Tryptophan Limitation', *Infection and Immunity*, 84(9), pp. 2703–2713. Available at: https://doi.org/10.1128/IAI.00377-16.

Paavonen, J. (1999) 'Chlamydia trachomatis: impact on human reproduction', *Human Reproduction Update*, 5(5), pp. 433–447. Available at: https://doi.org/10.1093/humupd/5.5.433.

Packiam, M. *et al.* (2015) 'Structural characterization of muropeptides from *Chlamydia trachomatis* peptidoglycan by mass spectrometry resolves "chlamydial anomaly"', *Proceedings of the National Academy of Sciences*, 112(37), pp. 11660–11665. Available at: https://doi.org/10.1073/pnas.1514026112.

Panzetta, M.E., Valdivia, R.H. and Saka, H.A. (2018a) 'Chlamydia Persistence: A Survival Strategy to Evade Antimicrobial Effects in-vitro and in-vivo', *Frontiers in Microbiology*, 9. Available at: https://doi.org/10.3389/fmicb.2018.03101.

Panzetta, M.E., Valdivia, R.H. and Saka, H.A. (2018b) 'Chlamydia Persistence: A Survival Strategy to Evade Antimicrobial Effects in-vitro and in-vivo', *Frontiers in Microbiology*, 9. Available at: https://doi.org/10.3389/fmicb.2018.03101.

Park, J.T. *et al.* (1998) *MppA, a Periplasmic Binding Protein Essential for Import of the Bacterial Cell Wall Peptide L-Alanyl-D-Glutamyl-meso-Diaminopimelate*, *JOURNAL OF BACTERIOLOGY*.

Park, J.T. and Strominger, J.L. (1957) 'Mode of Action of Penicillin', *Science*, 125(3238), pp. 99–101. Available at: https://doi.org/10.1126/science.125.3238.99.

Park, J.T. and Uehara, T. (2008) 'How Bacteria Consume Their Own Exoskeletons (Turnover and Recycling of Cell Wall Peptidoglycan)', *Microbiology and Molecular Biology Reviews*, 72(2), pp. 211–227. Available at: https://doi.org/10.1128/MMBR.00027-07.

Parquet, M. del C. *et al.* (2019) 'Antibiotic-Resistant *Acinetobacter baumannii* Is Susceptible to the Novel Iron-Sequestering Anti-infective DIBI *In Vitro* and in Experimental Pneumonia in Mice', *Antimicrobial Agents and Chemotherapy*, 63(9). Available at: https://doi.org/10.1128/AAC.00855-19.

Patin, D. *et al.* (2009) 'Functional and Biochemical Analysis of the *Chlamydia trachomatis* Ligase MurE', *Journal of Bacteriology*, 191(24), pp. 7430–7435. Available at: https://doi.org/10.1128/JB.01029-09.

Patin, D. *et al.* (2012) 'Biochemical characterisation of the chlamydial MurF ligase, and possible sequence of the chlamydial peptidoglycan pentapeptide stem', *Archives of Microbiology*, 194(6), pp. 505–512. Available at: https://doi.org/10.1007/s00203-011-0784-8.

Paysan-Lafosse, T. *et al.* (2023) 'InterPro in 2022.', *Nucleic acids research*, 51(D1), pp. D418–D427. Available at: https://doi.org/10.1093/nar/gkac993.

de Pedro, M.A. *et al.* (1997) 'Murein segregation in Escherichia coli', *Journal of Bacteriology*, 179(9), pp. 2823–2834. Available at: https://doi.org/10.1128/jb.179.9.2823-2834.1997.

Perez, D.R., Sklar, L.A. and Chigaev, A. (2019) 'Clioquinol: To harm or heal', *Pharmacology & Therapeutics*, 199, pp. 155–163. Available at: https://doi.org/10.1016/j.pharmthera.2019.03.009.

Pérez-Dorado, I. *et al.* (2010) 'Insights into pneumococcal fratricide from the crystal structures of the modular killing factor LytC', *Nature Structural & Molecular Biology*, 17(5), pp. 576–581. Available at: https://doi.org/10.1038/nsmb.1817.

Perkins, H.R. and Allison, A.C. (1963) 'Cell-wall Constituents of Rickettsiae and Psittacosis-Lymphogranuloma Organisms', *Journal of General Microbiology*, 30(3), pp. 469–480. Available at: https://doi.org/10.1099/00221287-30-3-469.

Peters, N.T., Dinh, T. and Bernhardt, T.G. (2011) 'A Fail-Safe Mechanism in the Septal Ring Assembly Pathway Generated by the Sequential Recruitment of Cell Separation Amidases and Their Activators', *Journal of Bacteriology*, 193(18), pp. 4973–4983. Available at: https://doi.org/10.1128/JB.00316-11.

Pettersen, E.F. *et al.* (2004) 'UCSF Chimera--a visualization system for exploratory research and analysis.', *Journal of computational chemistry*, 25(13), pp. 1605–12. Available at: https://doi.org/10.1002/jcc.20084.

Phillips Campbell, R. *et al.* (2012) 'Chlamydia muridarum enters a viable but non-infectious state in amoxicillin-treated BALB/c mice', *Microbes and Infection*, 14(13), pp. 1177–1185. Available at: https://doi.org/10.1016/j.micinf.2012.07.017.

Piekut, T. *et al.* (2022) 'Infectious agents and Alzheimer's disease', *Journal of Integrative Neuroscience*, 21(2), p. 073. Available at: https://doi.org/10.31083/j.jin2102073.

Pilhofer, M. *et al.* (2013) 'Discovery of chlamydial peptidoglycan reveals bacteria with murein sacculi but without FtsZ', *Nature Communications*, 4(1), p. 2856. Available at: https://doi.org/10.1038/ncomms3856.

Pillonel, T. *et al.* (2019) 'ChlamDB: a comparative genomics database of the phylum Chlamydiae and other members of the Planctomycetes-Verrucomicrobiae-Chlamydiae superphylum', *Nucleic Acids Research* [Preprint]. Available at: https://doi.org/10.1093/nar/gkz924.

Pizzetti, I. *et al.* (2016) 'Chlamydial seasonal dynamics and isolation of " <scp> *C* </scp> *andidatus* <scp>N</scp> eptunochlamydia vexilliferae" from a <scp>T</scp> yrrhenian coastal lake', *Environmental Microbiology*, 18(8), pp. 2405–2417. Available at: https://doi.org/10.1111/1462-2920.13111.

Van der Ploeg, R., Goudelis, S. and Den Blaauwen, T. (2015) 'Validation of FRET Assay for the Screening of Growth Inhibitors of Escherichia coli Reveals Elongasome Assembly Dynamics', *International Journal of Molecular Sciences*, 16(8), pp. 17637–17654. Available at: https://doi.org/10.3390/ijms160817637.

Pokorzynski, N.D. *et al.* (2020) 'The iron-dependent repressor YtgR is a tryptophan-dependent attenuator of the trpRBA operon in Chlamydia trachomatis', *Nature Communications*, 11(1), p. 6430. Available at: https://doi.org/10.1038/s41467-020-20181-5.

Pokorzynski, N.D., Thompson, C.C. and Carabeo, R.A. (2017) 'Ironing Out the Unconventional Mechanisms of Iron Acquisition and Gene Regulation in Chlamydia', *Frontiers in Cellular and Infection Microbiology*, 7. Available at: https://doi.org/10.3389/fcimb.2017.00394.

Potluri, L., de Pedro, M.A. and Young, K.D. (2012) '*Escherichia coli* low-molecular-weight penicillin-binding proteins help orient septal FtsZ, and their absence leads to asymmetric cell division and branching', *Molecular Microbiology*, 84(2), pp. 203–224. Available at: https://doi.org/10.1111/j.1365-2958.2012.08023.x.

von Prowazek, S. and Halberstädter, L. (1907) 'Zur Aetiologie des Trachoms', *DMW - Deutsche Medizinische Wochenschrift*, 33(32), pp. 1285–1287. Available at: https://doi.org/10.1055/s-0029-1188920.

Qi, L.S. *et al.* (2013) 'Repurposing CRISPR as an RNA-Guided Platform for Sequence-Specific Control of Gene Expression', *Cell*, 152(5), pp. 1173–1183. Available at: https://doi.org/10.1016/j.cell.2013.02.022.

Rajeeve, K. *et al.* (2020) 'Reprogramming of host glutamine metabolism during Chlamydia trachomatis infection and its key role in peptidoglycan synthesis', *Nature Microbiology*, 5(11), pp. 1390–1402. Available at: https://doi.org/10.1038/s41564-020-0762-5.

Ranjit, D.K., Liechti, G.W. and Maurelli, A.T. (2020) 'Chlamydial MreB Directs Cell Division and Peptidoglycan Synthesis in Escherichia coli in the Absence of FtsZ Activity', *mBio*, 11(1). Available at: https://doi.org/10.1128/mBio.03222-19.

Raskin, D.M. and de Boer, P.A.J. (1999) 'Rapid pole-to-pole oscillation of a protein required for directing division to the middle of *Escherichia coli*', *Proceedings of the National Academy of Sciences*, 96(9), pp. 4971–4976. Available at: https://doi.org/10.1073/pnas.96.9.4971.

Raulston, J.E. (1997) 'Response of Chlamydia trachomatis serovar E to iron restriction in vitro and evidence for iron-regulated chlamydial proteins', *Infection and Immunity*, 65(11), pp. 4539–4547. Available at: https://doi.org/10.1128/iai.65.11.4539-4547.1997.

Raulston, J.E. *et al.* (2007) 'Identification of an iron-responsive protein that is antigenic in patients with *Chlamydia trachomatis* genital infections', *FEMS Immunology & Medical Microbiology*, 51(3), pp. 569–576. Available at: https://doi.org/10.1111/j.1574-695X.2007.00336.x.

Reuter, J. *et al.* (2023) 'An NlpC/P60 protein catalyzes a key step in peptidoglycan recycling at the intersection of energy recovery, cell division and immune evasion in the intracellular pathogen

Chlamydia trachomatis', *PLOS Pathogens*, 19(2), p. e1011047. Available at: https://doi.org/10.1371/journal.ppat.1011047.

Reyes-Fernández, E.Z. and Schuldiner, S. (2020) 'Acidification of Cytoplasm in Escherichia coli Provides a Strategy to Cope with Stress and Facilitates Development of Antibiotic Resistance', *Scientific Reports*, 10(1), p. 9954. Available at: https://doi.org/10.1038/s41598-020-66890-1.

Ribeiro, M., Sousa, C.A. and Simões, M. (2022) 'Harnessing microbial iron chelators to develop innovative therapeutic agents', *Journal of Advanced Research*, 39, pp. 89–101. Available at: https://doi.org/10.1016/j.jare.2021.10.010.

Richmond, S.J., Hilton, A.L. and Clarke, S.K. (1972) 'Chlamydial infection. Role of Chlamydia subgroup A in non-gonococcal and post-gonococcal urethritis.', *Sexually Transmitted Infections*, 48(6), pp. 437–444. Available at: https://doi.org/10.1136/sti.48.6.437.

Rick, P.D. *et al.* (1998) 'Characterization of the lipid-carrier involved in the synthesis of enterobacterial common antigen (ECA) and identification of a novel phosphoglyceride in a mutant of Salmonella typhimurium defective in ECA synthesis.', *Glycobiology*, 8(6), pp. 557–67. Available at: https://doi.org/10.1093/glycob/8.6.557.

Riffaud, C.M., Rucks, E.A. and Ouellette, S.P. (2023a) 'Persistence of obligate intracellular pathogens: alternative strategies to overcome host-specific stresses', *Frontiers in Cellular and Infection Microbiology*, 13. Available at: https://doi.org/10.3389/fcimb.2023.1185571.

Riffaud, C.M., Rucks, E.A. and Ouellette, S.P. (2023b) 'Tryptophan Availability during Persistence of Chlamydia trachomatis Directly Impacts Expression of Chlamydial Cell Division Proteins', *Infection and Immunity*, 91(2). Available at: https://doi.org/10.1128/iai.00513-22.

Rocaboy, M. *et al.* (2013) 'The crystal structure of the cell division amidase <scp>AmiC</scp> reveals the fold of the <scp>AMIN</scp> domain, a new peptidoglycan binding domain', *Molecular Microbiology*, 90(2), pp. 267–277. Available at: https://doi.org/10.1111/mmi.12361.

Romeo, A.M. *et al.* (2001) 'Intracellular Chelation of Iron by Bipyridyl Inhibits DNA Virus Replication', *Journal of Biological Chemistry*, 276(26), pp. 24301–24308. Available at: https://doi.org/10.1074/jbc.M010806200.

Rosario, C.J., Hanson, B.R. and Tan, M. (2014) 'The transcriptional repressor <scp>EUO</scp> regulates both subsets of <scp> *C* </scp> *hlamydia* late genes', *Molecular Microbiology*, 94(4), pp. 888–897. Available at: https://doi.org/10.1111/mmi.12804.

Rovero, A., Kebbi-Beghdadi, C. and Greub, G. (2023) 'Spontaneous Aberrant Bodies Formation in Human Pneumocytes Infected with Estrella lausannensis', *Microorganisms*, 11(10), p. 2368. Available at: https://doi.org/10.3390/microorganisms11102368.

Rzomp, K.A. *et al.* (2003) 'Rab GTPases Are Recruited to Chlamydial Inclusions in Both a Species-Dependent and Species-Independent Manner', *Infection and Immunity*, 71(10), pp. 5855–5870. Available at: https://doi.org/10.1128/IAI.71.10.5855-5870.2003.

Rzomp, K.A., Moorhead, A.R. and Scidmore, M.A. (2006) 'The GTPase Rab4 Interacts with *Chlamydia trachomatis* Inclusion Membrane Protein CT229', *Infection and Immunity*, 74(9), pp. 5362–5373. Available at: https://doi.org/10.1128/IAI.00539-06.

Saka, H.A. *et al.* (2011) 'Quantitative proteomics reveals metabolic and pathogenic properties of *Chlamydia trachomatis* developmental forms', *Molecular Microbiology*, 82(5), pp. 1185–1203. Available at: https://doi.org/10.1111/j.1365-2958.2011.07877.x.

Salesa, B., Sabater i Serra, R. and Serrano-Aroca, Á. (2021) 'Zinc Chloride: Time-Dependent Cytotoxicity, Proliferation and Promotion of Glycoprotein Synthesis and Antioxidant Gene Expression in Human Keratinocytes', *Biology*, 10(11), p. 1072. Available at: https://doi.org/10.3390/biology10111072.

Scaioli, E. *et al.* (2019) 'Simkania negevensis in Crohn's Disease', *Digestive Diseases and Sciences*, 64(11), pp. 3284–3290. Available at: https://doi.org/10.1007/s10620-019-05632-4.

Scherler, A. *et al.* (2020) 'Diverse Stress-Inducing Treatments cause Distinct Aberrant Body Morphologies in the Chlamydia-Related Bacterium, Waddlia chondrophila', *Microorganisms*, 8(1), p. 89. Available at: https://doi.org/10.3390/microorganisms8010089.

Schleifer, K.H. and Kandler, O. (1972) 'Peptidoglycan types of bacterial cell walls and their taxonomic implications', *Bacteriological Reviews*, 36(4), pp. 407–477. Available at: https://doi.org/10.1128/br.36.4.407-477.1972.

Schmidt, D.M.Z., Hubbard, B.K. and Gerlt, J.A. (2001) 'Evolution of Enzymatic Activities in the Enolase Superfamily: Functional Assignment of Unknown Proteins in *Bacillus subtilis* and *Escherichia coli* as <scp>l</scp> -Ala- <scp>d</scp> / <scp>l</scp> -Glu Epimerases', *Biochemistry*, 40(51), pp. 15707–15715. Available at: https://doi.org/10.1021/bi011640x.

Schmidt, K.L. *et al.* (2004) 'A Predicted ABC Transporter, FtsEX, Is Needed for Cell Division in *Escherichia coli*', *Journal of Bacteriology*, 186(3), pp. 785–793. Available at: https://doi.org/10.1128/JB.186.3.785-793.2004.

Scholz, F. and Kahlert, H. (2019) *Chemical Equilibria in Analytical Chemistry*. Cham: Springer International Publishing. Available at: https://doi.org/10.1007/978-3-030-17180-3.

Schramm, N., Bagnell, C.R. and Wyrick, P.B. (1996) 'Vesicles containing Chlamydia trachomatis serovar L2 remain above pH 6 within HEC-1B cells', *Infection and Immunity*, 64(4), pp. 1208–1214. Available at: https://doi.org/10.1128/iai.64.4.1208-1214.1996.

Schroeder, U. *et al.* (1994) 'Peptidase D of *Escherichia coli* K-12, a metallopeptidase of low substrate specificity', *FEMS Microbiology Letters*, 123(1–2), pp. 153–159. Available at: https://doi.org/10.1111/j.1574-6968.1994.tb07215.x.

Schwarz, U., Asmus, A. and Frank, H. (1969) 'Autolytic enzymes and cell division of Escherichia coli', *Journal of Molecular Biology*, 41(3), pp. 419–429. Available at: https://doi.org/10.1016/0022-2836(69)90285-X.

Scott, C. *et al.* (2021) 'Iron Chelation in Local Infection', *Molecules*, 26(1), p. 189. Available at: https://doi.org/10.3390/molecules26010189.

Seo, B.-R. *et al.* (2015) 'The zinc ionophore clioquinol reverses autophagy arrest in chloroquine-treated ARPE-19 cells and in APP/mutant presenilin-1–transfected Chinese hamster ovary cells', *Neurobiology of Aging*, 36(12), pp. 3228–3238. Available at: https://doi.org/10.1016/j.neurobiolaging.2015.09.006.

Serkebaeva, Y.M. *et al.* (2013) 'Pyrosequencing-Based Assessment of the Bacteria Diversity in Surface and Subsurface Peat Layers of a Northern Wetland, with Focus on Poorly Studied Phyla and Candidate Divisions', *PLoS ONE*, 8(5), p. e63994. Available at: https://doi.org/10.1371/journal.pone.0063994.

Sham, L.-T. *et al.* (2014) 'MurJ is the flippase of lipid-linked precursors for peptidoglycan biogenesis', *Science*, 345(6193), pp. 220–222. Available at: https://doi.org/10.1126/science.1254522.

Shaw, E.I. *et al.* (2000) 'Three temporal classes of gene expression during the *Chlamydia trachomatis* developmental cycle', *Molecular Microbiology*, 37(4), pp. 913–925. Available at: https://doi.org/10.1046/j.1365-2958.2000.02057.x.

Shima, K. *et al.* (2018) 'The Genetic Transformation of Chlamydia pneumoniae', *mSphere*, 3(5). Available at: https://doi.org/10.1128/mSphere.00412-18.

Shima, K. *et al.* (2021) 'Regulation of the Mitochondrion-Fatty Acid Axis for the Metabolic Reprogramming of Chlamydia trachomatis during Treatment with β-Lactam Antimicrobials', *mBio*, 12(2). Available at: https://doi.org/10.1128/mBio.00023-21.

Shima, K., Kuhlenbäumer, G. and Rupp, J. (2010) 'Chlamydia pneumoniae infection and Alzheimer's disease: a connection to remember?', *Medical Microbiology and Immunology*, 199(4), pp. 283–289. Available at: https://doi.org/10.1007/s00430-010-0162-1.

Shockman, G.D. *et al.* (1996) 'Bacterial Walls, Peptidoglycan Hydrolases, Autolysins, and Autolysis', *Microbial Drug Resistance*, 2(1), pp. 95–98. Available at: https://doi.org/10.1089/mdr.1996.2.95.

Shockman, G.D. and Höltje, J.-V. (1994) ‘Chapter 7 Microbial peptidoglycan (murein) hydrolases’, in, pp. 131–166. Available at: https://doi.org/10.1016/S0167-7306(08)60410-X.

Shostak, K. and Schirch, V. (1988) ‘Serine hydroxymethyltransferase: mechanism of the racemization and transamination of D- and L-alanine’, *Biochemistry*, 27(21), pp. 8007–8014. Available at: https://doi.org/10.1021/bi00421a006.

Sieger, B. *et al.* (2013) ‘The lipid <scp>II</scp> flippase <scp>RodA</scp> determines morphology and growth in *<scp>C</scp> orynebacterium glutamicum* ’, *Molecular Microbiology*, 90(5), pp. 966–982. Available at: https://doi.org/10.1111/mmi.12411.

Siegrist, M.S. *et al.* (2013) ‘<scp>d</scp> -Amino Acid Chemical Reporters Reveal Peptidoglycan Dynamics of an Intracellular Pathogen’, *ACS Chemical Biology*, 8(3), pp. 500–505. Available at: https://doi.org/10.1021/cb3004995.

Sievers, F. *et al.* (2011) ‘Fast, scalable generation of high-quality protein multiple sequence alignments using Clustal Omega.’, *Molecular systems biology*, 7, p. 539. Available at: https://doi.org/10.1038/msb.2011.75.

Simpson, B.W. *et al.* (2024) ‘*Escherichia coli* CadB is capable of promiscuously transporting muropeptides and contributing to peptidoglycan recycling’, *Journal of Bacteriology*, 206(1). Available at: https://doi.org/10.1128/jb.00369-23.

Simunek, T. *et al.* (2005) ‘SIH—a novel lipophilic iron chelator—protects H9c2 cardiomyoblasts from oxidative stress-induced mitochondrial injury and cell death’, *Journal of Molecular and Cellular Cardiology*, 39(2), pp. 345–354. Available at: https://doi.org/10.1016/j.yjmcc.2005.05.008.

Singh, R., Liechti, G., *et al.* (2020) ‘Chlamydia trachomatis Oligopeptide Transporter Performs Dual Functions of Oligopeptide Transport and Peptidoglycan Recycling’, *Infection and Immunity*, 88(5). Available at: https://doi.org/10.1128/IAI.00086-20.

Singh, R., Slade, J.A., *et al.* (2020) ‘Competing Substrates for the Bifunctional Diaminopimelic Acid Epimerase/Glutamate Racemase Modulate Peptidoglycan Synthesis in Chlamydia trachomatis’, *Infection and Immunity*, 89(1). Available at: https://doi.org/10.1128/IAI.00401-20.

Singh, S.K. *et al.* (2012) ‘Three redundant murein endopeptidases catalyse an essential cleavage step in peptidoglycan synthesis of *<scp>E</scp> scherichia coli* <scp>K</scp> 12’, *Molecular Microbiology*, 86(5), pp. 1036–1051. Available at: https://doi.org/10.1111/mmi.12058.

Skilton, R.J. *et al.* (2009) ‘Penicillin Induced Persistence in Chlamydia trachomatis: High Quality Time Lapse Video Analysis of the Developmental Cycle’, *PLoS ONE*, 4(11), p. e7723. Available at: https://doi.org/10.1371/journal.pone.0007723.

Slade, J.A. *et al.* (2019) ‘Fosmidomycin, an inhibitor of isoprenoid synthesis, induces persistence in Chlamydia by inhibiting peptidoglycan assembly’, *PLOS Pathogens*, 15(10), p. e1008078. Available at: https://doi.org/10.1371/journal.ppat.1008078.

Solomon, A.W. *et al.* (2022) ‘Trachoma’, *Nature Reviews Disease Primers*, 8(1), p. 32. Available at: https://doi.org/10.1038/s41572-022-00359-5.

Sonke, T. *et al.* (2005) ‘<scp>l</scp> -Selective Amidase with Extremely Broad Substrate Specificity from *Ochrobactrum anthropi* NCIMB 40321’, *Applied and Environmental Microbiology*, 71(12), pp. 7961–7973. Available at: https://doi.org/10.1128/AEM.71.12.7961-7973.2005.

de Souza, R.F. *et al.* (2008a) ‘AMIN domains have a predicted role in localization of diverse periplasmic protein complexes’, *Bioinformatics*, 24(21), pp. 2423–2426. Available at: https://doi.org/10.1093/bioinformatics/btn449.

de Souza, R.F. *et al.* (2008b) ‘AMIN domains have a predicted role in localization of diverse periplasmic protein complexes’, *Bioinformatics*, 24(21), pp. 2423–2426. Available at: https://doi.org/10.1093/bioinformatics/btn449.

Spratt, B.G. (1977) ‘The mechanism of action of mecillinam’, *Journal of Antimicrobial Chemotherapy*, 3(suppl B), pp. 13–19. Available at: https://doi.org/10.1093/jac/3.suppl_B.13.

Sriramam, K. (1972) ‘Some new applications of ferroin as redox indicator in titrations with dichromate’, *Talanta*, 19(11), pp. 1445–1448. Available at: https://doi.org/10.1016/0039-9140(72)80140-1.

Stephens, R.S. *et al.* (1998a) ‘Genome Sequence of an Obligate Intracellular Pathogen of Humans: *Chlamydia trachomatis*’, *Science*, 282(5389), pp. 754–759. Available at: https://doi.org/10.1126/science.282.5389.754.

Stephens, R.S. *et al.* (1998b) ‘Genome Sequence of an Obligate Intracellular Pathogen of Humans: *Chlamydia trachomatis*’, *Science*, 282(5389), pp. 754–759. Available at: https://doi.org/10.1126/science.282.5389.754.

Studier, F.W. (2005) ‘Protein production by auto-induction in high density shaking cultures.’, *Protein expression and purification*, 41(1), pp. 207–234. Available at: https://doi.org/10.1016/j.pep.2005.01.016.

Su, H. *et al.* (1996) ‘A recombinant Chlamydia trachomatis major outer membrane protein binds to heparan sulfate receptors on epithelial cells.’, *Proceedings of the National Academy of Sciences*, 93(20), pp. 11143–11148. Available at: https://doi.org/10.1073/pnas.93.20.11143.

Subtil, A., Collingro, A. and Horn, M. (2014) ‘Tracing the primordial Chlamydiae: extinct parasites of plants?’, *Trends in Plant Science*, 19(1), pp. 36–43. Available at: https://doi.org/10.1016/j.tplants.2013.10.005.

Suchland, R.J., Geisler, W.M. and Stamm, W.E. (2003) ‘Methodologies and Cell Lines Used for Antimicrobial Susceptibility Testing of *Chlamydia* spp’, *Antimicrobial Agents and Chemotherapy*, 47(2), pp. 636–642. Available at: https://doi.org/10.1128/AAC.47.2.636-642.2003.

Swoboda, A.R. *et al.* (2023) ‘The Periplasmic Tail-Specific Protease, Tsp, Is Essential for Secondary Differentiation in *Chlamydia trachomatis*’, *Journal of Bacteriology*, 205(5). Available at: https://doi.org/10.1128/jb.00099-23.

Taguchi, A. *et al.* (2019) ‘FtsW is a peptidoglycan polymerase that is functional only in complex with its cognate penicillin-binding protein’, *Nature Microbiology*, 4(4), pp. 587–594. Available at: https://doi.org/10.1038/s41564-018-0345-x.

Tartoff, K.D. and Hobbs, C.A. (1987) ‘Improved Media for Growing Plasmid and Cosmid Clones’, *Bethesda Research Laboratories Focus*, 9(12).

Tatar, L.D. *et al.* (2007) ‘An Escherichia coli undecaprenyl-pyrophosphate phosphatase implicated in undecaprenyl phosphate recycling’, *Microbiology*, 153(8), pp. 2518–2529. Available at: https://doi.org/10.1099/mic.0.2007/006312-0.

Taylor, B.D. and Haggerty, C.L. (2011) ‘Management of Chlamydia trachomatis genital tract infection: screening and treatment challenges.’, *Infection and drug resistance*, 4, pp. 19–29. Available at: https://doi.org/10.2147/IDR.S12715.

Taylor, H.R. (2009) ‘Doyne Lecture: trachoma, is it history?’, *Eye*, 23(11), pp. 2007–2022. Available at: https://doi.org/10.1038/eye.2008.432.

Taylor-Brown, A. *et al.* (2015) ‘Twenty years of research into Chlamydia-like organisms: a revolution in our understanding of the biology and pathogenicity of members of the phylum Chlamydiae’, *Pathogens and Disease*, 73(1), pp. 1–15. Available at: https://doi.org/10.1093/femspd/ftu009.

Teil, M. *et al.* (2022) ‘The Zinc Ionophore Clioquinol Reduces Parkinson’s Disease Patient-Derived Brain Extracts-Induced Neurodegeneration.’, *Molecular neurobiology*, 59(10), pp. 6245–6259. Available at: https://doi.org/10.1007/s12035-022-02974-5.

Terns, M.P. and Terns, R.M. (2011) ‘CRISPR-based adaptive immune systems’, *Current Opinion in Microbiology*, 14(3), pp. 321–327. Available at: https://doi.org/10.1016/j.mib.2011.03.005.

Thao, M.L. *et al.* (2003) ‘Phylogenetic Evidence for Two New Insect-Associated Chlamydia of the Family Simkaniaceae’, *Current Microbiology*, 47(1), pp. 46–50. Available at: https://doi.org/10.1007/s00284-002-3953-9.

Thompson, C.C. *et al.* (2012) 'Cleavage of a putative metal permease in *Chlamydia trachomatis* yields an iron-dependent transcriptional repressor', *Proceedings of the National Academy of Sciences*, 109(26), pp. 10546–10551. Available at: https://doi.org/10.1073/pnas.1201398109.

Thompson, C.C. and Carabeo, R.A. (2011) 'An Optimal Method of Iron Starvation of the Obligate Intracellular Pathogen, Chlamydia Trachomatis', *Frontiers in Microbiology*, 2. Available at: https://doi.org/10.3389/fmicb.2011.00020.

Timms, P. *et al.* (2009) 'Differential transcriptional responses between the interferon-gamma-induction and iron-limitation models of persistence for Chlamydia pneumoniae.', *Journal of microbiology, immunology, and infection = Wei mian yu gan ran za zhi*, 42(1), pp. 27–37.

Tomioka, S. *et al.* (1983) 'Mutation of the N-acetylmuramyl-L-alanine amidase gene of Escherichia coli K-12', *Journal of Bacteriology*, 156(1), pp. 463–465. Available at: https://doi.org/10.1128/jb.156.1.463-465.1983.

Tschachler, E. *et al.* (2007) 'Streptococcal infections of the skin and mucous membranes', *Journal der Deutschen Dermatologischen Gesellschaft*, 6(5), pp. 527–532.

Uehara, T. *et al.* (2005) 'Recycling of the anhydro-N-acetylmuramic acid derived from cell wall murein involves a two-step conversion to N-acetylglucosamine-phosphate.', *Journal of bacteriology*, 187(11), pp. 3643–9. Available at: https://doi.org/10.1128/JB.187.11.3643-3649.2005.

Uehara, T. *et al.* (2006) 'MurQ Etherase Is Required by *Escherichia coli* in Order To Metabolize Anhydro- *N* -Acetylmuramic Acid Obtained either from the Environment or from Its Own Cell Wall', *Journal of Bacteriology*, 188(4), pp. 1660–1662. Available at: https://doi.org/10.1128/JB.188.4.1660-1662.2006.

Uehara, T. *et al.* (2010) 'Daughter cell separation is controlled by cytokinetic ring-activated cell wall hydrolysis', *The EMBO Journal*, 29(8), pp. 1412–1422. Available at: https://doi.org/10.1038/emboj.2010.36.

Uehara, T., Dinh, T. and Bernhardt, T.G. (2009) 'LytM-Domain Factors Are Required for Daughter Cell Separation and Rapid Ampicillin-Induced Lysis in *Escherichia coli*', *Journal of Bacteriology*, 191(16), pp. 5094–5107. Available at: https://doi.org/10.1128/JB.00505-09.

Uehara, T. and Park, J.T. (2004) 'The N-acetyl-D-glucosamine kinase of Escherichia coli and its role in murein recycling.', *Journal of bacteriology*, 186(21), pp. 7273–9. Available at: https://doi.org/10.1128/JB.186.21.7273-7279.2004.

Uehara, T. and Park, James T. (2007) 'An Anhydro- *N* -Acetylmuramyl- <scp>l</scp> -Alanine Amidase with Broad Specificity Tethered to the Outer Membrane of *Escherichia coli*', *Journal of Bacteriology*, 189(15), pp. 5634–5641. Available at: https://doi.org/10.1128/JB.00446-07.

Uehara, T. and Park, James T (2007) 'An anhydro-N-acetylmuramyl-L-alanine amidase with broad specificity tethered to the outer membrane of Escherichia coli.', *Journal of bacteriology*, 189(15), pp. 5634–41. Available at: https://doi.org/10.1128/JB.00446-07.

Ursinus, A., Steinhaus, H. and Höltje, J. V (1992) 'Purification of a nocardicin A-sensitive LD-carboxypeptidase from Escherichia coli by affinity chromatography', *Journal of Bacteriology*, 174(2), pp. 441–446. Available at: https://doi.org/10.1128/jb.174.2.441-446.1992.

Vallee, B.L. *et al.* (1960) 'The Role of Zinc in Carboxypeptidase', *Journal of Biological Chemistry*, 235(1), pp. 64–69. Available at: https://doi.org/10.1016/S0021-9258(18)69586-9.

Vallee, B.L. and Neurath, H. (1955) 'Carboxypeptidase, a zinc metalloenzyme.', *The Journal of biological chemistry*, 217(1), pp. 253–61.

Vermylen, C. (2008) 'What is new in iron overload?', *European Journal of Pediatrics*, 167(4), pp. 377–381. Available at: https://doi.org/10.1007/s00431-007-0604-y.

Vollmer, W. *et al.* (2008a) 'Bacterial peptidoglycan (murein) hydrolases', *FEMS Microbiology Reviews*, 32(2), pp. 259–286. Available at: https://doi.org/10.1111/j.1574-6976.2007.00099.x.

Vollmer, W. *et al.* (2008b) 'Bacterial peptidoglycan (murein) hydrolases', *FEMS Microbiology Reviews*, 32(2), pp. 259–286. Available at: https://doi.org/10.1111/j.1574-6976.2007.00099.x.

Vollmer, W. and Bertsche, U. (2008) 'Murein (peptidoglycan) structure, architecture and biosynthesis in Escherichia coli', *Biochimica et Biophysica Acta (BBA) - Biomembranes*, 1778(9), pp. 1714–1734. Available at: https://doi.org/10.1016/j.bbamem.2007.06.007.

Vollmer, W., Blanot, D. and De Pedro, M.A. (2008) 'Peptidoglycan structure and architecture', *FEMS Microbiology Reviews*, 32(2), pp. 149–167. Available at: https://doi.org/10.1111/j.1574-6976.2007.00094.x.

Vollmuth, N. *et al.* (2022) 'c-Myc plays a key role in IFN-γ-induced persistence of Chlamydia trachomatis', *eLife*, 11. Available at: https://doi.org/10.7554/eLife.76721.

Vouga, M., Baud, D. and Greub, G. (2017) '*Simkania negevensis* , an insight into the biology and clinical importance of a novel member of the *Chlamydiales* order', *Critical Reviews in Microbiology*, 43(1), pp. 62–80. Available at: https://doi.org/10.3109/1040841X.2016.1165650.

Wang, Y. *et al.* (2011) 'Development of a Transformation System for Chlamydia trachomatis: Restoration of Glycogen Biosynthesis by Acquisition of a Plasmid Shuttle Vector', *PLoS Pathogens*, 7(9), p. e1002258. Available at: https://doi.org/10.1371/journal.ppat.1002258.

Wanic, A. (1967) '[Therapeutic trials of various skin diseases using chinoline and chinaldine derivatives].', *Zeitschrift fur Haut- und Geschlechtskrankheiten*, 42(1), pp. 27–32.

Weiss, E. (1950) 'The Effect of Antibiotics on Agents of the Psittacosis-Lymphogranuloma Group: 1. The Effect of Penicillin', *Journal of Infectious Diseases*, 87(3), pp. 249–263. Available at: https://doi.org/10.1093/infdis/87.3.249.

Welter-Stahl, L. *et al.* (2006) 'Stimulation of the cytosolic receptor for peptidoglycan, Nod1, by infection with Chlamydia trachomatis or Chlamydia muridarum', *Cellular Microbiology*, 8(6), pp. 1047–1057. Available at: https://doi.org/10.1111/j.1462-5822.2006.00686.x.

Whitfield, C. and Trent, M.S. (2014) 'Biosynthesis and Export of Bacterial Lipopolysaccharides', *Annual Review of Biochemistry*, 83(1), pp. 99–128. Available at: https://doi.org/10.1146/annurev-biochem-060713-035600.

WHO (2021) *World Health Organization. WHO Alliance for the Global Elimination of Trachoma by 2020: progress report on elimination of trachoma, 2020.*

Wickstrum, J. *et al.* (2013) 'Conditional Gene Expression in Chlamydia trachomatis Using the Tet System', *PLoS ONE*, 8(10), p. e76743. Available at: https://doi.org/10.1371/journal.pone.0076743.

Wiedenheft, B., Sternberg, S.H. and Doudna, J.A. (2012) 'RNA-guided genetic silencing systems in bacteria and archaea', *Nature*, 482(7385), pp. 331–338. Available at: https://doi.org/10.1038/nature10886.

Wilkins, M.R. *et al.* (1999) 'Protein identification and analysis tools in the ExPASy server.', *Methods in molecular biology (Clifton, N.J.)*, 112, pp. 531–52. Available at: https://doi.org/10.1385/1-59259-584-7:531.

Wilks, J.C. and Slonczewski, J.L. (2007) 'pH of the Cytoplasm and Periplasm of *Escherichia coli* : Rapid Measurement by Green Fluorescent Protein Fluorimetry', *Journal of Bacteriology*, 189(15), pp. 5601–5607. Available at: https://doi.org/10.1128/JB.00615-07.

Winter, W.E., Bazydlo, L.A.L. and Harris, N.S. (2014) 'The Molecular Biology of Human Iron Metabolism', *Laboratory Medicine*, 45(2), pp. 92–102. Available at: https://doi.org/10.1309/LMF28S2GIMXNWHMM.

Wolle, M.A. and West, S.K. (2019) 'Ocular *Chlamydia trachomatis* infection: elimination with mass drug administration', *Expert Review of Anti-infective Therapy*, 17(3), pp. 189–200. Available at: https://doi.org/10.1080/14787210.2019.1577136.

Wood, H. *et al.* (2003) 'Regulation of tryptophan synthase gene expression in *Chlamydia trachomatis*', *Molecular Microbiology*, 49(5), pp. 1347–1359. Available at: https://doi.org/10.1046/j.1365-2958.2003.03638.x.

Wood, N.A. *et al.* (2020) 'The ClpX and ClpP2 Orthologs of Chlamydia trachomatis Perform Discrete and Essential Functions in Organism Growth and Development', *mBio*, 11(5). Available at: https://doi.org/10.1128/mBio.02016-20.

Xiao, J. and Goley, E.D. (2016) 'Redefining the roles of the FtsZ-ring in bacterial cytokinesis', *Current Opinion in Microbiology*, 34, pp. 90–96. Available at: https://doi.org/10.1016/j.mib.2016.08.008.

Xie, J. *et al.* (2023) 'Cuproptosis: mechanisms and links with cancers.', *Molecular cancer*, 22(1), p. 46. Available at: https://doi.org/10.1186/s12943-023-01732-y.

Xu, Q. *et al.* (2015) 'Insights into Substrate Specificity of NlpC/P60 Cell Wall Hydrolases Containing Bacterial SH3 Domains.', *mBio*, 6(5), pp. e02327-14. Available at: https://doi.org/10.1128/mBio.02327-14.

Yakhnina, A.A. and Bernhardt, T.G. (2020) 'The Tol-Pal system is required for peptidoglycan-cleaving enzymes to complete bacterial cell division', *Proceedings of the National Academy of Sciences*, 117(12), pp. 6777–6783. Available at: https://doi.org/10.1073/pnas.1919267117.

Yamamoto, H. *et al.* (2008) 'Post-translational control of vegetative cell separation enzymes through a direct interaction with specific inhibitor IseA in *Bacillus subtilis*', *Molecular Microbiology*, 70(1), pp. 168–182. Available at: https://doi.org/10.1111/j.1365-2958.2008.06398.x.

Yang, C. *et al.* (2019) 'Chlamydia trachomatis Lipopolysaccharide Evades the Canonical and Noncanonical Inflammatory Pathways To Subvert Innate Immunity', *mBio*, 10(2). Available at: https://doi.org/10.1128/mBio.00595-19.

Yang, D.C. *et al.* (2011) 'An ATP-binding cassette transporter-like complex governs cell-wall hydrolysis at the bacterial cytokinetic ring', *Proceedings of the National Academy of Sciences*, 108(45). Available at: https://doi.org/10.1073/pnas.1107780108.

Yang, D.C. *et al.* (2012a) 'A conformational switch controls cell wall-remodelling enzymes required for bacterial cell division', *Molecular Microbiology*, 85(4), pp. 768–781. Available at: https://doi.org/10.1111/j.1365-2958.2012.08138.x.

Yang, D.C. *et al.* (2012b) 'A conformational switch controls cell wall-remodelling enzymes required for bacterial cell division', *Molecular Microbiology*, 85(4), pp. 768–781. Available at: https://doi.org/10.1111/j.1365-2958.2012.08138.x.

Yang, X. *et al.* (2021) 'A two-track model for the spatiotemporal coordination of bacterial septal cell wall synthesis revealed by single-molecule imaging of FtsW', *Nature Microbiology*, 6(5), pp. 584–593. Available at: https://doi.org/10.1038/s41564-020-00853-0.

Yu, H., Lou, J.R. and Ding, W.-Q. (2010) 'Clioquinol independently targets NF-kappaB and lysosome pathways in human cancer cells.', *Anticancer research*, 30(6), pp. 2087–92.

Zhu, Y. *et al.* (2021) 'Clioquinol Attenuates Pulmonary Fibrosis through Inactivation of Fibroblasts via Iron Chelation', *American Journal of Respiratory Cell and Molecular Biology*, 65(2), pp. 189–200. Available at: https://doi.org/10.1165/rcmb.2020-0279OC.

Zoll, S. *et al.* (2010) 'Structural Basis of Cell Wall Cleavage by a Staphylococcal Autolysin', *PLoS Pathogens*, 6(3), p. e1000807. Available at: https://doi.org/10.1371/journal.ppat.1000807.

Zomorodipour, A. and Andersson, S.G.E. (1999) 'Obligate intracellular parasites: *Rickettsia prowazekii* and *Chlamydia trachomatis*', *FEBS Letters*, 452(1–2), pp. 11–15. Available at: https://doi.org/10.1016/S0014-5793(99)00563-3.

Veröffentlichungen

Teile dieser Arbeit wurden bereits veröffentlicht:

Reuter J, Otten C, Jacquier N, Lee J, Mengin-Lecreulx D, Löckener I, Kluj R, Mayer C, Corona F, **Dannenberg J**, Aeby S, Bühl H, Greub G, Vollmer W, Ouellette SP, Schneider T, Henrichfreise B. (2023) An NlpC/P60 protein catalyzes a key step in peptidoglycan recycling at the intersection of energy recovery, cell division and immune evasion in the intracellular pathogen *Chlamydia trachomatis*. PLoS Pathog 19(2): e1011047. doi:10.1371/journal.ppat.1011047